NASA/TM—2017–219693

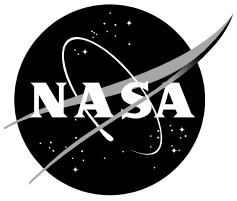

Aerodynamic Coefficients from Aeroballistic Range Testing of Deployed- and Stowed-SIAD SFDT Models

Michael C. Wilder
Ames Research Center, Moffett Field, California

Jeffrey D. Brown
Engineering Research & Consulting, Inc.
Ames Research Center, Moffett Field, California

David W. Bogdanoff
Engineering Research & Consulting, Inc.
Ames Research Center, Moffett Field, California

Leslie A. Yates
Aerospace Computing, Inc.

Artem A. Dyakonov
Langley Research Center, Hampton, Virginia

Ian G. Clark
Jet Propulsion Laboratory, California Institute of Technology, Pasadena, California

Jay H. Grinstead
Ames Research Center, Moffett Field, California

November 2017

NASA STI Program ... in Profile

Since its founding, NASA has been dedicated to the advancement of aeronautics and space science. The NASA scientific and technical information (STI) program plays a key part in helping NASA maintain this important role.

The NASA STI program operates under the auspices of the Agency Chief Information Officer. It collects, organizes, provides for archiving, and disseminates NASA's STI. The NASA STI program provides access to the NTRS Registered and its public interface, the NASA Technical Reports Server, thus providing one of the largest collections of aeronautical and space science STI in the world. Results are published in both non-NASA channels and by NASA in the NASA STI Report Series, which includes the following report types:

- TECHNICAL PUBLICATION. Reports of completed research or a major significant phase of research that present the results of NASA Programs and include extensive data or theoretical analysis. Includes compilations of significant scientific and technical data and information deemed to be of continuing reference value. NASA counterpart of peer-reviewed formal professional papers but has less stringent limitations on manuscript length and extent of graphic presentations.

- TECHNICAL MEMORANDUM. Scientific and technical findings that are preliminary or of specialized interest, e.g., quick release reports, working papers, and bibliographies that contain minimal annotation. Does not contain extensive analysis.

- CONTRACTOR REPORT. Scientific and technical findings by NASA-sponsored contractors and grantees.

- CONFERENCE PUBLICATION. Collected papers from scientific and technical conferences, symposia, seminars, or other meetings sponsored or co-sponsored by NASA.

- SPECIAL PUBLICATION. Scientific, technical, or historical information from NASA programs, projects, and missions, often concerned with subjects having substantial public interest.

- TECHNICAL TRANSLATION. English-language translations of foreign scientific and technical material pertinent to NASA's mission.

Specialized services also include organizing and publishing research results, distributing specialized research announcements and feeds, providing information desk and personal search support, and enabling data exchange services.

For more information about the NASA STI program, see the following:

- Access the NASA STI program home page at http://www.sti.nasa.gov

- E-mail your question to help@sti.nasa.gov

- Phone the NASA STI Information Desk at 757-864-9658

- Write to:
  NASA STI Information Desk
  Mail Stop 148
  NASA Langley Research Center
  Hampton, VA 23681-2199

NASA/TM—2017–219693

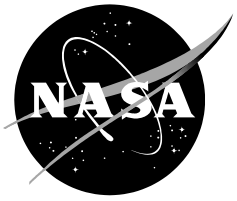

Aerodynamic Coefficients from Aeroballistic Range Testing of Deployed- and Stowed-SIAD SFDT Models

Michael C. Wilder
Ames Research Center, Moffett Field, California

Jeffrey D. Brown
Engineering Research & Consulting, Inc.
Ames Research Center, Moffett Field, California

David W. Bogdanoff
Engineering Research & Consulting, Inc.
Ames Research Center, Moffett Field, California

Leslie A. Yates
Aerospace Computing, Inc.

Artem A. Dyakonov
Langley Research Center, Hampton, Virginia

Ian G. Clark
Jet Propulsion Laboratory, California Institute of Technology, Pasadena, California

Jay H. Grinstead
Ames Research Center, Moffett Field, California

National Aeronautics and
Space Administration

Ames Research Center
Moffett Field, CA 94035-1000

November 2017

Acknowledgments

This work was supported by NASA's Low Density Supersonic Decelerators (LDSD) Project, led by the NASA Jet Propulsion Laboratory for the Space Technology Mission Directorate. The Local Technical Project Manager for the LDSD Project at NASA Ames Research Center was Jay Grinstead, the Principal Investigator for the LDSD Project was Ian Clark of the Jet Propulsion Laboratory, and the Aerosciences Manager for the LDSD Project was Chuck Player of the NASA Langley Research Center.

The authors wish to acknowledge the tireless efforts of the HFFAF crew, Chuck Cornelison, Don Holt, Don Bowling, Freddy Perez, and Jon-Pierre Wiens. Models and sabots were machined by Shawn Meszaros and Jim Scott of the NASA Ames machine shop, Everfab, Inc. of East Aurora, NY, Roncelli Plastics of Monrovia, CA and EVJ Machine of Pacoima, CA.

David W. Bogdanoff, Jeffrey D. Brown, and Leslie A. Yates (via a subcontract to ERC, Inc.) were supported by Contract NNA10DE12C from the NASA Ames Research Center to ERC, Inc. At the time of publication, David W. Bogdanoff and Jeffrey D. Brown were employed by Analytical Mechanics Associates, Inc. under contract to NASA Ames Research Center, and Artem A. Dyakonov was with Blue Origin in Kent, WA.

Available from:

NASA Center for AeroSpace Information
7115 Standard Drive
Hanover, MD 21076-1320
443-757-5802

Table of Contents

List of Figures

List of Tables

Abstract

This report documents a ballistic-range test campaign conducted in 2012 in order to estimate the aerodynamic stability characteristics of two configurations of the Supersonic Flight Dynamics Test (SFDT) vehicle prior to its initial flight in 2014. The SFDT vehicle was a test bed for demonstrating several new aerodynamic decelerator technologies then being developed under the Low-Density Supersonic Decelerator (LDSD) Project. Of particular interest here is the Supersonic Inflatable Aerodynamic Decelerator (SIAD), an inflatable attached torus used to increase the drag surface area of an entry vehicle during the supersonic portion of the entry trajectory. Two model configurations were tested in the ballistic range: one representing the SFDT vehicle prior to deployment of the SIAD, and the other representing the nominal shape with the SIAD inflated. Both models were fabricated from solid metal, and therefore, the effects of the flexibility of the inflatable decelerator were not considered. The test conditions were chosen to match, as close as possible, the Mach number, Reynolds number, and motion dynamics expected for the SFDT vehicle in flight, both with the SIAD stowed and deployed. For SFDT models with the SIAD stowed, 12 shots were performed covering a Mach number range of 3.2 to 3.7. For models representing the deployed SIAD, 37 shots were performed over a Mach number range of 2.0 to 3.8. Pitch oscillation amplitudes covered a range from 0.7 to 20.6 degrees RMS.

Portions of this report (data analysis approach, aerodynamic modeling, and resulting aerodynamic coefficients) were originally published as an internal LDSD Project report [1] in 2012. In addition, this report provides a description of the test design approach, the test facility, and experimental procedures. Estimated non-linear aerodynamic coefficients, including pitch damping, for both model configurations are reported, and the shot-by-shot trajectory measurements, plotted in comparison with calculated trajectories based on the derived non-linear aerodynamic coefficients, are provided as appendices.

Since the completion of these tests, two full-scale SFDT flights have been successfully conducted: one in June 2014 [2, 3], and one in June 2015 [3].

Nomenclature

Symbols

a	- speed of sound
A	- model, or vehicle, frontal area
C_D	- drag coefficient
C_{D_0}, $C_{D_{(M\text{-}M_{ref})}}$	- functional parameters for non-linear drag coefficient
C_L	- lift coefficient
C_{L_σ}, $C_{L_{\sigma(M\text{-}M_{ref})}}$	- functional parameters for non-linear lift coefficient
C_m	- pitching moment coefficient
$C_{m_{\sigma,1}}$, $C_{m_{\sigma,2}}$ …	- functional parameters for non-linear pitching moment coefficient
C_{m_q}	- pitch damping coefficient
$C^*_{m_q}$, $C^*_{m_{q,0}}$ …	- functional parameters for non-linear pitch damping coefficient
C_{m_α}	- moment curve slope, $\partial C_m / \partial \alpha$
d	- model, or vehicle, diameter
I_{xx}, I_{yy}, I_{zz}	- moments of inertia about length, cross, and vertical axes, respectively
l	- model length, from geometric nose to base of the rocket nozzle
M	- Mach number, u_∞/a
$\bar{M}$	- average Mach number for a shot (averaged from the first to the last shadowgraph station)
q	- model angular rate (non-dimensional)
Re_d	- Freestream Reynolds number, $\rho_\infty u_\infty d/\mu_\infty$
R_n	- Nose radius
t	- time
u_∞	- freestream velocity
V	- velocity
x, y, z	- longitudinal, transverse, and vertical facility coordinates, respectively, or - axial, transverse, and vertical model coordinates, respectively
α	- angle of attack

β - yaw angle
θ - measured angle relative to horizontal plane
λ - pitch oscillation wavelength
μ - fluid viscosity
σ - total angle of attack [$= \cos^{-1}(\cos\alpha * \cos\beta)$]
ρ - fluid density
ψ - measured angle relative to vertical plane
ω - angular oscillation frequency (dimensional)

Subscripts
∞ - at freestream conditions
CG - at the center of gravity of the model

Abbreviations and Acronyms
CADRA - Comprehensive Automatic Data Reduction system for Aeroballistic ranges
DOF - degrees of freedom
HFFAF - Hypervelocity Free-Flight Aerodynamics Facility
LDSD - Low Density Supersonic Decelerator
RMS - root mean square
SFDT - Supersonic Flight Dynamics Test
SIAD - Supersonic Inflatable Aerodynamic Decelerator
SSR - sum of the squares of the residuals

1. Introduction

The Low-Density Supersonic Decelerator (LDSD) Project developed and tested several technologies to meet the needs of landing higher-mass payloads in potential future Mars exploration missions [4, 5]. This included the supersonic inflatable aerodynamic decelerator (SIAD), which is an inflatable attached torus (also referred to as SIAD-R, with 'R' designating use in robotic exploration missions). The SIAD, attached to the outer rim of a capsule-like atmospheric entry vehicle, is intended to inflate after the vehicle has passed through the hypersonic, high-heating, portion of the entry when the vehicle is flying at Mach 3 to 4. The added surface area will allow the vehicle to decelerate to around Mach 2, where it becomes safe to deploy a supersonic parachute while still at a safe altitude. The LDSD Project conducted two flight tests in the Earth's atmosphere, designated the Supersonic Flight Dynamics Test (SFDT) [2-6], of the SIAD and other technologies in 2014 and 2015. To achieve flight conditions relevant to Mars entry, the 4.7 meter-diameter capsule was dropped from a high altitude balloon and propelled with a rocket motor to a Mach number of approximately 4 at an altitude between 45 and 50 km, as illustrated in Figure 1. After a brief coasting period, a single-torus SIAD was deployed, expanding the diameter to 6 m. The vehicle descended un-powered through the atmosphere in this configuration until slowing to roughly Mach 2, when it deployed a parachute for landing. Figure 2 shows drawings of the SFDT vehicle before, and after, deploying the SIAD.

The SFDT vehicle was not equipped with a reaction control system and relied, instead, on favorable pitch damping to limit the growth of oscillations during the test phase. Noting the general tendency in blunt entry vehicles for small oscillations to grow with deceleration [7-9], the potential for high oscillation amplitude at the beginning of the SFDT test phase caused by perturbations during balloon drop, and the tight requirement for angle of attack at parachute opening, the need for well-characterized aerodynamics and uncertainties as an input for SFDT flight simulation is evident. Therefore, prior to the first SFDT flight, a ballistic-range test campaign was conducted in order to estimate the aerodynamic stability characteristics of the vehicle, both before and after deployment of the SIAD. These tests were performed in the Hypervelocity Free-Flight Aerodynamics Facility (HFFAF) at NASA's Ames Research Center from January to April of 2012.

The ballistic range tests concentrated on the SFDT test period, indicated in Figure 1, from deployment of the SIAD to release of the PDD (a ram-air inflated Parachute Deployment Device, also being developed by the LDSD Project). Thirty-seven shots were made over a Mach number range of 2.0 – 3.8 for models of the SFTD vehicle with the SIAD deployed. Data were obtained over pitch oscillation amplitudes ranging from 0.7 to 20.6 degrees RMS (root mean square). The models, including the representation of the SIAD, were fabricated from solid metal, and therefore, evaluation of any effects of the flexibility of the inflatable decelerator was not part of this test campaign. In addition, a smaller number of tests were made to assess the aerodynamic characteristics of the SFDT vehicle in

the period between despin and SIAD deployment, also shown in Figure 1. Twelve shots were made over a Mach number range of 3.2 – 3.7 for models of the SFTD with the SIAD stowed. RMS pitch oscillation amplitudes ranged from 1.6 to 17.2 degrees. Test conditions were chosen to match, as close as possible, the Mach number, Reynolds number, the normalized deceleration rates, and the normalized pitch-oscillation wavelengths of those expected for the flight vehicle. Static aerodynamic coefficients for lift, drag and pitching moment were obtained, as well as the dynamic stability pitch damping coefficients.

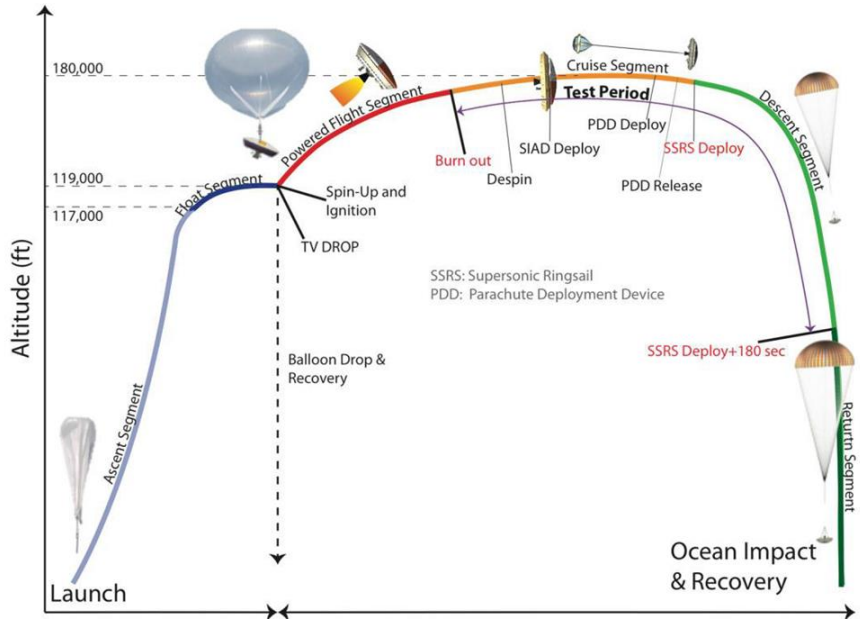

Figure 1. Supersonic Flight Dynamics Test trajectory overview (from Ref. 4).

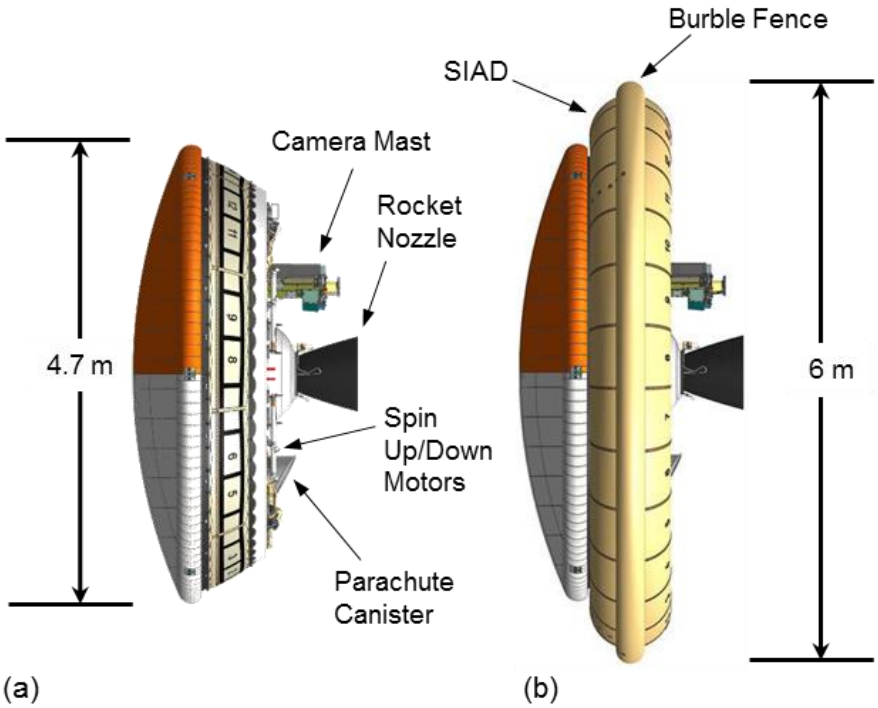

Figure 2. Supersonic Flight Dynamics Test (SFDT) vehicle with (a) SIAD stowed, and (b) SIAD deployed (from Ref. 6).

2. Experimental Setup and Approach

2.1. Test Facility

The tests were conducted in the Hypervelocity Free-Flight Aerodynamics Facility (HFFAF) at the NASA Ames Research Center. Initially developed for the study of hypersonic planetary entry phenomena [10, 11], the facility is capable of testing over the full speed range, from hypersonic to subsonic, experienced by an entry vehicle [12, 13]. The HFFAF is shown schematically in Figure 3(a), and a photograph of the test section is shown in Figure 3(b). Two smooth-bore powder-gun launchers, shown in Figure 4, were used for the SFDT test series: a 20 mm bore-diameter gun for the stowed-SIAD models and a 44 mm bore gun for the deployed-SIAD configuration. Launched into the test section, a model flies an unconstrained (6-degree-of-freedom) trajectory through a quiescent test gas at ambient room temperature. The test-section pressure and gas composition are selectable to allow simulation of flight at different altitudes and in different planetary atmospheres. Since the SFDT flight tests were conducted in Earth's atmosphere, all tests in this campaign were conducted in air. The HFFAF can be operated at pressures from about 0.1 Torr to a maximum of 760 Torr (1 atm). The test section is approximately 1 m across and 23 m long with 16 shadowgraph stations evenly spaced every 1.524 m (5 ft). Each shadowgraph station has two orthogonal imaging systems, providing side and top views of the model from which the instantaneous position and orientation of the model are measured relative to a system of calibrated fiducial wires, as described in Section 3.1. Elapsed-time data are provided by 16 high-speed digital counters synchronized with the shadowgraphs. Example side-view shadowgraph images of each model configuration are shown in Figure 5. These images have been cropped to emphasize the flow structure. The pair of vertical lines seen in these images are part of the fiducial system.

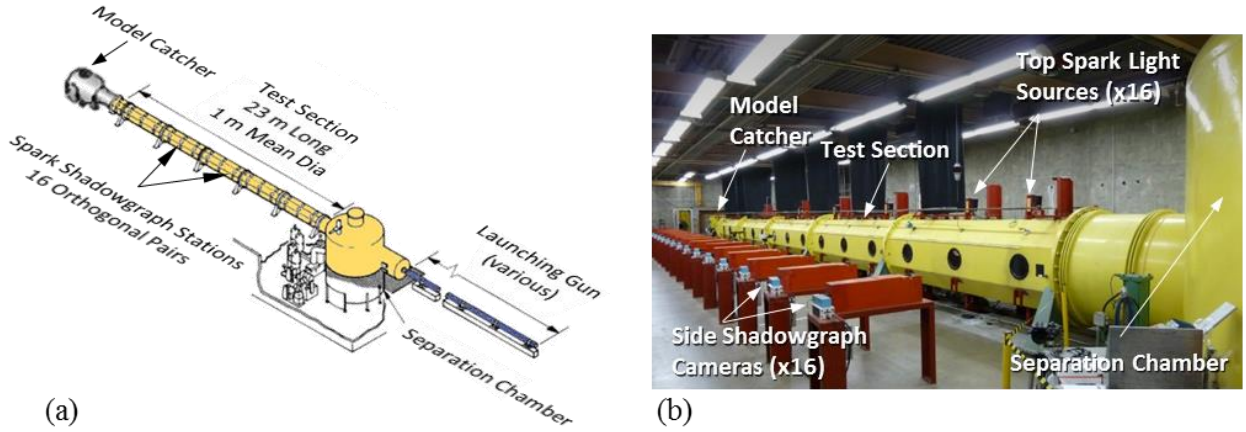

Figure 3. The Hypervelocity Free Flight Aerodynamic Facility. (a) Schematic of the facility; (b) Photograph of the test section.

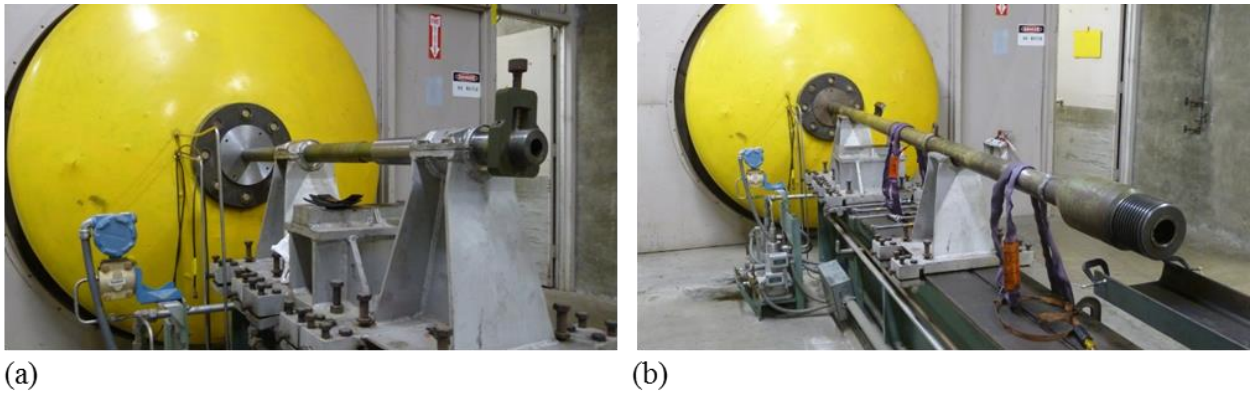

Figure 4. Powder gun launchers in the HFFAF: (a) 20 mm gun; (b) 44 mm gun.

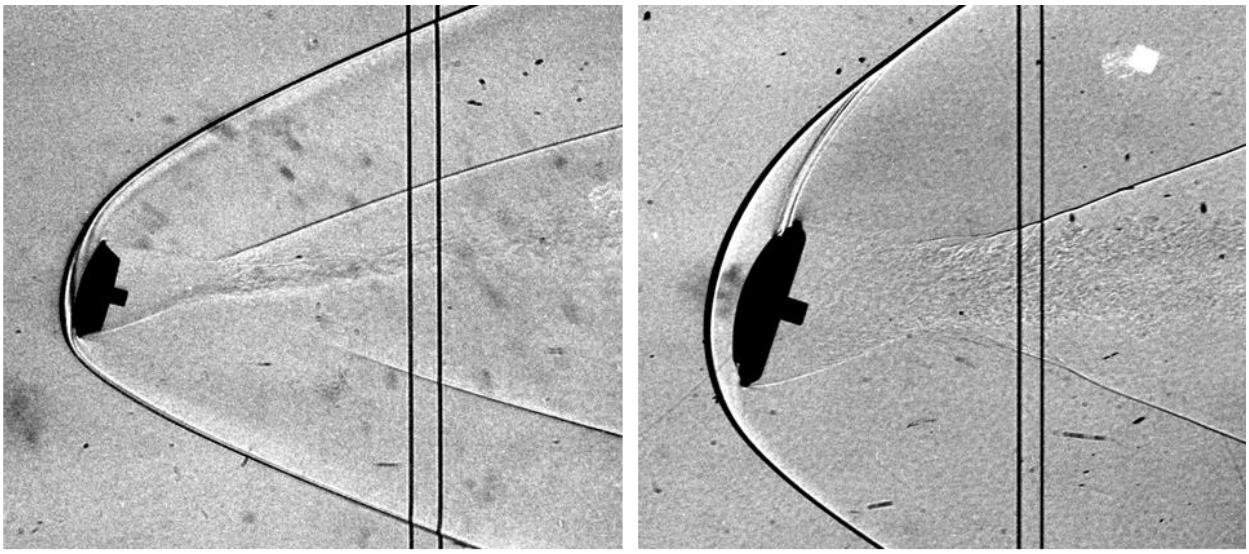

(a) (b)

Figure 5. Example side-view shadowgraphs of test models in flight: (a) SIAD stowed configuration (shot 2670, station 2); (b) SIAD deployed configuration (shot 2650, station 3).

2.2. Test and Model Design

Static aerodynamic similitude is generally achieved by matching the full-scale free stream Mach number and Reynolds number.

$$M_\infty = \frac{u_\infty}{a} \tag{1}$$

$$Re_d = \frac{\rho_\infty u_\infty d}{\mu_\infty} \tag{2}$$

The gun launchers of the HFFAF can easily match SFDT flight Mach numbers. Despite the small model dimensions, flight Reynolds numbers can be attained by testing at higher freestream density (test section pressure), relative to the atmospheric density at flight altitude. In order to achieve dynamic similarity with flight, we attempt to match two additional similarity parameters: the vehicle-to-fluid mass moment of inertia ratio, $I/\rho_\infty d^5$, and the vehicle-to-fluid mass ratio, $m/\rho_\infty d^3$ [14-16]. These can be related, respectively, to the normalized pitch oscillation wavelength, λ/d (from Ref. 17), and to the relative deceleration over one characteristic length (vehicle diameter) of movement, $\Delta u/u$ per d:

$$\frac{\lambda}{d} = \frac{1}{d}\sqrt{\frac{8\pi^2 I}{-C_{m_\alpha}\rho_\infty A d}} \propto \sqrt{\frac{I}{\rho_\infty d^5}} \tag{3}$$

$$\left.\frac{\Delta u}{u}\right|_d = \frac{1}{2}\rho_\infty C_D \frac{A}{m} d \propto \frac{\rho_\infty d^3}{m} \tag{4}$$

In designing the model and test conditions, the wavelength and deceleration forms of these similarity parameters (eqns. 3 and 4) are used because the allowable values of these quantities are constrained by facility and data-acquisition requirements. Specifically, at least three well-defined peaks in the pitch oscillation waveform (1.5 cycles of oscillation) are necessary to determine whether the oscillation amplitude is damping or growing, and at least 5 samples (shadowgraphs) per cycle are needed to reliably define the peak amplitudes (resulting in ~3 cycles of oscillation over the 16 shadowgraph stations of the HFFAF test section) (Refer to the error analysis discussion in Ref. 18 for further details). Consequently λ is typically constrained such that the model performs between 1.5 and 3

cycles of pitch oscillation over the length of the test section. To determine the drag coefficient, the deceleration of the model must be large enough to be measured accurately, but not so large that it significantly alters the flight conditions. Typically, the drop in speed through the test section is between 5% and 10%. Additional design constraints are placed on the model diameter, mass, and mass moment of inertia due to the bore size of available guns, and the densities of materials available for model fabrication. The model diameter is typically 70% to 85% of the gun bore diameter, based on the need for structural integrity of the model-carrying sabot and the competing need to be able to cleanly separate the sabot from the model.

It can be seen from equations 1-4 that one similarity parameter may depend inversely relative to another on the same design parameter. For example, Reynolds number (eqn. 2) and relative deceleration (eqn. 4) both increase with increasing freestream density, while the oscillation wavelength (eqn. 3) decreases with density. The pattern is similar for model size, but the inverse for model mass. As a consequence, it may not be possible to match all four similarity parameters at all trajectory points for a single model design (size and mass). Models are typically designed to have the closest similarity to flight conditions at the flight condition where dynamic stability is considered most critical. If flight conditions vary too much over a trajectory, multiple model designs may be required.

In general, an initial model diameter is determined that satisfies $(\lambda/d)_{test} = (\lambda/d)_{flight}$ at the most critical trajectory point, subject to the constraints that $\lambda_{test} \approx$ half the test-section length and $d \approx 80\%$ of the gun bore. Then, for each trajectory point, the test gas density required to match the flight Reynolds number is determined from eqn. 2, and eqn. 3 is used to determine the required model moment of inertia, I. The required model material density is determined from I and the known model geometry, and the material closest in density is selected. A second iteration is performed to adjust d and ρ_∞ for the selected material density, subject to the facility constraints.

Initial estimates of the SFDT vehicle mass properties and static aerodynamic coefficients at several trajectory points were provided by the LDSD Project for use in model and test-condition design. The methodologies for determining the aerodynamic coefficients are discussed in more detail in Ref. 19, which also presents post-flight simulations of the SFDT-1 flight. The values at trajectory points prior to inflation of the SIAD are given in Table 1, and after the SIAD is deployed in Table 2.

Table 1. Flight Conditions and Similarity Parameters for the SFDT Vehicle with the SIAD Stowed.

M_∞	Re_d (x 10^{-6})	V_∞, m/sec	ρ_∞, kg/m^3	C_{m_α}	C_D	λ/d	$\Delta u/u\|_\lambda$
4.23	0.454	1384	0.00117	0.119	1.51	740	0.039
3.50	0.340	1144	0.00106	0.119	1.53	778	0.037

Mass = 1370 kg, Diameter = 4.7 m, Moment of inertia = 1740 kg-m^2

Table 2. Flight Conditions and Similarity Parameters for the SFDT Vehicle with the SIAD Deployed.

M_∞	Re_d (x 10^{-6})	V_∞, m/sec	ρ_∞, kg/m^3	C_{m_α}	C_D	λ/d	$\Delta u/u\|_\lambda$
3.96	0.513	1295	0.00111	0.196	1.43	352	0.034
3.50	0.434	1144	0.00106	0.188	1.45	368	0.035
3.00	0.382	982	0.00109	0.180	1.46	370	0.036
2.48	0.400	811	0.00138	0.173	1.46	336	0.042
2.37	0.422	774	0.00152	0.171	1.45	321	0.044

Mass = 1370 kg, Diameter = 6.0 m, Moment of inertia = 2077 kg-m^2

The model design process described above resulted in a model diameter of 1.699 cm (0.669 in) for the stowed-SIAD configuration, and 3.556 cm (1.400 in) for the deployed-SIAD configuration. The model profiles are shown in Figure 6 (compare with the flight vehicle profiles shown in Figure 2). Detailed dimensional drawings are given in Figure 7 and Figure 8 for the stowed and deployed configurations, respectively, and photographs of each model type are shown in Figure 9.

The stowed-SIAD models were assembled from two materials in order to correctly position the longitudinal center of gravity (CG) at x/d = 0.1973 measured from the geometric nose. The main body was made of tungsten, and a steel insert in the nose was used to position the CG, as shown in Figure 7.

The deployed-SIAD models were machined from a solid piece of steel, and the longitudinal center of gravity was x/d = 0.1577 measured from the geometric nose, which was sufficiently close to the expected CG of the flight vehicle that no adjustments were required.

The forward surface and the aft cone surface of each configuration, as well as the torus and burble fence of the inflated SIAD, were accurately scaled on the models. The rear surfaces were greatly simplified to reduce machining costs. For both configurations, the rocket motor nozzle was represented as a solid cylinder. For the deployed-SIAD configuration all other aft details were eliminated, including the camera mast, electronics boxes, parachute canister, and spin up/down motors. It was assumed that these simplifications would have little or no effect on the stability characteristics of the vehicle and model since these surfaces lie in the low velocity wake region. For the stowed-SIAD configuration an attempt was made to capture some aft detail, namely the non-axisymmetric placement of the spin up/down motors. This was done by machining cut outs on the outer diameter of the base, as seen in Figure 7 and the photographs of Figure 9(a).

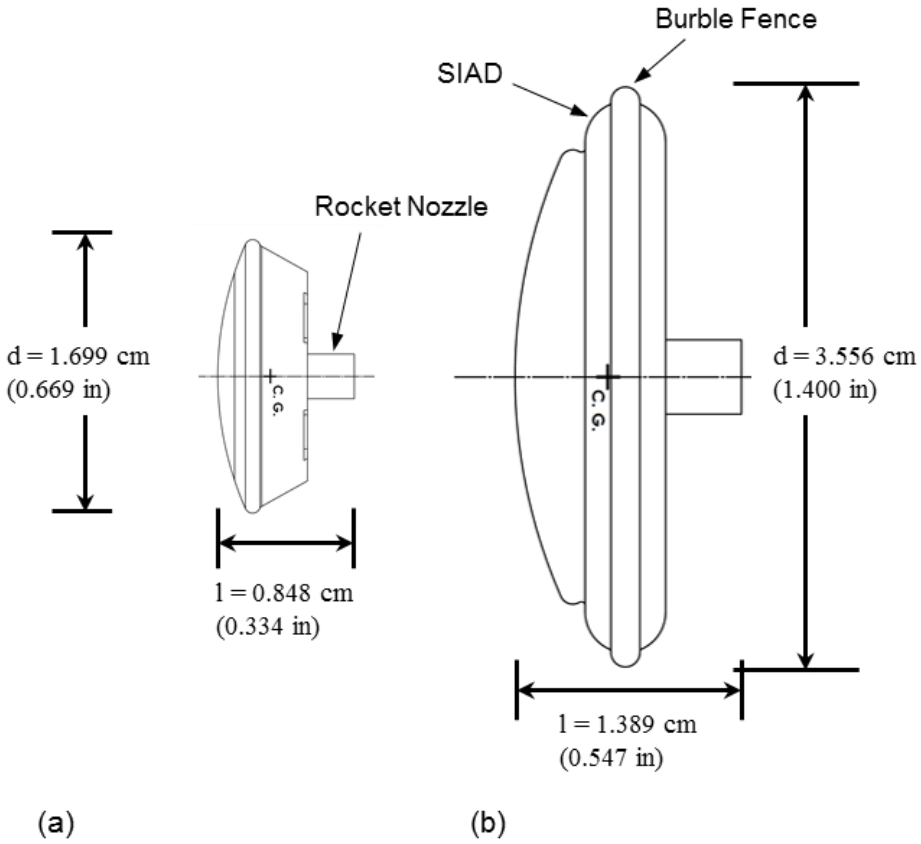

Figure 6. Drawings of ballistic-range models of the SFDT vehicle with the SIAD (a) stowed, and (b) deployed.

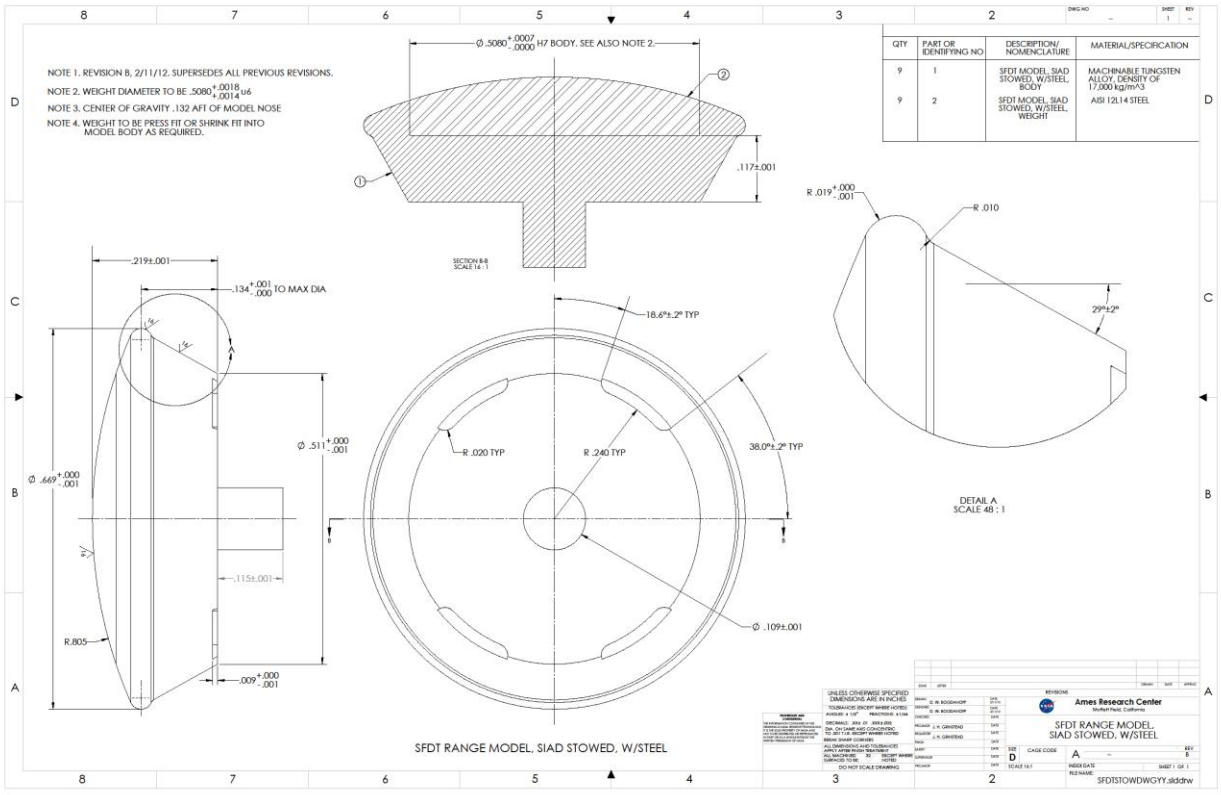

Figure 7. Detailed drawings of the stowed-SIAD ballistic range model. Dimension in inches.

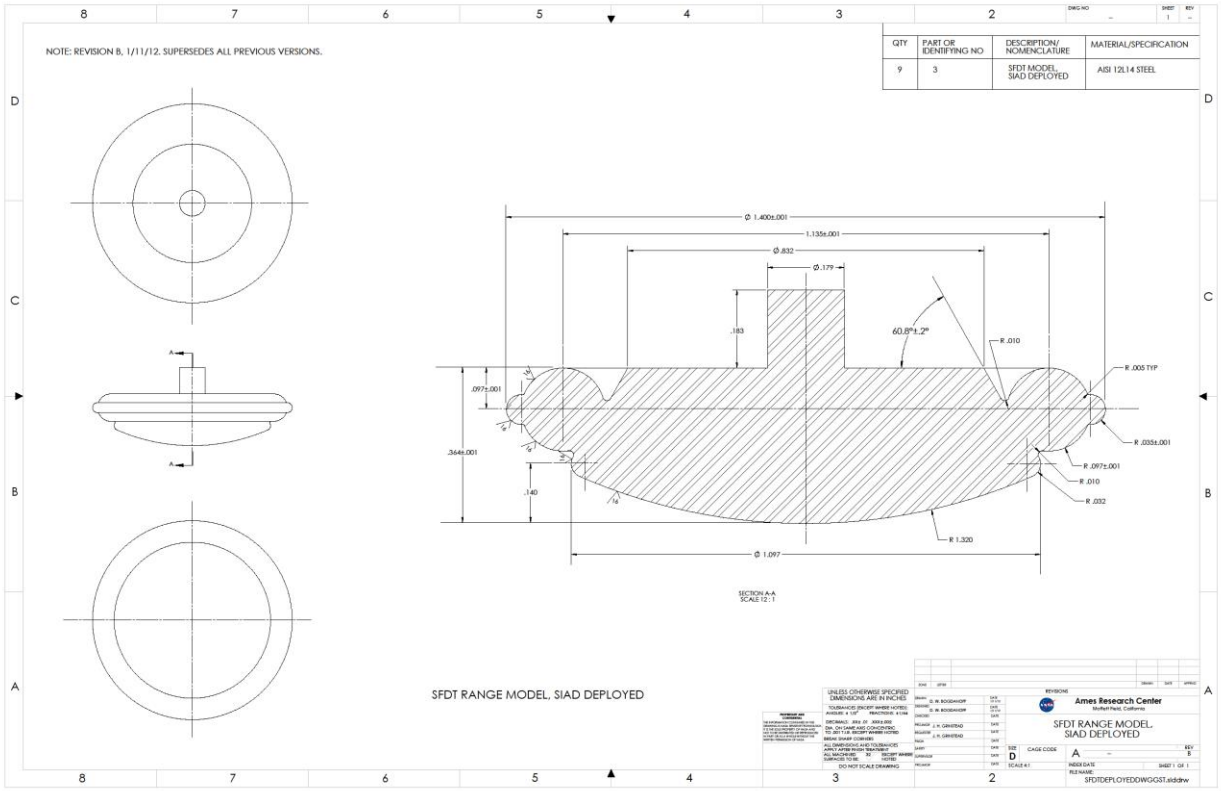

Figure 8. Detailed drawings of the deployed-SIAD ballistic range model. Dimension in inches.

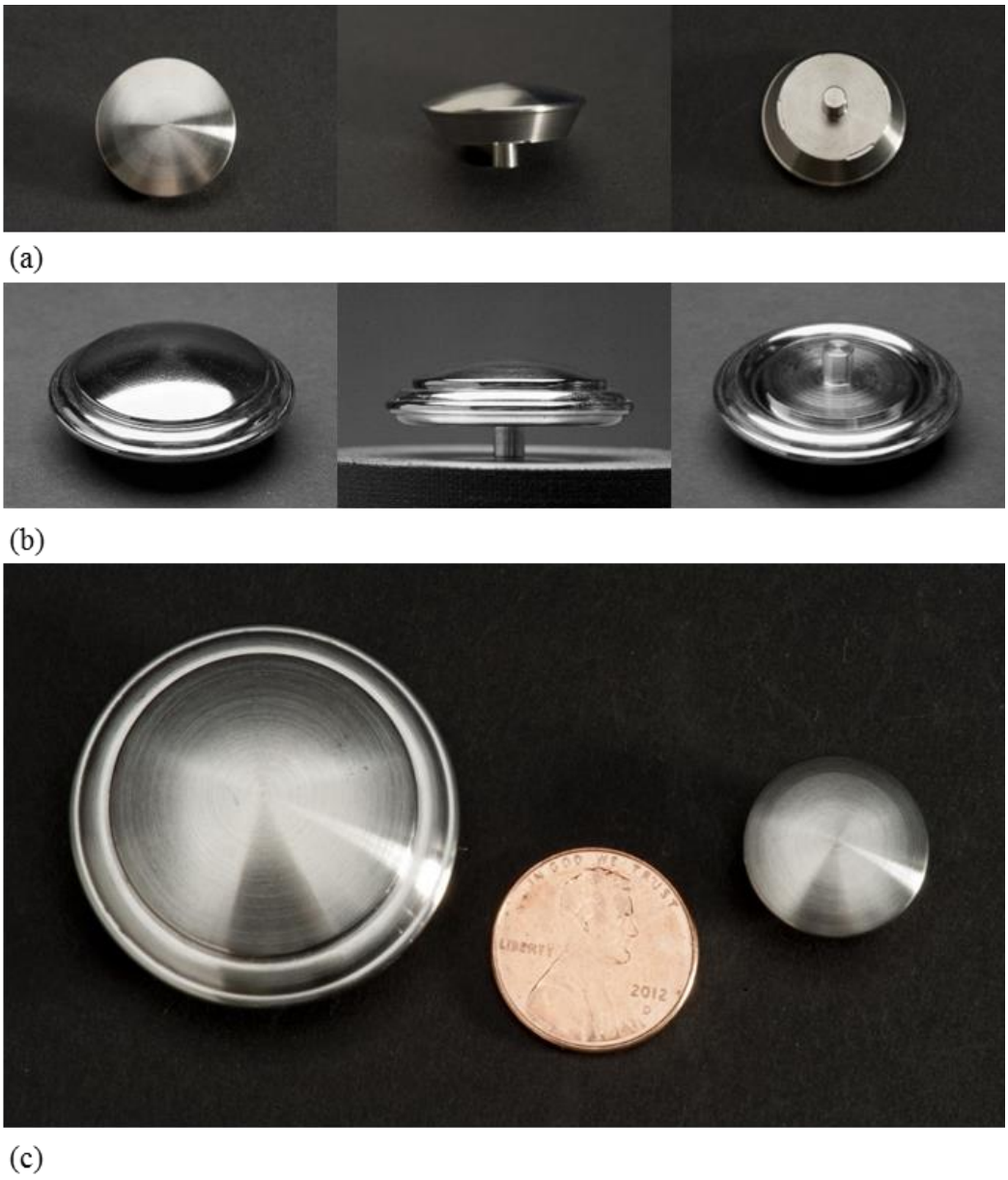

Figure 9. Photographs of ballistic-range models of SFDT vehicle: (a) SIAD stowed (front, side, and aft views from left to right), (b) SIAD deployed (front, side, and aft views from left to right), (c) front view of both model configurations shown with a penny for scale.

All models were launched at a nominal zero-degree angle of attack. During launch from the gun, each model was packaged inside a segmented Nylon cylindrical carrier, called a sabot. Figure 10 shows each model design in a launch sabot, with one segment removed to show the internal detail. When the launch package exits the muzzle, aerodynamic loads on forward bevels rotate the sabot segments away from the model. Five meters from the gun muzzle the model passes through an opening from the separation chamber (refer to Figure 3) to the test section, at which point the sabot segments have separated far enough from the model to be trapped in the separation chamber. For some test conditions, a cavity in the base of the sabot (see the larger sabot in Figure 10) was used to improve separation. Propellant gases from the gun (muzzle blast) pressurize the cavity, causing the sabot to open from the rear upon exiting the barrel. Properly balanced with the aerodynamic separation on the front of the sabot results in the sabot segments moving axially away from the model, thus reducing the chance of a sabot segment imparting unwanted perturbations to the attitude of the model. An example of this effect is given in Figure 11, which shows the early stage of sabot separation without, and with, a base cavity. The cleaner release of the model seen in Figure

11(b) with the base cavity is critical for achieving launches having small initial angle of attack and angular rates. Further details about the launch techniques developed and employed in these tests can be found in Ref. 19.

In order to fully characterize the aerodynamics of a model, a number of shots must be made with the model having a wide range of amplitudes of pitch oscillations. Since all models were launched at a nominal zero-degree angle of attack, a method was used to mechanically induce a pitch oscillation after the sabot separation. A sheet of paper, or cardstock, was positioned at the entrance to the test section such that half the model would impact the sheet. The mass density of the sheet was used to control the amplitude of the resulting model pitch oscillations. Figure 12 shows an example impact sequence that resulted in an RMS angle of attack of 8.8°. Further details about this technique can be found in Refs. 19 and 16.

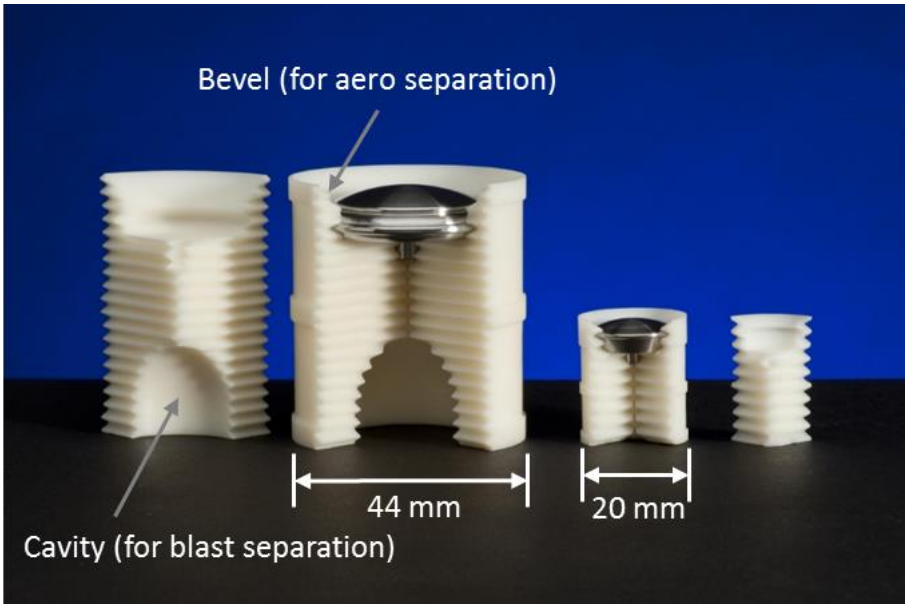

Figure 10. Photograph of ballistic-range models in launch sabots, with one sabot segment removed to show internal detail. Left: The deployed-SIAD model and sabot for the 44 mm gun; Right: The stowed-SIAD model and sabot for the 20 mm gun.

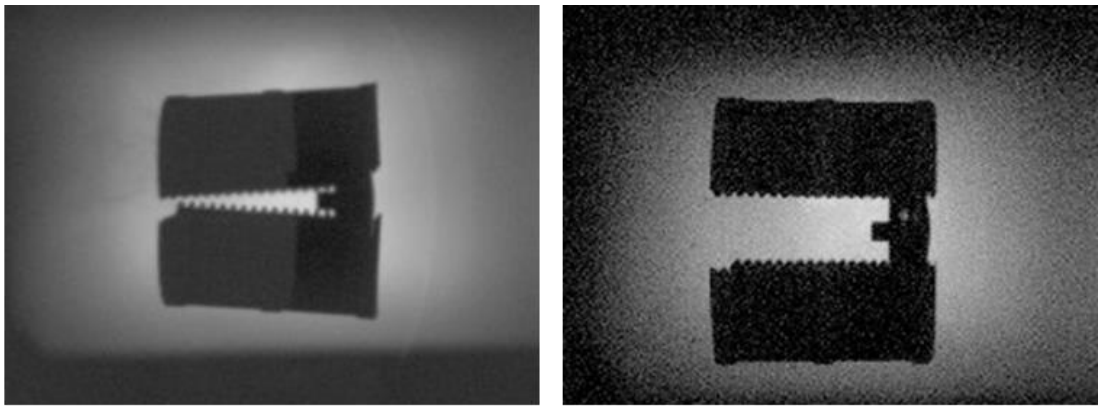

Figure 11. Sabot separation from the deployed-SIAD model at 1.14 m distance from the gun muzzle at M = 2.9, P_∞ = 163 Torr. (a) Sabot without base cavity; (b) Sabot with base cavity.

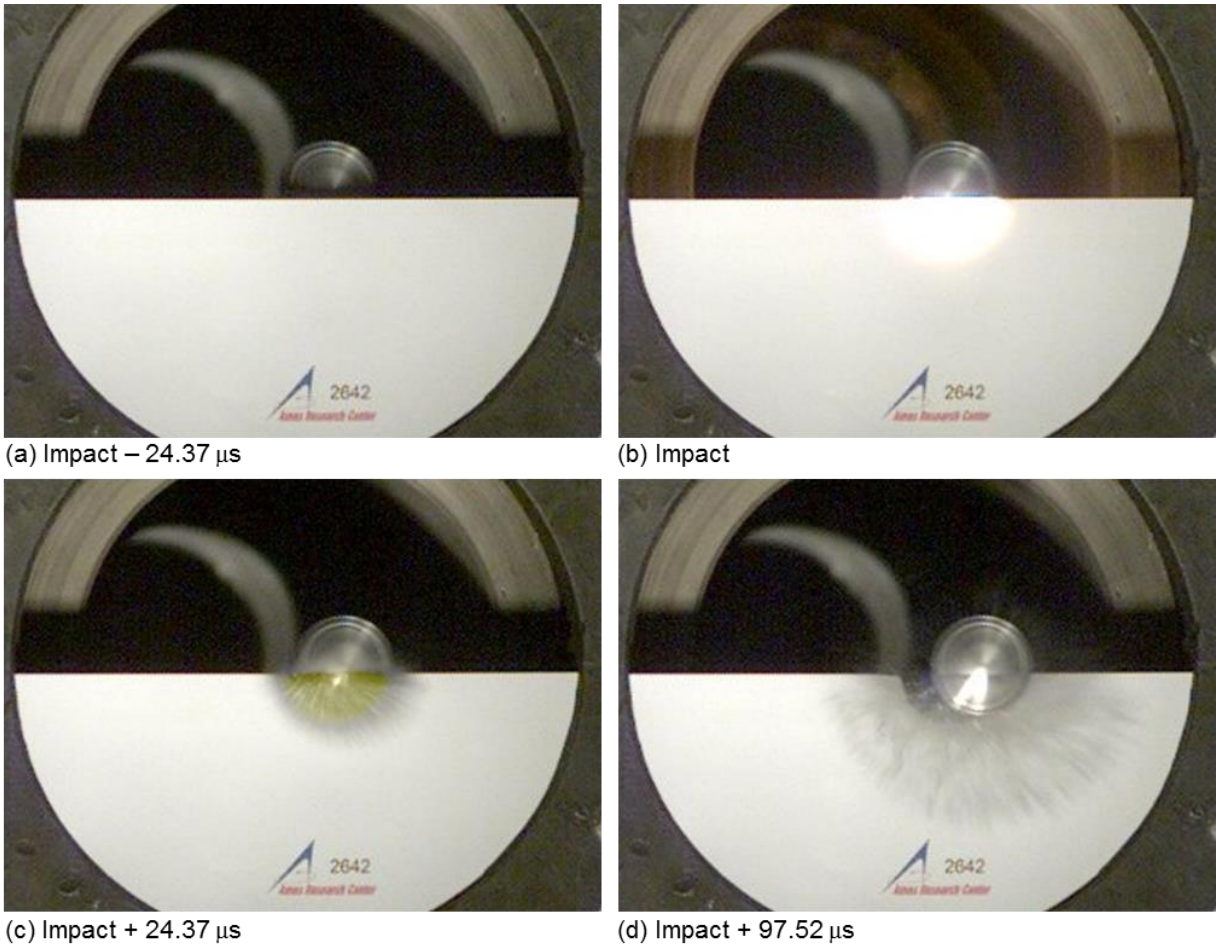

Figure 12. Sequence of images showing impact with a sheet of paper to induce angle oscillations for shot 2642.

2.3. Test Conditions and Model Properties

As mentioned in the Introduction, this test series was primarily concerned with the dynamic stability characteristics of the SFDT vehicle with the SIAD deployed while decelerating to parachute deployment speed. Thirty-seven shots of models in the deployed-SIAD configuration were made, covering average Mach numbers from 2.03 to 3.84, and total angle of attack, σ_{RMS}, values between 0.7° and 20.6°. Tables 3 and 4 list the model properties and test conditions, respectively, for each shot of the deployed-SIAD configuration. Additionally, 12 shots were made of models in the stowed-SIAD configuration to determine the aerodynamic characteristics of the SFDT vehicle after despin and prior to deployment of the SIAD. Eleven of the 12 shots were made at two nominal Mach numbers of 3.15 and 3.50, and RMS angles between 1.6° and 17.2°. One shot was made at a higher Mach number of 3.67 to explore any possible Mach-number dependencies in the coefficients. Tables 5 and 6 list the model properties and test conditions, respectively, for the stowed-SIAD shots. Figure 13 shows the coverage of data in the Mach-σ_{RMS} space for both configurations. Figure 14 shows the test-condition coverage compared with the SFDT trajectory design points presented in Tables 1 and 2: (a) in terms of Mach and Reynolds numbers; and (b) in terms of normalized deceleration and normalized oscillation wavelength. The velocity (Mach and Reynolds numbers) given in Tables 3 and 5 and Figure 14 are the average values in the test section. Full trajectory data are given in Appendix A for shots of the deployed-SIAD models, and in Appendix B for the stowed-SIAD models.

As discussed in the previous section, models and test conditions were designed to the flight trajectory points where dynamic stability was considered most critical, in this case the low Mach number points where either SIAD or parachute deployment will occur. These points are highlighted in the plots in Figure 14. With the exception of normalized deceleration and oscillation wavelength for the stowed-SIAD model, all flight similarity parameters were matched at the trajectory design-to points. As seen from eqn. 3, to increase λ/d for the stowed-SIAD model would require either decreasing ρ_∞ and/or model diameter, both of which would result is a decrease of Reynolds

number, or increasing model mass (moment of inertia), which is not practicable as it would require a material ~1.5 times more dense than tungsten. In this case, it was decided to prioritize Mach and Reynolds number similarity. At trajectory points other than the design-to points it was not possible to exactly match the expected flight parameters while satisfying the facility constraint on λ, as seen in Figure 14; however, no significant Reynolds number effects were expected over the range of expected flight conditions.

Five shots were also made to calibrate the reference wire and timing systems used to measure model trajectories. Spheres were shot through an evacuated test section (thus, only gravitational force acted on the projectile) at velocities spanning the test conditions. These shots provided measurements that were used to precisely determine the station-to-station spacing and identify any biases in the timing data.

The mass, diameter, center of gravity, and moments of inertias all enter into the equations of motion, and errors in the measurements of the mass properties propagate into uncertainties in the aerodynamic coefficients. As a measure of the manufacturing repeatability Tables 3 and 5 give, in addition to the properties of each model, the average properties of each model type and the nominal design, or "as-drawn", properties. The model coordinate system is illustrated in Figure 15 for the stowed-SIAD models. Moments of inertia were measured about the center of gravity (CG), and the axial CG location, x_{CG}/d, given in Tables 3 and 5 represent the distance of the CG from the geometric nose along the x axis. For the deployed-SIAD models, the orientation of the y and z axes was arbitrarily selected since the models were symmetric about the x axis. Due to the cutouts on the base of the stowed-SIAD models, these models had two planes of symmetry, and the orientation of the y-z plane was defined as shown in Figure 15. All models were launched with the z axis oriented up. The models were manufactured to a dimensional tolerance of ±0.00254 cm (±0.001 in), except where noted in Figure 7 and Figure 8. The lengths and diameters were measured to ±0.000254 cm (±0.0001 in).

Model mass was measured with a Mettler Toledo model MS304S digital balance. The instrument specifications quote a repeatability of 0.0001 g, standard deviation. For each model, a minimum of five readings were averaged, and the standard deviation was less than 0.0002 g for all models.

The center of gravity of each model was determined with a modified equal-arm-type analytical balance as described in Ref. 21. The balance was calibrated using accurately machined right circular cylinders with known centers of gravity. This calibration was performed 14 separate times over the duration of this test. Each calibration used the average measurement of two different right circular cylinders: one having a CG location near that of the models, and one having a CG location further from the fulcrum. The standard deviation of all right circular cylinder CG measurements was 0.001 cm (0.0004 in). The maximum variation (minimum value to maximum value) was 0.003 cm (0.0012 in). The axial, x, CG location was measured at least twice for each model and averaged. Each model was rotated 90° about the x-axis between each measurement as a check for any gross asymmetries (none were detected). For approximately 30% of the models the x CG measurement was repeated between 3 and 7 times, and averaged. The maximum variation between repeat measurements was 0.001 cm (0.0004 in). Due to the method of attaching the model to the balance, the CG location was measured relative to the flat base of the model. The CG location relative to the geometric nose was determined by subtracting the CG relative to the base from the thickness of the model, which in turn was determined by subtracting the measurements of the rocket-motor length from the model total length. The resultant uncertainty in the dimensionless CG location relative to the nose, x_{CG}/d, is 0.12% for the deployed-SIAD models, and 0.26% for the stowed-SIAD models. The axial center of gravity location relative to the nose given in Tables 3 and 5 are plotted in Figure 16 versus the total length of each model. Also shown on each plot is the nominal design location. The y- and z-CG location was measured for 17 of the 37 axisymmetric deployed-SIAD models, and for 5 of the 15 stowed-SIAD models. All were within the limit of measurement accuracy of the expected location (0, 0).

Moments of inertia were measured using a Space Electronics, Inc. model XKR1A4 moment of inertia instrument. The instrument operates on the principle of the inverted torsion pendulum. The test object rests on a table attached to precision low friction bearings which constrain the motion of this torsion member to pure rotation. A sensing device produces timing pulses which start and stop a digital period counter (HP 53131A Universal Counter) to determine the period of the oscillating system. The moment of inertia about the axis of the torsion rod is proportional to the square of the period of oscillation. The proportionality constant is determined by measuring the oscillation period of a precision sphere of known mass and diameter. The instrument specifications quotes an accuracy of 0.5%, and 1.5 g-cm^2 as the minimum moment of inertia that can be measured with the rated accuracy. Repeated measurements of reference spheres gave an accuracy of 1.2% for a sphere having a 1.5 g-cm^2 moment of inertia, and less that 0.5% for spheres having a moment of inertia greater than 2.5 g-cm^2. The moments of inertia given in Tables 3 and 5 were measured about axes through the center of gravity of each model. As can be seen from the data in the tables, there was no measureable difference between the moments of inertia about the pitch axis (I_{yy}) and the yaw axis (I_{zz}). The moments of inertia about the pitch axis (I_{yy}) are plotted versus the model mass and versus

the roll moment of inertia (I_{xx}) for the deployed-SIAD models in Figure 17, and for the stowed-SIAD models in Figure 18. Also shown in each plot is a linear trend line through the data, and the as-drawn values. The error bars represent a ±0.5% uncertainty (the quoted instrument accuracy) for all moments except for the stowed-SIAD I_{yy} uncertainty, which is ±1%, based on the reference sphere measurements described above.

Table 3. Mass properties for each of the deployed -SIAD configuration models.

Shot	Diameter, d (cm)	Total Length, l (cm)	Rocket Length, l_r (cm)	Mass (g)	x_{CG}/d (from nose)	y_{CG} (cm)	z_{CG} (cm)	I_{xx} (g-cm^2)	I_{yy} (g-cm^2)	I_{zz} (g-cm^2)
2614	3.551	1.402	0.478	46.6240	0.159	0.000	0.001	56.45	30.76	30.77
2616	3.553	1.385	0.462	46.0246	0.160	-0.002	0.000	55.79	30.39	30.37
2617	3.554	1.385	0.462	45.7386	0.160	0.001	-0.001	55.07	30.00	30.02
2619	3.557	1.382	0.465	45.6833	0.158	0.002	-0.001	55.12	29.92	29.88
2620	3.550	1.388	0.464	45.9724	0.160	0.000	0.002	55.55	30.13	30.14
2621	3.557	1.386	0.463	45.9330	0.160	-0.002	0.001	55.58	30.16	30.20
2622	3.557	1.388	0.469	45.6594	0.159	0.001	-0.002	55.24	29.94	29.90
2623	3.551	1.394	0.467	45.9336	0.161	0.002	0.001	55.59	30.20	30.18
2624	3.555	1.390	0.463	45.7303	0.158	0.000	0.000	55.14	29.82	29.82
2625	3.552	1.395	0.467	45.8586	0.161			55.26	30.14	30.12
2626	3.557	1.389	0.463	45.7758	0.158			55.18	30.07	30.07
2627	3.556	1.390	0.464	45.7465	0.158			55.17	29.89	29.92
2628	3.555	1.390	0.463	45.7575	0.158			55.13	29.94	29.92
2629	3.556	1.390	0.463	45.7799	0.158	0.000	0.000	55.14	29.96	29.93
2630	3.554	1.390	0.464	45.7479	0.159			55.11	30.00	29.97
2631	3.554	1.390	0.463	45.7470	0.158			55.06	30.00	29.99
2632	3.555	1.390	0.464	45.7149	0.159			55.04	29.96	29.97
2635	3.556	1.390	0.464	45.7613	0.159			55.10	29.97	29.97
2636	3.555	1.391	0.465	46.0921	0.160	0.001	0.003	55.59	30.35	30.28
2637	3.553	1.399	0.473	45.9728	0.159	-0.003	-0.002	55.46	30.11	30.10
2638	3.552	1.399	0.471	45.9288	0.160			55.13	30.09	30.10
2639	3.557	1.389	0.464	45.8190	0.159	0.000	0.000	55.14	30.07	30.06
2640	3.554	1.396	0.472	45.8860	0.159			55.10	30.05	30.06
2641	3.556	1.392	0.463	45.8674	0.160			55.13	30.05	30.06
2642	3.555	1.389	0.463	45.7620	0.159			55.06	30.05	30.04
2643	3.558	1.391	0.464	45.8569	0.159			55.09	30.05	30.06
2644	3.556	1.390	0.464	45.8018	0.159	0.001	0.000	55.17	30.01	30.02
2645	3.556	1.390	0.464	45.7445	0.159	0.000	0.000	55.03	30.02	30.01
2646	3.557	1.390	0.464	45.8266	0.158			55.09	30.05	30.05
2647	3.554	1.391	0.464	45.8332	0.159			55.08	30.07	30.07
2648	3.557	1.390	0.464	45.8553	0.159			55.18	30.07	30.07
2649	3.556	1.389	0.464	45.7266	0.159			55.05	30.04	30.05
2650	3.557	1.391	0.464	45.8948	0.158			55.31	30.07	30.06
2651	3.557	1.393	0.464	45.9457	0.159			55.27	30.08	30.08
2652	3.557	1.392	0.464	45.8947	0.158			55.38	30.08	30.08
2653	3.555	1.391	0.464	45.8631	0.159	0.000	0.001	55.27	30.01	30.01
2654	3.556	1.388	0.464	45.7526	0.158	0.000	0.000	55.15	29.92	29.94
mean	**3.555**	**1.391**	**0.465**	**45.8517**	**0.159**	**0.000**	**0.000**	**55.25**	**30.07**	**30.06**
st dev	**0.0020**	**0.0040**	**0.0033**	**0.1640**	**0.0007**	**0.001**	**0.001**	**0.28**	**0.16**	**0.16**
% of mean	**0.06%**	**0.28%**	**0.71%**	**0.36%**	**0.43%**			**0.51%**	**0.56%**	**0.56%**
as drawn	**3.556**	**1.389**	**0.465**	**46.2443**	**0.1577**	**0.000**	**0.000**	**55.6770**	**30.2329**	**30.2329**
% diff	**-0.03%**	**0.09%**	**0.05%**	**-0.85%**	**0.81%**			**-0.76%**	**-0.55%**	**-0.56%**

Table 4. Test conditions for each shot of the deployed-SIAD configuration models.

Shot	$\bar{M}_\infty$	$\overline{Re}_d$ (x 10^{-6})	$\bar{V}_\infty$ (m/s)	P_∞ (Torr)	T_∞ (K)	ρ_∞ (kg/m^3)	σ_{RMS} (deg)	$\Delta u/u\|_\lambda$	λ/d
2614	2.33	0.407	800	166.0	293.3	0.263	1.1	0.041	292
2616	2.56	0.441	878	164.2	293.8	0.260	1.5	0.043	308
2617	2.97	0.499	1023	160.5	294.4	0.253	1.7	0.039	292
2619	2.06	0.365	708	169.0	294.1	0.267	1.7	0.046	317
2620	2.39	0.425	818	169.4	292.8	0.269	5.2	0.043	300
2621	2.11	0.376	723	169.4	293.1	0.268	7.1	0.047	326
2622	2.13	0.380	732	169.4	293.3	0.268	2.5	0.046	317
2623	2.03	0.362	697	169.4	292.8	0.269	12.9	0.047	334
2624	2.08	0.369	715	169.4	294.2	0.267	1.9	0.045	309
2625	2.36	0.420	809	169.4	293.1	0.268	1.5	0.037	257
2626	2.84	0.484	976	162.4	294.2	0.256	1.0	0.040	300
2627	3.47	0.564	1190	155.0	293.7	0.245	0.9	0.037	292
2628	2.90	0.495	995	162.4	293.3	0.257	5.3	0.040	292
2629	2.42	0.426	832	167.7	293.9	0.265	3.2	0.043	300
2630	2.26	0.399	776	167.7	293.1	0.266	15.8	0.044	325
2631	2.42	0.428	830	167.7	292.7	0.266	0.7	0.043	300
2632	2.34	0.399	803	162.7	293.7	0.257	14.7	0.044	334
2635	2.76	0.472	947	163.1	294.0	0.258	18.4	0.042	334
2636	3.39	0.552	1165	155.0	293.7	0.245	20.5	0.039	343
2637	3.45	0.559	1184	155.0	294.4	0.245	3.5	0.037	291
2638	3.78	0.590	1300	149.0	294.2	0.235	8.1	0.037	309
2639	2.64	0.454	907	164.2	294.0	0.259	3.0	0.040	291
2640	3.24	0.536	1115	158.0	293.8	0.250	4.1	0.038	292
2641	2.37	0.418	813	166.5	291.9	0.265	9.7	0.043	309
2642	2.91	0.495	999	161.5	293.2	0.256	8.8	0.041	308
2643	3.31	0.538	1141	155.0	294.3	0.245	6.0	0.038	299
2644	2.64	0.449	905	161.5	293.0	0.256	19.7	0.041	334
2645	2.27	0.404	779	169.4	293.7	0.268	20.6	0.044	334
2646	2.47	0.421	848	163.0	294.3	0.257	12.3	0.042	317
2647	2.88	0.490	992	163.0	295.1	0.257	10.7	0.042	318
2648	3.49	0.573	1197	155.0	292.2	0.246	11.1	0.040	317
2649	3.17	0.526	1088	158.0	293.6	0.250	15.7	0.040	325
2650	2.67	0.458	919	163.0	293.8	0.258	14.2	0.043	326
2651	3.84	0.611	1323	152.0	294.5	0.240	16.0	0.040	343
2652	3.62	0.564	1248	149.0	294.9	0.235	1.3	0.037	301
2653	3.10	0.513	1071	158.0	294.4	0.249	0.7	0.039	292
2654	2.74	0.473	936	163.0	291.5	0.260	5.8	0.040	292

Table 5. Mass properties for each of the stowed-SIAD configuration models.

Shot	Diameter, d (cm)	Total Length, l (cm)	Rocket Length, l_r (cm)	Mass (g)	x_{CG}/d (from nose)	y_{CG} (cm)	z_{CG} (cm)	I_{xx} (g-cm^2)	I_{yy} (g-cm^2)	I_{zz} (g-cm^2)
2659	1.698	0.848	0.292	12.5957	0.196	0.000	0.000	3.66	2.10	2.10
2660	1.699	0.849	0.294	12.5975	0.196			3.66	2.09	2.09
2661	1.698	0.849	0.292	12.5992	0.196			3.66	2.10	2.08
2662	1.699	0.849	0.292	12.6658	0.196			3.70	2.12	2.12
2663	1.699	0.848	0.292	12.6215	0.196	0.000	0.000	3.65	2.07	2.09
2664	1.698	0.847	0.293	12.5345	0.196	-0.001	-0.001	3.63	2.08	2.07
2665	1.698	0.847	0.292	12.5514	0.196			3.62	2.12	2.11
2666	1.698	0.848	0.293	12.6776	0.195	0.000	0.000	3.72	2.12	2.13
2667	1.698	0.848	0.293	12.5656	0.196			3.63	2.12	2.12
2668	1.698	0.848	0.292	12.5822	0.196			3.70	2.11	2.14
2669	1.697	0.848	0.292	12.6075	0.196	0.000	0.000	3.68	2.12	2.13
2670	1.698	0.849	0.292	12.5628	0.197			3.66	2.12	2.13
mean	**1.698**	**0.848**	**0.293**	**12.5968**	**0.196**	**0.000**	**0.000**	**3.67**	**2.11**	**2.11**
st dev	**0.0004**	**0.0007**	**0.0005**	**0.0430**	**0.0003**	**0.0004**	**0.0004**	**0.03**	**0.02**	**0.02**
% of mean	**0.02%**	**0.08%**	**0.16%**	**0.34%**	**0.17%**			**0.82%**	**0.81%**	**1.04%**
as drawn	**1.699**	**0.848**	**0.292**	**12.8152**	**0.1973**	**0.000**	**0.000**	**3.7513**	**2.1271**	**2.1301**
% diff	**-0.05%**	**-0.03%**	**0.16%**	**-1.70%**	**-0.63%**			**-2.29%**	**-1.01%**	**-1.06%**

Table 6. Test conditions for each shot of the stowed-SIAD configuration models.

Shot	$\bar{M}_\infty$	$\overline{Re}_d$ (x 10^{-6})	$\bar{V}_\infty$ (m/s)	P_∞ (Torr)	T_∞ (K)	ρ_∞ (kg/m^3)	σ_{RMS} (deg)	$\Delta u/u\|_\lambda$	λ/d
2659	3.46	0.341	1187	195.0	292.3	0.310	1.9	0.044	628
2660	3.44	0.338	1181	195.0	293.0	0.309	7.6	0.043	626
2661	3.46	0.339	1190	195.0	293.9	0.308	1.6	0.042	611
2662	3.51	0.344	1202	195.0	292.8	0.309	10.4	0.042	627
2663	3.45	0.338	1188	195.0	293.5	0.309	4.9	0.043	626
2664	3.48	0.343	1192	195.0	292.0	0.310	13.9	0.041	609
2665	3.20	0.312	1103	195.0	294.6	0.307	17.2	0.040	627
2666	3.17	0.308	1092	195.0	295.1	0.307	2.0	0.043	628
2667	3.18	0.310	1095	195.0	294.5	0.308	11.4	0.042	627
2668	3.18	0.310	1094	195.0	294.7	0.307	3.0	0.043	627
2669	3.18	0.310	1095	195.0	294.2	0.308	5.8	0.043	627
2670	3.67	0.357	1265	194.8	295.2	0.307	16.2	0.040	627

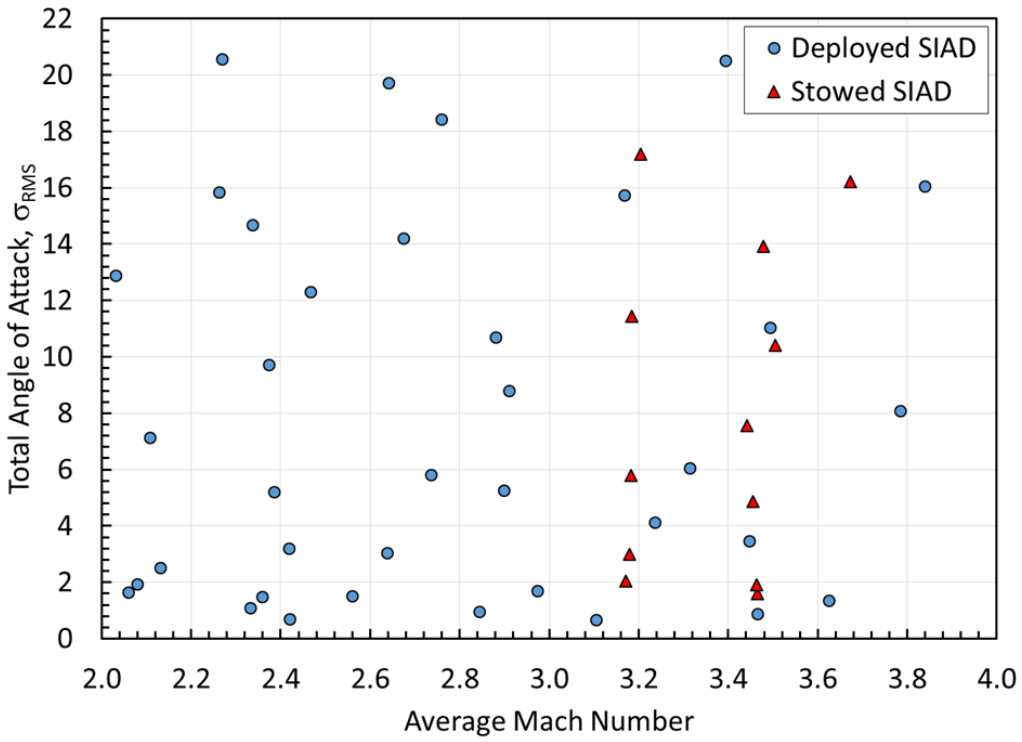

Figure 13. Distribution of test conditions in terms of Mach number and total angle of attack.

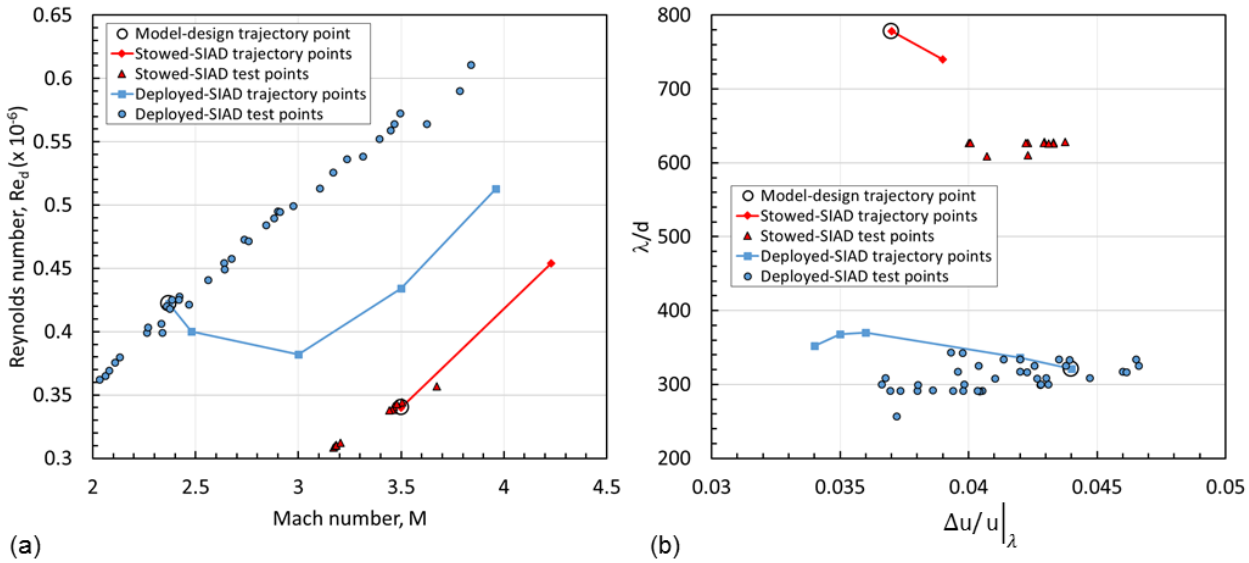

Figure 14. Distribution of test conditions compared with the SFDT trajectory design points: (a) in terms of Mach and Reynolds numbers; (b) in terms of normalized deceleration and normalized oscillation wavelength.

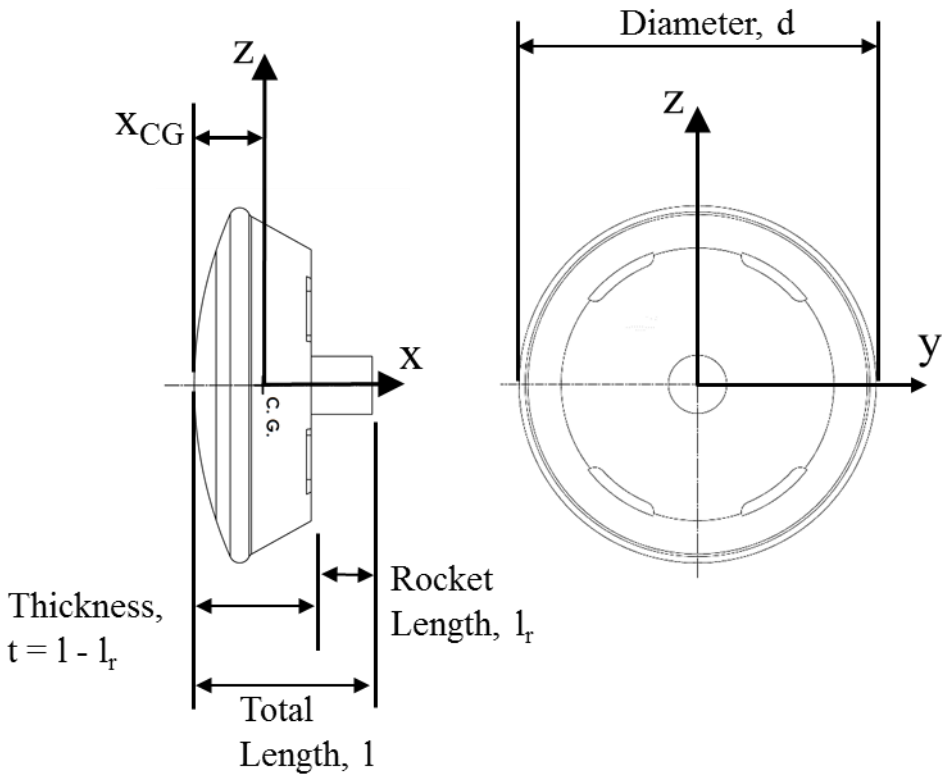

Figure 15. Coordinate system orientation for the stowed-SIAD models.

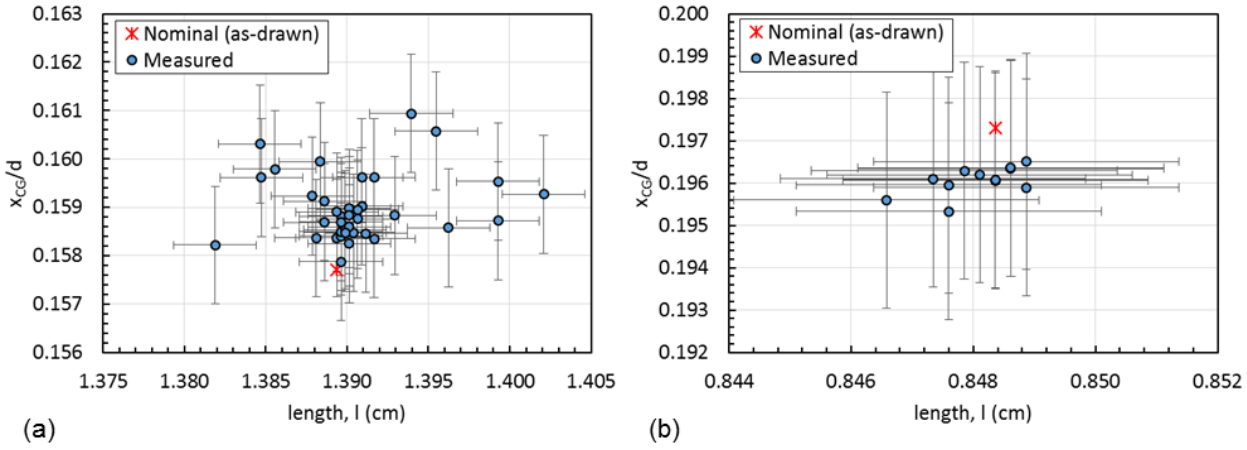

Figure 16. Center of gravity location relative to the model nose vs. model total length. (a) Deployed-SIAD models, (b) Stowed-SIAD models.

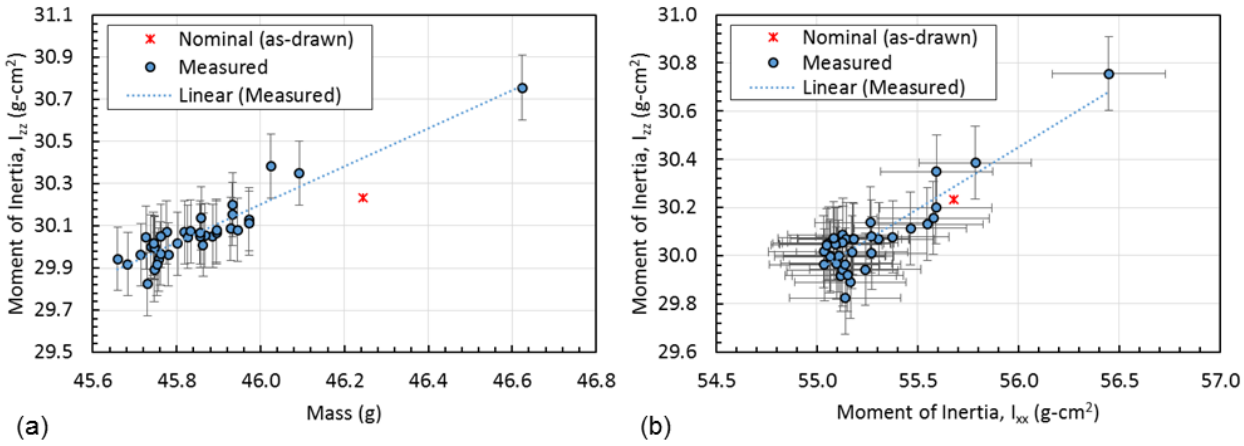

Figure 17. Moments of inertia about the center of gravity of the deployed-SIAD models. (a) Pitch moment of inertia vs. model mass; (b) Pitch moment of inertia vs. the roll moment of inertia.

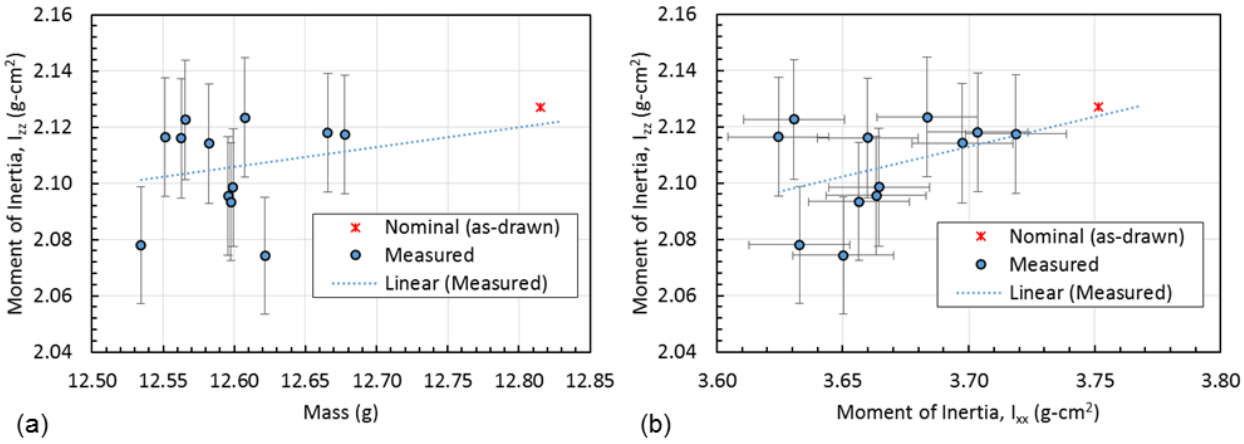

Figure 18. Moments of inertia about the center of gravity of the stowed-SIAD models. (a) Pitch moment of inertia vs. model mass; (b) Pitch moment of inertia vs. the roll moment of inertia.

Data Acquisition and Analysis

3.1. Test Data

The data acquired for each shot include horizontal and vertical shadowgraph images at the 16 measurement stations, and the time at which each image pair was captured. Also recorded are the temperature and pressure of the test gas. Figure 19 shows an example orthogonal image pair of a deployed-SIAD model. The vertical and horizontal lines in the images are part of the fiducial system described in detail in Ref. 22. The wires are located outside the test section, with a duplicate set on each side of the test section. The catenary and taut wires run the full length of the test section. At each station, the position and orientation of the model was measured relative to the fiducial wires, as described in the next section. The majority of the images were recorded on film, specifically, 8" x 10" Ilford HP5 Plus ISO 400 black and white film, which was push-processed to ISO 3200. Exposure times were approximately 40 ns using Kerr cell electro-optical shutters described in Ref. 23. Five of the 32 images (stations 4 side and top, and the top view at stations 8, 10, and 13) were recorded using gated digital cameras (Princeton Instruments PI-MAX 1024x1024 ICCD cameras), gated at 5 ns. The film images were digitized using a commercially-available flat-bed scanner with the capability of scanning transparencies. Scan resolution was selected to give approximately 200 pixels on the diameter of the model image. This was achieved for the larger deployed-SIAD models with a scan resolution of 300 dots-per-inch (dpi), and for the smaller stowed-SIAD models with a scan resolution of 600 dpi. At 600 dpi, the digitized images were approaching the film grain resolution.

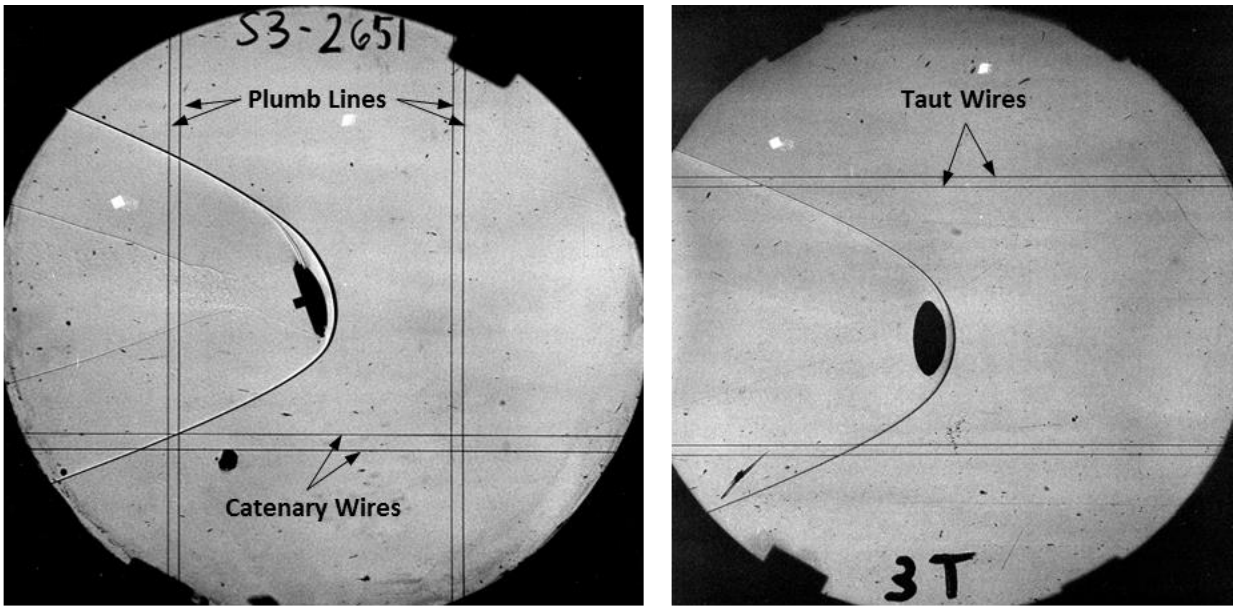

Figure 19. Shadowgraph image pair of a deployed-SIAD model taken at range station 3 for shot 2651. (a) Horizontal (side) view; (b) Vertical (top) view.

3.2. Data Analysis

The instantaneous position and orientation of the model was measured using a version of the film reading program CADRA1 [24]. With CADRA1, the position and orientation of models are identified using the centroid method (a weighted, least-squares method). All the pixels identified as belonging to the model are used, and edge pixels are weighted less than center pixels; the weighting is based on the pixel's gray-scale value (% of pixel covered by the model). In order to transform the centroid measurements to CG locations, the nose and tail locations, relative to the centroid, are also found. During the transformation of film-reading coordinates to facility coordinates, the tail and nose locations, along with dimensional information about the model, provide the necessary information for transferring the centroid measurements to CG location. The output of CADRA1 is the trajectory measured in facility coordinates defined by the fiducial wires shown in Figure 19. For each station the file contains the time of arrival at that station, the x, y, z location of the CG of the model relative to the facility origin, and the pitch, yaw, roll (if measured) attitude of the model. Roll angle was not measured in the tests reported here. The measured pitch (θ) and yaw (ψ) angles are relative to the facility coordinate system axes, and therefore are slightly different from α and β, the pitch and yaw angles relative to the wind line. The CADRA1 trajectory measurements, along with data on the test conditions, the model dimensions, and the model mass properties, are input to the parameter-identification software CADRA2. CADRA2 models the aerodynamic forces, identifies the aerodynamic coefficients by fitting calculated trajectories to the experimental data, and characterizes the measurement biases and aerodynamic modeling errors. The details of the algorithms CADRA2 employs for identifying the unknown aerodynamic parameters are given in Refs. 24-26.

Systematic errors in the position and orientation of a model occur when the recording system does not conform to the geometric relationships assumed for it. Such errors are introduced by optical refraction, misalignment of the photographic and fiducial wires, and timing errors. Systematic errors in the position and timing were determined from five calibration shots of spherical projectiles fired through an evacuated test section (vacuum) by comparing the measured trajectories to the expected parabolic trajectories. Systematic errors in the orientation measurements were determined from the actual deployed-SIAD test data by examining the residual errors at each station between the measured position and orientation and the corresponding values from the best curve-fit, 6-DOF trajectory determined using CADRA2.

After removing the identified biases, the errors are expected to be at a minimum when the base of the model is parallel to the fiducial line used as the 0 degree reference. The calculated biases in the location measurements were

compared to those obtained from the calibration shots and were in relatively good agreement. Identifying and removing the biases improved the trajectory fits, particularly for the down range position measurements (x) and for the angle measurements in the horizontal plane (ψ).

The uncertainties in the film-reading measurements are functions of the number of pixels, distortions due to shocks, and model shape. The film-reading uncertainties in the angle measurements are largest as the aspect ratio of the model approaches one, as is often the case for blunt entry vehicles. CADRA1 has been updated to reduce uncertainties in the angle measurements by estimating the orientation of the model image from a comparison of the upper and lower back edges of the image and correcting the front surface if distorted. For the deployed-SIAD models, uncertainty in θ and ψ are $\pm 0.1^o$ and $\pm 0.7^o$, respectively. These values are also comparable to the RMS of the biases. The uncertainties for the angle measurements of the stowed configuration were larger, by about 50%, than those of the deployed model. Although the stowed model was smaller, the number of pixels in the digitized images was increased to keep the pixels per model approximately constant. However, the stowed configuration had a smaller flat region on the back surface than the deployed configuration, reducing the accuracy of the methods for estimating the angle and for reducing optical distortions. Positional uncertainties, and the RMS of the measured biases, were less than ±1 mm for both model configurations.

The digitized images were read and reduced to trajectory coordinates. For each shot, the measured values of the models' down range (x), transverse (y) and vertical (z) trajectory coordinates and angles relative to the facility horizontal (θ) and vertical (ψ) planes are tabulated as functions of time (t) in Appendix A for the deployed-SIAD configuration, and in Appendix B for the stowed-SIAD configuration. Plots of these values are also given in the appendices. The down-range positions are plotted as a distance decrement, $(x\text{-}x_0) - V_0(t\text{-}t_0)$, where the subscript 0 refers to the value at the first measurement station. The distance decrement is the difference between the actual position and the position at the same time of a projectile traveling V_0 but experiencing no drag.

3.3. Analysis Approach

The aerodynamic coefficients are found by fitting 6-DOF simulated trajectories to the trajectory measurements (positions and orientations); the fits are obtained using a quasi-linear adaptation to standard least squares or minimum variance methods [25]. To illustrate this approach, consider a simple, 1-DOF case for the angle of attack. The first step is to form the sum of the squares of the residuals, $\mathrm{SSR} = \sum_{i=1}^{n}(\alpha_{\mathrm{exp}_i} - \alpha_{\mathrm{calc}_i})^2$.

The subscripts exp_i and calc_i refer to the experimental and calculated values of the angle of attack at the i^{th} station and the summation is over all n stations. The value of α_{calc} is a function of the unknown aerodynamic coefficients and the initial conditions, and it can be written as $\alpha_{calc} = \alpha_{calc}(C_1, C_2, \ldots, C_r)$.

Expanding the unknowns and the angle of attack in terms of an initial estimate and correction,

$$C_j = C_j^0 + \Delta C_j \quad \text{and} \quad \alpha_{\mathrm{calc}_i} = \alpha^0_{\mathrm{calc}_i} + \sum_{j=1}^{r} \frac{\partial \alpha^0_{\mathrm{calc}_i}}{\partial C_j} \Delta C_j$$

and substituting the expansions into the SSR gives

$$\mathrm{SSR} = \sum_{i=1}^{n} \left(\alpha_{\mathrm{exp}_i} - \alpha^0_{\mathrm{calc}_i} + \sum_{j=1}^{r} \frac{\partial \alpha^0_{\mathrm{calc}_i}}{\partial C_j} \Delta C_j \right)^2$$

Differentiating by the correction to the k^{th} unknown, ΔC_k,

$$\frac{\partial \mathrm{SSR}}{\partial \Delta C_k} = 2 \sum_{i=1}^{n} \left(\alpha_{\mathrm{exp}_i} - \alpha^0_{\mathrm{calc}_i} + \sum_{j=1}^{r} \frac{\partial \alpha^0_{\mathrm{calc}_i}}{\partial C_j} \Delta C_j \right) \frac{\partial \alpha^0_{\mathrm{calc}_i}}{\partial C_k}$$

and setting the result equal to zero and rearranging,

$$\sum_{i=1}^{n} \sum_{j=1}^{r} \frac{\partial \alpha^0_{\mathrm{calc}_i}}{\partial C_j} \frac{\partial \alpha^0_{\mathrm{calc}_i}}{\partial C_k} \Delta C_j = \sum_{i=1}^{n} \left(\alpha_{\mathrm{exp}_i} - \alpha^0_{\mathrm{calc}_i} \right) \frac{\partial \alpha^0_{\mathrm{calc}_i}}{\partial C_k}$$

gives r equations for r unknowns ΔC_k. This can be written in matrix form as $\bar{A}\underline{\Delta C} = \underline{R}$; the corrections vector is given by $\underline{\Delta C} = \underline{A}^{-1}\underline{R}$ where the elements of the A matrix and the column vector R are:

$$A_{j,k} = \sum_{i=1}^{n} \frac{\partial \alpha^0_{\mathrm{calc}_i}}{\partial C_j} \frac{\partial \alpha^0_{\mathrm{calc}_i}}{\partial C_k} \quad \text{and} \quad R_k = \sum_{i=1}^{n} \left(\alpha_{\mathrm{exp}_i} - \alpha^0_{\mathrm{calc}_i} \right) \frac{\partial \alpha^0_{\mathrm{calc}_i}}{\partial C_k}$$

To solve for the corrections, the partial derivatives with respect to the r unknowns must be calculated. Generally, there are no closed form solutions for these derivatives; instead, they are specified by partial differential

equations derived from the 6-DOF equations of motion. For example, consider a 1-DOF oscillatory equation for the angle of attack with a nonlinear dynamics stability coefficient and a nonlinear pitching moment coefficient

$$\frac{\partial^2\alpha}{\partial t^2} + f(C_{m+1}, C_2, \ldots, C_{r-2}, \alpha)\frac{\partial\alpha}{\partial t} + g(C_1, C_2, \ldots, C_m, \alpha) = 0$$

with initial conditions $\alpha(0) = C_{r\text{-}1}$ and $\dot{\alpha}(0) = C_r$. Differentiating with respect to the aerodynamic terms and two initial conditions gives

$$\frac{\partial^2 P_k}{\partial t^2} + f\frac{\partial P_k}{\partial t} + \left(\frac{\partial f}{\partial\alpha}\frac{\partial\alpha}{\partial t} + \frac{\partial g}{\partial\alpha}\right)P_k = -\frac{\partial f}{\partial C_k}\frac{\partial\alpha}{\partial t} - \frac{\partial g}{\partial C_k}$$

where $P_k = \partial\alpha/\partial C_k$. The initial conditions for this parametric differential equation are $P_k(0) = 0$ and $\partial P_k/\partial t(0) = 1$. During the least-squares process, the parametric equations are integrated simultaneously along with the original dynamics equation. The corrections, ΔC_j, are then calculated, and the coefficients updated: $C_j^1 = C_j^0 + \Delta C_j$. This process is repeated until the corrections meet a preset convergence criterion.

This process also yields a matrix for estimating the errors for each of the coefficients and for the initial conditions, which is shown by starting with the equation for the corrections to C_k, $\underline{\Delta C} = \underline{A}^{-1}\underline{R}$. Multiplying times the transpose gives

$$\underline{\Delta C}\left(\underline{\Delta C}\right)^T = \overline{A^{-1}}\,\underline{R}\left(\overline{A^{-1}}\,\underline{R}\right)^T \quad \text{or} \quad \overline{\underline{\Delta C}\left(\underline{\Delta C}\right)^T} = \overline{\underline{R}\left(\underline{R}\right)^T}.$$

If the errors in the angle of attack are statistically independent, the estimated errors for the C_k are given by:

$$\overline{\underline{\Delta C}\left(\underline{\Delta C}\right)^T} = \overline{Cov(C)} = \overline{A^{-1}}\,Var(\alpha).$$

One needs to keep in mind that these are the errors for the coefficients of the selected math model or function used in the analysis for describing the aerodynamic coefficients. They do not include errors that result from inadequacies of the math model itself.

When more than one type of variable is treated, such as angles and distances, this least squares method is replaced by a minimum variance approach, for example,

$$SSR = \sum_{i=1}^{n}\left[\frac{\left(\alpha_{exp_i} - \alpha_{calc_i}\right)^2}{SD(\alpha)^2} + \frac{\left(x_{exp_i} - x_{calc_i}\right)^2}{SD(x)^2}\right]$$

where $SD(\alpha)$ and $SD(x)$ are the expected errors in the angle and down range measurements. Without the additional weighting functions, one of the variables may drive the solutions and poor fits will be obtained for the other terms.

3.4. Aerodynamic Modeling

Specifying the functional form of the aerodynamic coefficients is an important step in the estimation of the aerodynamic coefficients. For a single data set with two or three cycles of motion, the agreement of the calculated and measured trajectory values can be insensitive to the functional form used to describe the coefficients. Quasi-linear fits, that is, fits to the trajectory data assuming linear aerodynamics, are generally very good for a single data set. An unlimited number of aerodynamic functions can also provide good fits as long as the "average" over a cycle is correct.

The selection of the functional forms for the aerodynamic coefficients is guided by the quasi-linear aerodynamics obtained from multiple data sets covering the Mach–σ regime of interest. An example of the coefficients calculated using quasi-linear aerodynamics is illustrated in Figure 20 for the drag coefficient (C_D). It is evident from these plots that there is a dependence on Mach number and angle of attack, and the function describing the drag coefficient should include these terms. From these plots, it appears that polynomials in the Mach number and angle of attack could be used to describe the dependencies.

The test of the non-linear functions selected to describe the aerodynamic coefficients is the comparison of the calculated and measured trajectory values over the range of Mach numbers and angles of attack covered by the test series. The fits should be nearly as good as the quasi-linear fits. The residual errors for the trajectory fits using the non-linear coefficients are generally a little larger than those for the single data set quasi-linear fits. It is presumed this is the result of small differences in the models or errors in measuring the diameter, pressure, temperature, etc. For example, for two test runs with the same RMS angles of attack and Mach number, the drag coefficient can be slightly different.

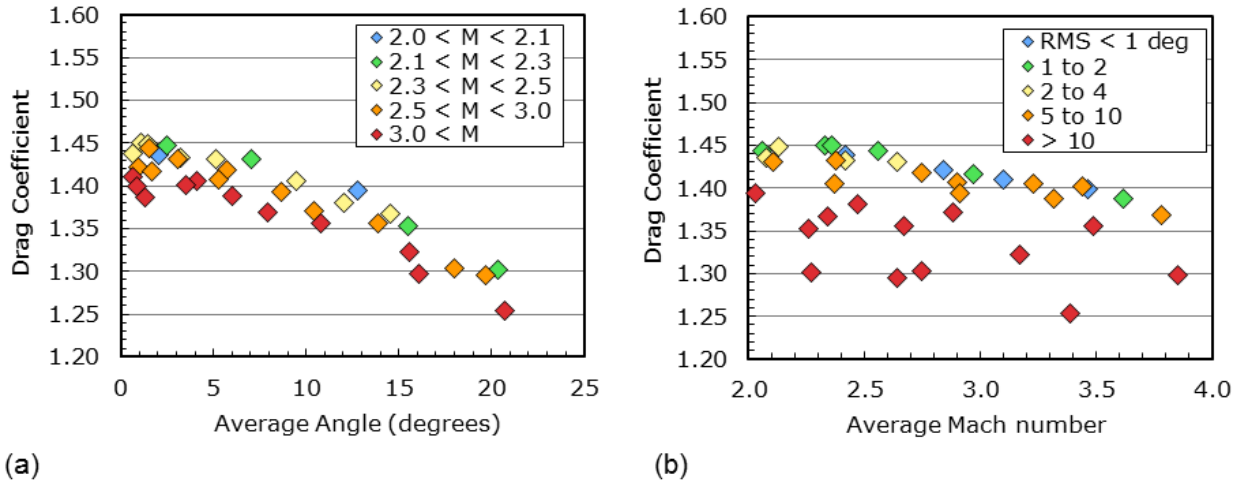

Figure 20. Quasi-linear fits for drag coefficient: (a) vs. RMS angle; (b) vs. average Mach number.

4. Results

The quasi-linear aerodynamic forces and moments, the nonlinear functions developed from the quasi-linear results, the processes for identifying the function parameters, and the results are described in the following sections, first for the deployed configuration and then for the stowed.

The simulated and measured trajectories for the deployed- and stowed-SIAD models are plotted in Appendices A and B, respectively, along with the measured values.

4.1. Drag Coefficient (Deployed SIAD)

The quasi-linear results for C_D of the deployed-SIAD models (Figure 21a) exhibited variations in Mach number and angle of attack, which were modeled using simple polynomials in M and sin σ.

$$C_D = \left[C_{D_0} + C_{D_{(M-M_{ref})}}(M - M_{ref}) + C_{D_{(M-M_{ref})^2}}(M - M_{ref})^2\right]\cos\sigma + \left[C_{D_{\sigma^2}} + C_{D_{\sigma^2,(M-M_{ref})}}(M - M_{ref}) + C_{D_{\sigma^2,(M-M_{ref})^2}}(M - M_{ref})^2\right]\sin^2\sigma + \left[C_{D_{\sigma^4}} + C_{D_{\sigma^4,(M-M_{ref})}}(M - M_{ref}) + C_{D_{\sigma^4,(M-M_{ref})^2}}(M - M_{ref})^2\right]\sin^4\sigma$$

The Mach variation at small angles was identified by first using the shots with $2.05 \le M \le 2.11$ to tie down the value of the drag coefficient at the low end of the Mach regime. Then, the ten data sets (or, test shots) with the smallest σ_{RMS} were used to define the Mach variation at zero angle of attack.

The variations with M and σ at moderate to large amplitude were identified using multiple data sets with moderate to large σ_{RMS}. The parameter-identification software, CADRA2, is currently limited to reducing 10 data sets simultaneously, and it was not possible to simultaneously fit all the data. Therefore, three different groups of moderate to large angle test runs were used to estimate the moderate to large angle behavior of the drag coefficient. There were minimal variations in the estimated drag coefficients for the three groups; the largest variations were at the extremes of the test regime (M = 2 and M = 3.8). The bracketed Mach terms multiplying $\sin^4\sigma$ resulted in unrealistic variations and did not improve the fits appreciably. Therefore, the associated parameters were set equal to zero. The nonlinear drag coefficient is plotted in Figure 21b. The estimated parameter values and errors* for the SFDT deployed-SIAD drag coefficient are given in the table below.

---

* *Note, the estimated errors for the aerodynamic coefficients are functions of the Mach number, total angle of attack, pitching rate, and the covariance matrix, which is calculated during the least-squares process. The reported error estimates for the individual terms in the coefficient expansions are the square roots of the variance terms - the diagonal terms of the covariance matrix. The best estimate of the errors should also include the off diagonal terms. These terms are typically negative and, when included in the formulation of the error estimate, reduce the total estimated error. The minimum error typically occurs at the Mach number and angle of attack where the data is concentrated.*

C_{D_0}	=	1.449467	±	0.000727
$C_{D_{(M-M_{ref})}}$	=	-0.012836	±	0.002102
$C_{D_{(M-M_{ref})^2}}$	=	-0.018142	±	0.001638
$C_{D_{\sigma^2}}$	=	-0.436271	±	0.015453
$C_{D_{\sigma^2,(M-M_{ref})}}$	=	-0.460018	±	0.028559
$C_{D_{\sigma^2,(M-M_{ref})^2}}$	=	0.306234	±	0.016133
$C_{D_{\sigma^4}}$	=	0.421109	±	0.096385
$C_{D_{\sigma^4,(M-M_{ref})}}$	=	0	±	0
$C_{D_{\sigma^4,(M-M_{ref})^2}}$	=	0	±	0
M_{ref}	=	2.06		

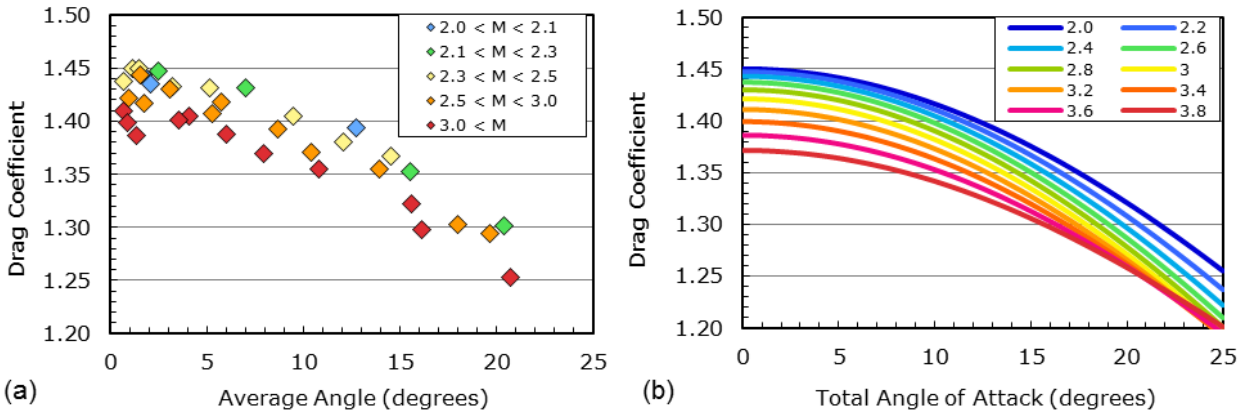

Figure 21. Drag coefficient for the deployed-SIAD configuration: (a) quasi-linear; (b) non-linear.

4.2. Lift Coefficient (Deployed SIAD)

The quasi-linear results for the lift coefficient (C_L) in the deployed-SIAD case (Figure 22a) exhibited significant scatter at small angles. The lift is estimated from the swerve motion, and at small angles the measurement errors are large compared to the swerve due to lift. In addition, any errors in translating the centroid measurements to the model CG location may add errors that are proportional to the angle, thus introducing additional uncertainties to C_L.

At moderate to large oscillation amplitudes, the quasi-linear lift exhibited some possible variations with M and σ. The lift coefficient was modeled using:

$$C_L = \left\{ C_{L_\sigma} + C_{L_{\sigma,(M-M_{ref})}} \left(M - M_{ref}\right) + \left[C_{L_{\sigma^3}} + C_{L_{\sigma^3,(M-M_{ref})}} \left(M - M_{ref}\right) \right] \sin^2\sigma \right\} \sin\sigma$$

To reduce the estimated errors, the Mach variations at small angles were identified using data sets with σ_{RMS} of about 2 degrees, and therefore slightly larger swerve due to lift.

The Mach and σ variations in C_L at moderate to large σ_{RMS} were identified similarly to how they were for C_D. Three different groups of test shots with moderate to large σ_{RMS} were used to estimate the moderate to large angle behavior, and there were minimal variations in the estimated C_L. The largest variations were at the extremes of the test regime, M = 2 and M = 3.8. The nonlinear lift coefficient is plotted in Figure 22b; the corresponding parameters, with errors*, are:

$$C_{L_\sigma} = -1.162136 \pm 0.025146$$

$$C_{L_{\sigma,(M-Mref)}} = 0.130873 \pm 0.059953$$

$$C_{L_{\sigma^3}} = 0.168101 \pm 0.045305$$

$$C_{L_{\sigma^3,(M-Mref)}} = -0.442989 \pm 0.07691$$

$$M_{ref} = 2.06$$

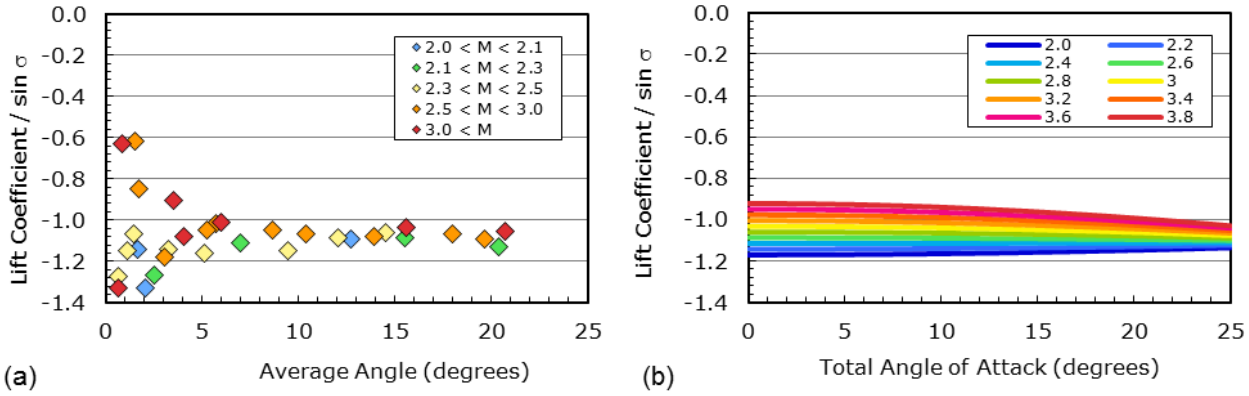

Figure 22. Lift coefficient for the deployed-SIAD configuration: (a) quasi-linear; (b) non-linear.

4.3. Pitching Moment Coefficient (Deployed SIAD)

The quasi-linear results (Figure 23a) for the pitching moment coefficient (C_m) exhibited variations in Mach number and angle of attack, which were modeled as:

$$C_m = \left\{\left[C_{m_{\sigma,1}} f + C_{m_{\sigma,2}}(1-f)\right]g + (C^{**}_{m_{\sigma,1}} + C^{**}_{m_{\sigma,2}} f)(1-g)\right\} \sin\sigma$$

where $$f = \exp\left[C^{*}_{m_{(M\text{-}M_{ref})}}(M\text{-}M_{ref})\right]$$

and $$g = \exp\left[C^{**}_{m_{\sigma^2}} \sin^2\sigma\right]$$

The Mach variation at small angles was identified by first using the shots with $2.05 \le M \le 2.11$ to tie down the value of C_m for the low end of the Mach number space. Then, the ten test shots with the smallest σ_{RMS} were used to define the Mach variation at zero angle of attack.

As with drag and lift, the Mach and angle variations in C_m at moderate to large σ_{RMS} were identified using three different groups of ten moderate-to-large amplitude data sets. The differences between the resulting estimated coefficients were minimal, being largest at M = 2 and M = 3.8. The estimated nonlinear C_m is shown in Figure 23b; the associated parameters with errors* are:

$$C_{m_{\sigma,1}} = -0.201444 \pm 0.003155$$

$$C_{m_{\sigma,2}} = -0.261817 \pm 0.006220$$

$$C^{*}_{m_{(M-M_{ref})}} = -1.986651 \pm 0.477588$$

$$C^{**}_{m_{\sigma,1}} = -0.165781 \pm 0.000696$$

$$C^{**}_{m_{\sigma,2}} = -0.0132 \pm 0.001262$$

$$C^{**}_{m_{\sigma^2}} = -8.41941 \pm 0.01740$$

$$M_{ref} = 2.06$$

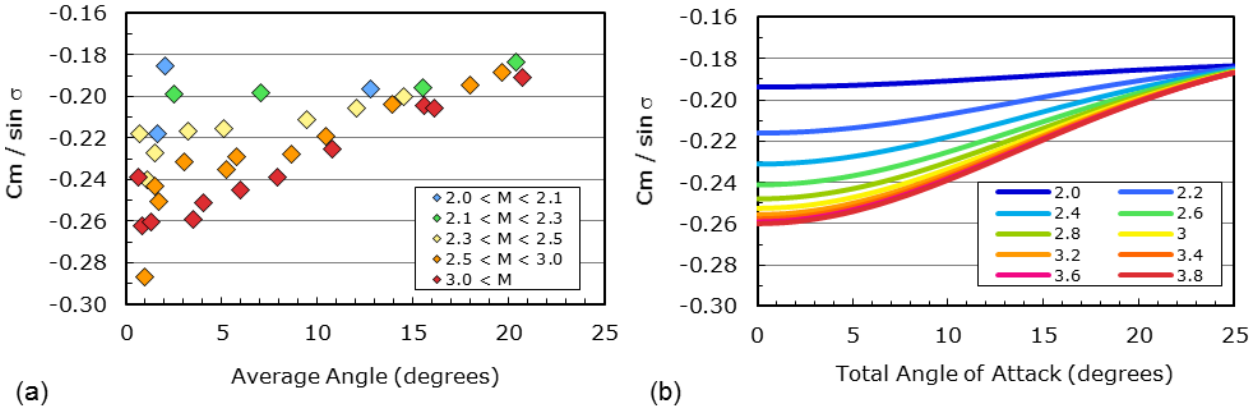

Figure 23. Pitching moment coefficient for the deployed-SIAD configuration: (a) quasi-linear; (b) non-linear.

4.4. Pitch Damping Coefficient (Deployed SIAD)

The quasi-linear results for the pitch-damping coefficient (C_{m_q}), in Figure 24a, show large variations with Mach and angle of attack variations with apparent instabilities for small amplitude motions. The peak instability magnitude appears to be Mach dependent, with the highest peak at lower M. As σ increases, the damping coefficient rapidly approaches a slightly negative asymptote.

In this study, a new functional form was considered for C_{m_q}. There are a variety of entry probe configurations that are dynamically unstable at small angles and stable at large ones for which it has been difficult to identify a pitch-damping coefficient that works well over the entire angle-of-attack range. Solutions could be found for small and large angles, but the amplitude growth rate at moderate angles was always too large. And, if the amplitude growth were matched at moderate angles, it would not be at small and large angles. Forcing the width of the instability region to decrease resulted in an increased peak value for C_{m_q} at σ = 0°, with no appreciable improvement in the solutions. If the asymptote were allowed to become more negative, the peak value and rate of fall-off with σ would have to be adjusted, and the solution could become unrealistic without much improvement in fitting the entire angle-of-attack range. The estimated values for C_{m_q} often ended up being a compromise, sometimes under predicting the small amplitude growth rate in order to reduce the over prediction of the growth at moderate angles, or simply allowing the growth rate at moderate angles to be over predicted. It appears that, as the amplitude of the angular motion increases, the positive pitch damping near zero degrees angle of attack, multiplied by the pitching rate, introduces too large of a dynamic instability into the solution.

A number of approaches were considered for this problem, including offsetting the effects of the peak C_{m_q} (at σ = 0°) by a negative peak at a small non-zero angle. However, to simulate the trajectories, the negative peak might have to be large and physically unrealistic. The solution implemented here was to turn off the peak as the amplitude of the motion and, therefore, the non-dimensional pitching rate (q) at small angles, increased. A functional model that achieves this is:

$$C_{m_q} = C^{*}_{m_q}(\sigma, M)e^{-f(M)q^2} + \left[1 - e^{-f(M)q^2}\right]C_{m_q,\,asymptote}$$

The parameter $C^{*}_{m_q}(\sigma, M)$, a function of the total angle of attack, would be similar to ones used in previous analyses of ballistic range tests. Note that a quasi-linear analysis will not differentiate between pitch damping models that are functions of σ alone and those that are functions of both σ and q. Assuming a sinusoidal motion of the form $\sigma = A\sin\omega t$, the non-dimensional pitching rate can be written as $q = (d/V)A\omega\cos\omega t$, and its square as $q^2 = (d/V)^2A^2\omega^2(1 - \sin^2\omega t)$, or $q^2 = (d/V)^2(A^2\omega^2 - \omega^2\sigma^2)$, where d, V, and ω are the model diameter, average

velocity, and pitch-oscillation frequency, respectively. It is readily apparent that when averaged over a cycle of motion, the quasi-linear results will appear to be functions of σ.

Parametric studies indicated that good simulations of the experimental trajectories over the entire σ range could be obtained by replacing $C^*_{m_q}(\sigma, M)$ with a function of Mach number alone, and that the trajectory simulations using this formulation of C_{m_q} captured small, moderate and large angle behaviors better than simulations using the traditional form. It may be that there is a relatively wide peak in σ which is attenuated by a relatively sharp peak in q. This would explain some ballistic range evidence of the peak C_{m_q} moving to the trim angle for lifting models, as well as some evidence of frequency dependence in the pitch damping results from forced oscillation tests. This approach to modeling the pitch damping should be further, and carefully investigated.

The quasi-linear estimates for C_{m_q} exhibited strong instabilities at small angles at the lower Mach numbers. This instability appeared to disappear for the mid-range Mach numbers, where the quasi-linear results appeared to reach a plateau. The instabilities then reappeared at the higher Mach numbers (two of the small angle data sets appeared to exhibit positive quasi-linear values for the pitch damping). These variations were modeled with the following equation:

$$C^*_{m_q} = C^*_{m_{q,0}} \exp\left(-C^*_{m_{q,2}} C^*_{m_{q,2}} q^2\right) + \left[1 - \exp(-C^*_{m_{q,2}} C^*_{m_{q,2}} q^2)\right] C_{m_{q,\,\text{asymptote}}}$$

where

$$C^*_{m_{q,0}} = Max\left[C^{**}_{m_{q,0}} + C^{**}_{m_{q,M=M_{ref}}}(M - M_{ref}),\ \ C^{***}_{m_{q,\,\text{plateau}}},\ \ C^{****}_{m_{q,0}} + C^{****}_{m_{q,M=M_{ref}}}(M - M^{****}_{ref})\right]$$

The large angle asymptote, $C_{m_{q,\,\text{asymptote}}}$, was identified using all of the large amplitude shots.

At small angles, errors in exponential decay with the square of the pitching rate can be offset by changes in peak value and vice versa. It is difficult for the parameter-identification process to identify the ideal solution in the small angle regime due to the larger ratio of the measurement errors relative to the measured angles. The peak pitch damping at M = 2.06 was estimated by taking segments of three small amplitude motions, calculating the quasi-linear value for the damping coefficient, plotting these values against the RMS angle of attack (or q), and extrapolating to $\sigma = 0°$ (or, q = 0). All of the data clustered in the region of $2 < M < 2.15$ were then used to identify a value for $C^*_{m_{q,2}}$. At larger Mach numbers, the quasi-linear values of the pitch damping at small angles were smaller, making it more difficult to identify $C^*_{m_{q,2}}$. Therefore, $C^*_{m_{q,2}}$ was assumed constant for the entire Mach range.

Test runs with $\sigma_{RMS} < 5°$ and $2.06 \le M \le 2.56$ were used to identify the fall off with Mach number of the peak C_{m_q}. Multiple quasi-linear fits of the small angle data indicated that C_{m_q} reached a plateau between M = 2.5 and M = 3.2. The small angle data sets with average Mach numbers ranging from 2.56 to 3.23 were used to define this plateau region.

Quasi-linear fits for two of the high-M small-σ data sets indicated that pitch damping at small angles appeared to increase. Limited data were available in this Mach range, and a peak value was identified using only the small-σ, M = 3.62 shot. The change with Mach number was identified using all small angle data sets with Mach numbers ranging from 3.4 to 3.62.

The nonlinear pitch-damping coefficient is plotted versus the non-dimensional pitching rate in Figure 24b. The estimated values and errors* for the corresponding functional parameters are:

$C_{m_{q,\text{asymptote}}}$	=	-0.1068	±	0.0089
$C^*_{m_{q,2}}$	=	1,140	±	140
$C^{**}_{m_{q,0}}$	=	2.5	±	0
$C^{**}_{m_{q,M=Mref}}$	=	-4.35	±	0.76
$C^{***}_{m_{q,plateau}}$	=	0.09	±	0.34
$C^{****}_{m_{q,0}}$	=	1.38	±	0.43
$C^{*****}_{m_{q,M=Mref}}$	=	6.5	±	2.4

M_{ref} = 2.06

M^{****}_{ref} = 3.62

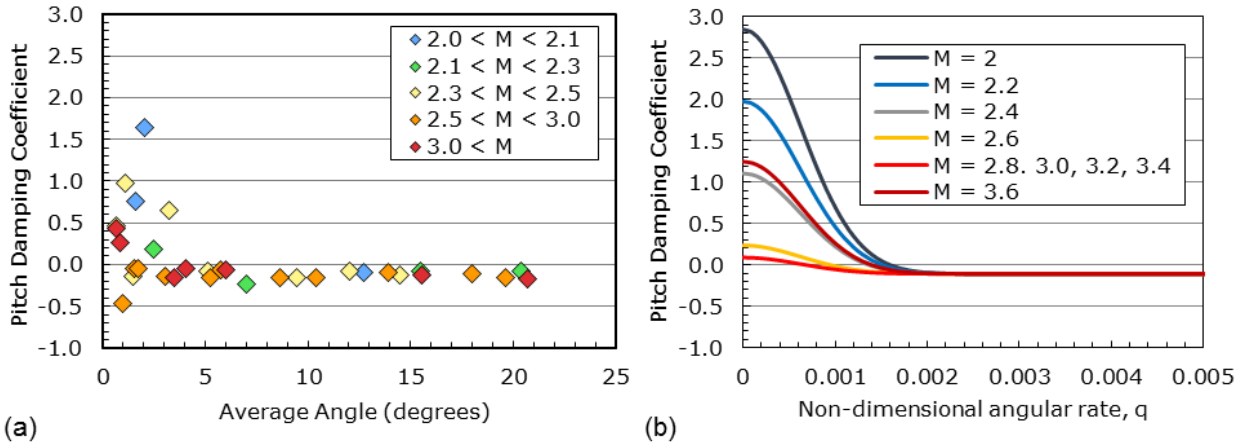

Figure 24. Pitch damping coefficient for the deployed-SIAD configuration: (a) quasi-linear; (b) non-linear.

4.5. Pitch Damping Coefficient Alternate, σ, Formulation (Deployed SIAD)

In the previous section a new functional form for C_{m_q}, dependent on the non-dimensional angular rate, q, was developed. Since this formulation for the pitch-damping coefficient has not been thoroughly evaluated, an alternate formulation, dependent on the total angle of attack, σ, was also developed. The previously used formulations of this form, though over or under predicting the amplitude growth for segments of the ground test regime, have been successfully used for mission planning [13, 27]. Therefore, a function of the form

$$C^*_{m_q} = C^*_{m_{q,0}} \exp\left(-C^*_{m_{\sigma,2}} C^*_{m_{\sigma,2}} \sin^2\sigma\right) + \left[1 - \exp(-C^*_{m_{\sigma,2}} C^*_{m_{\sigma,2}} \sin^2\sigma)\right] C^*_{m_{q,\,\text{asymptote}}}$$

where

$$C^*_{m_{q,0}} = Max\left[C^{**}_{m_{q,0}} + C^{**}_{m_{q,M=M_{ref}}}(M - M_{ref}),\ C^{***}_{m_{q,\,\text{plateau}}},\ C^{****}_{m_{q,0}} + C^{****}_{m_{q,M=M_{ref}}}(M - M^{****}_{ref})\right]$$

and

$$C^*_{m_{q,\,\text{asymptote}}} = C^*_{m_{q,asy,0}} + C^*_{m_{q,asy,1}}(M - M_{ref}) + C^*_{m_{q,asy,2}}(M - M_{ref})^2$$

was also employed to describe the measured pitch-damping behavior for the SFDT models. Note the similarity to the pitching rate formulation used in the previous section. The differences are that the exponential decay is now in terms of the square of the sine of the angle of attack, and the large angle asymptote is a function of M.

The approach for identifying the various pitch damping parameters was similar to that described in the last section for C_{m_q} as a function of pitching rate. The peak pitch damping at Mach 2.06 was estimated by taking segments of three small amplitude motions, calculating the quasi-linear value for the damping coefficient, plotting these values against the σ_{RMS}, and extrapolating to σ at 0°. All of the data in the region of 2 < M < 2.15 were used to identify a value for $C^*_{m_{\sigma,2}}$. For larger M, the quasi-linear C_{m_q} at 0° were smaller, making it more difficult to identify $C^*_{m_{\sigma,2}}$. Therefore, $C^*_{m_{\sigma,2}}$ was assumed constant over the full Mach range. Instead of using a large angle asymptote calculated from the large-σ shots, a first estimate of it was identified using the data from the region 2 < M < 2.15.

As described in the previous sections, shots with σ_{RMS} < 5° and 2.06 ≤ M ≤ 2.56 were used to identify the fall off with M of the peak C_{m_q}. The small angle data sets with M ranging from 2.56 to 3.23 were used to define the plateau region between Mach 2.5 and 3.2. Quasi-linear fits for two of the high-M small-σ shots indicated that C_{m_q} increased at small angles. Limited data were available in this Mach range, and a peak value was identified using only the small-σ, Mach 3.62 shot. The change with Mach number was identified using all small angle data sets having M between 3.4 and 3.62.

The next step in the parameter-identification process was to identify the Mach dependency of the asymptote term. The terms describing the amplitude growth at small angles were fixed and four groupings of the test runs with σ_{RMS} ranging from 7.0° to 20.7° were used to identify the large angle asymptote terms. These terms were then fixed, and the terms governing the small angle behavior were re-identified. This process was repeated until a converged solution was obtained.

The nonlinear pitch-damping coefficient modeled as a function of angle of attack is plotted in Figure 25, and the corresponding estimated parameter values and errors* are:

$$C_{m_{q,asy,0}} = -0.518 \pm 0.083$$

$$C_{m_{q,asy,1}} = 1.088 \pm 0.060$$

$$C_{m_{q,asy,2}} = -0.572 \pm 0.042$$

$$C^{*}_{m_{\sigma,2}} = 35.5 \pm 5.0$$

$$C^{**}_{m_{q,0}} = 2.5 \pm 0$$

$$C^{**}_{m_{q,M=Mref}} = -5.03 \pm 0.65$$

$$C^{****}_{m_{q,plateau}} = -0.23 \pm 0.20$$

$$C^{****}_{m_{q,0}} = 1.23 \pm 0.39$$

$$C^{****}_{m_{q,M=Mref}} = 7.32 \pm 1.20$$

$$M_{ref} = 2.06$$

$$M^{****}_{ref} = 3.62$$

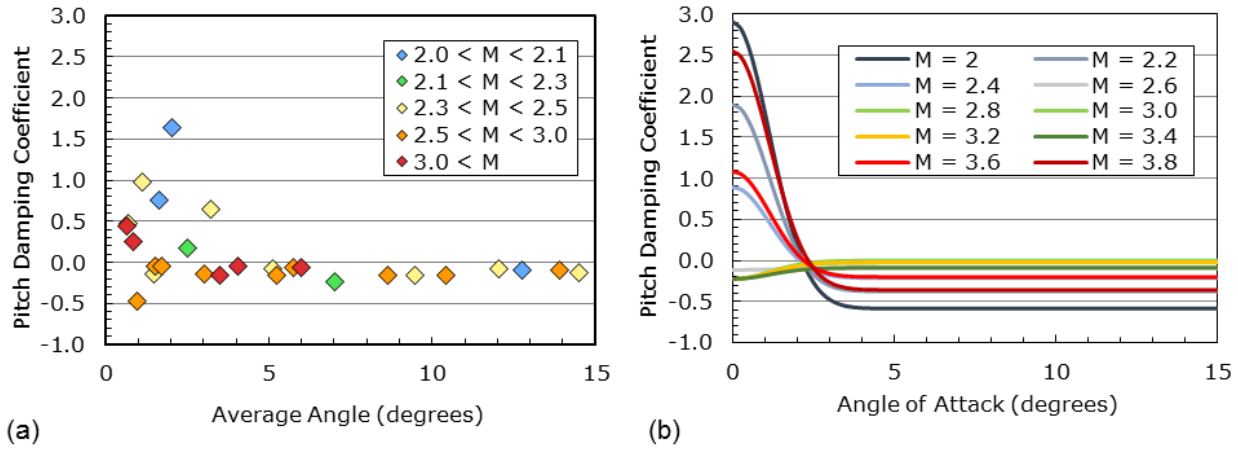

Figure 25. Pitch damping coefficient, alternative (angle) formulation, for the deployed-SIAD configuration: (a) quasi-linear; (b) non-linear.

Note that there are similarities in the two pitch damping models (Figure 24b and Figure 25b). The peak pitch damping values at zero degrees for the two models exhibit similar changes with Mach number. The main difference is in the asymptotic behavior. At Mach numbers with a strong instability at zero degrees, the large angle asymptote for the pitch damping modeled as a function of angle of attack is significantly more negative than that of the quasi-linear results. This results, presumably, from the necessity to counteract the positive peak so that the averages for the majority of the angle-of-attack regime are correct. The pitch damping model using angle of attack has a small negative peak in the presumed plateau region – the large angle asymptote in this region is less negative than the quasi-linear results, and this small negative peak decreases the "average" value of the pitch damping.

To test the sensitivity of the large angle asymptote to the peak pitch damping at zero degrees, a parametric study was performed for a fixed Mach number; all the data with an average Mach number between 2.06 and 2.15 were used for this study. The pitch-damping coefficient was simplified to

$$C_{m_q} = A_1 \exp\left(-A_2 * A_2 \sin^2\sigma\right) + \left[1 - \exp\left(-A_2 * A_2 \sin^2\sigma\right)\right] A_3$$

where A_1, A_2 and A_3 are independent of Mach number and angle of attack. The peak pitch damping coefficient at zero degrees, A_1, was fixed at values ranging from 1 to 5, and A_2 and A_3 were obtained by fitting calculated trajectories to the measured trajectory data. The results of this parametric study are shown in Figure 26. As A_1 increases, the peak becomes narrower, and the large angle asymptote shows very little variation. A peak pitch damping value of 20 did reduce the asymptote to a value of about -0.35, still significantly larger than the quasi-linear result.

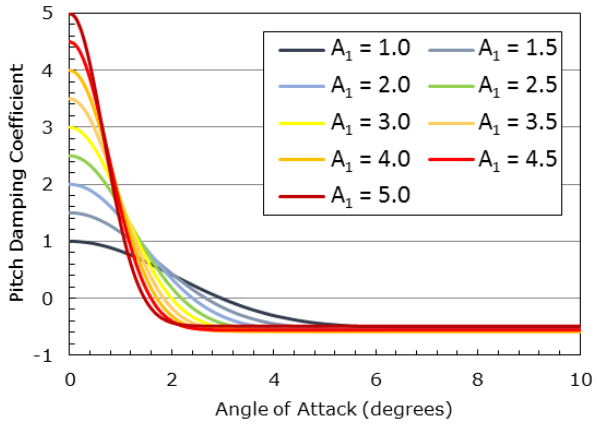

Figure 26. Pitch damping coefficient asymptote parameter study.

In the vast majority of cases, the simulated trajectories for the two pitch damping models are nearly identical. They deviate at the extremes of the test regime, i.e., at 1) small M and small σ_{RMS}; 2) small M and large σ_{RMS}; and 3) large M and large σ_{RMS}. It is at the small and large Mach numbers where the pitch damping at zero degrees is largest and where the large angle asymptotes have the largest downward adjustments to offset the contributions to the pitch damping from the small angle instability. At the largest angles, this downward adjustment is too large, and the angle-based trajectory simulations are over damped. For the small Mach number and small angle cases, the C_{m_q} model based on pitching rate appears to better capture the amplitude growth, especially for test shot 2624. The angles, θ and ψ, for shot 2624 from the two models are compared in Figure 27.

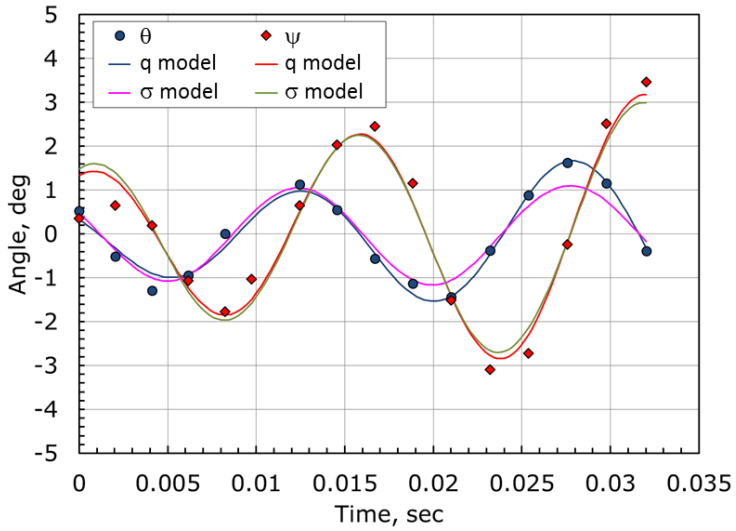

Figure 27. Comparison of the angles from the two pitch damping models for shot 2624.

Whether the proper dependent variable for C_{m_q} is the pitching rate or the angle of attack, it appears that the best models will include an amplitude dependent term that turns off the small angle instability as the amplitude of the motion increases. The pitching rate formulation does minimize the contribution of the instability region as the amplitude of the motion increases, and it appears to give the correct "average" C_{m_q} for a more extended Mach-angle regime than the corresponding σ formulation. Whether it provides the correct C_{m_q} for discrete values of σ and q is unknown.

4.6. Test of aerodynamic force and moment modeling (Deployed SIAD)

Some of the functions used to model the aerodynamic forces and moments for the deployed configuration are fairly complicated and have large M and σ variations. During the parameter identification process, simulated trajectories were simultaneously fit to multiple data sets, and the residual errors in the fits of the position and orientation measurements were generally within the expected range – that is, only slightly larger than those obtained when fitting individual data sets with quasi-linear coefficients.

To further test the functions selected for modeling the aerodynamic forces and moments, an approach was developed that adds multipliers or constants to each of the nonlinear coefficients. The values of the multipliers or constants were then obtained from the best fits between the simulated 6-DOF trajectories and the measured trajectories. The results are shown in Figure 28. In addition to errors in modeling the aerodynamic coefficients, the sources of the corrections may include small errors in measuring the model properties (e.g., mass, diameter, length, inertias) and facility conditions (e.g., pressure and temperature).

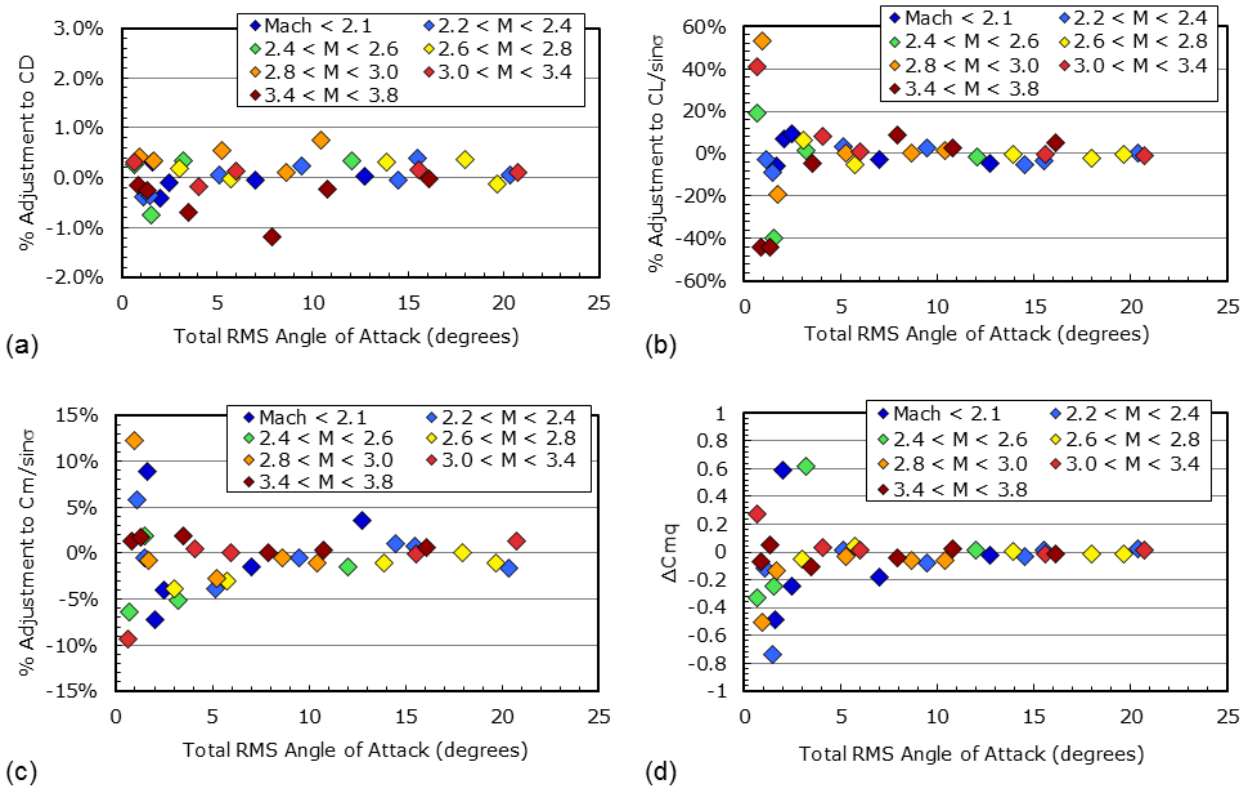

Figure 28. Corrections to non-linear aerodynamic coefficients for individual shots: (a) drag, (b) lift, (c) pitching moment and (d) pitch damping.

Multiplicative factors were added to the drag, lift, and pitching moment coefficients. For the drag coefficient, the corrections were small, typically less than 1%, and there was no discernible pattern to the corrections. It can therefore be concluded that the function selected for the nonlinear drag coefficient models the drag force over the Mach–σ regime. For the lift and pitching moment, the corrections are larger, particularly at small angles (RMS angles less than 3° to 4°). The lift coefficient values are extracted from small oscillations in the swerve motion which are proportional to the angular motion, and the magnitudes of the adjustments at small angles are driven by

errors in the swerve and angle measurements. The corrections do not seem to correlate with Mach number or angle of attack, and it can therefore be assumed that the function modeling the lift forces is reasonable. The correction factors for the pitching moment coefficient are not as large as that for the lift coefficient, but, as with the lift coefficient, they are larger at small angles. Again, the corrections appear to be independent of Mach number and angle of attack and are presumably driven by uncertainties in the angle measurements, not by deficiencies in the function describing the pitching moment coefficient.

For the pitch damping modeled as a function of the pitching rate, a constant correction was added to the nonlinear coefficients. For RMS angles greater than 4°, minimal adjustments were required to optimize the fit to each data set; for RMS angles less than 4°, the adjustments were larger; this is partially due to the larger error to measurement ratio for the angular measurements. There appears to be no discernible pattern in the adjustments, and for all but three cases, it might be surmised that the pitch-damping model is overestimating the instability.

4.7. Drag Coefficient (Stowed SIAD)

The quasi-linear results for the drag coefficient (Figure 29a) exhibited strong angle-of-attack effects and possible Mach effects. The drag coefficient for the stowed configuration was modeled using the function:

$$C_D = \left[C_{D_0} + C_{D_{(M-M_{ref})}}(M - M_{ref}) + C_{D_{(M-M_{ref})^2}}(M - M_{ref})^2\right]\cos\sigma + \left[C_{D_{\sigma^2}}\sin^2\sigma + C_{D_{\sigma^4}}\sin^4\sigma\right]\left[1 + C^*_{D_{(M-M_{ref})}}(M - M_{ref})\right]$$

When identifying the parameters in the C_D equation, the applicable M–σ range was divided into two overlapping regimes: small to moderate angles ($\sigma_{RMS} < 10°$) for all M, and moderate to large angles ($\sigma_{RMS} > 4°$) for all M.

The zero and second order terms in σ were identified using the small to moderate angle data sets. Test comparisons between the calculated and measured trajectories showed that neither the second order terms in σ nor in M improved fit accuracy. Therefore, the parameters in these terms were set to zero.

Once an estimate of the lower order terms was obtained, the fourth order terms in angle of attack were identified using the moderate to large angle data sets. The higher order terms were then fixed, and the lower order terms re-estimated. This process was repeated until the solutions converged.

The nonlinear drag coefficient for the stowed configuration is plotted in Figure 29b; the estimated parameter values and errors* for C_D are:

C_{D_0}	=	1.51851	±	0.00087
$C_{D_{(M-M_{ref})}}$	=	0.0125	±	0.0040
$C_{D_{(M-M_{ref})^2}}$	=	0		
$C_{D_{\sigma^2}}$	=	0		
$C_{D_{\sigma^4}}$	=	-4.87	±	0.13
$C^*_{D_{(M-M_{ref})}}$	=	0.858	±	0.099
M_{ref}	=	3.5		

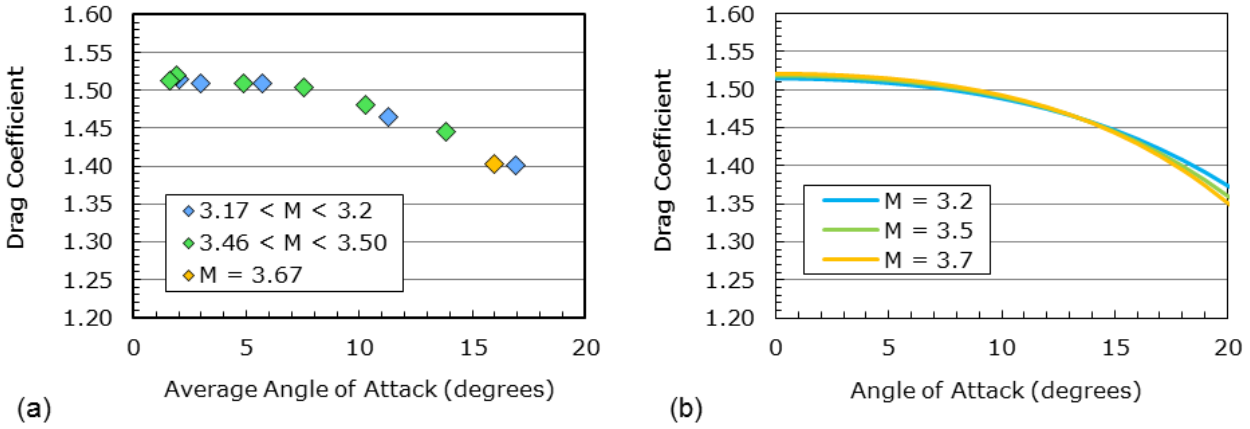

Figure 29. Drag coefficient for the stowed-SIAD configuration: (a) quasi-linear; (b) non-linear.

4.8. Lift Coefficient (Stowed SIAD)

The quasi-linear results for the lift coefficient (Figure 30a) exhibited significant scatter at small angles. At small angles the measurement errors are large compared to the swerve due to lift. In addition, any errors in translating the measured model centroid location to the CG location may add errors that are proportional to the angle, thus introducing additional uncertainties to the C_L. At large angles, the quasi-linear results exhibited some angle-of-attack effects and possible Mach effects. The lift coefficient for the stowed configuration was modeled using the function:

$$C_L = \left[C_{L_\sigma} + C_{L_{\sigma^3}} \sin^2\sigma + C_{L_{\sigma,(M-M_{ref})}} (M - M_{ref}) \right] \sin\sigma$$

The terms in the lift coefficient were identified using only the moderate- to large-amplitude data sets. Parametric studies indicated that the inclusion of a Mach number term in the lift coefficient function did not improve the fit accuracy, and the corresponding parameter was set to zero. The nonlinear lift coefficient for the stowed configuration is plotted in Figure 30b; the estimated values and errors* for its functional parameters are:

$$C_{L_\sigma} = -1.514 \pm 0.047$$

$$C_{L_{\sigma^3}} = 1.38 \pm 0.46$$

$$C_{L_{\sigma,(M-M_{ref})}} = 0$$

$$M_{ref} = 3.5$$

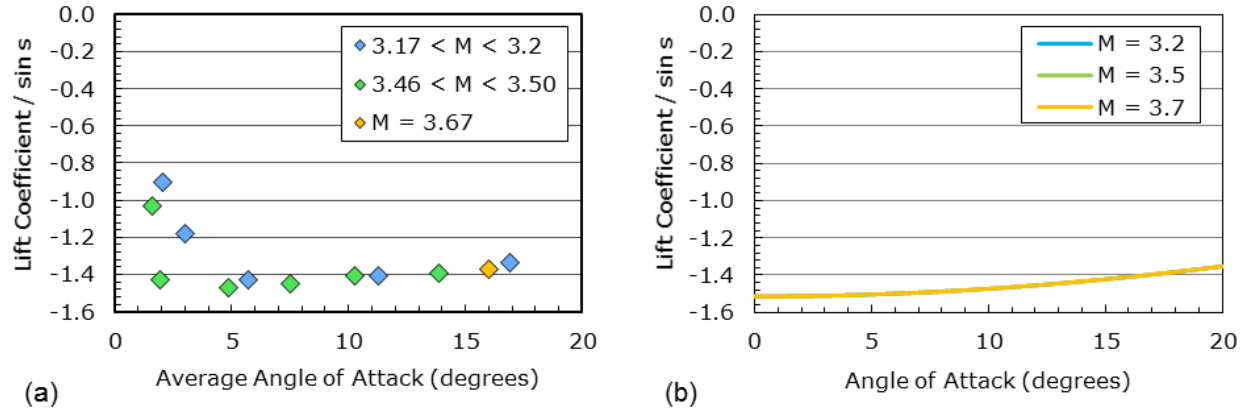

Figure 30. Lift coefficient for the stowed-SIAD configuration: (a) quasi-linear; (b) non-linear.

4.9. Pitching Moment Coefficient (Stowed SIAD)

The quasi-linear results for the pitching moment coefficient (Figure 31a) exhibited possible angle-of-attack and Mach effects. The pitching moment coefficient for the stowed configuration was modeled using the function:

$$C_m = \left[C_{m_\sigma} + C_{m_{\sigma,(M-M_{ref})}}(M - M_{ref})\right]\sin\sigma + \left[C_{m_{\sigma^3}} + C_{m_{\sigma^3,(M-M_{ref})}}(M - M_{ref})\right]\sin^3\sigma + \left[C_{m_{\sigma^5}} + C_{m_{\sigma^5,(M-M_{ref})}}(M - M_{ref})\right]\sin^5\sigma$$

When identifying the parameters in the C_m equation, the applicable M–σ range was divided into two overlapping regimes: small to moderate angles ($\sigma_{RMS} < 10°$) for all M, and moderate to large angles ($\sigma_{RMS} > 4°$) for all M.

The first and third order terms in angle of attack were identified using the small to moderate amplitude shots. Test comparisons between the calculated and measured trajectories showed that the third order terms in σ did not improve the fit accuracy. Thus, the corresponding parameters were therefore set to zero.

Once an estimate of the lower order terms was obtained, the fifth order terms in σ were identified using the moderate to large angle data sets. The higher order terms were then fixed, and the lower order terms re-estimated. This process was repeated until the solutions converged.

The nonlinear pitching moment coefficient for the stowed configuration is plotted in Figure 31b, and the estimated values and errors* for the associated functional parameters are:

C_{m_σ}	=	-0.12695	±	0.00046
$C_{m_{\sigma,(M-M_{ref})}}$	=	0.0018	±	0.0023
$C_{m_{\sigma^3}}$	=	0	±	0
$C_{m_{\sigma^3,(M-M_{ref})}}$	=	0	±	0
$C_{m_{\sigma^5}}$	=	-0.570	±	0.048
$C_{m_{\sigma^5,(M-M_{ref})}}$	=	-0.241	±	0.012
M_{ref}	=	3.5		

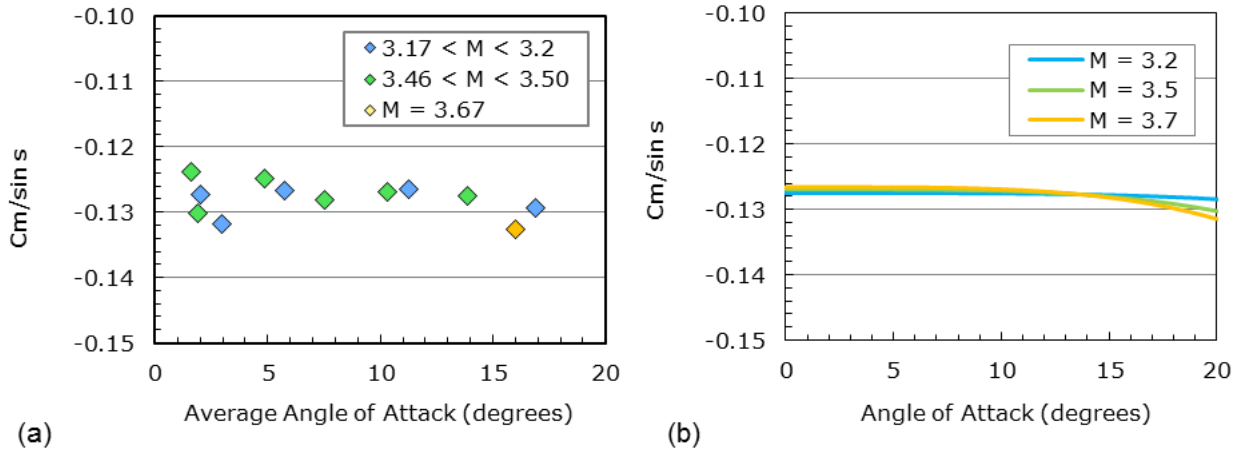

Figure 31. Pitching moment coefficient for the stowed-SIAD configuration: (a) quasi-linear; (b) non-linear.

4.10. Pitch Damping Coefficient (Stowed SIAD)

For the pitch-damping coefficient, the results of the quasi-linear analysis of the individual data sets (Figure 32a) indicated no discernible functional variations in Mach number or angle of attack. Test comparisons between the calculated trajectories and measured trajectories showed that, for data sets with comparable angular amplitudes but different Mach numbers, adding a Mach term did not improve the fits. For data sets with similar Mach numbers but varying amplitudes, adding an angle-of-attack or pitching rate term did not improve the fits. The shots were divided into groups with similar σ_{RMS}, and the quasi-linear values for C_{m_q} were estimated for each group. The results are shown, with estimated error bars, in Figure 32b; again, there is no discernible pattern.

Since there were no identifiable Mach or angle-of-attack variations, the pitch-damping coefficient was modeled using a constant:

$$C_{m_q} = C_{m_{q,0}}$$

and the estimated value and error* for the non-linear pitch-damping coefficient of the stowed configuration are:

$$C_{m_{q,0}} = -0.140 \pm 0.017$$

Referring to Figure 32b, the non-linear value is in good agreement with the quasi-linear results for all but one group. For the data sets with $\sigma_{RMS} \approx 6°$, the measured trajectories were first fit using $C_{m_{q,0}} = -0.140$; then $C_{m_{q,0}}$ was allowed to vary. The difference in the residual errors for the fits was only 0.02 degrees; therefore, the assumption of a constant C_{m_q} is reasonable.

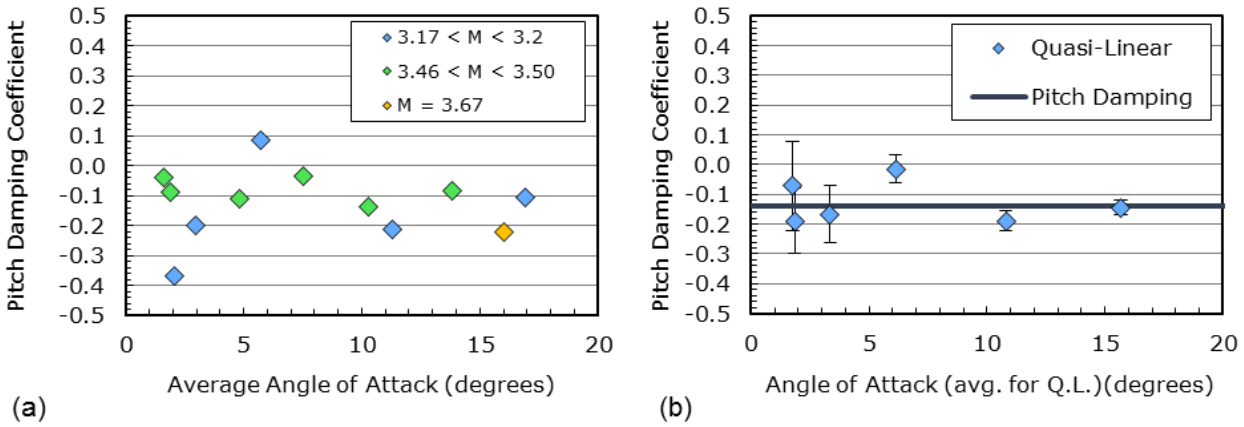

Figure 32. Pitch damping coefficient for the stowed-SIAD configuration: (a) quasi-linear; (b) non-linear.

5. Conclusions

A ballistic-range aerodynamics test campaign was performed in order to estimate the aerodynamic stability characteristics of the Supersonic Flight Dynamics Test (SFDT) vehicle prior to its first flight. SFDT was a flight demonstration of a Supersonic Inflatable Aerodynamic Decelerator (SIAD) concept developed by NASA under the Low-Density Supersonic Decelerator (LDSD) Project for possible use in future robotic entry missions to Mars. The SFDT flight tests took place in Earth's atmosphere at high altitude in order to achieve Mars-relevant flight conditions. The ground tests reported here were conducted in the Hypervelocity Free-Flight Aerodynamics Facility (HFFAF) at NASA's Ames Research Center. The test conditions were chosen to match, as close as possible, the Mach number, Reynolds number, and dynamics of those expected for the SFDT vehicle in flight, both with the SIAD stowed and deployed. The ballistic-range model of the SIAD was rigid, solid metal, and evaluation of the effect of the flexibility of the inflatable decelerator was not part of this test campaign. Static aerodynamics coefficients for lift, drag and pitching moment were obtained, as well as the dynamic stability pitch damping coefficients. Twelve shots were made over a Mach number range of 3.2 – 3.7 for a SFDT model with the SIAD

stowed. Thirty-seven shots were made over a Mach number range of 2.0 – 3.8 for a SFDT model with the SIAD deployed. Data were obtained over RMS pitch oscillation amplitudes ranging from ~1.5 to ~20 degrees.

For each shot, the positions and orientations of the models were photographically recorded at 16 stations along the flight trajectory through the ballistic range. Biases in the measured positions and orientations were identified and removed from the data. After removal of the biases, the uncertainties in the measured locations and orientations were relatively small. The uncertainties for the stowed configuration trajectory measurements were larger, by about 50%, for the angle measurements. Although the stowed-SIAD model diameter was 0.48 times smaller than the deployed-SIAD diameter, the resolution of the digitized images was increased to keep the number of pixels per model diameter approximately constant. However, the deployed-SIAD configuration had a larger flat region on its base, which improved the angle measurements.

For both the deployed and stowed configurations, the Mach and angle-of-attack trends were identified for the force and moment coefficients. The values of the various M- and σ-term parameters in the functions used to model the aerodynamic coefficients were identified by fitting calculated trajectories to the measured trajectories obtained from ballistic range tests. Trajectory simulations of the ballistic range tests were in good agreement with the measured trajectories.

For the deployed-SIAD configuration, the quasi-linear results for the pitch-damping coefficient (C_{m_q}) show large variations with Mach number, and angle of attack variations with apparent instabilities for small amplitude motions. The peak instability magnitude appears to be Mach dependent, with the highest peak at lower M. As σ increases, the damping coefficient rapidly approaches a slightly negative asymptote. Non-linear pitch-damping was modeled in two ways: as a function of the sine of the total angle of attack, σ, which has traditionally been used in analyzing ballistic-range data; and using a proposed new model in terms of the non-dimensional pitch rate, q. Parametric studies indicated that the trajectory simulations using this formulation of C_{m_q} captured small, moderate and large angle behaviors better than simulations using the traditional form. It is recommended that this new model should be further investigated by re-analyzing existing data for trimmed and untrimmed models, and by future experiments designed to test its assumptions.

For the stowed-SIAD configuration, the quasi-linear results for the pitch-damping coefficient indicated no discernible functional variations in Mach number or angle of attack, and the non-linear pitch-damping coefficient was modeled using a constant.

References

1. Yates, L., "Aerodynamic Coefficients from Aeroballistic Range Testing of Deployed and Stowed-SIAD SFDT Models," Final Report, May 22, 2012.
2. Clark, I. G., Adler, M., and Manning, R., "Summary of the First High-Altitude, Supersonic Flight Dynamics Test for the Low-Density Supersonic Decelerator Project," AIAA 2015-2100, 23rd AIAA Aerodynamic Decelerator Systems Technology Conference, Daytona Beach, FL, 30 Mar - 2 Apr 2015.
3. Van Norman, J.W., Dyakonov, A., Schoenenberger, M., Davis, J., Muppidi, S., Tang, C., Bose, D., Mobley, B. and Clark, I., "Aerodynamic Models for the Low Density Supersonic Decelerator (LDSD) Test Vehicles," AIAA 2016-3883, 34th AIAA Applied Aerodynamics Conference, Washington, D.C., 13-17 June 2016.
4. Clark, I.G., Adler, M., and Rivellini, T.P., "Development and Testing of a New Family of Supersonic Decelerators," AIAA 2013-1252, AIAA Aerodynamic Decelerator Systems (ADS) Conference, Daytona Beach, FL, 25-28 March 2013.
5. National Aeronautics and Space Administration, "Low Density Supersonic Decelerators," NASAfacts, JPL 400-1530 3/13, http://www.jpl.nasa.gov/news/fact_sheets/LDSD.pdf (accessed 9/29/2017).
6. Cook, B. T., Blando, G., Kennett, A., Von Der Heydt, M., Wolff, J.L, and Yerdon, M., "High Altitude Supersonic Decelerator Test Vehicle," AIAA 2013-1353, AIAA Aerodynamic Decelerator Systems (ADS) Conference, Daytona Beach, FL, 25-28 March 2013.
7. Desai, P., Mitcheltree, R., Cheatwood, F., "Entry Dispersion Analysis for the Stardust Comet Sample Return Capsule," Journal of Spacecraft and Rockets, Vol. 36, No. 3, May-June 1999, p. 463.
8. Desai, P., Mitcheltree, R., Cheatwood, F., "Mars Exploration Rover Six-Degree-of-Freedom Entry Trajectory Analysis," Journal of Spacecraft and Rockets, Vol. 43, No. 5, September-October, 2006, pp. 1019 – 1025.
9. Kazemba, C. D., Braun, R. D., Clark, I. G., and Schoenenberger, M., "Survey of Blunt-Body Supersonic Dynamic Stability," *Journal of Spacecraft and Rockets*, Vol. 54, No. 1, 2017, pp. 109-127.
10. De Rose, C.E., "Trim Attitude, Lift and Drag of the Apollo Command Module with Offset Center-Of-Gravity Positions at Mach Numbers to 29," NASA TN D-5276, June 1969.

11. Intrieri, P. F., De Rose, C. E., and Kirk, D. B., "Flight Characteristics of Probes in the Atmospheres of Mars, Venus and the Outer Planets," Acta Astronautica, Vol. 4, pp. 789-799, 1977.
12. Ramsey, A. L. and Chapman, G. T., "A Study of Reynolds Number Effects on Supersonic Flow Over Blunt Bodies," AIAA 2000-1010, 38th Aerospace Sciences Meeting & Exhibit, Reno, NV, 10-13 January 2000.
13. Brown, J. D., Bogdanoff, D. W., Yates, L. A., and Chapman, G.T., "Transonic Aerodynamics of a Lifting Orion Crew Capsule from Ballistic Range Data," Journal of Spacecraft and Rockets, Vol. 47, No. 1, January–February 2010, pp. 36 – 47.
14. Cruz, J. R., "Nondimensional Scaling of Aerodynamic Decelerator Tests," 20th AIAA Aerodynamic Decelerator Systems Technology Conference and Seminar, Parachute Systems Tests and Evaluation: Processes and Technology, May 4, 2009.
15. Dyakonov, A. A. and Bogdanoff, D. W., "Selection of Ballistic Range for LDSD Testing," White Paper to LDSD Project Team, August 19, 2011
16. Bogdanoff, D. W., "Design Guide for Aerodynamics Testing of Earth and Planetary Entry Vehicles in a Ballistic Range," NASA TM-2017-219473, January 2017.
17. Canning, T. N., Seiff, A., and James, C. S. (Ed.), "Ballistic Range Technology," AGARDograph No. 138, 1970, p. 103.
18. *Ibid*, pp. 323-325.
19. Tang, C., Muppidi, S., Bose, D., Van Norman, J. W., Tanimoto, R., and Clark, I., "Post-Flight Aerodynamic and Aerothermal Model Validation of a Supersonic Inflatable Aerodynamic Decelerator," AIAA 2015-2136, 23rd AIAA Aerodynamic Decelerator Systems Technology Conference, Daytona Beach, FL, 30 Mar-2 Apr 2015.
20. Bogdanoff, D. W., Brown, J. D., Dyakonov, A. A., and Wilder, M. C., "New Developments in Diagnostic, Launch and Model Control Techniques in the NASA Ames Ballistic Ranges," 63rd Meeting of the Aeroballistic Range Association, Brussels, Belgium, September-October, 2012.
21. Canning, T. N., Seiff, A., and James, C. S. (Ed.), "Ballistic Range Technology," AGARDograph No. 138, 1970, p. 114.
22. *Ibid*, pp. 207-210.
23. *Ibid*, pp. 205-206.
24. Yates, L. A., "A Comprehensive Automated Aerodynamic Reduction System for Ballistic Ranges," Wright Laboratory, Armament Directorate, WL-TR-95-7059, Oct. 1996.
25. Chapman, G. T., and Kirk, D. B., "A Method of Extracting Aerodynamic Coefficients from Free-Flight Data," AIAA J., Vol. 8, No. 4, April 1970.
26. Yates, L. A. and Chapman, G. T., "Aerodynamic Ballistic Range Analysis using Generalized Math Models," AIAA 1996-3360, AIAA Atmospheric Flight Mechanics Conference, San Diego, CA, July 29-31, 1996.
27. Schoenenberger, M., Yates, L., Hathaway, W., "Dynamic Stability Testing of the Mars Science Laboratory Entry Capsule," AIAA 2009-3917, 41st AIAA Thermophysics Conference, 22 - 25 June 2009.

Appendix A: Measured Trajectory Values and Simulated Trajectories for the Deployed-SIAD Configuration

The data were grouped for analysis by the RMS amplitude of the total angle of attack, σ_{RMS}, and are presented in this appendix in order of increasing Mach number within the groups of increasing σ_{RMS}. The table below gives the test conditions (from Table 4) sorted in the order presented in this appendix.

Test conditions for each shot of the deployed-SIAD configuration models.

Shot	$\bar{M}_\infty$	$\overline{Re}_d$ (x 10^{-6})	$\bar{V}_\infty$ (m/s)	P_∞ (Torr)	T_∞ (K)	ρ_∞ (kg/m^3)	σ_{RMS} (deg)
2619	2.06	0.365	708	169.0	294.1	0.267	1.7
2624	2.08	0.369	715	169.4	294.2	0.267	1.9
2622	2.13	0.380	732	169.4	293.3	0.268	2.5
2614	2.33	0.407	800	166.0	293.3	0.263	1.1
2625	2.36	0.420	809	169.4	293.1	0.268	1.5
2631	2.42	0.428	830	167.7	292.7	0.266	0.7
2616	2.56	0.441	878	164.2	293.8	0.260	1.5
2626	2.84	0.484	976	162.4	294.2	0.256	1.0
2617	2.97	0.499	1023	160.5	294.4	0.253	1.7
2653	3.10	0.513	1071	158.0	294.4	0.249	0.7
2627	3.47	0.564	1190	155.0	293.7	0.245	0.9
2652	3.62	0.564	1248	149.0	294.9	0.235	1.3
2620	2.39	0.425	818	169.4	292.8	0.269	5.2
2629	2.42	0.426	832	167.7	293.9	0.265	3.2
2639	2.64	0.454	907	164.2	294.0	0.259	3.0
2654	2.74	0.473	936	163.0	291.5	0.260	5.8
2628	2.90	0.495	995	162.4	293.3	0.257	5.3
2640	3.24	0.536	1115	158.0	293.8	0.250	4.1
2643	3.31	0.538	1141	155.0	294.3	0.245	6.0
2637	3.45	0.559	1184	155.0	294.4	0.245	3.5
2621	2.11	0.376	723	169.4	293.1	0.268	7.1
2642	2.91	0.495	999	161.5	293.2	0.256	8.8
2638	3.78	0.590	1300	149.0	294.2	0.235	8.1
2623	2.03	0.362	697	169.4	292.8	0.269	12.9
2641	2.37	0.418	813	166.5	291.9	0.265	9.7
2646	2.47	0.421	848	163.0	294.3	0.257	12.3
2647	2.88	0.490	992	163.0	295.1	0.257	10.7
2648	3.49	0.573	1197	155.0	292.2	0.246	11.1
2630	2.26	0.399	776	167.7	293.1	0.266	15.8
2632	2.34	0.399	803	162.7	293.7	0.257	14.7
2650	2.67	0.458	919	163.0	293.8	0.258	14.2
2649	3.17	0.526	1088	158.0	293.6	0.250	15.7
2651	3.84	0.611	1323	152.0	294.5	0.240	16.0
2645	2.27	0.404	779	169.4	293.7	0.268	20.6
2644	2.64	0.449	905	161.5	293.0	0.256	19.7
2635	2.76	0.472	947	163.1	294.0	0.258	18.4
2636	3.39	0.552	1165	155.0	293.7	0.245	20.5

Shot	$\bar{M}_\infty$	$\overline{Re}_d$ (x 10^{-6})	$\bar{V}_\infty$ (m/s)	P_∞ (Torr)	T_∞ (K)	ρ_∞ (kg/m^3)	σ_{RMS} (deg)
2619	2.06	0.365	708	169.0	294.1	0.267	1.7

Station	time, s	x, m	y, m	z, m	V, m/s	M	Re_d (x 10^{-6})	ψ, deg	θ, deg
1	0.00000000	0.045	0.056	0.060	742.10	2.16	0.383	0.2	0.6
2	0.00206712	1.573	0.055	0.059	737.46	2.15	0.380	1.6	0.3
3	0.00414962	3.104	0.054	0.056	732.83	2.13	0.378	1.6	0.0
4	0.00621675		0.052		728.29	2.12	0.375	0.6	
5	0.00832618	6.146	0.050	0.050	723.71	2.11	0.373	-1.0	0.9
6	0.01044991	7.677	0.048	0.048	719.16	2.09	0.371	-2.1	0.8
7	0.01255942	9.190	0.047	0.046	714.69	2.08	0.368	-1.3	0.7
8	0.01470663	10.719		0.043	710.19	2.07	0.366		-0.4
9	0.01686479	12.247	0.043	0.039	705.72	2.05	0.364	1.4	-1.6
10	0.01903156	13.771	0.042	0.037	701.30	2.04	0.361	1.9	-1.3
11	0.02121370	15.297	0.040	0.034	696.90	2.03	0.359	1.0	-0.3
12	0.02341136	16.824	0.038	0.032	692.52	2.01	0.357	-0.9	1.5
13	0.02561727	18.348	0.036	0.029	688.19	2.00	0.355	-1.9	2.2
14	0.02784028	19.872	0.035	0.026	683.89	1.99	0.353	-1.0	1.5
15	0.03006868	21.392	0.034	0.023	679.63	1.98	0.350	0.9	1.1
16	0.03232372	22.919	0.032	0.020	675.38	1.96	0.348	2.4	-0.5

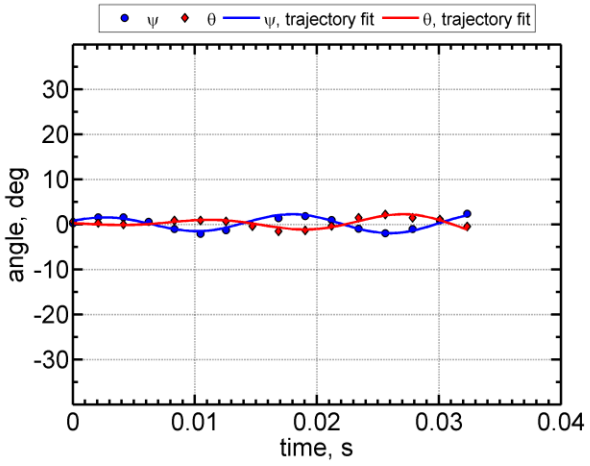

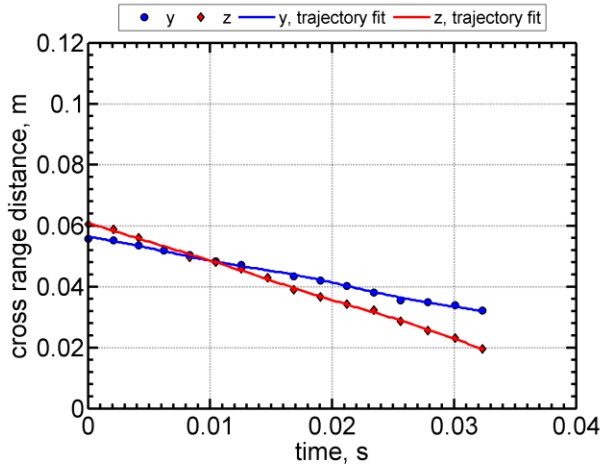

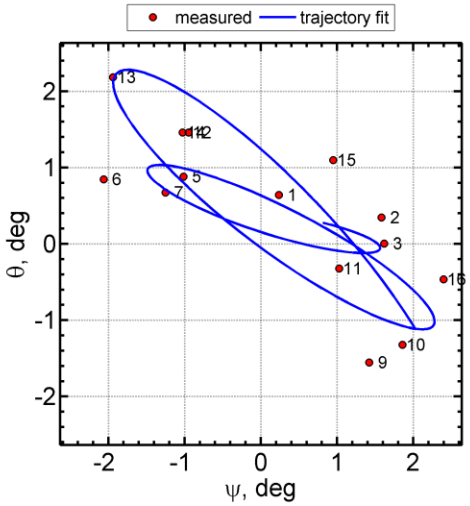

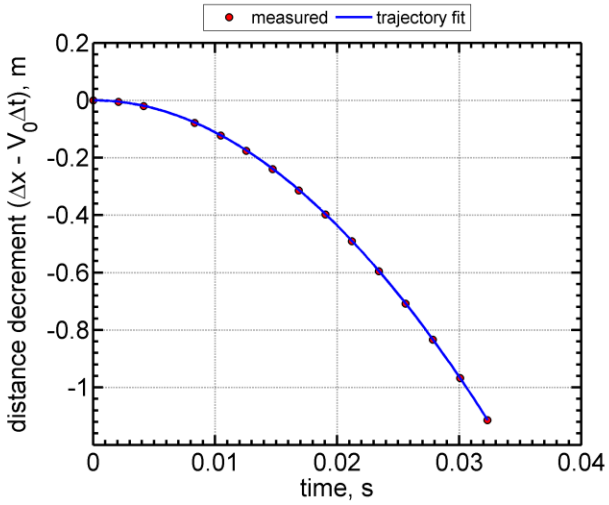

Shot	$\bar{M}_\infty$	$\overline{Re}_d$ (x 10^{-6})	$\bar{V}_\infty$ (m/s)	P_∞ (Torr)	T_∞ (K)	ρ_∞ (kg/m^3)	σ_{RMS} (deg)
2624	2.08	0.369	715	169.4	294.2	0.267	1.9

Station	time, s	x, m	y, m	z, m	V, m/s	M	Re_d (x 10^{-6})	ψ, deg	θ, deg
1	0.00000000	0.046	0.056	0.061	749.05	2.18	0.387	0.4	0.5
2	0.00204882	1.576	0.056	0.059	744.36	2.16	0.384	0.7	-0.5
3	0.00410979	3.105	0.054	0.056	739.70	2.15	0.382	0.2	-1.3
4	0.00615644	4.615	0.053	0.053	735.12	2.14	0.380	-1.1	-0.9
5	0.00824589	6.147	0.051	0.049	730.50	2.12	0.377	-1.8	0.0
6	0.00973486		0.051		727.24	2.12	0.376	-1.0	
7	0.01244049	9.191	0.049	0.047	721.39	2.10	0.373	0.7	1.1
8	0.01456421	10.719	0.048	0.044	716.86	2.08	0.370	2.0	0.5
9	0.01670595	12.249	0.047	0.040	712.35	2.07	0.368	2.5	-0.6
10	0.01884835	13.770	0.045	0.038	707.89	2.06	0.366	1.2	-1.1
11	0.02101181	15.297	0.044	0.035	703.45	2.05	0.363	-1.5	-1.4
12	0.02318838	16.823	0.042	0.033	699.04	2.03	0.361	-3.1	-0.4
13	0.02537470	18.347	0.040	0.030	694.66	2.02	0.359	-2.7	0.9
14	0.02757590	19.871	0.041	0.027	690.32	2.01	0.357	-0.2	1.6
15	0.02978539	21.392	0.040	0.025	686.02	2.00	0.354	2.5	1.2
16	0.03201945	22.918	0.039	0.021	681.74	1.98	0.352	3.5	-0.4

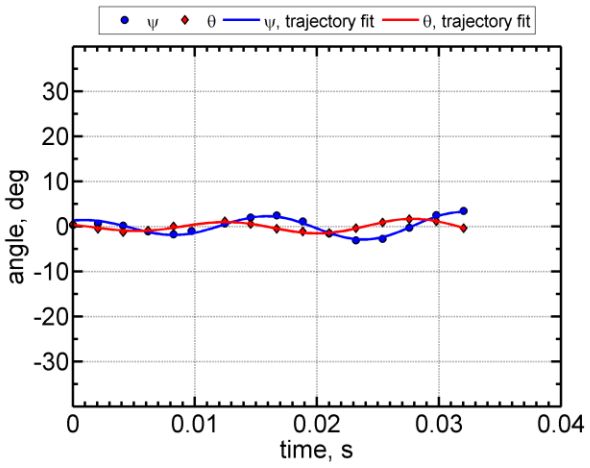

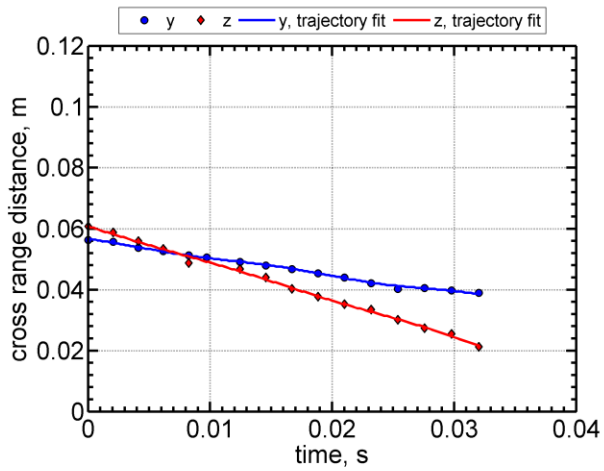

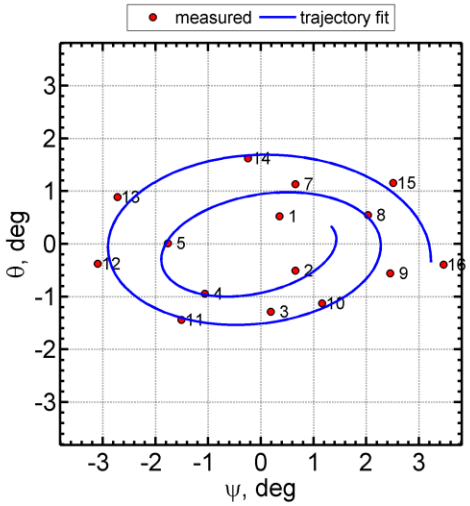

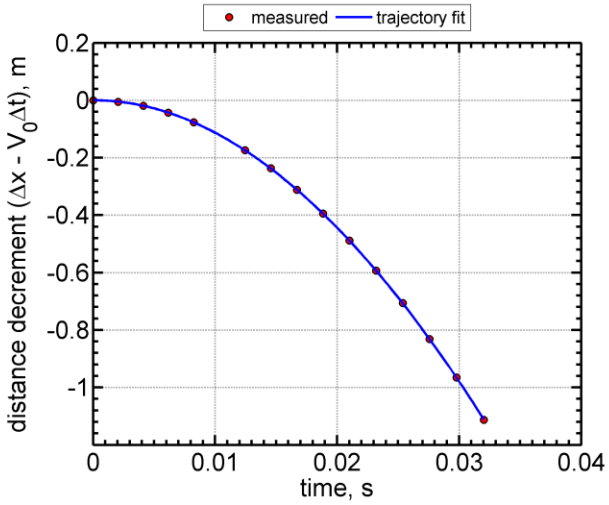

Shot	$\bar{M}_\infty$	$\overline{Re}_d$ (x 10^{-6})	$\bar{V}_\infty$ (m/s)	P_∞ (Torr)	T_∞ (K)	ρ_∞ (kg/m^3)	σ_{RMS} (deg)
2622	2.13	0.380	732	169.4	293.3	0.268	2.5

Station	time, s	x, m	y, m	z, m	V, m/s	M	Re_d (x 10^{-6})	ψ, deg	θ, deg
1	0.00000000	0.046	0.058	0.060	766.75	2.23	0.398	-1.9	0.4
2	0.00199974	1.574	0.057	0.059	761.94	2.22	0.396	-1.3	2.4
3	0.00401488	3.105	0.057	0.056	757.14	2.21	0.393	-1.0	2.8
4	0.00601496	4.615	0.056	0.053	752.44	2.19	0.391	0.1	1.6
5	0.00805663	6.146	0.055	0.049	747.69	2.18	0.388	0.6	-1.5
6	0.01011220	7.678	0.055	0.047	742.96	2.16	0.386	0.4	-3.6
7	0.01215409	9.190	0.054	0.046	738.32	2.15	0.383	-0.3	-2.7
8	0.01423102	10.719		0.044	733.66	2.14	0.381		-0.3
9	0.01632360	12.249	0.053	0.041	729.02	2.12	0.379	-1.4	2.5
10	0.01842948	13.779	0.053	0.039	724.42	2.11	0.376	-1.2	3.8
11	0.02053068	15.297	0.053	0.036	719.88	2.10	0.374	-0.3	2.5
12	0.02265861	16.824	0.053	0.033	715.34	2.08	0.372	0.0	-0.2
13	0.02479477	18.348	0.052	0.030	710.84	2.07	0.369	0.2	-3.0
14	0.02694751	19.872	0.053	0.027	706.37	2.06	0.367	0.4	-3.4
15	0.02910514	21.392	0.053	0.025	701.96	2.04	0.365	0.2	-1.6
16	0.03128809	22.919	0.053	0.023	697.55	2.03	0.362	0.1	1.9

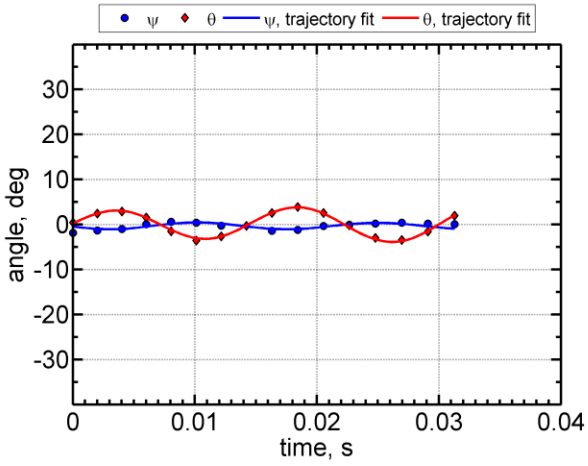

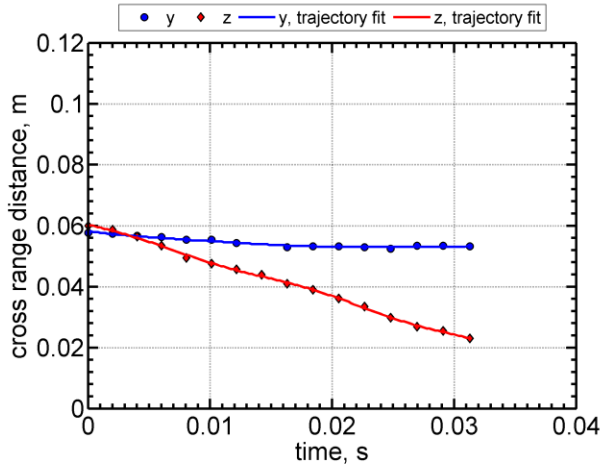

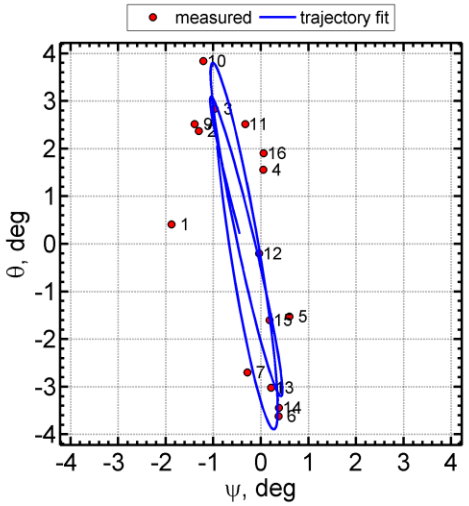

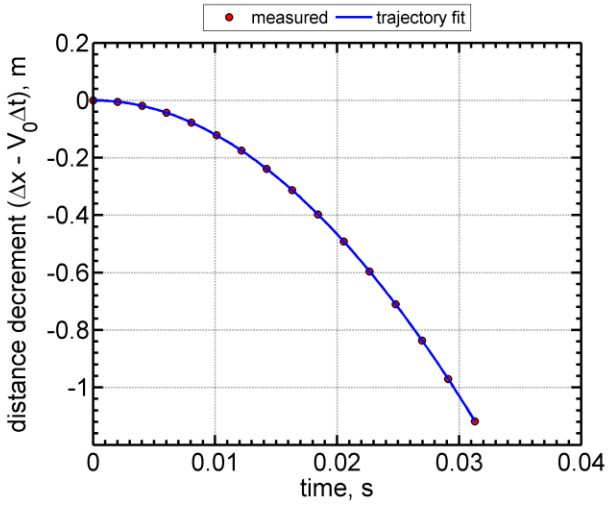

Shot	$\bar{M}_\infty$	$\overline{Re_d}$ (x 10^{-6})	$\bar{V}_\infty$ (m/s)	P_∞ (Torr)	T_∞ (K)	ρ_∞ (kg/m^3)	σ_{RMS} (deg)
2614	2.33	0.407	800	166.0	293.3	0.263	1.1

Station	time, s	x, m	y, m	z, m	V, m/s	M	Re_d (x 10^{-6})	ψ, deg	θ, deg
1	0.00000000	0.047	0.074	0.055	836.94	2.44	0.425	-0.2	-0.7
2	0.00183271	1.576	0.077	0.053	831.93	2.42	0.423	0.9	-0.7
3	0.00367771	3.106	0.078	0.049	826.93	2.41	0.420	0.5	0.1
4	0.00551042		0.079		822.01	2.39	0.418	-0.3	
5	0.00737707	6.148	0.081	0.043	817.06	2.38	0.415	-1.0	1.0
6	0.00925589	7.678	0.083	0.040	812.14	2.37	0.413	-0.9	1.4
7	0.01112712	9.193	0.085	0.038	807.29	2.35	0.410	-0.3	0.8
8	0.01302662	10.722	0.086	0.035	802.42	2.34	0.408	0.0	-0.2
9	0.01493946	12.252	0.088	0.030	797.57	2.32	0.405	0.7	-0.5
10	0.01685439	13.775	0.090	0.027	792.78	2.31	0.403	0.0	-0.4
11	0.01878302	15.300	0.092	0.025	788.01	2.30	0.400	-0.9	0.2
12	0.02072848	16.828	0.094	0.022	783.26	2.28	0.398	-2.1	0.3
13	0.02268170	18.353	0.095	0.018	778.55	2.27	0.396	-1.8	-0.1
14	0.02464265	19.875	0.099	0.014	773.88	2.25	0.393	-0.7	-0.5
15	0.02661424	21.396	0.101	0.012	769.25	2.24	0.391	0.9	-0.4
16	0.02860401	22.921	0.104	0.009	764.64	2.23	0.388	1.7	-1.0

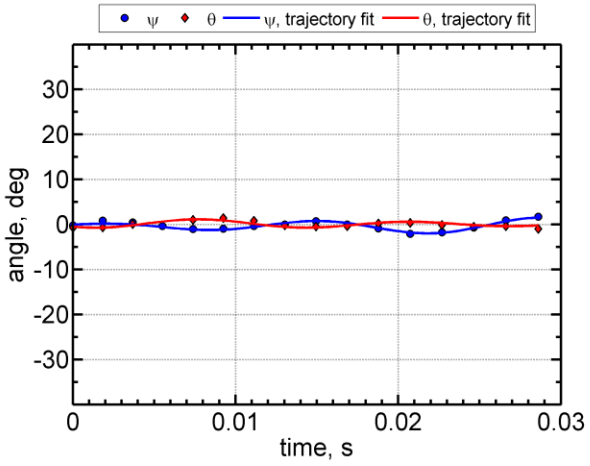

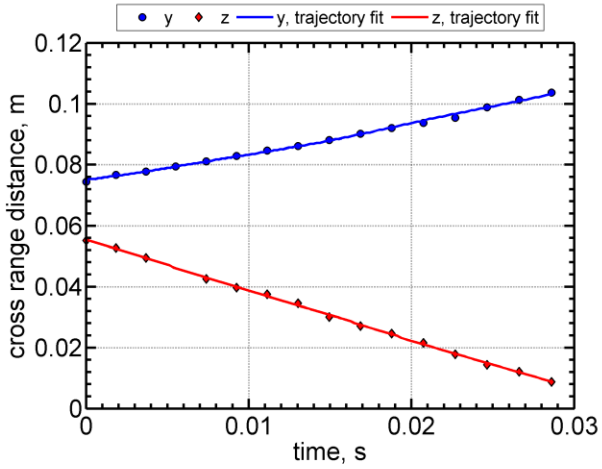

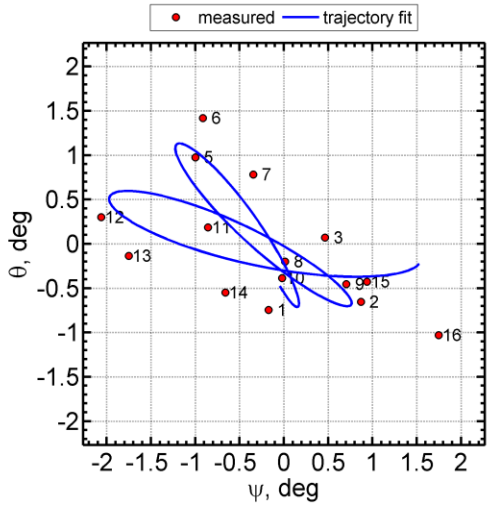

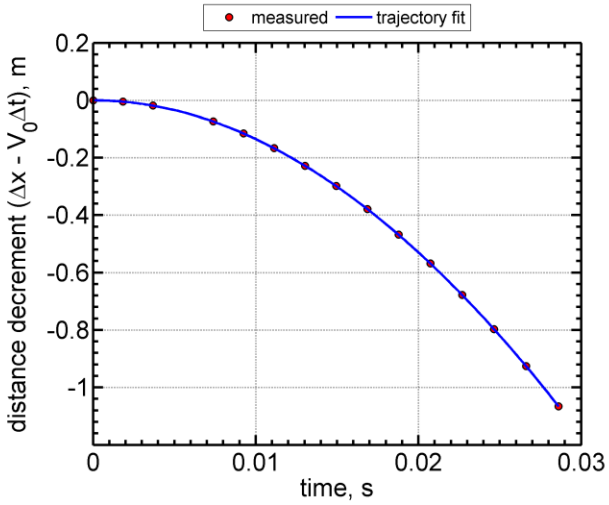

Shot	$\bar{M}_\infty$	$\overline{Re}_d$ (x 10^{-6})	$\bar{V}_\infty$ (m/s)	P_∞ (Torr)	T_∞ (K)	ρ_∞ (kg/m^3)	σ_{RMS} (deg)
2625	2.36	0.420	809	169.4	293.1	0.268	1.5

Station	time, s	x, m	y, m	z, m	V, m/s	M	Re_d (x 10^{-6})	ψ, deg	θ, deg
1	0.00000000	0.047	0.056	0.060	847.91	2.47	0.440	0.8	0.4
2	0.00180938	1.576	0.055	0.059	842.64	2.46	0.437	0.0	1.8
3	0.00362998	3.106	0.054	0.056	837.39	2.44	0.435	-0.6	1.6
4	0.00543795	4.615	0.053	0.054	832.23	2.42	0.432	-0.3	0.4
5	0.00728436	6.148	0.052	0.050	827.03	2.41	0.429	-0.1	-1.4
6	0.00914022	7.677	0.050	0.049	821.85	2.39	0.427	0.6	-2.5
7	0.01098865	9.192	0.048	0.047	816.76	2.38	0.424	0.4	-1.1
8	0.01286403	10.720	0.046	0.046	811.66	2.36	0.421	-0.1	0.4
9	0.01475417	12.248	0.044	0.043	806.57	2.35	0.419	-0.3	1.7
10	0.01664879	13.771	0.043	0.041	801.54	2.34	0.416	-0.4	2.1
11	0.01855880	15.297	0.042	0.039	796.53	2.32	0.413	0.1	0.4
12	0.02048045	16.823	0.040	0.037	791.55	2.31	0.411	0.7	-1.2
13	0.02241221	18.349	0.038	0.033	786.62	2.29	0.408	0.7	-2.0
14	0.02435594	19.872	0.037	0.031	781.72	2.28	0.406	0.5	-1.4
15	0.02630606	21.392	0.035	0.030	776.87	2.26	0.403	-0.1	0.6
16	0.02827949	22.919	0.033	0.026	772.02	2.25	0.401	-0.5	1.9

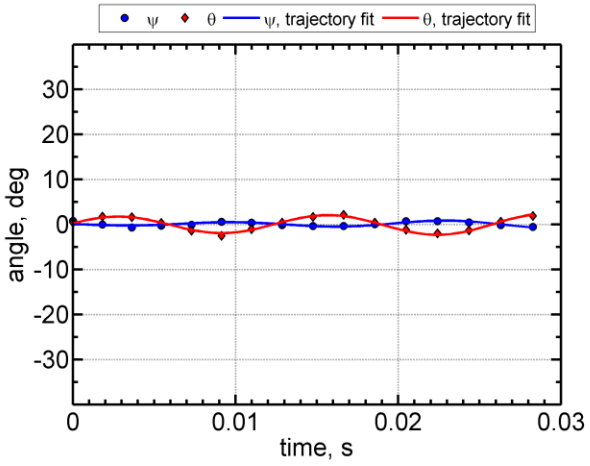

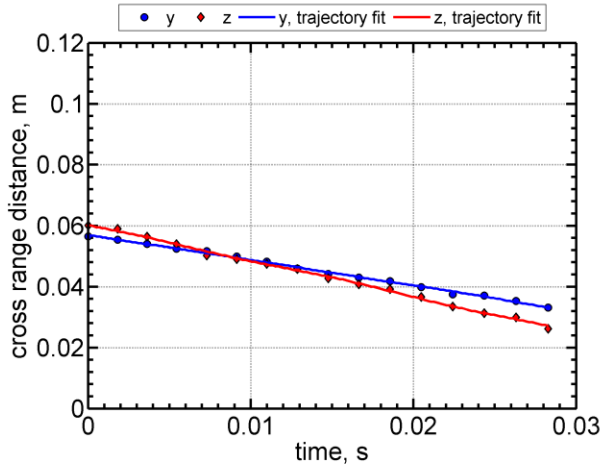

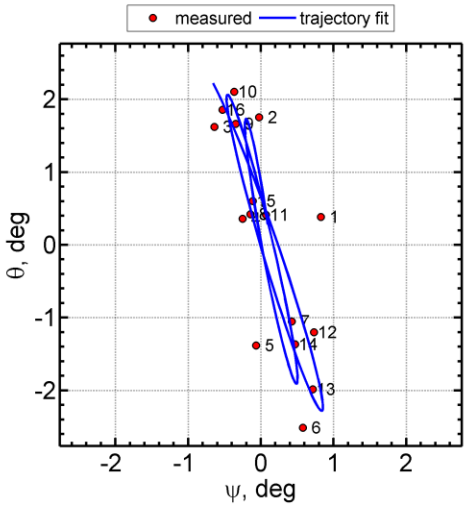

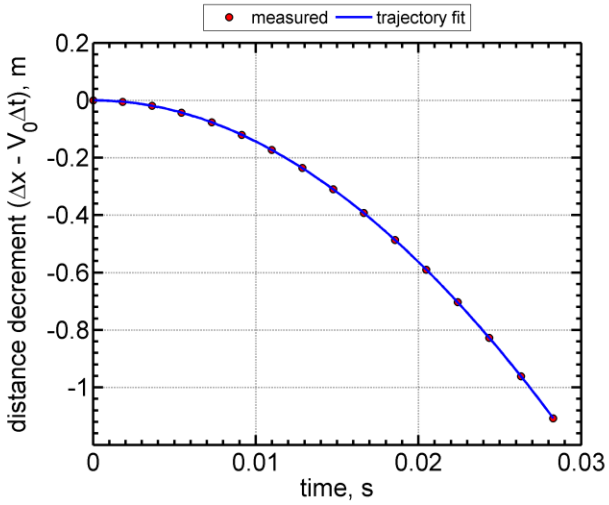

Shot	$\bar{M}_\infty$	$\overline{Re}_d$ (x 10^{-6})	$\bar{V}_\infty$ (m/s)	P_∞ (Torr)	T_∞ (K)	ρ_∞ (kg/m^3)	σ_{RMS} (deg)
2631	2.42	0.428	830	167.7	292.7	0.266	0.7

Station	time, s	x, m	y, m	z, m	V, m/s	M	Re_d (x 10^{-6})	ψ, deg	θ, deg
1	0.00000000	0.048	0.057	0.059	869.29	2.53	0.448	-1.1	-0.4
2	0.00176686	1.578	0.056	0.057	863.91	2.52	0.445	-0.2	0.0
3	0.00354272	3.108	0.055	0.054	858.56	2.50	0.443	0.5	0.2
4	0.00530540	4.616	0.054	0.052	853.30	2.49	0.440	0.6	0.6
5	0.00710776	6.150	0.053	0.048	847.99	2.47	0.437	0.1	0.6
6	0.00891831	7.680	0.052	0.046	842.71	2.46	0.435	-0.5	0.3
7	0.01071992	9.193	0.051	0.044	837.52	2.44	0.432	-0.8	0.2
8	0.01254890	10.722	0.049	0.041	832.31	2.43	0.429	-0.6	0.0
9	0.01439235	12.250	0.048	0.038	827.13	2.41	0.427	0.2	-0.1
10	0.01624245	13.775	0.048	0.035	821.98	2.40	0.424	0.6	0.3
11	0.01810223	15.299	0.047	0.033	816.88	2.38	0.421	0.8	0.7
12	0.01997653	16.826	0.045	0.030	811.80	2.37	0.419	0.2	0.4
13	0.02185999	18.351	0.043	0.027	806.77	2.35	0.416	-0.1	-0.1
14	0.02375572	19.875	0.043	0.023	801.76	2.34	0.413	-0.9	-0.8
15	0.02565645	21.395	0.042	0.021	796.81	2.32	0.411	-0.8	-0.7
16	0.02758055	22.923	0.042	0.019	791.87	2.31	0.408	-0.4	-0.6

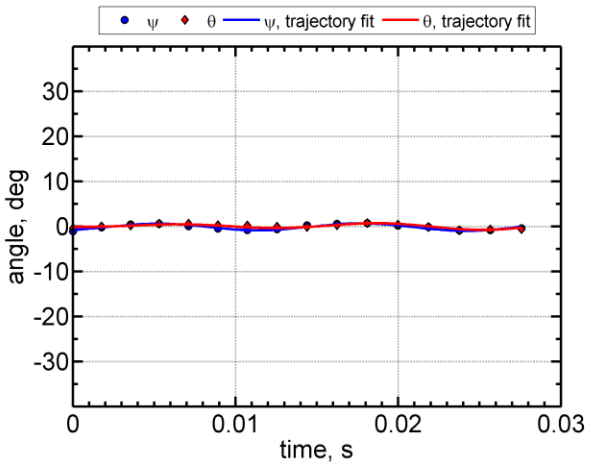

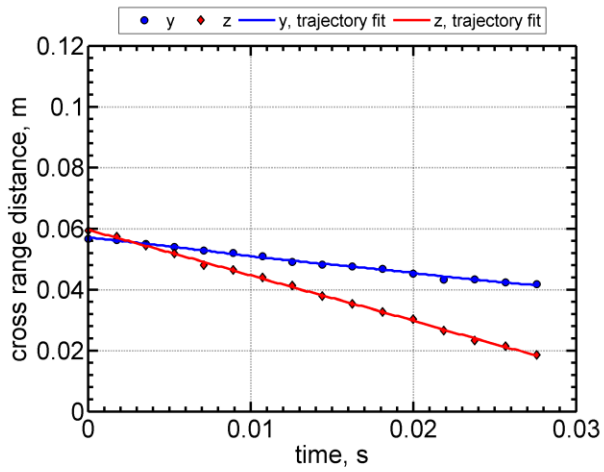

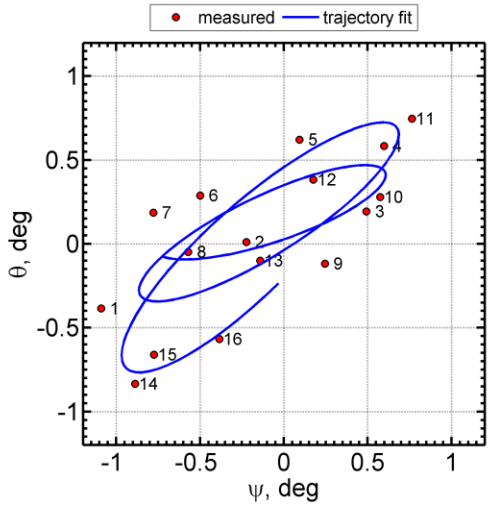

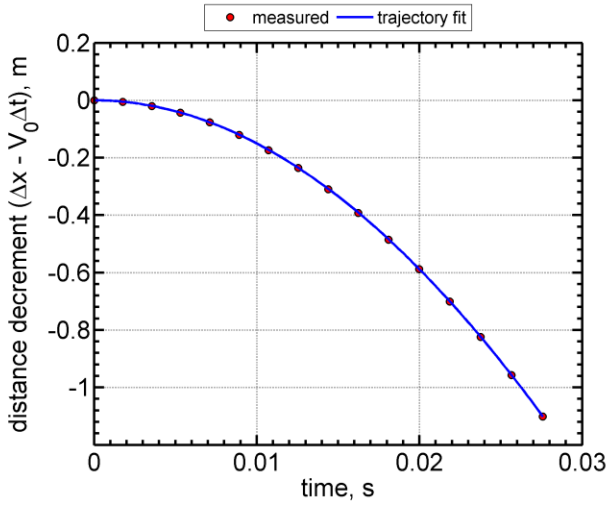

Shot	$\bar{M}_\infty$	$\overline{Re_d}$ (x 10^{-6})	$\bar{V}_\infty$ (m/s)	P_∞ (Torr)	T_∞ (K)	ρ_∞ (kg/m^3)	σ_{RMS} (deg)
2616	2.56	0.441	878	164.2	293.8	0.260	1.5

Station	time, s	x, m	y, m	z, m	V, m/s	M	Re_d (x 10^{-6})	ψ, deg	θ, deg
1	0.00000000	0.047	0.058	0.064	918.31	2.67	0.460	-0.6	0.4
2	0.00166945	1.576	0.058	0.063	912.83	2.66	0.457	-1.9	-0.3
3	0.00335089	3.106	0.057	0.061	907.37	2.64	0.455	-2.2	-0.7
4	0.00501922		0.056		902.00	2.63	0.452	-1.0	
5	0.00672218	6.148	0.056	0.056	896.59	2.61	0.449	0.5	0.0
6	0.00843753	7.681	0.055	0.055	891.19	2.59	0.447	1.5	0.3
7	0.01013836	9.192	0.055	0.054	885.90	2.58	0.444	1.0	0.5
8	0.01186867	10.720	0.053	0.052	880.58	2.56	0.441	-0.7	0.3
9	0.01360902	12.248	0.053	0.049	875.28	2.55	0.439	-2.6	-0.5
10	0.01532308		0.052		870.13	2.53	0.436	-2.1	
11	0.01711337	15.297	0.052	0.046	864.82	2.52	0.433	-0.3	-0.8
12									
13	0.02066504	18.349	0.051	0.043	854.46	2.49	0.428	1.6	0.4
14	0.02245416	19.873	0.052	0.041	849.34	2.47	0.426	0.8	0.4
15	0.02424834	21.392	0.053	0.040	844.28	2.46	0.423	-0.5	0.6
16	0.02606305	22.919	0.052	0.038	839.22	2.44	0.421	-2.4	0.2

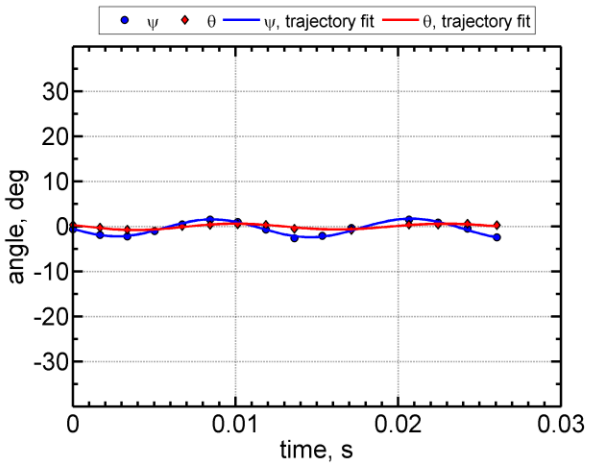

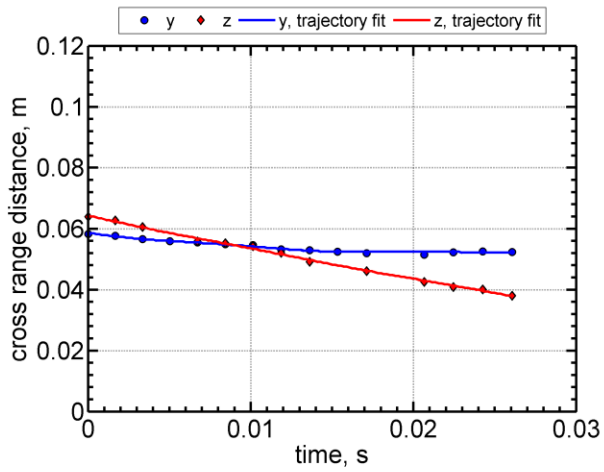

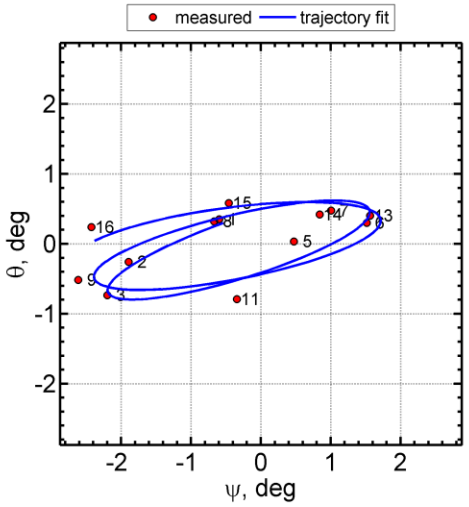

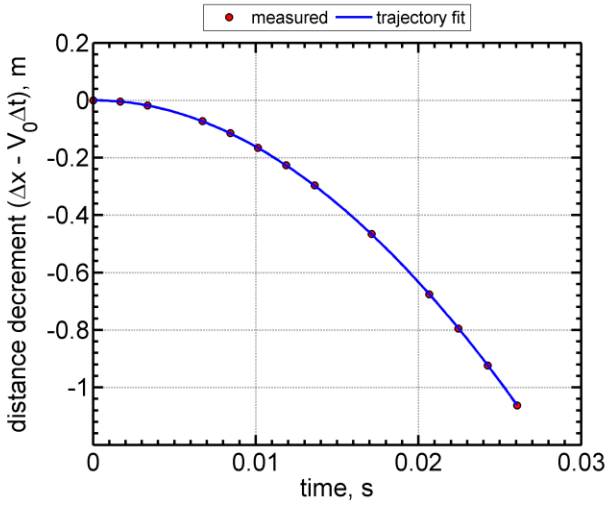

Shot	$\bar{M}_\infty$	$\overline{Re_d}$ (x 10^{-6})	$\bar{V}_\infty$ (m/s)	P_∞ (Torr)	T_∞ (K)	ρ_∞ (kg/m^3)	σ_{RMS} (deg)
2626	2.84	0.484	976	162.4	294.2	0.256	1.0

Station	time, s	x, m	y, m	z, m	V, m/s	M	Re_d (x 10^{-6})	ψ, deg	θ, deg
1	0.00000000	0.049	0.058	0.058	1020.36	2.97	0.505	-0.6	1.0
2	0.00154597	1.581	0.057	0.055	1014.17	2.95	0.502	-0.7	0.6
3	0.00301749	3.109	0.056	0.052	1008.33	2.93	0.499	-1.3	-0.4
4	0.00452368	4.623	0.054	0.049	1002.43	2.92	0.496	-0.5	-0.9
5	0.00605198	6.151	0.054	0.045	996.49	2.90	0.493	0.1	-0.8
6	0.00759188	7.680	0.053	0.043	990.58	2.88	0.490	0.8	-0.1
7	0.00912660	9.196	0.052	0.041	984.75	2.86	0.488	0.8	0.4
8	0.01068050	10.723	0.050	0.039	978.91	2.85	0.485	-0.5	0.7
9	0.01224833	12.252	0.049	0.035	973.09	2.83	0.482	-0.5	0.5
10	0.01381917	13.776	0.048	0.032	967.32	2.81	0.479	-1.3	0.1
11	0.01540051	15.301	0.048	0.029	961.58	2.80	0.476	-0.6	-0.6
12									
13	0.01859244	18.354	0.045	0.024	950.20	2.76	0.470	0.7	0.2
14	0.02020288	19.878	0.045	0.021	944.57	2.75	0.468	0.8	0.8
15	0.02181452	21.397	0.045	0.019	938.99	2.73	0.465	-0.3	1.2
16	0.02344644	22.925	0.044	0.015	933.42	2.71	0.462	-0.9	0.8

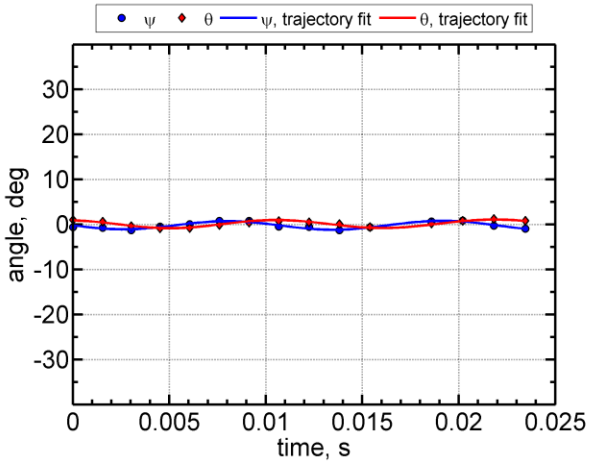

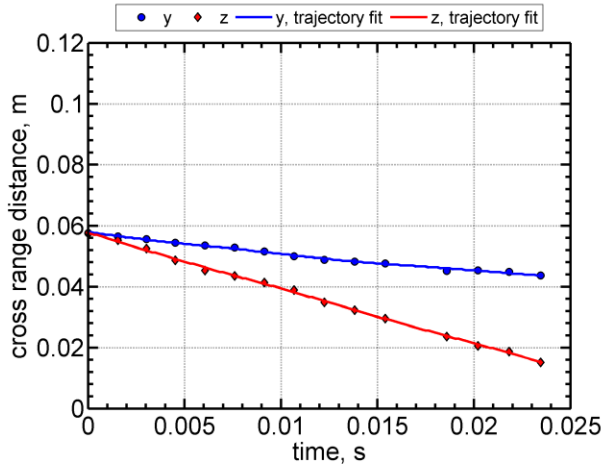

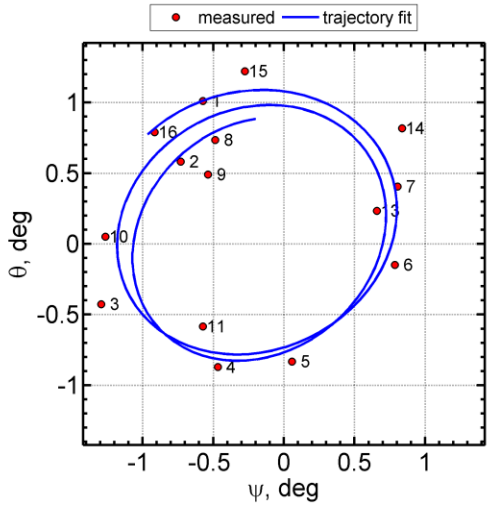

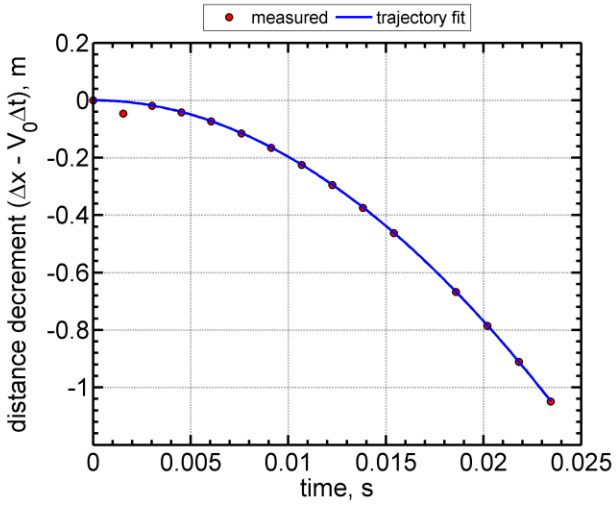

Shot	$\bar{M}_\infty$	$\overline{Re}_d$ (x 10^{-6})	$\bar{V}_\infty$ (m/s)	P_∞ (Torr)	T_∞ (K)	ρ_∞ (kg/m^3)	σ_{RMS} (deg)
2617	2.97	0.499	1023	160.5	294.4	0.253	1.7

Station	time, s	x, m	y, m	z, m	V, m/s	M	Re_d (x 10^{-6})	ψ, deg	θ, deg
1	0.00000000	0.049	0.057	0.065	1061.77	3.09	0.518	0.0	1.4
2	0.00144467	1.578	0.057	0.063	1055.61	3.07	0.515	-0.6	-0.8
3	0.00289732	3.106	0.055	0.061	1049.48	3.05	0.512	-0.9	-1.9
4	0.00434088	4.618	0.055	0.059	1043.45	3.03	0.510	-0.5	-1.9
5	0.00581455	6.150	0.054	0.056	1037.35	3.02	0.507	-0.1	0.6
6	0.00730716	7.694	0.053	0.056	1031.25	3.00	0.504	0.1	1.9
7	0.00876625	9.194	0.052	0.054	1025.35	2.98	0.501	0.2	2.3
8	0.01026073	10.722	0.050	0.052	1019.37	2.96	0.498	-0.5	0.8
9	0.01176356	12.250	0.049	0.049	1013.42	2.95	0.495	-0.7	-1.1
10	0.01327199	13.774	0.049	0.047	1007.52	2.93	0.492	-0.4	-2.0
11	0.01478945	15.299		0.046	1001.65	2.91	0.489		-1.4
12	0.01631839	16.825	0.048	0.045	995.80	2.90	0.486	0.4	0.5
13	0.01785488	18.351	0.046	0.042	990.00	2.88	0.483	0.3	2.2
14	0.01939727	19.874	0.047	0.039	984.25	2.86	0.481	-0.2	2.5
15									
16									

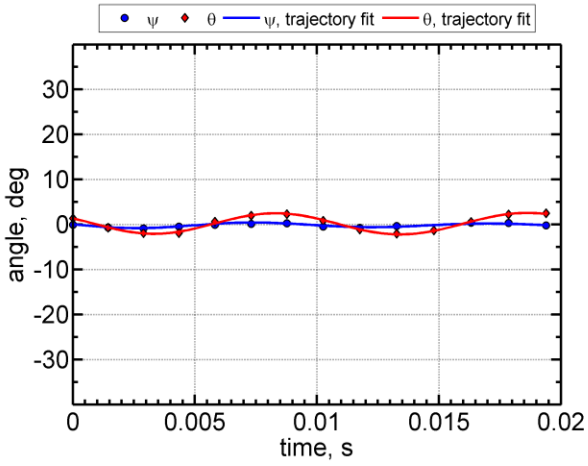

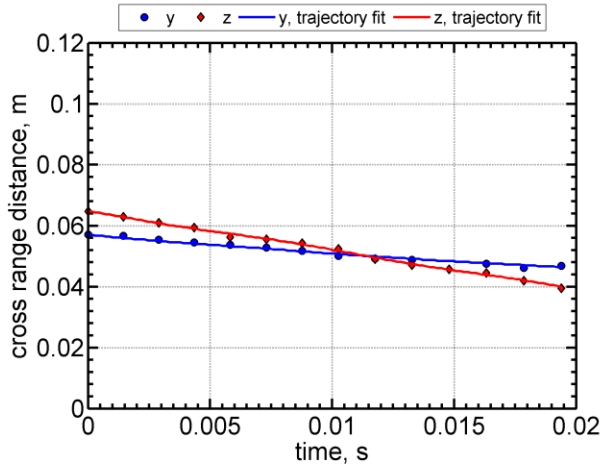

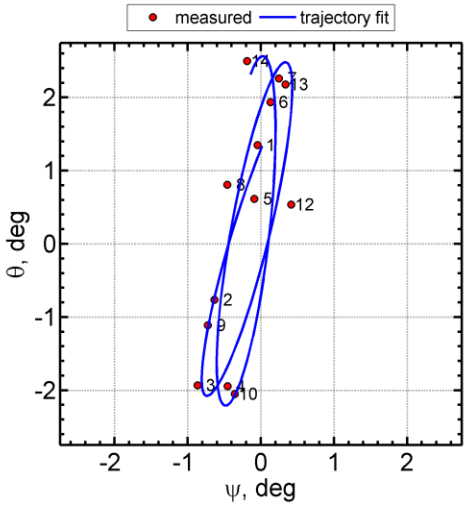

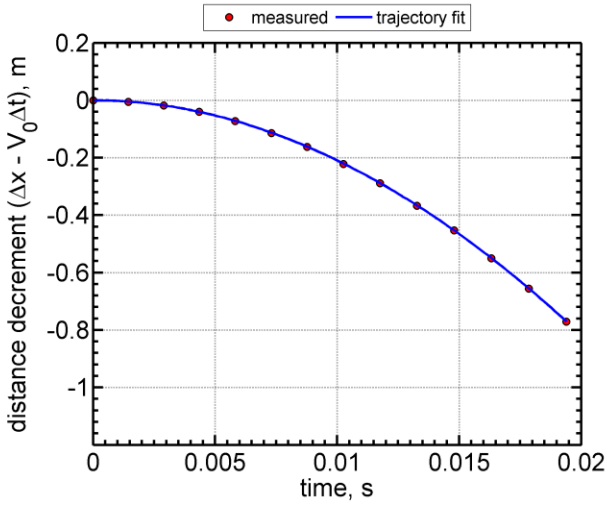

Shot	$\bar{M}_\infty$	$\overline{Re}_d$ (x 10^{-6})	$\bar{V}_\infty$ (m/s)	P_∞ (Torr)	T_∞ (K)	ρ_∞ (kg/m^3)	σ_{RMS} (deg)
2653	3.10	0.513	1071	158.0	294.4	0.249	0.7

Station	time, s	x, m	y, m	z, m	V, m/s	M	Re_d (x 10^{-6})	ψ, deg	θ, deg
1	0.00000000	0.050	0.056	0.058	1113.86	3.24	0.536	0.3	-0.1
2	0.00138004	1.582	0.055	0.056	1107.53	3.22	0.533	-0.1	0.5
3	0.00276569	3.113	0.054	0.053	1101.24	3.20	0.530	-0.3	0.7
4	0.00413705	4.618	0.053	0.050	1095.07	3.18	0.527	-0.3	0.7
5	0.00554014	6.151	0.052	0.046	1088.83	3.17	0.524	-0.8	-0.1
6	0.00695367	7.685	0.050	0.045	1082.60	3.15	0.521	-0.4	-0.4
7	0.00835409	9.197	0.050	0.042	1076.49	3.13	0.518	0.4	-0.7
8	0.00977547	10.724	0.047	0.040	1070.36	3.11	0.515	0.2	-0.5
9	0.01121161	12.255	0.046	0.036	1064.23	3.09	0.512	0.0	0.6
10	0.01264050	13.772	0.045	0.034	1058.19	3.08	0.509	-0.4	0.9
11	0.01409049	15.302	0.044	0.032	1052.14	3.06	0.506	-0.7	1.0
12	0.01554951	16.832	0.043	0.029	1046.12	3.04	0.503	-0.3	0.2
13	0.01700739	18.355	0.041	0.025	1040.17	3.02	0.500	0.1	0.0
14	0.01848200	19.883	0.041	0.023	1034.22	3.01	0.497	0.6	-0.6
15	0.01994974	21.398	0.041	0.020	1028.37	2.99	0.495	0.7	-0.1
16	0.02144035		0.039		1022.50	2.97	0.492	-0.4	

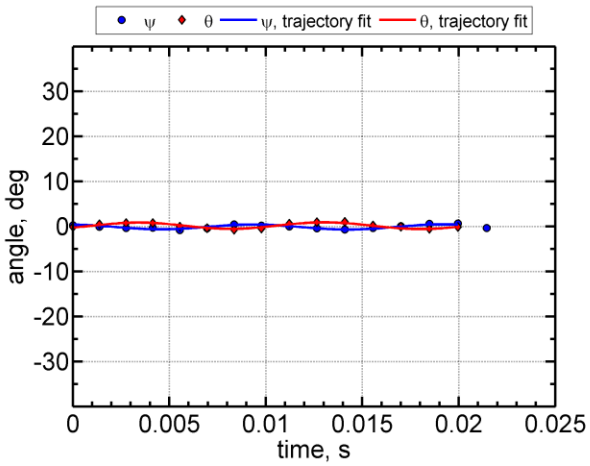

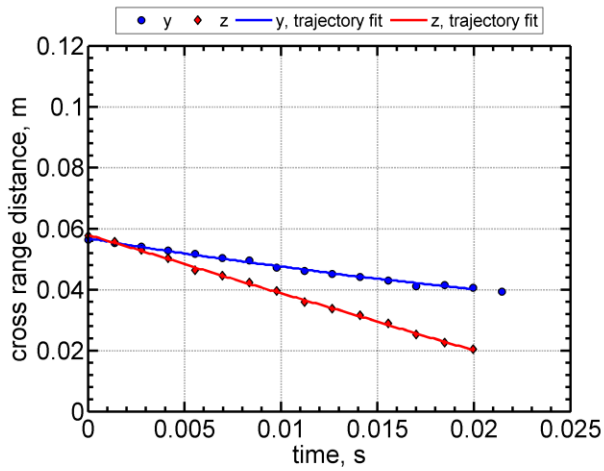

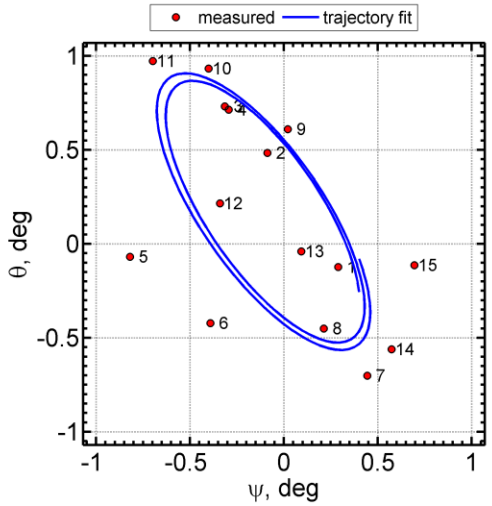

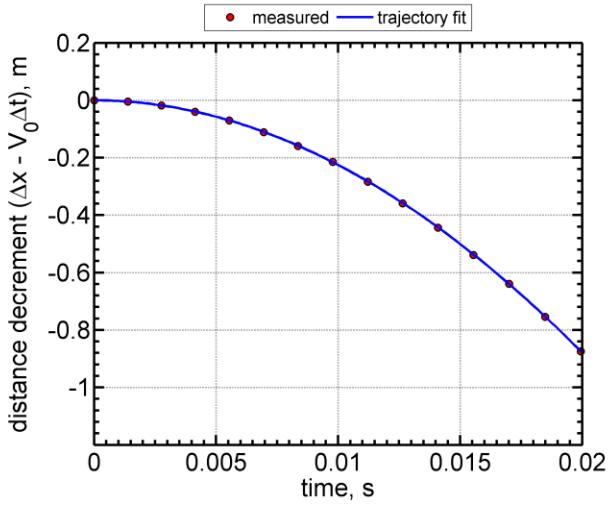

Shot	$\bar{M}_\infty$	$\overline{Re_d}$ (x 10^{-6})	$\bar{V}_\infty$ (m/s)	P_∞ (Torr)	T_∞ (K)	ρ_∞ (kg/m^3)	σ_{RMS} (deg)
2627	3.47	0.564	1190	155.0	293.7	0.245	0.9

Station	time, s	x, m	y, m	z, m	V, m/s	M	Re_d (x 10^{-6})	ψ, deg	θ, deg
1	0.00000000	0.051	0.059	0.058	1240.51	3.61	0.588	-1.2	0.3
2	0.00123843	1.582	0.058	0.056	1233.69	3.59	0.584	-0.3	-0.1
3	0.00248100	3.111	0.057	0.053	1226.90	3.57	0.581	0.4	-0.6
4	0.00371311	4.619	0.056	0.050	1220.23	3.55	0.578	0.9	-0.2
5	0.00497237	6.152	0.055	0.046	1213.47	3.53	0.575	0.4	0.2
6	0.00623867	7.684	0.054	0.044	1206.75	3.51	0.572	-0.8	0.1
7	0.00749675	9.198	0.054	0.042	1200.13	3.49	0.569	-1.1	0.1
8	0.00877171	10.725	0.052	0.040	1193.50	3.47	0.565	-1.0	0.2
9	0.01005770	12.254	0.051	0.036	1186.87	3.45	0.562	0.4	-0.3
10	0.01134761	13.781	0.051	0.033	1180.29	3.44	0.559	1.0	-0.2
11	0.01264089	15.303	0.050	0.031	1173.76	3.42	0.556	0.9	-0.1
12	0.01394585	16.830	0.049	0.029	1167.24	3.40	0.553	0.0	0.4
13	0.01525570	18.356	0.047	0.025	1160.77	3.38	0.550	-0.8	0.4
14	0.01657345	19.880	0.048	0.022	1154.33	3.36	0.547	-1.5	0.2
15	0.01789154	21.398	0.048	0.020	1147.96	3.34	0.544	-0.8	0.3
16	0.01922754	22.927	0.047	0.017	1141.57	3.32	0.541	0.0	-0.7

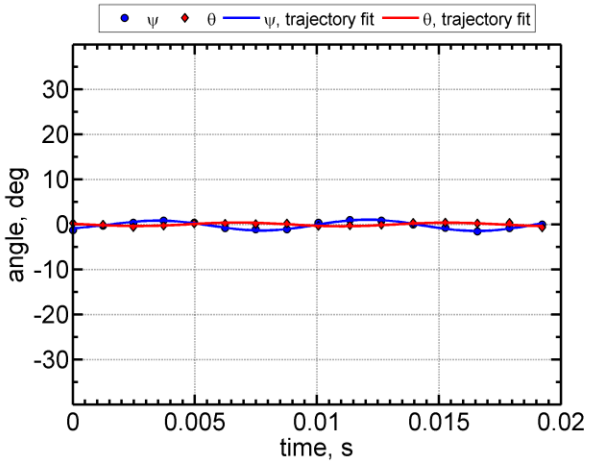

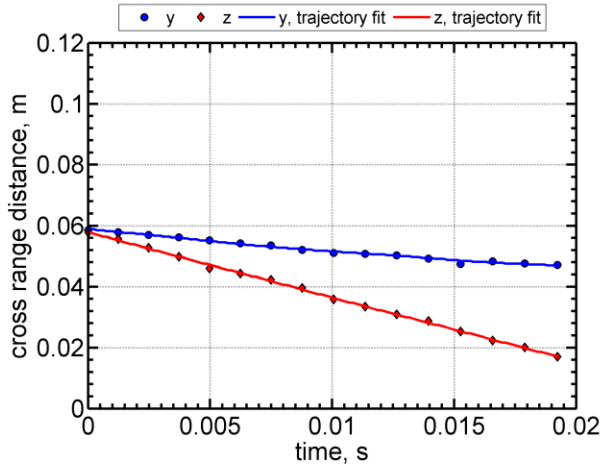

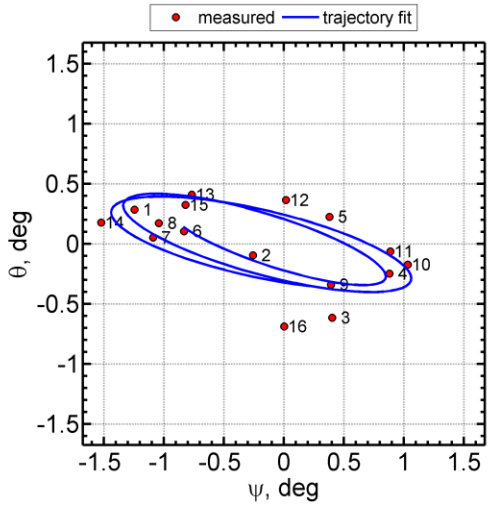

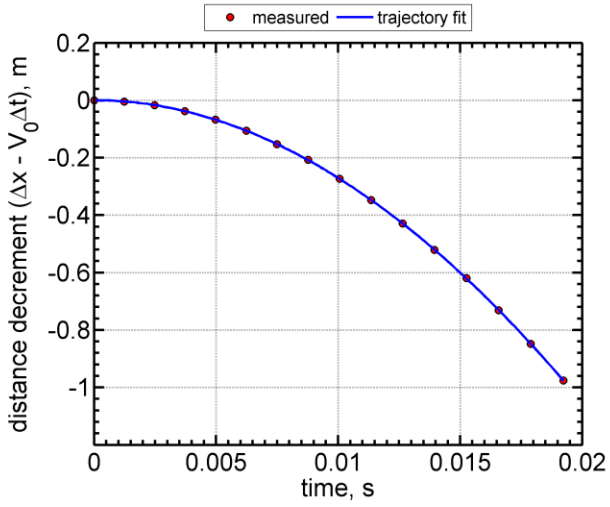

Shot	$\bar{M}_\infty$	$\overline{Re}_d$ (x 10^{-6})	$\bar{V}_\infty$ (m/s)	P_∞ (Torr)	T_∞ (K)	ρ_∞ (kg/m^3)	σ_{RMS} (deg)
2652	3.62	0.564	1248	149.0	294.9	0.235	1.3

Station	time, s	x, m	y, m	z, m	V, m/s	M	Re_d (x 10^{-6})	ψ, deg	θ, deg
1	0.00000000	0.051	0.058	0.060	1297.40	3.77	0.587	0.6	-0.6
2	0.00118599	1.586	0.057	0.059	1290.62	3.75	0.584	0.4	-0.1
3	0.00237045	3.111	0.056	0.056	1283.90	3.73	0.581	-1.0	1.1
4	0.00354808	4.619	0.055	0.054	1277.29	3.71	0.578	-1.1	1.2
5	0.00475086	6.152	0.054	0.051	1270.59	3.69	0.575	-0.9	0.1
6	0.00596679	7.692	0.052	0.050	1263.88	3.67	0.572	0.5	-0.7
7	0.00716177	9.199	0.052	0.048	1257.35	3.65	0.569	0.7	-1.5
8	0.00837669	10.724	0.050	0.045	1250.77	3.63	0.566	0.7	-1.2
9	0.00960661		0.049		1244.17	3.61	0.563	0.1	
10	0.01083003	13.775	0.048	0.040	1237.67	3.60	0.560	-0.9	1.2
11	0.01206721	15.302	0.048	0.038	1231.16	3.58	0.557	-1.4	2.0
12	0.01331319	16.831	0.046	0.037	1224.66	3.56	0.554	-0.8	0.8
13	0.01456051	18.356	0.045	0.034	1218.23	3.54	0.551	0.2	-0.9
14	0.01581935	19.884	0.045	0.031	1211.80	3.52	0.548	1.5	-1.3
15	0.01707019	21.396	0.045	0.030	1205.48	3.50	0.545	1.7	-0.6
16	0.01834151	22.925	0.043	0.027	1199.13	3.48	0.542	-0.1	0.5

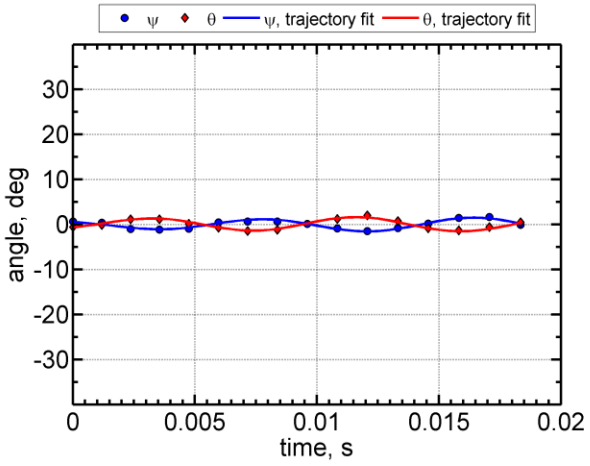

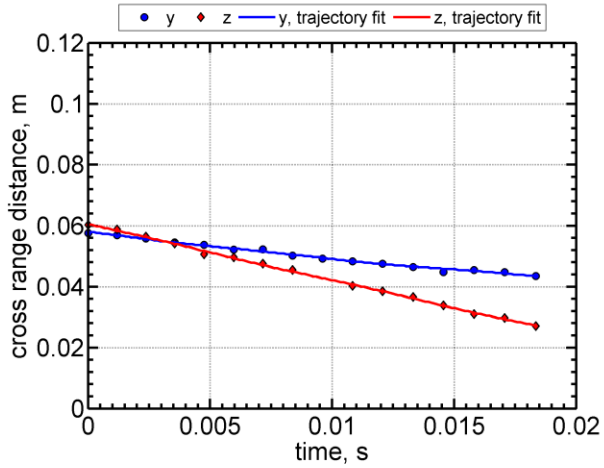

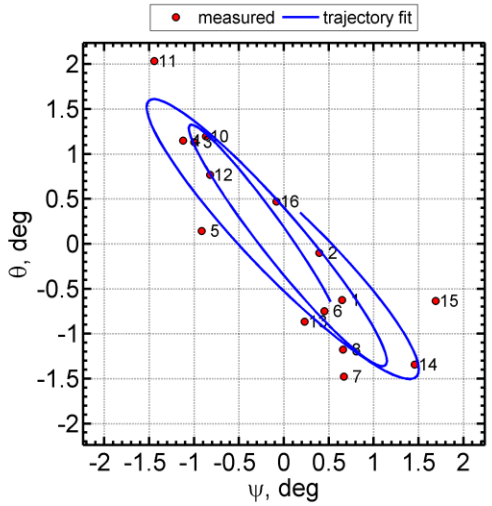

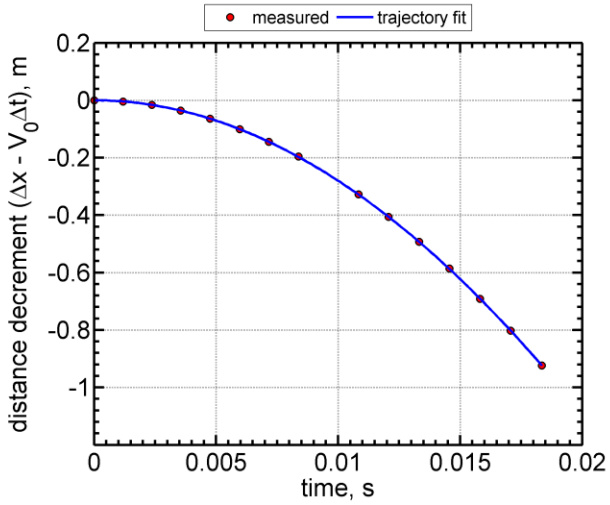

Shot	$\bar{M}_\infty$	$\overline{Re}_d$ (x 10^{-6})	$\bar{V}_\infty$ (m/s)	P_∞ (Torr)	T_∞ (K)	ρ_∞ (kg/m^3)	σ_{RMS} (deg)
2620	2.39	0.425	818	169.4	292.8	0.269	5.2

Station	time, s	x, m	y, m	z, m	V, m/s	M	Re_d (x 10^{-6})	ψ, deg	θ, deg
1	0.00000000	0.046	0.057	0.064	856.62	2.50	0.445	0.5	-1.2
2	0.00179024	1.575	0.056	0.064	851.35	2.48	0.443	-0.1	4.5
3	0.00359436	3.106	0.054	0.063	846.09	2.47	0.440	-1.0	7.4
4	0.00538309	4.616	0.053	0.062	840.94	2.45	0.437	-1.0	4.9
5	0.00720938	6.146	0.052	0.058	835.73	2.44	0.435	-0.2	-1.1
6	0.00905397	7.682	0.051	0.058	830.54	2.42	0.432	1.0	-6.5
7	0.01087502	9.191	0.050	0.056	825.46	2.41	0.429	1.4	-7.0
8	0.01273203	10.719	0.047	0.057	820.35	2.39	0.427	0.6	-2.3
9	0.01460072	12.247	0.045	0.055	815.27	2.38	0.424	-0.7	3.8
10	0.01649106	13.783	0.044	0.056	810.19	2.36	0.421	-1.9	6.9
11	0.01836291	15.295	0.043	0.055	805.22	2.35	0.419	-1.3	5.3
12	0.02026399	16.821	0.041	0.053	800.24	2.33	0.416	-0.2	-0.3
13	0.02217388	18.346	0.039	0.051	795.30	2.32	0.413	1.4	-5.9
14	0.02409716	19.869	0.039	0.049	790.39	2.30	0.411	2.4	-7.5
15	0.02602489	21.389	0.038	0.049	785.54	2.29	0.408	1.0	-3.6
16	0.02797503	22.916	0.035	0.049	780.70	2.28	0.406	-0.8	2.6

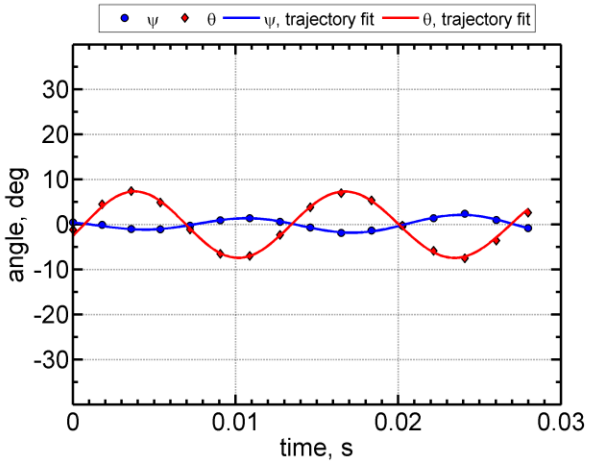

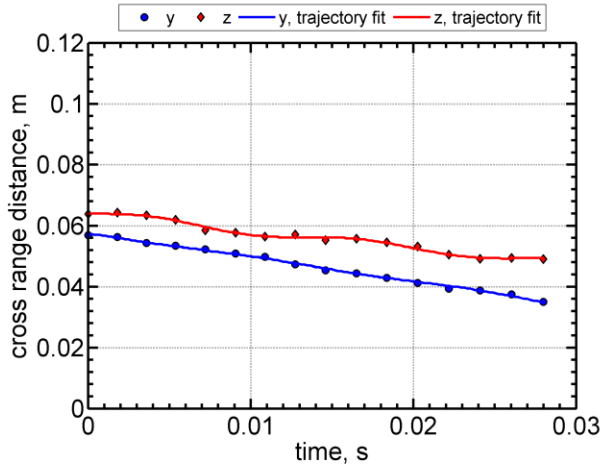

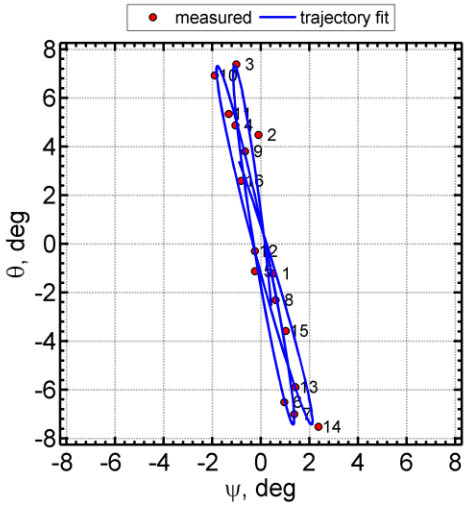

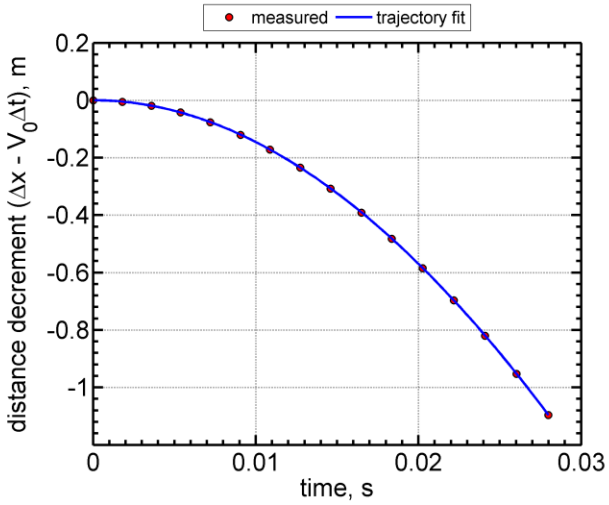

Shot	$\bar{M}_\infty$	$\overline{Re}_d$ (x 10^{-6})	$\bar{V}_\infty$ (m/s)	P_∞ (Torr)	T_∞ (K)	ρ_∞ (kg/m^3)	σ_{RMS} (deg)
2629	2.42	0.426	832	167.7	293.9	0.265	3.2

Station	time, s	x, m	y, m	z, m	V, m/s	M	Re_d (x 10^{-6})	ψ, deg	θ, deg
1	0.00000000	0.047	0.057	0.062	871.20	2.53	0.446	-0.9	-1.5
2	0.00176218	1.577	0.056	0.062	865.84	2.52	0.443	-0.9	1.3
3	0.00353362	3.105	0.055	0.060	860.52	2.50	0.441	0.5	3.3
4	0.00529362	4.615	0.054	0.058	855.28	2.49	0.438	1.4	3.0
5	0.00708970	6.147	0.054	0.055	850.00	2.47	0.435	0.8	-0.1
6									
7	0.01069341	9.191	0.051	0.053	839.58	2.44	0.430	-1.2	-4.5
8	0.01251873	10.719	0.049	0.051	834.39	2.43	0.427	-1.9	-2.0
9	0.01435740	12.248	0.048	0.049	829.23	2.41	0.424	-1.0	1.5
10	0.01620497	13.775	0.048	0.048	824.11	2.40	0.422	0.4	4.3
11	0.01805689	15.297	0.047	0.046	819.04	2.38	0.419	1.5	3.7
12	0.01992687	16.823	0.046	0.045	813.98	2.37	0.417	1.5	0.7
13	0.02180386	18.348	0.044	0.041	808.97	2.35	0.414	0.5	-3.1
14	0.02369509	19.872	0.044	0.039	803.99	2.34	0.412	-1.1	-5.2
15	0.02558987	21.392	0.043	0.038	799.06	2.33	0.409	-2.5	-3.0
16	0.02750724	22.919	0.043	0.037	794.15	2.31	0.407	-2.2	1.2

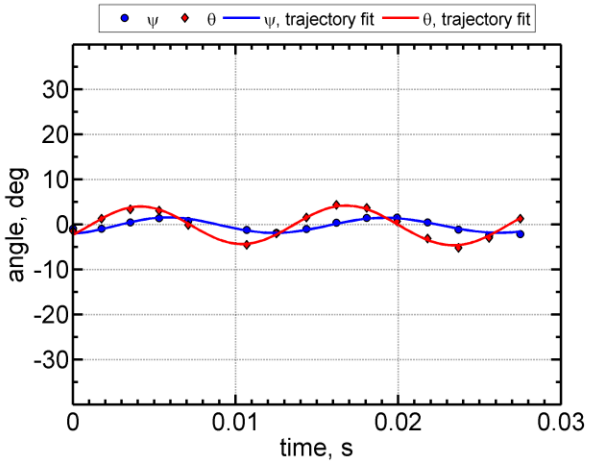

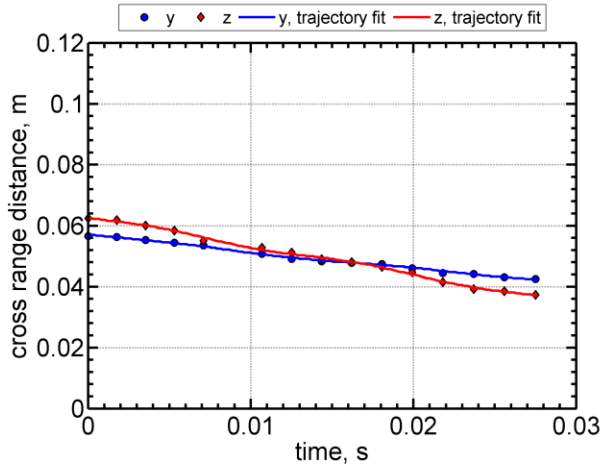

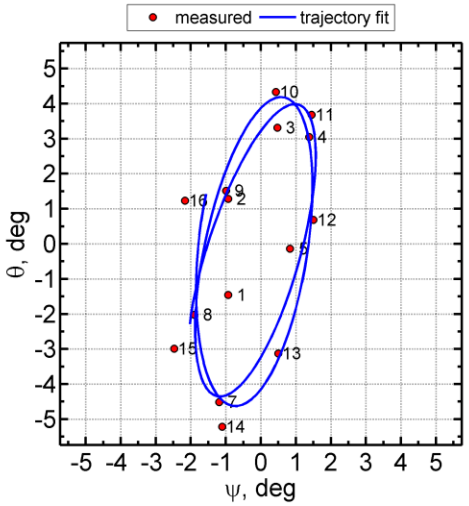

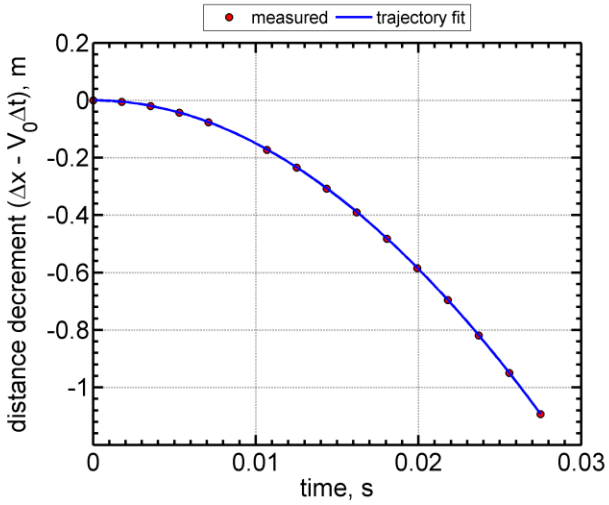

Shot	$\bar{M}_\infty$	$\overline{Re}_d$ (x 10^{-6})	$\bar{V}_\infty$ (m/s)	P_∞ (Torr)	T_∞ (K)	ρ_∞ (kg/m^3)	σ_{RMS} (deg)
2639	2.64	0.454	907	164.2	294.0	0.259	3.0

Station	time, s	x, m	y, m	z, m	V, m/s	M	Re_d (x 10^{-6})	ψ, deg	θ, deg
1	0.00000000	0.048	0.057	0.061	948.97	2.76	0.476	-0.6	-0.7
2	0.00161956	1.580	0.057	0.061	943.29	2.74	0.473	0.5	2.5
3	0.00324446	3.108	0.056	0.059	937.64	2.73	0.470	1.2	4.3
4	0.00485804	4.617	0.055	0.057	932.09	2.71	0.467	0.7	2.7
5	0.00650753	6.150	0.054	0.053	926.47	2.70	0.464	-0.7	-1.0
6									
7	0.00981376	9.194	0.053	0.051	915.40	2.66	0.459	-1.7	-3.7
8	0.01148578	10.721	0.051	0.049	909.90	2.65	0.456	-0.9	-0.7
9	0.01317503	12.253	0.051	0.047	904.41	2.63	0.453	0.9	2.4
10	0.01485551	13.768	0.051	0.046	899.00	2.62	0.451	2.0	4.3
11	0.01656285	15.298	0.050	0.045	893.58	2.60	0.448	1.4	2.0
	0.01827775	16.826	0.049	0.043	888.20	2.58	0.445	-0.7	-0.7
13	0.01999787	18.350	0.047	0.040	882.86	2.57	0.442	-2.0	-3.4
14	0.02173237	19.876	0.047	0.038	877.56	2.55	0.440	-2.4	-3.5
15	0.02346495	21.393	0.047	0.037	872.32	2.54	0.437	-0.8	-0.6
16	0.02522420	22.923	0.046	0.036	867.07	2.52	0.435	1.2	2.2

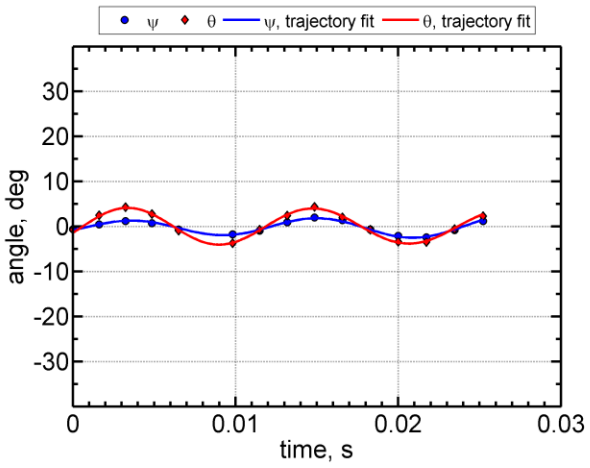

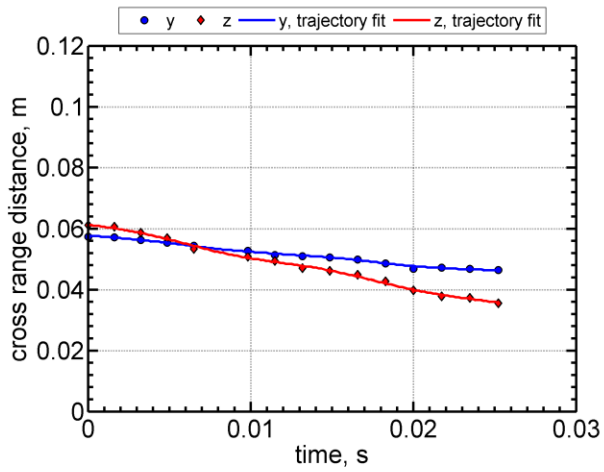

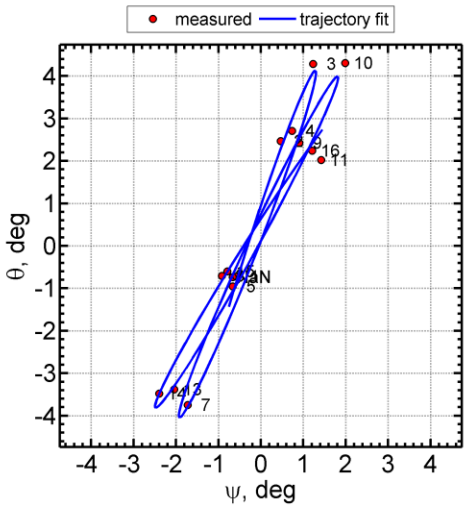

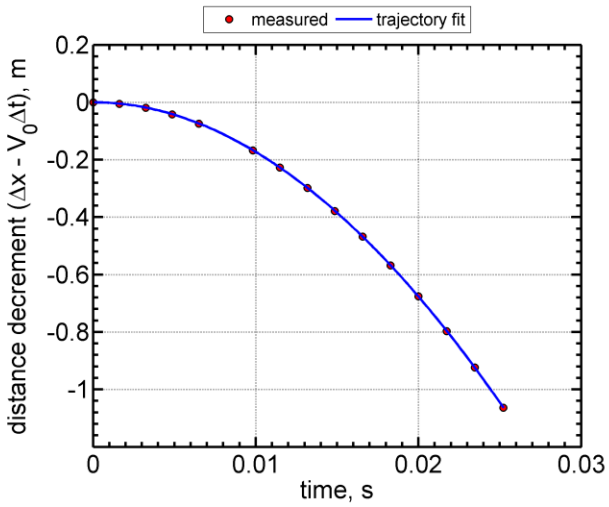

Shot	$\bar{M}_\infty$	$\overline{Re}_d$ (x 10^{-6})	$\bar{V}_\infty$ (m/s)	P_∞ (Torr)	T_∞ (K)	ρ_∞ (kg/m^3)	σ_{RMS} (deg)
2654	2.74	0.473	936	163.0	291.5	0.260	5.8

Station	time, s	x, m	y, m	z, m	V, m/s	M	Re_d (x 10^{-6})	ψ, deg	θ, deg
1	0.00000000	0.049	0.056	0.060	978.94	2.86	0.495	-0.7	-2.2
2	0.00156975	1.581	0.056	0.060	973.12	2.84	0.492	0.2	4.9
3	0.00314641	3.111	0.055	0.058	967.33	2.83	0.489	0.5	8.3
4	0.00470799	4.617	0.054	0.056	961.66	2.81	0.486	0.1	5.6
5	0.00630494	6.148	0.052	0.052	955.92	2.79	0.483	-0.4	-1.2
6	0.00791486	7.682	0.051	0.050	950.19	2.78	0.480	-0.6	-7.4
7	0.00951002	9.194	0.050	0.049	944.58	2.76	0.477	-0.6	-8.2
8	0.01113165	10.722	0.048	0.048	938.94	2.74	0.474	-0.2	-2.2
9	0.01276773	12.253	0.047	0.046	933.32	2.73	0.471	0.4	4.9
10	0.01439932	13.770	0.047	0.045	927.77	2.71	0.469	-0.2	8.4
11	0.01605150	15.299	0.046	0.043	922.22	2.69	0.466	-0.3	6.1
12	0.01771625	16.829	0.045	0.041	916.70	2.68	0.463	-0.5	-1.0
13	0.01937928	18.351	0.043	0.037	911.25	2.66	0.460	-0.3	-6.8
14	0.02105984	19.876	0.043	0.035	905.81	2.65	0.458	0.2	-7.8
15	0.02273918	21.393	0.042	0.035	900.44	2.63	0.455	0.9	-2.9
16	0.02444241	22.922	0.042	0.033	895.06	2.62	0.452	0.9	

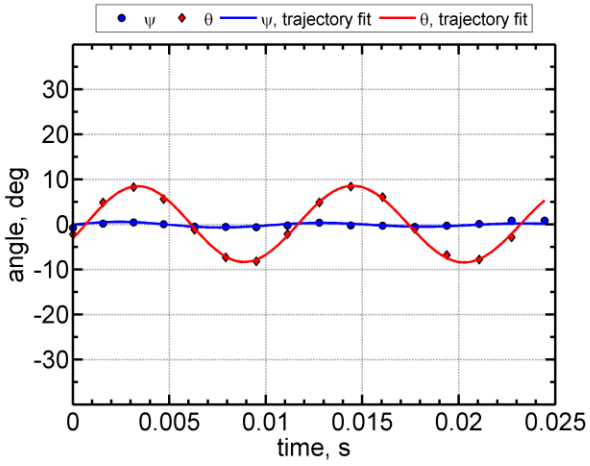

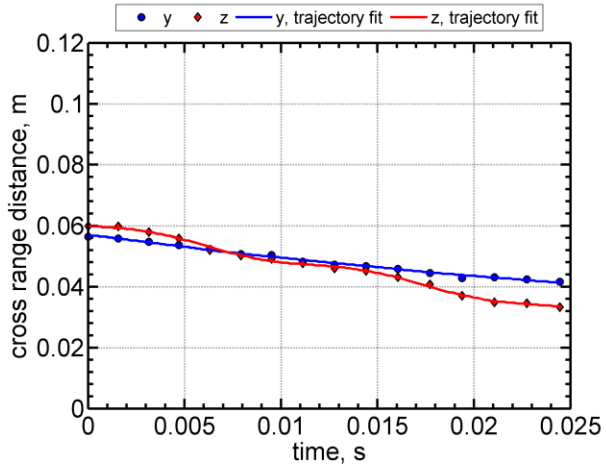

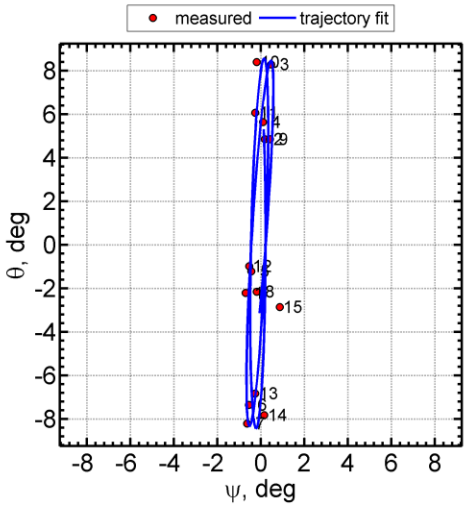

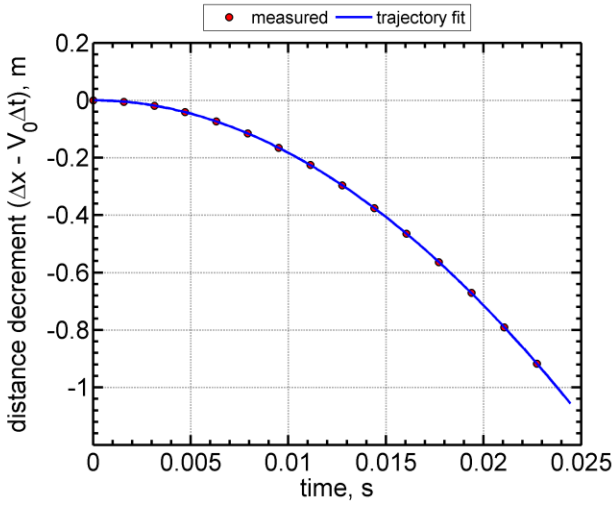

Shot	$\bar{M}_\infty$	$\overline{Re_d}$ (x 10^{-6})	$\bar{V}_\infty$ (m/s)	P_∞ (Torr)	T_∞ (K)	ρ_∞ (kg/m^3)	σ_{RMS} (deg)
2628	2.90	0.495	995	162.4	293.3	0.257	5.3

Station	time, s	x, m	y, m	z, m	V, m/s	M	Re_d (x 10^{-6})	ψ, deg	θ, deg
1	0.00000000	0.049	0.057	0.062	1039.71	3.03	0.517	0.4	-1.9
2	0.00147756		0.056		1033.61	3.01	0.514	-0.2	
3	0.00296024	3.108	0.055	0.061	1027.55	2.99	0.511	-0.3	7.7
4	0.00443365	4.617	0.054	0.059	1021.60	2.98	0.508	-0.6	4.8
5	0.00593775	6.149	0.053	0.056	1015.58	2.96	0.505	-0.3	-1.7
6	0.00745098	7.681	0.052	0.054	1009.59	2.94	0.502	-0.1	-7.4
7	0.00895362	9.193	0.052	0.053	1003.70	2.92	0.499	0.3	-7.0
8	0.01047905	10.721	0.050	0.053	997.79	2.91	0.497	0.3	-1.7
9	0.01201672	12.250	0.049	0.051	991.90	2.89	0.494	-0.1	4.8
10	0.01355764	13.773	0.048	0.051	986.06	2.87	0.491	-1.1	7.1
11	0.01510846	15.299	0.047	0.049	980.26	2.86	0.488	-1.0	4.6
12	0.01667097	16.825	0.046	0.047	974.48	2.84	0.485	-0.3	-1.5
13	0.01823815	18.350	0.045	0.044	968.75	2.82	0.482	0.5	-7.0
14	0.01981699	19.873	0.045	0.042	963.04	2.81	0.479	0.7	-7.0
15	0.02139767	21.392	0.044	0.042	957.40	2.79	0.476	0.7	-1.5
16	0.02299802	22.920	0.043	0.042	951.77	2.77	0.474	-0.6	5.0

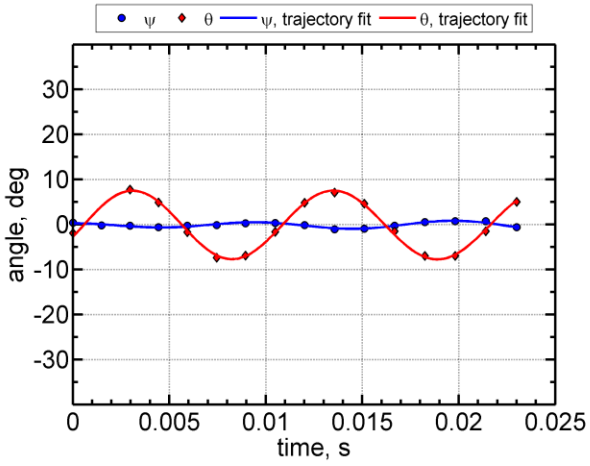

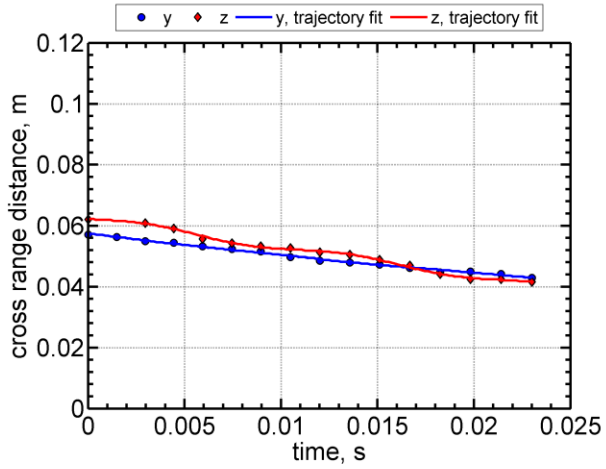

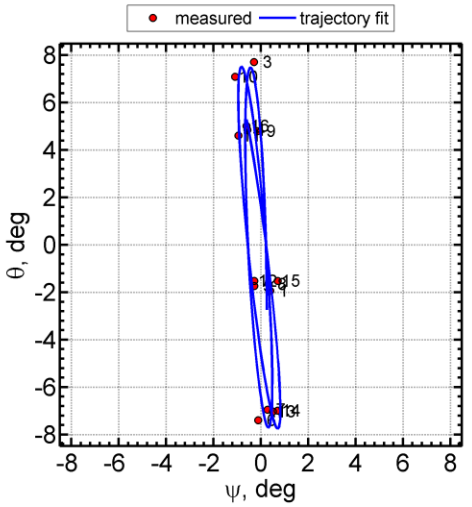

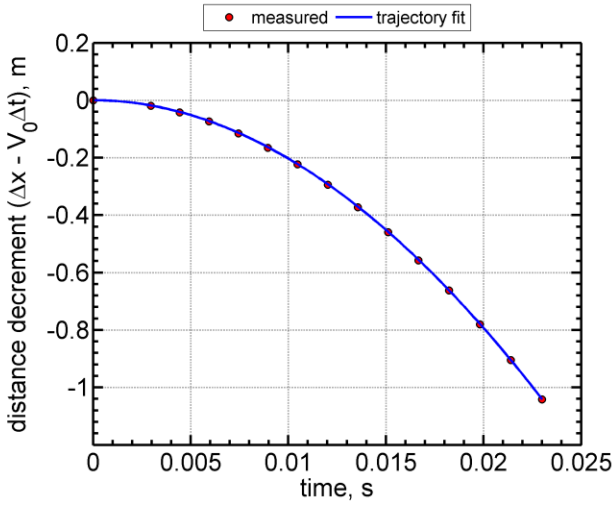

Shot	$\bar{M}_\infty$	$\overline{Re}_d$ (x 10^{-6})	$\bar{V}_\infty$ (m/s)	P_∞ (Torr)	T_∞ (K)	ρ_∞ (kg/m^3)	σ_{RMS} (deg)
2640	3.24	0.536	1115	158.0	293.8	0.250	4.1

Station	time, s	x, m	y, m	z, m	V, m/s	M	Re_d (x 10^{-6})	ψ, deg	θ, deg
1	0.00000000	0.050	0.056	0.060	1159.33	3.37	0.559	-0.9	0.9
2	0.00132578	1.583	0.055	0.056	1152.81	3.35	0.556	0.7	-3.7
3	0.00265268	3.108	0.054	0.053	1146.33	3.34	0.553	1.9	-5.0
4	0.00397312	4.618	0.053	0.051	1139.96	3.32	0.550	1.1	-2.7
5	0.00532098	6.150	0.051	0.047	1133.51	3.30	0.547	-0.2	2.8
6	0.00667796	7.684	0.050	0.046	1127.09	3.28	0.544	-2.3	5.0
7	0.00802355	9.196	0.049	0.044	1120.78	3.26	0.541	-2.8	4.3
8	0.00938833	10.723	0.047	0.040	1114.46	3.24	0.538	-0.7	0.4
9	0.01076776	12.255	0.046	0.036	1108.13	3.22	0.535	1.6	-4.4
10	0.01214014	13.771	0.045	0.033	1101.90	3.21	0.532	2.3	-4.9
11	0.01353312	15.302	0.044	0.031	1095.65	3.19	0.529	1.2	-1.1
12	0.01493150	16.829	0.042	0.029	1089.44	3.17	0.526	-0.9	3.2
13	0.01633513	18.355	0.040	0.025	1083.28	3.15	0.523	-2.7	5.6
14	0.01774744	19.879	0.041	0.022	1077.15	3.13	0.520	-2.7	4.0
15	0.01916052	21.398	0.040	0.019	1071.09	3.12	0.517	-0.3	-0.2
16	0.02059066	22.925		0.015	1065.04	3.10	0.514		-4.4

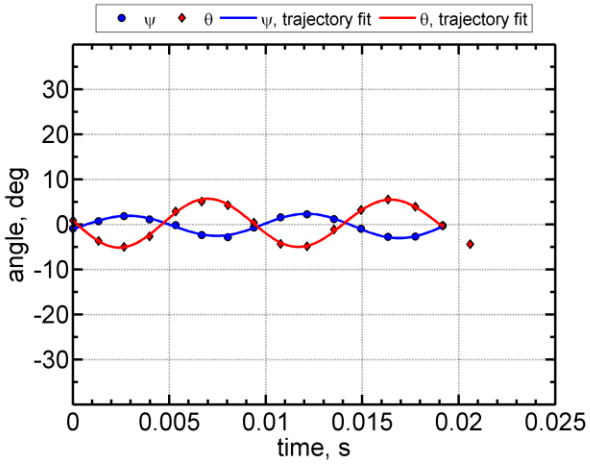

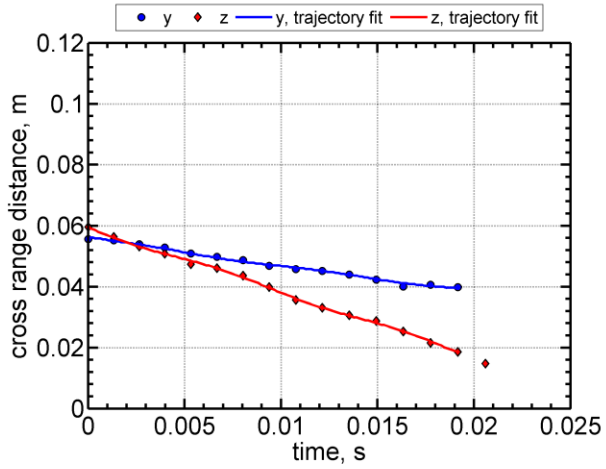

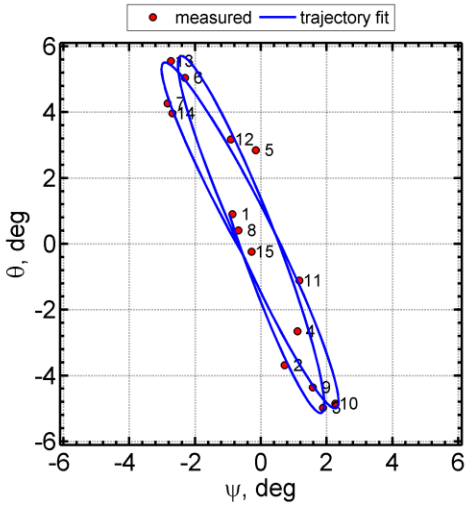

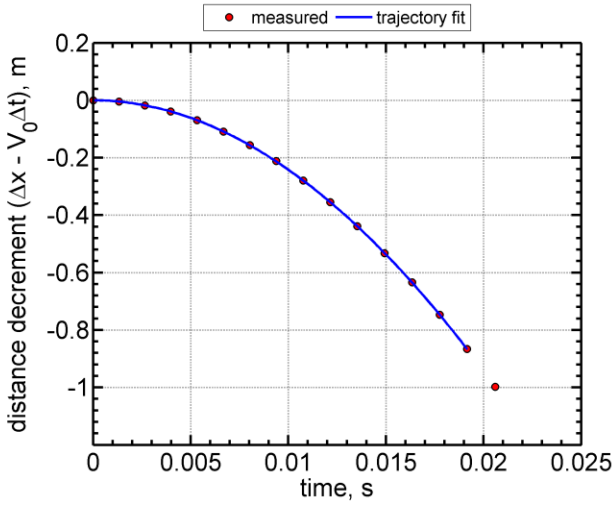

Shot	$\bar{M}_\infty$	$\overline{Re}_d$ (x 10^{-6})	$\bar{V}_\infty$ (m/s)	P_∞ (Torr)	T_∞ (K)	ρ_∞ (kg/m^3)	σ_{RMS} (deg)
2643	3.31	0.538	1141	155.0	294.3	0.245	6.0

Station	time, s	x, m	y, m	z, m	V, m/s	M	Re_d (x 10^{-6})	ψ, deg	θ, deg
1	0.00000000	0.050	0.059	0.066	1188.55	3.46	0.561	0.7	-1.6
2	0.00129268	1.582	0.058	0.066	1182.04	3.44	0.558	-0.7	5.7
3	0.00258808	3.109	0.058	0.066	1175.57	3.42	0.555	-1.9	8.6
4	0.00387394	4.617	0.057	0.065	1169.22	3.40	0.552	-1.8	5.2
5	0.00518771	6.149	0.056	0.062	1162.79	3.38	0.549	-0.2	-2.0
6									
7	0.00782099	9.193	0.055	0.062	1150.08	3.34	0.543	3.2	-7.1
8	0.00915141	10.721	0.053	0.062	1143.76	3.33	0.540	1.2	-1.4
9	0.01049483	12.252	0.052	0.062	1137.44	3.31	0.537	-1.6	5.3
10	0.01183043	13.766	0.051	0.061	1131.22	3.29	0.534	-4.0	7.7
11	0.01318660	15.297	0.051	0.061	1124.97	3.27	0.531	-3.6	4.5
12	0.01455002	16.826	0.051	0.060	1118.75	3.25	0.528	0.3	-1.9
13	0.01591340	18.349	0.050	0.058	1112.61	3.24	0.526	4.7	-6.3
14	0.01728823	19.873	0.050	0.057	1106.47	3.22	0.523	5.4	-5.6
15	0.01866327	21.390	0.049	0.058	1100.41	3.20	0.520	1.8	-1.2
16	0.02005607	22.919	0.048	0.058	1094.33	3.18	0.517	-3.7	4.4

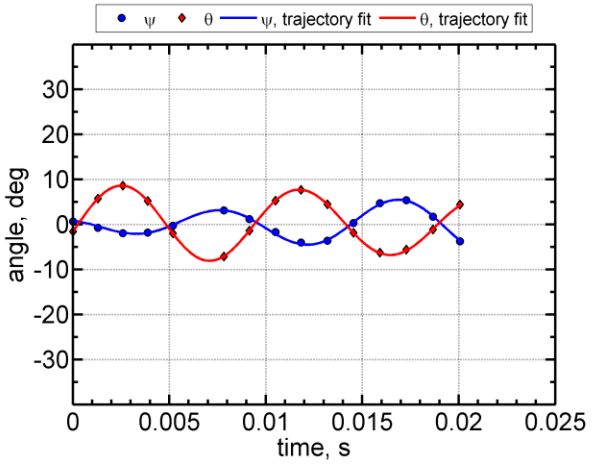

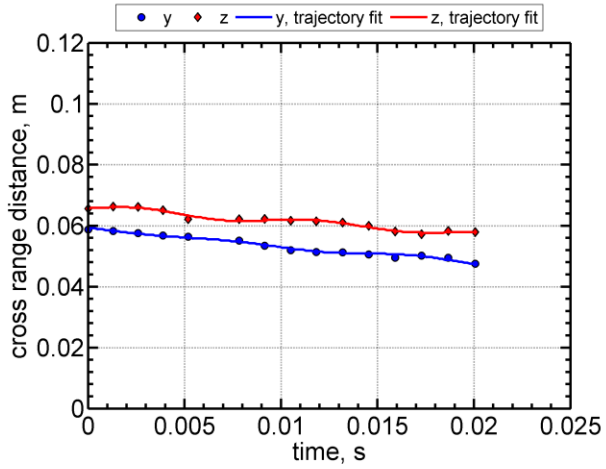

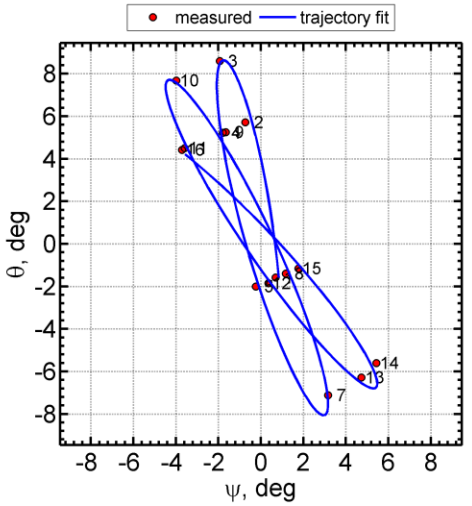

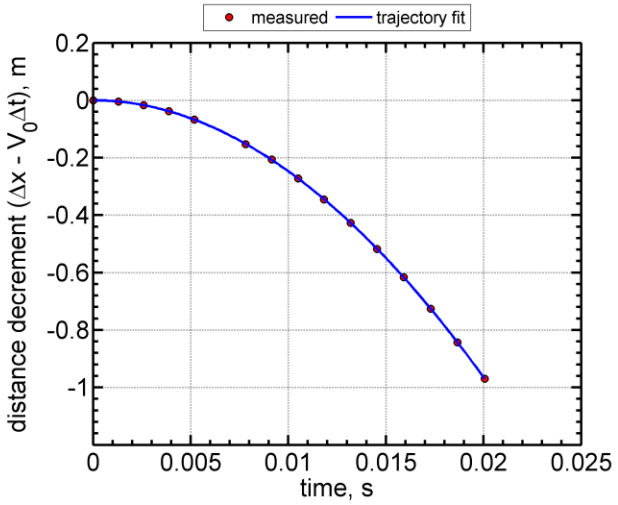

Shot	$\bar{M}_\infty$	$\overline{Re_d}$ (x 10^{-6})	$\bar{V}_\infty$ (m/s)	P_∞ (Torr)	T_∞ (K)	ρ_∞ (kg/m^3)	σ_{RMS} (deg)
2637	3.45	0.559	1184	155.0	294.4	0.245	3.5

Station	time, s	x, m	y, m	z, m	V, m/s	M	Re_d (x 10^{-6})	ψ, deg	θ, deg
1	0.00000000	0.050	0.055	0.061	1233.23	3.59	0.581	-0.3	-1.0
2	0.00124539	1.582	0.055	0.060	1226.52	3.57	0.578	0.3	3.1
3	0.00249397	3.110	0.053	0.059	1219.84	3.55	0.575	1.0	4.8
4	0.00373370	4.618	0.052	0.056	1213.27	3.53	0.572	1.1	2.7
5	0.00499989	6.151	0.050	0.053	1206.63	3.51	0.569	0.2	-1.7
6	0.00626981	7.679	0.049	0.052	1200.03	3.49	0.566	-0.5	-5.0
7	0.00753732	9.196	0.047	0.051	1193.51	3.47	0.563	-0.4	-4.5
8	0.00882104	10.724	0.045	0.049	1186.96	3.45	0.560	-0.3	-0.2
9	0.01011344	12.253	0.043	0.047	1180.44	3.43	0.557	0.1	3.9
10	0.01140285	13.771	0.042	0.046	1174.00	3.41	0.554	-0.2	5.0
11	0.01270885	15.300	0.041	0.044	1167.55	3.39	0.550	0.2	2.6
13	0.01533838	18.353	0.036	0.040	1154.75	3.36	0.544	1.3	-4.7
14	0.01666190	19.877	0.035	0.037	1148.42	3.34	0.541	0.9	-3.5
15	0.01798662	21.394	0.034	0.037	1142.15	3.32	0.538	-0.4	0.5
16	0.01933070	22.924	0.033	0.035	1135.85	3.30	0.536	-1.7	3.6

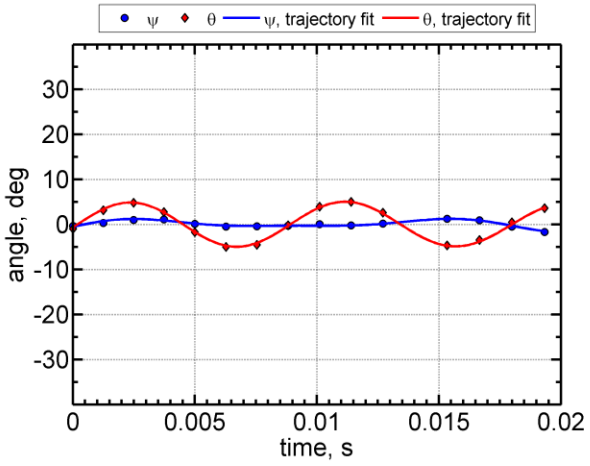

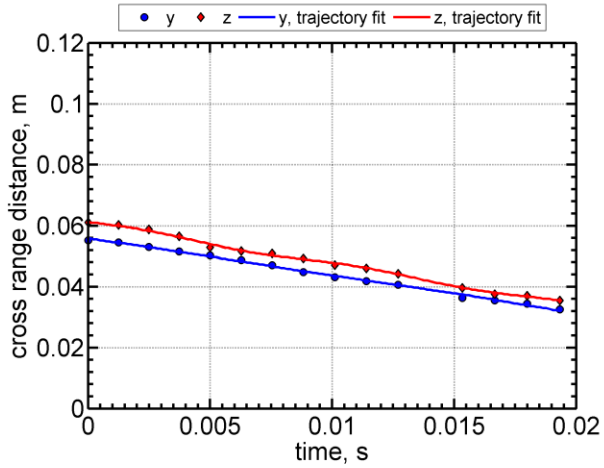

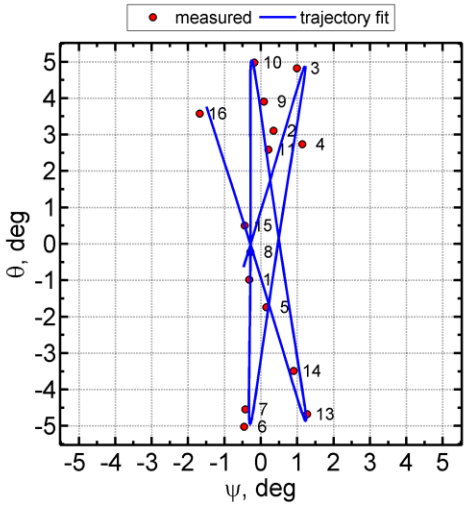

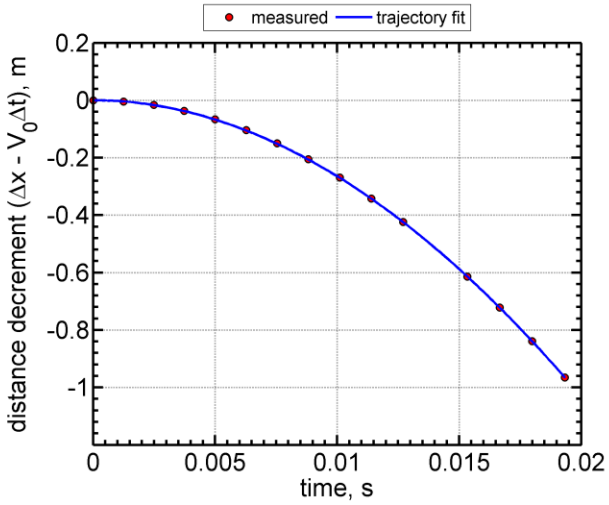

Shot	$\bar{M}_\infty$	$\overline{Re_d}$ (x 10^{-6})	$\bar{V}_\infty$ (m/s)	P_∞ (Torr)	T_∞ (K)	ρ_∞ (kg/m^3)	σ_{RMS} (deg)
2621	2.11	0.376	723	169.4	293.1	0.268	7.1

Station	time, s	x, m	y, m	z, m	V, m/s	M	Re_d (x 10^{-6})	ψ, deg	θ, deg
1	0.00000000	0.046	0.056	0.064	757.29	2.21	0.394	0.2	-4.7
2	0.00202442	1.574	0.056	0.065	752.61	2.19	0.391	-0.5	4.1
3	0.00406389	3.104	0.055	0.065	747.95	2.18	0.389	-0.5	9.9
4	0.00608926	4.615	0.054	0.064	743.38	2.17	0.386	-0.7	8.8
5	0.00815382	6.145	0.053	0.060	738.76	2.15	0.384	0.0	2.0
6	0.01027743	7.708	0.052	0.059	734.07	2.14	0.382	0.5	-6.3
7	0.01229962	9.188	0.052	0.058	729.66	2.13	0.379	0.8	-10.2
8	0.01440059	10.717	0.050	0.057	725.13	2.11	0.377	0.3	-7.4
9	0.01651523	12.245	0.049	0.057	720.63	2.10	0.375	-0.2	0.3
10	0.01863635	13.768	0.048	0.057	716.16	2.09	0.372	-1.2	7.5
11	0.02077196	15.294	0.048	0.057	711.73	2.07	0.370	-1.4	9.4
12	0.02292286	16.819	0.047	0.056	707.32	2.06	0.368	-1.3	5.4
13	0.02508293	18.344	0.046	0.053	702.94	2.05	0.365	-0.1	-2.5
14	0.02725876	19.867	0.046	0.051	698.60	2.04	0.363	0.7	-9.1
15	0.02943961	21.386	0.046	0.050	694.30	2.02	0.361	1.0	-9.3
16	0.03164702	22.914	0.045	0.050	690.02	2.01	0.359	-0.4	-4.1

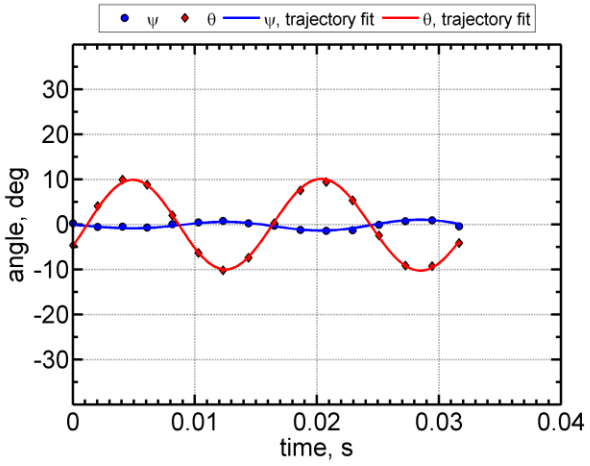

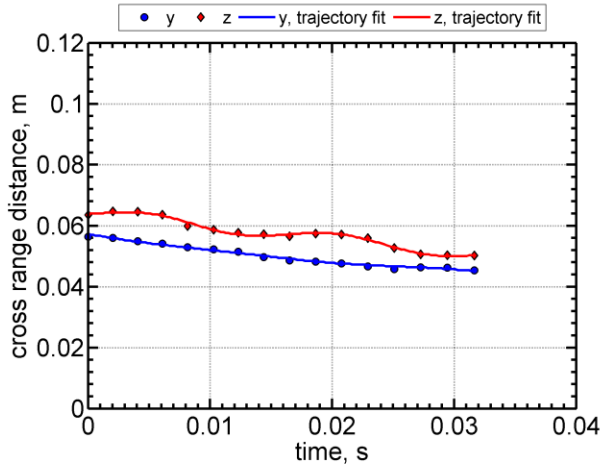

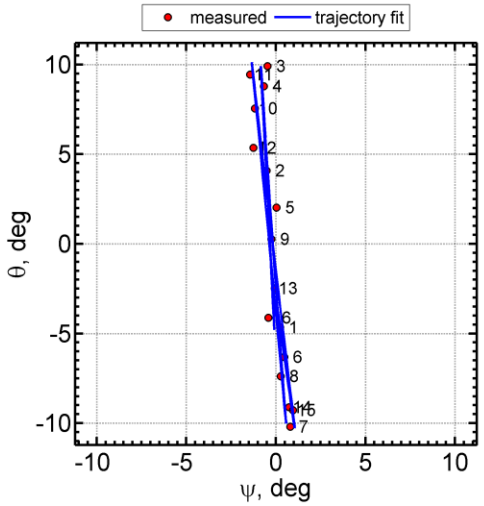

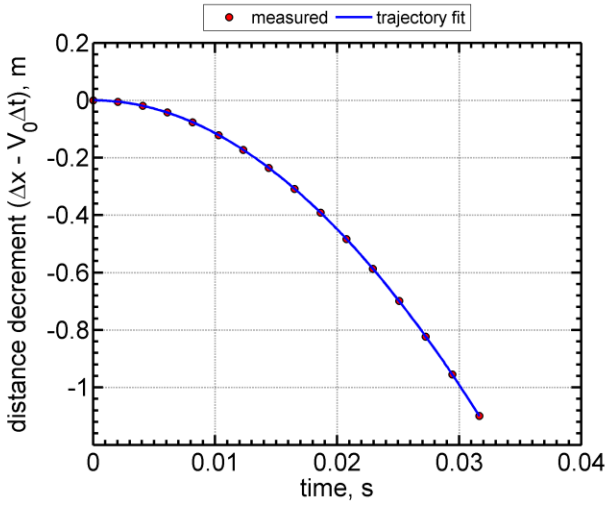

Shot	$\bar{M}_\infty$	$\overline{Re}_d$ (x 10^{-6})	$\bar{V}_\infty$ (m/s)	P_∞ (Torr)	T_∞ (K)	ρ_∞ (kg/m^3)	σ_{RMS} (deg)
2642	2.91	0.495	999	161.5	293.2	0.256	8.8

Station	time, s	x, m	y, m	z, m	V, m/s	M	Re_d (x 10^{-6})	ψ, deg	θ, deg
1	0.00000000	0.049	0.057	0.065	1042.96	3.04	0.516	-0.2	-4.8
2	0.00147467	1.582	0.056	0.067	1036.96	3.02	0.513	0.1	6.5
3	0.00295039	3.108	0.055	0.067	1031.01	3.00	0.510	-1.0	12.6
4	0.00441801	4.617	0.054	0.066	1025.15	2.99	0.507	-1.0	10.2
5	0.00591534	6.147	0.053	0.062	1019.24	2.97	0.505	-0.4	-0.5
6	0.00742054	7.677	0.052	0.062	1013.36	2.95	0.502	0.7	-10.1
7	0.00891952	9.191	0.051	0.061	1007.56	2.94	0.499	1.2	-11.9
8	0.01043988	10.720	0.049	0.061	1001.74	2.92	0.496	0.8	-5.9
9	0.01197360	12.251	0.048	0.061	995.94	2.90	0.493	-0.2	5.1
10	0.01349960	13.766	0.047	0.062	990.23	2.88	0.490	-2.2	11.9
11	0.01504897	15.296	0.047	0.062	984.50	2.87	0.487	-2.3	10.8
12	0.01660613	16.824	0.045	0.060	978.81	2.85	0.485	-0.9	1.2
13	0.01816499	18.347	0.044	0.057	973.17	2.84	0.482	1.5	-8.3
14	0.01973760	19.872	0.045	0.056	967.56	2.82	0.479	2.6	-12.2
15	0.02131003	21.389	0.044	0.057	962.01	2.80	0.476	2.1	-7.0
16	0.02290266	22.917	0.042	0.057	956.46	2.79	0.473	-0.5	3.6

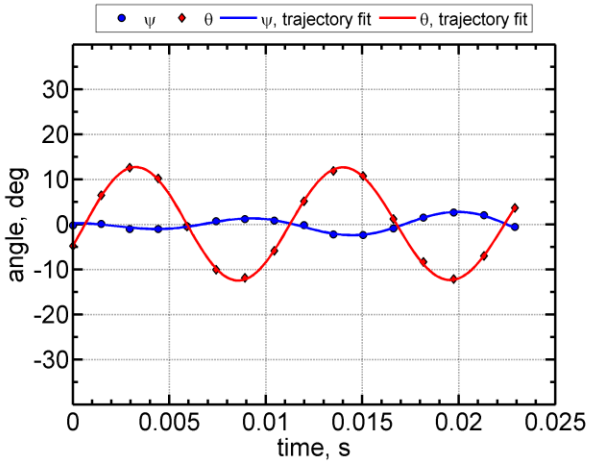

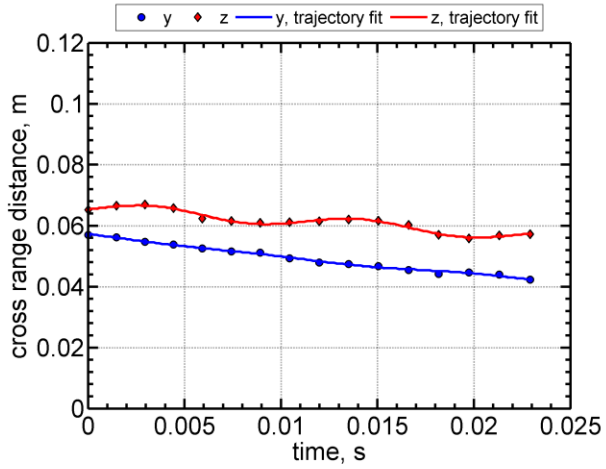

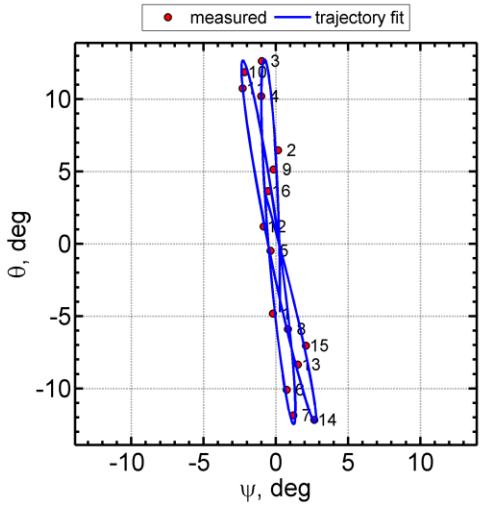

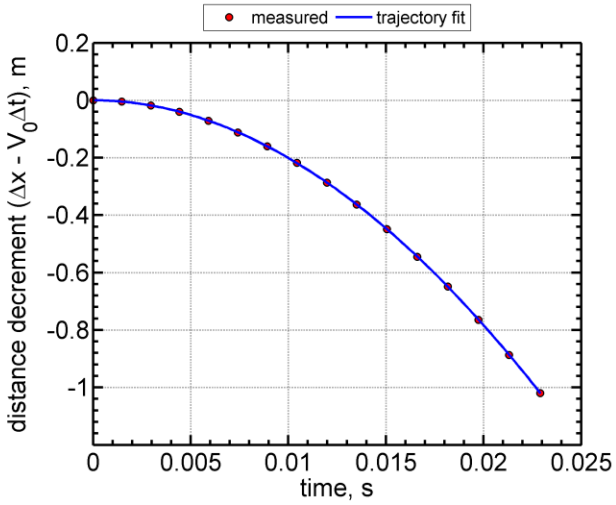

Shot	$\bar{M}_\infty$	$\overline{Re}_d$ (x 10^{-6})	$\bar{V}_\infty$ (m/s)	P_∞ (Torr)	T_∞ (K)	ρ_∞ (kg/m^3)	σ_{RMS} (deg)
2638	3.78	0.590	1300	149.0	294.2	0.235	8.1

Station	time, s	x, m	y, m	z, m	V, m/s	M	Re_d (x 10^{-6})	ψ, deg	θ, deg
1	0.00000000	0.052	0.059	0.062	1350.05	3.93	0.612	0.1	-4.7
2	0.00113709	1.584	0.059	0.063	1343.16	3.91	0.609	0.2	5.2
3	0.00227591	3.110	0.058	0.063	1336.33	3.89	0.606	-0.8	11.1
4	0.00340691	4.618	0.057	0.061	1329.60	3.87	0.603	-0.9	9.6
5	0.00456163	6.150	0.057	0.057	1322.80	3.85	0.600	-0.3	0.9
6	0.00571994	7.679	0.057	0.057	1316.03	3.83	0.597	-0.3	-7.9
7	0.00687504	9.195	0.056	0.055	1309.34	3.81	0.594	0.6	-11.7
8	0.00804458	10.723	0.055	0.055	1302.63	3.79	0.591	0.6	-7.0
9	0.00922419		0.055		1295.93	3.77	0.588	0.7	
10	0.01039568	13.769	0.055	0.055	1289.33	3.75	0.585	-0.9	10.1
11	0.01158544	15.299	0.055	0.054	1282.70	3.73	0.582	-1.7	10.9
13	0.01397955	18.353	0.053	0.050	1269.54	3.69	0.576	-0.5	-5.6
14	0.01518237	19.876	0.055	0.048	1263.03	3.67	0.573	0.5	-11.6
15	0.01638699	21.393	0.055	0.048	1256.58	3.65	0.570	0.8	-8.7
16	0.01760736	22.923	0.055	0.049	1250.11	3.64	0.567	-0.3	-0.4

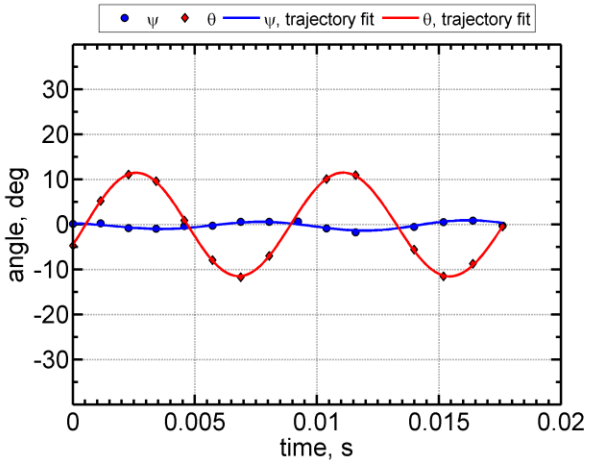

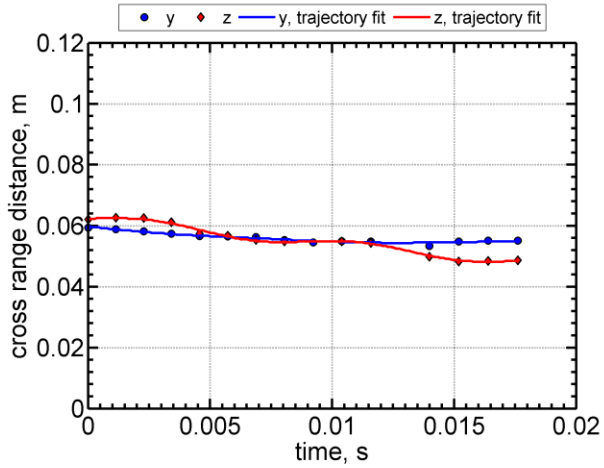

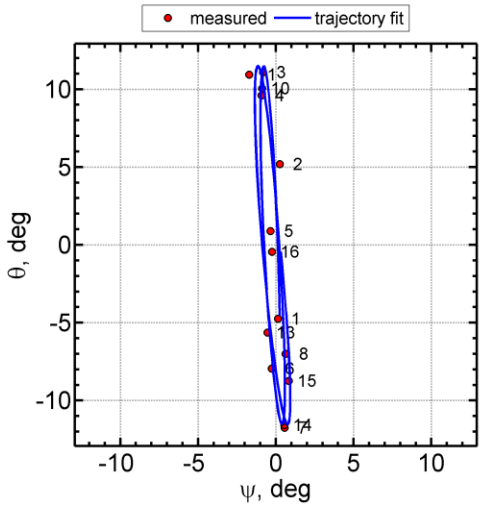

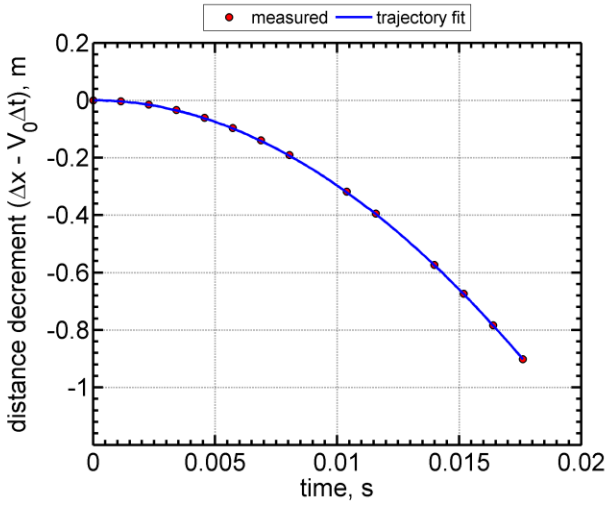

Shot	$\bar{M}_\infty$	$\overline{Re}_d$ (x 10^{-6})	$\bar{V}_\infty$ (m/s)	P_∞ (Torr)	T_∞ (K)	ρ_∞ (kg/m^3)	σ_{RMS} (deg)
2623	2.03	0.362	697	169.4	292.8	0.269	12.9

Station	time, s	x, m	y, m	z, m	V, m/s	M	Re_d (x 10^{-6})	ψ, deg	θ, deg
1	0.00000000	0.044	0.057	0.069	728.88	2.12	0.379	0.2	-7.8
2	0.00210442	1.573	0.056	0.073	724.50	2.11	0.377	-1.2	7.1
3	0.00422119	3.102	0.055	0.075	720.14	2.10	0.374	-1.7	17.0
4	0.00632334	4.611	0.054	0.076	715.86	2.09	0.372	-2.0	15.9
5	0.00846918	6.143	0.054	0.073	711.54	2.07	0.370	-0.6	4.6
6	0.01062634	7.673	0.053	0.072	707.24	2.06	0.368	1.2	-10.9
7	0.01277194	9.185	0.052	0.073	703.02	2.05	0.365	2.2	-17.8
8	0.01495102	10.713	0.050	0.074	698.78	2.04	0.363	2.1	-14.3
9	0.01714504	12.242	0.050	0.076	694.55	2.02	0.361	-0.6	-1.3
10	0.01934295	13.763	0.048	0.080	690.38	2.01	0.359	-2.4	12.7
11	0.02155856	15.289	0.048	0.082	686.22	2.00	0.357	-3.9	18.1
12	0.02378890	16.814	0.047	0.082	682.08	1.99	0.355	-2.7	11.9
13	0.02602831	18.338	0.046	0.080	677.98	1.98	0.352	0.2	-2.0
14	0.02828361	19.861	0.047	0.078	673.91	1.96	0.350	3.1	-15.0
15	0.03054361	21.380	0.047	0.080	669.88	1.95	0.348	3.4	-17.6
16	0.03283027	22.908	0.045	0.082	665.85	1.94	0.346	2.1	-9.3

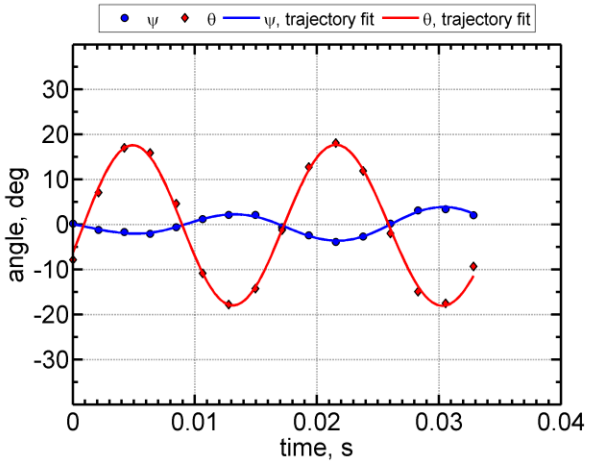

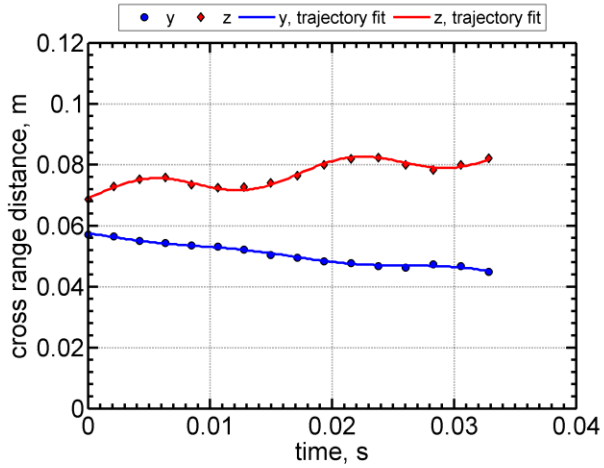

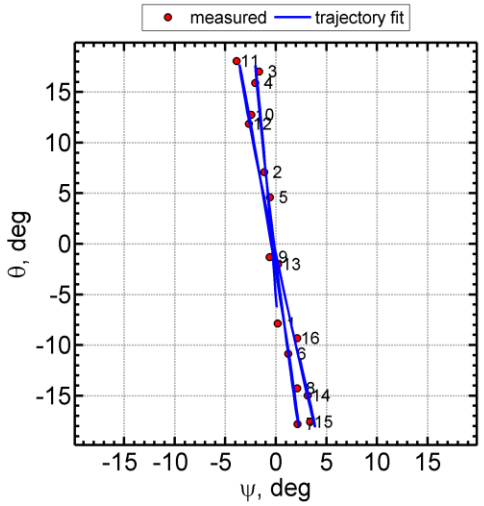

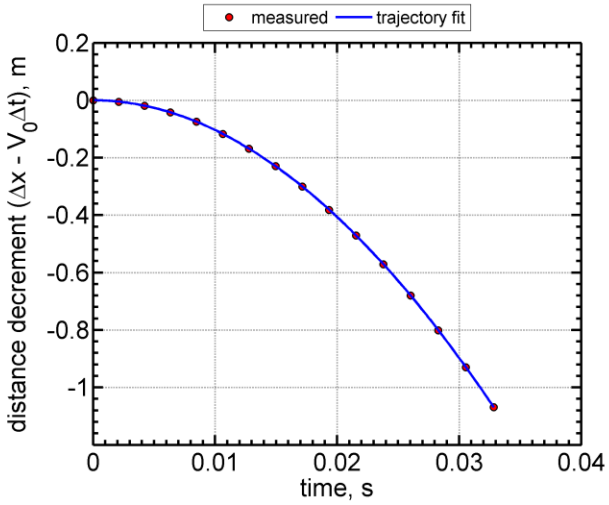

Shot	$\bar{M}_\infty$	$\overline{Re}_d$ (x 10^{-6})	$\bar{V}_\infty$ (m/s)	P_∞ (Torr)	T_∞ (K)	ρ_∞ (kg/m^3)	σ_{RMS} (deg)
2641	2.37	0.418	813	166.5	291.9	0.265	9.7

Station	time, s	x, m	y, m	z, m	V, m/s	M	Re_d (x 10^{-6})	ψ, deg	θ, deg
1	0.00000000	0.048	0.058	0.064	850.69	2.48	0.438	0.1	-4.2
2	0.00180507	1.578	0.058	0.066	845.58	2.47	0.435	0.1	7.4
3	0.00361794	3.106	0.057	0.066	840.51	2.45	0.432	0.3	14.3
4	0.00541805	4.615	0.056	0.065	835.52	2.44	0.430	-0.4	11.3
5	0.00725577	6.146	0.055	0.061	830.49	2.42	0.427	-0.4	0.0
6									
7	0.01094367	9.190	0.054	0.059	820.56	2.40	0.422	0.1	-13.6
8	0.01281026	10.718	0.052	0.060	815.62	2.38	0.420	0.2	-6.6
9	0.01469424	12.249	0.051	0.060	810.69	2.37	0.417	-0.1	4.2
10	0.01656995	13.765	0.050	0.061	805.84	2.35	0.415	-0.4	12.8
11	0.01847346	15.294	0.050	0.061	800.97	2.34	0.412	-0.9	12.8
12	0.02038441	16.820	0.049	0.059	796.15	2.32	0.410	-0.6	3.6
13	0.02230382	18.345	0.047	0.055	791.37	2.31	0.407	0.8	-7.4
14	0.02423639	19.868	0.048	0.053	786.62	2.30	0.405	1.0	-13.5
15	0.02617293	21.388	0.047	0.054	781.91	2.28	0.402	0.9	-10.1
16	0.02813214	22.915	0.046	0.054	777.22	2.27	0.400	0.2	1.0

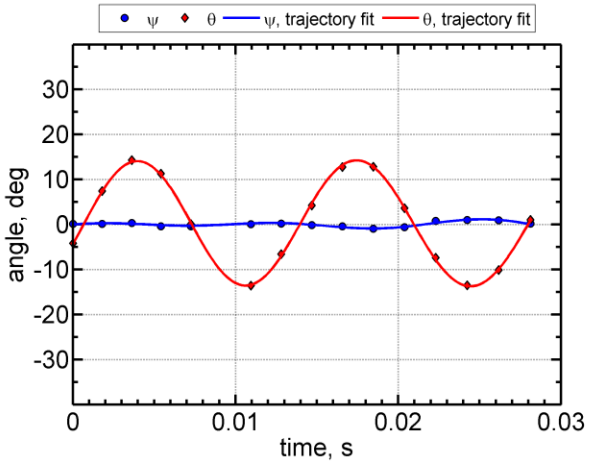

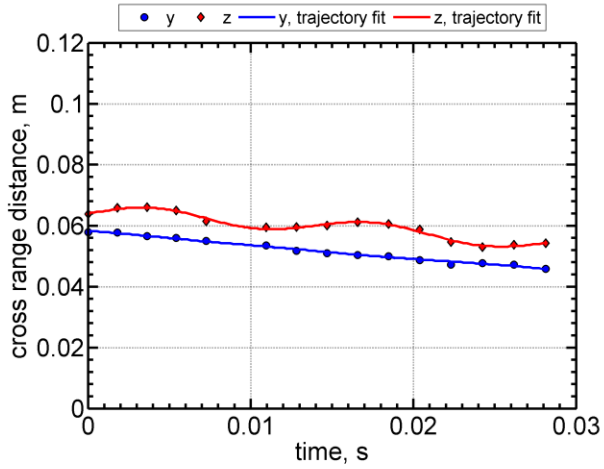

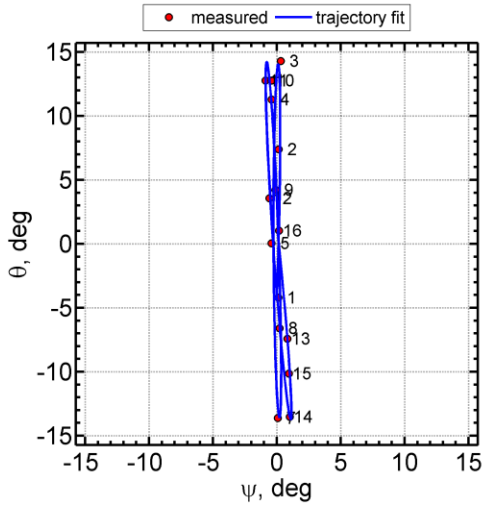

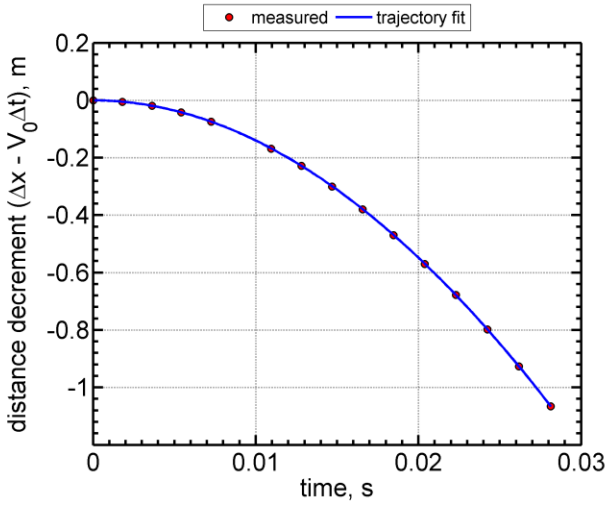

Shot	$\bar{M}_\infty$	$\overline{Re}_d$ (x 10^{-6})	$\bar{V}_\infty$ (m/s)	P_∞ (Torr)	T_∞ (K)	ρ_∞ (kg/m^3)	σ_{RMS} (deg)
2646	2.47	0.421	848	163.0	294.3	0.257	12.3

Station	time, s	x, m	y, m	z, m	V, m/s	M	Re_d (x 10^{-6})	ψ, deg	θ, deg
1	0.00000000	0.047	0.057	0.067	885.63	2.58	0.440	-0.1	-8.6
2	0.00173495	1.579	0.057	0.071	880.54	2.56	0.437	0.3	5.4
3	0.00347659	3.108	0.055	0.073	875.48	2.55	0.435	0.3	15.7
4	0.00520162	4.614	0.055	0.073	870.52	2.53	0.432	-0.5	16.0
5	0.00696526	6.145	0.054	0.070	865.50	2.52	0.430	-0.3	5.7
6	0.00874336	7.679	0.052	0.069	860.49	2.50	0.427	-0.5	-9.2
7	0.01050418	9.190	0.052	0.068	855.59	2.49	0.425	0.4	-16.4
8	0.01229250	10.717		0.069	850.66	2.47	0.422		-13.6
9	0.01409855	12.248	0.049	0.070	845.74	2.46	0.420	0.4	-1.6
10	0.01589612	13.763	0.049	0.073	840.90	2.45	0.418	-0.6	11.7
11	0.01772053	15.294	0.048	0.074	836.05	2.43	0.415	-1.4	17.1
12	0.01955251	16.820	0.046	0.074	831.23	2.42	0.413	-1.4	12.1
13	0.02138815	18.344	0.045	0.070	826.46	2.40	0.410	-0.3	-1.1
14	0.02323996	19.868	0.045	0.068	821.71	2.39	0.408	1.3	-14.0
15	0.02509119	21.385	0.045	0.069	817.02	2.38	0.406	1.9	-16.9
16	0.02696647	22.913	0.044	0.070	812.32	2.36	0.403	1.6	-8.8

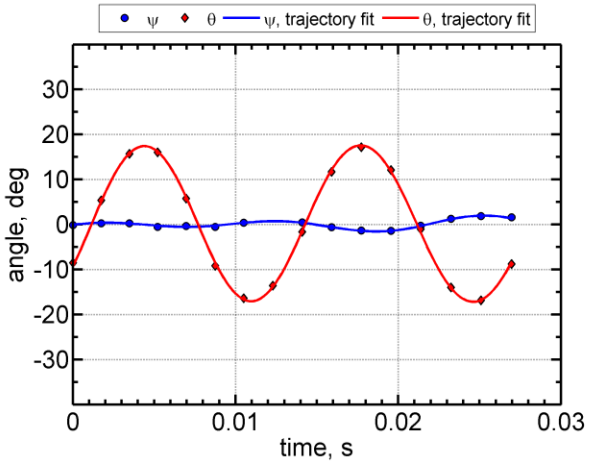

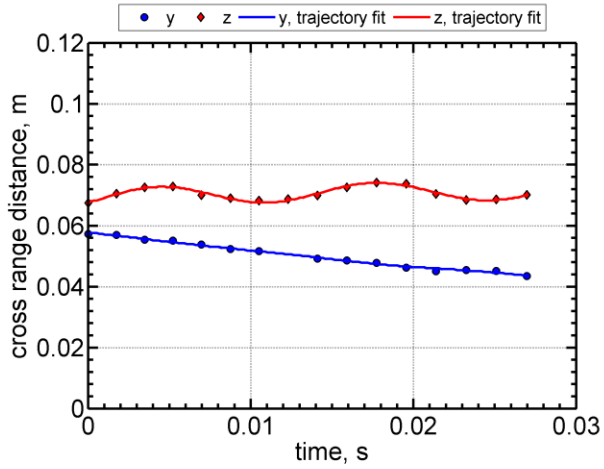

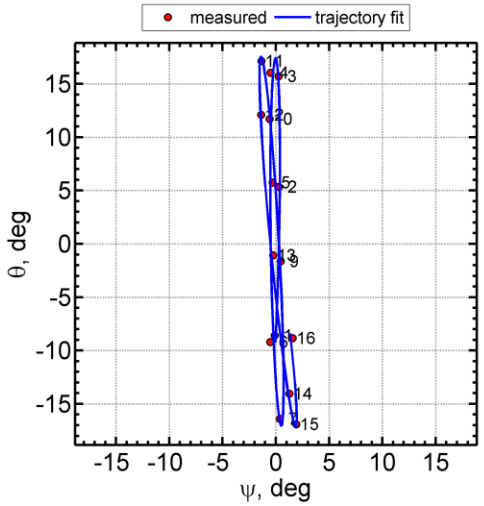

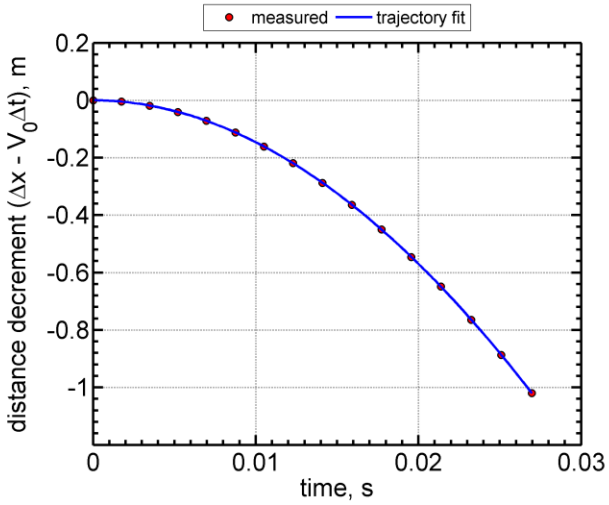

Shot	$\bar{M}_\infty$	$\overline{Re_d}$ (x 10^{-6})	$\bar{V}_\infty$ (m/s)	P_∞ (Torr)	T_∞ (K)	ρ_∞ (kg/m^3)	σ_{RMS} (deg)
2647	2.88	0.490	992	163.0	295.1	0.257	10.7

Station	time, s	x, m	y, m	z, m	V, m/s	M	Re_d (x 10^{-6})	ψ, deg	θ, deg
1	0.00000000	0.049	0.057	0.069	1034.87	3.01	0.511	0.0	-5.9
2	0.00148424	1.580	0.057	0.071	1028.97	2.99	0.508	-0.1	7.0
3	0.00297214	3.106	0.056	0.073	1023.12	2.97	0.505	-0.1	15.0
4	0.00445131	4.615	0.055	0.073	1017.35	2.95	0.502	0.1	12.6
5	0.00596093	6.147	0.054	0.070	1011.53	2.94	0.499	-0.4	1.4
6	0.00747939	7.678	0.052	0.070	1005.74	2.92	0.497	-0.9	-11.2
7	0.00898925	9.192	0.052	0.070	1000.04	2.90	0.494	-0.5	-15.4
8	0.01051954	10.719	0.050	0.071	994.32	2.89	0.491	-0.4	-8.8
9	0.01206449	12.250	0.049	0.072	988.61	2.87	0.488	0.5	3.5
10	0.01360062	13.763	0.049	0.074	983.00	2.85	0.485	0.4	13.8
11	0.01516112	15.294	0.048	0.075	977.37	2.84	0.483	0.7	14.1
12	0.01672909	16.822	0.046	0.074	971.77	2.82	0.480	0.5	5.2
13	0.01829945	18.345	0.045	0.072	966.23	2.81	0.477	-1.1	-7.6
14	0.01988589	19.872	0.045	0.071	960.70	2.79	0.474	-1.3	-14.6
15	0.02146619	21.386	0.045	0.073	955.26	2.77	0.472	-1.2	-11.6
16	0.02307016	22.915	0.043	0.075	949.80	2.76	0.469	0.3	-0.3

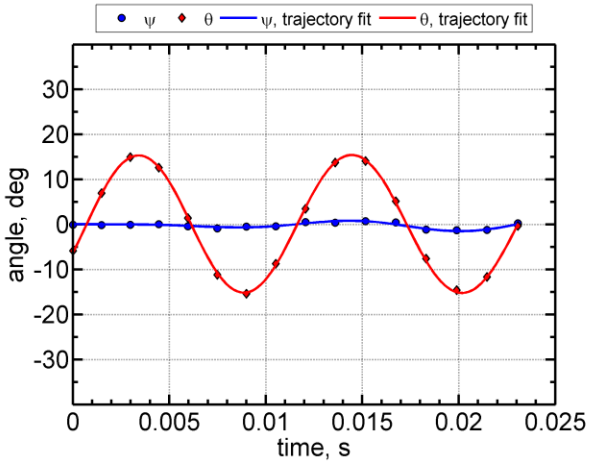

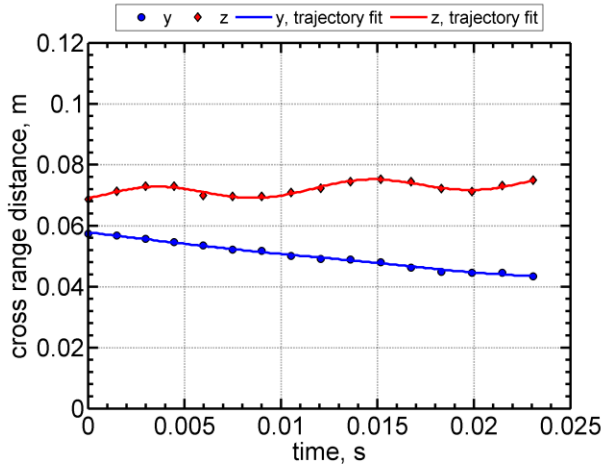

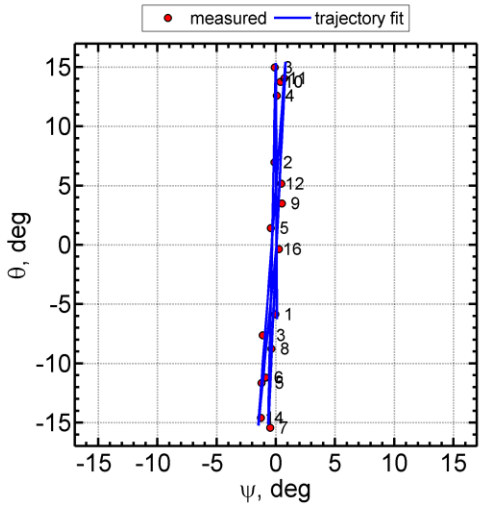

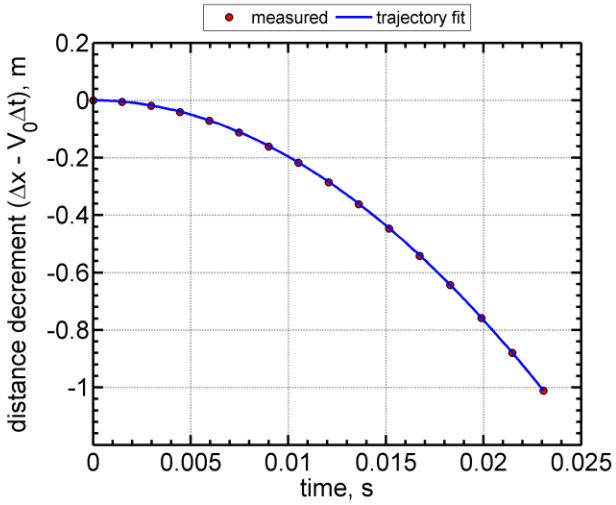

Shot	$\bar{M}_\infty$	$\overline{Re}_d$ (x 10^{-6})	$\bar{V}_\infty$ (m/s)	P_∞ (Torr)	T_∞ (K)	ρ_∞ (kg/m^3)	σ_{RMS} (deg)
2648	3.49	0.573	1197	155.0	292.2	0.246	11.1

Station	time, s	x, m	y, m	z, m	V, m/s	M	Re_d (x 10^{-6})	ψ, deg	θ, deg
1	0.00000000	0.052	0.056	0.065	1245.93	3.64	0.596	-0.5	-6.9
2	0.00123157	1.582	0.056	0.067	1239.26	3.62	0.593	-0.3	6.4
3	0.00246887	3.111	0.055	0.067	1232.62	3.60	0.590	0.6	14.7
4	0.00369356	4.617	0.053	0.066	1226.10	3.58	0.587	1.2	14.0
5	0.00494590	6.149	0.053	0.063	1219.51	3.56	0.583	0.3	2.7
6	0.00615475		0.051		1213.20	3.54	0.580	-0.6	
7	0.00745640	9.194	0.050	0.061	1206.47	3.52	0.577	-1.1	-15.7
8	0.00872469	10.721	0.048	0.061	1199.98	3.50	0.574	-1.3	-10.4
9	0.01000565	12.253	0.048	0.061	1193.50	3.48	0.571	-0.6	2.7
10	0.01127814	13.767	0.047	0.062	1187.12	3.46	0.568	0.7	13.2
11	0.01257050	15.297	0.046	0.063	1180.71	3.45	0.565	1.4	16.1
12	0.01387022	16.827	0.045	0.061	1174.34	3.43	0.562	0.9	7.4
13	0.01516841	18.350	0.043	0.058	1168.03	3.41	0.559	-0.4	-6.0
14	0.01647859	19.873	0.043	0.056	1161.74	3.39	0.556	-1.6	-14.1
15	0.01778763	21.390	0.042	0.056	1155.53	3.37	0.553	-2.3	-13.3
16	0.01911345	22.919	0.041	0.056	1149.30	3.35	0.550	-0.8	-2.1

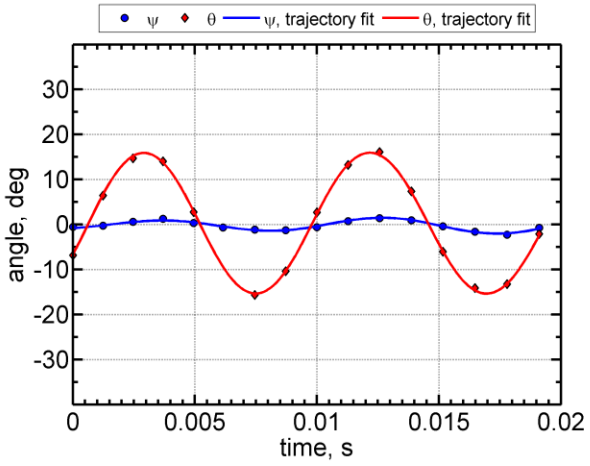

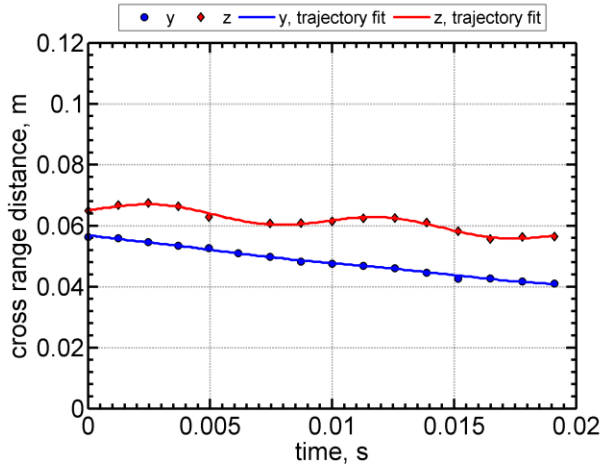

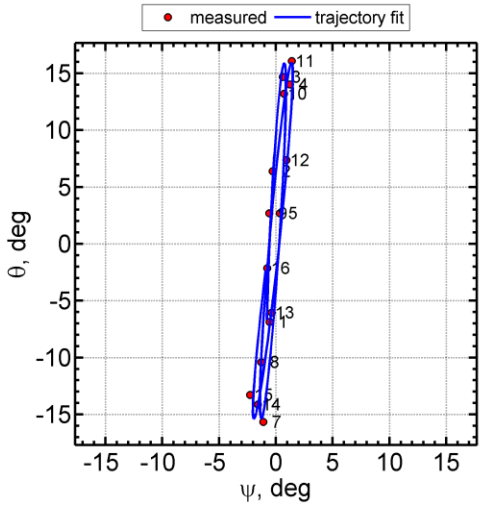

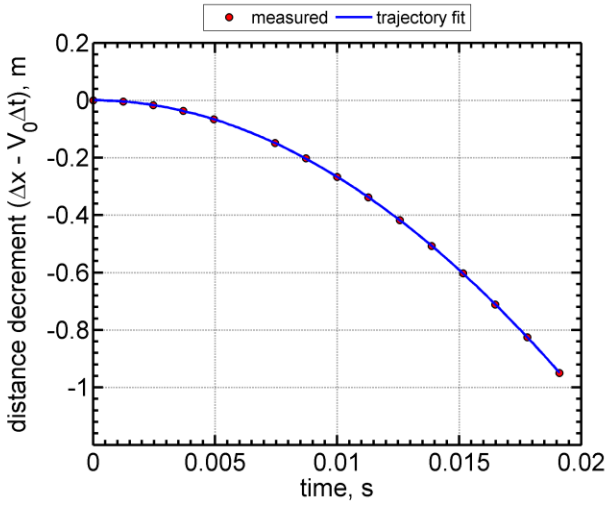

Shot	$\bar{M}_\infty$	$\overline{Re_d}$ (x 10^{-6})	$\bar{V}_\infty$ (m/s)	P_∞ (Torr)	T_∞ (K)	ρ_∞ (kg/m^3)	σ_{RMS} (deg)
2630	2.26	0.399	776	167.7	293.1	0.266	15.8

Station	time, s	x, m	y, m	z, m	V, m/s	M	Re_d (x 10^{-6})	ψ, deg	θ, deg
1	0.00000000	0.045	0.058	0.071	810.74	2.36	0.417	-1.4	-9.4
2	0.00189254	1.575	0.058	0.076	806.03	2.35	0.414	-1.2	8.5
3	0.00379349	3.103	0.057	0.079	801.36	2.33	0.412	0.0	20.7
4	0.00568226	4.612	0.057	0.081	796.76	2.32	0.410	0.5	19.8
5	0.00760939	6.143	0.056	0.078	792.13	2.31	0.407	0.9	6.0
6	0.00954747	7.674	0.055	0.077	787.51	2.29	0.405	0.2	-12.4
7	0.01147418	9.187	0.054	0.077	782.97	2.28	0.403	-0.4	-21.5
8	0.01342927	10.714	0.053	0.079	778.42	2.27	0.400	-1.5	-17.6
9	0.01539991	12.243	0.052	0.083	773.88	2.25	0.398	-1.2	-2.3
10	0.01737668	13.768	0.052	0.087	769.39	2.24	0.396	-0.4	15.2
11	0.01935954	15.289	0.051	0.090	764.93	2.23	0.393	0.3	22.2
12	0.02136129	16.815	0.050	0.090	760.48	2.22	0.391	1.1	15.7
13	0.02336874	18.339	0.048	0.087	756.07	2.20	0.389	1.0	-1.3
14	0.02538842	19.860	0.048	0.086	751.70	2.19	0.387	-0.4	-17.5
15	0.02741610	21.380	0.048	0.087	747.36	2.18	0.384	-1.1	-22.4
16	0.02946605	22.908	0.047	0.089	743.03	2.16	0.382	-1.6	-12.9

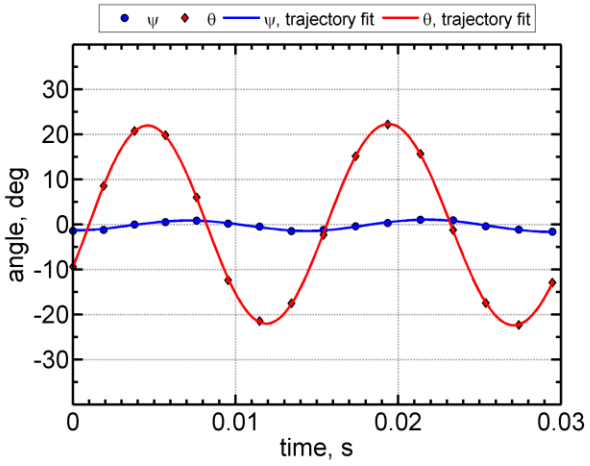

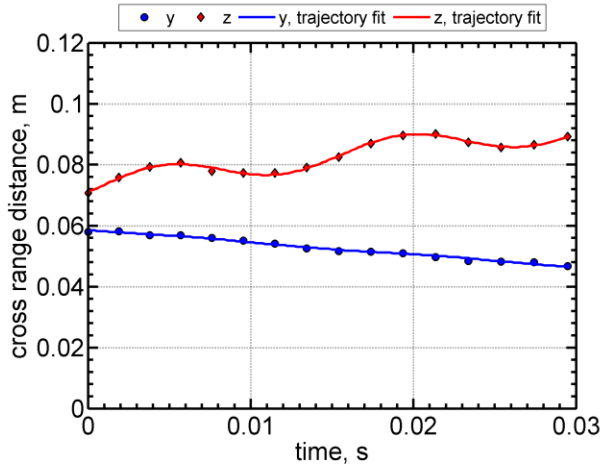

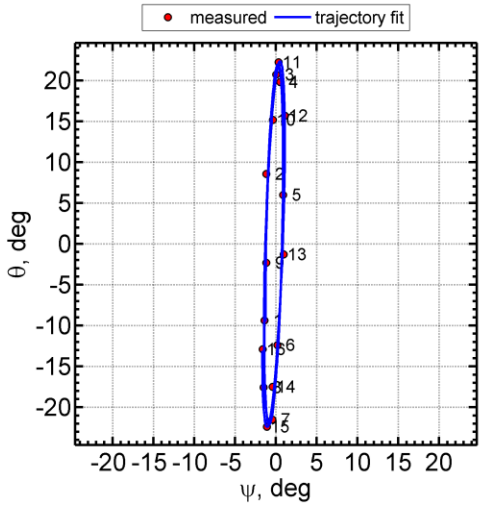

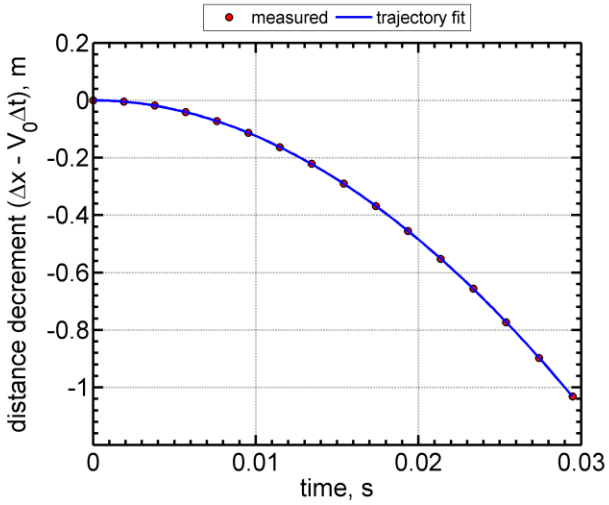

Shot	$\bar{M}_\infty$	$\overline{Re_d}$ (x 10^{-6})	$\bar{V}_\infty$ (m/s)	P_∞ (Torr)	T_∞ (K)	ρ_∞ (kg/m^3)	σ_{RMS} (deg)
2632	2.34	0.399	803	162.7	293.7	0.257	14.7

Station	time, s	x, m	y, m	z, m	V, m/s	M	Re_d (x 10^{-6})	ψ, deg	θ, deg
1	0.00000000	0.046	0.055	0.073	837.64	2.44	0.417	0.1	-9.8
2	0.00183189	1.576	0.055	0.078	832.89	2.42	0.414	1.1	6.7
3	0.00367096	3.103	0.054	0.081	828.16	2.41	0.412	1.1	19.0
4	0.00549808	4.612	0.052	0.083	823.51	2.40	0.410	0.7	19.1
5	0.00736240	6.143	0.051	0.081	818.82	2.38	0.407	-0.6	7.1
6	0.00923490	7.672	0.050	0.081	814.15	2.37	0.405	-1.7	-10.2
7	0.01110008	9.186	0.049	0.081	809.55	2.36	0.403	-2.3	-20.1
8	0.01299265	10.714	0.047	0.083	804.94	2.34	0.400	-1.1	-17.4
9	0.01489919	12.245	0.046	0.085	800.34	2.33	0.398	0.6	-3.4
10	0.01680469	13.764	0.045	0.090	795.80	2.32	0.396	1.9	12.7
11	0.01872496	15.289	0.045	0.093	791.27	2.30	0.394	2.3	21.1
12	0.02069796	16.845	0.042	0.094	786.67	2.29	0.391	1.1	15.5
13	0.02260061	18.339	0.040	0.092	782.29	2.28	0.389	-1.1	0.8
14	0.02455498	19.862	0.040	0.090	777.85	2.26	0.387	-3.2	-14.4
15	0.02651159	21.379	0.039	0.091	773.45	2.25	0.385	-3.0	-19.9
16	0.02849194	22.908	0.038	0.094	769.06	2.24	0.382	-1.5	-13.3

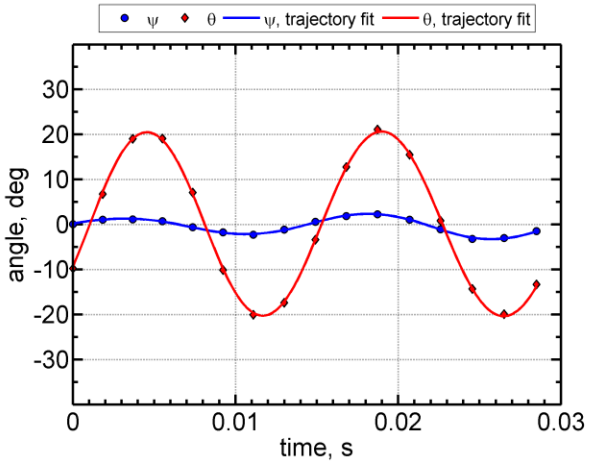

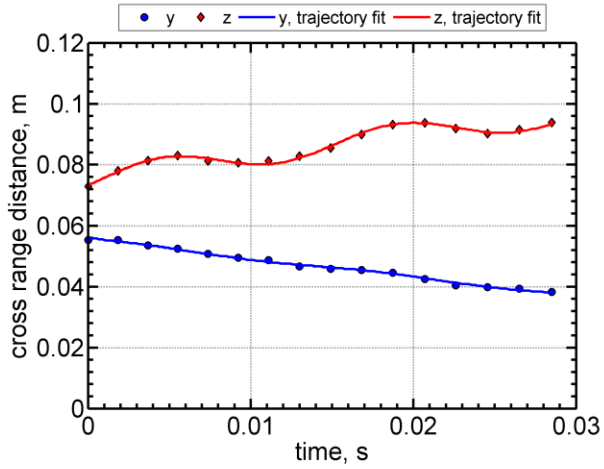

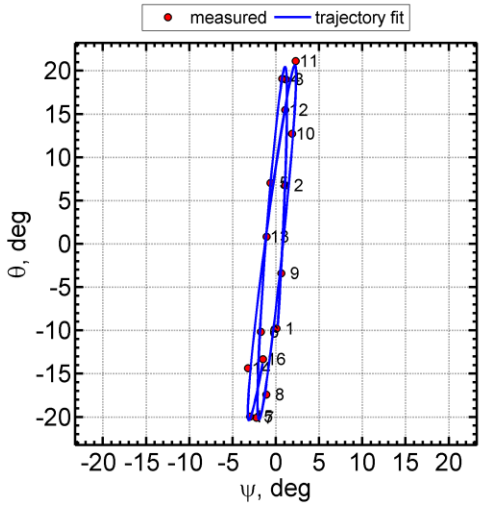

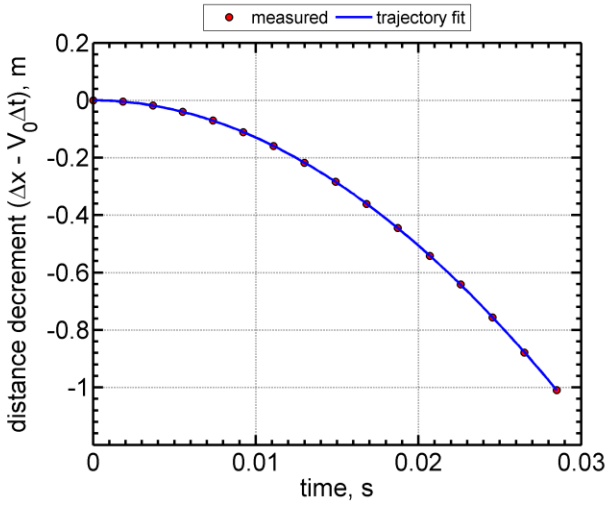

Shot	$\bar{M}_\infty$	$\overline{Re}_d$ (x 10^{-6})	$\bar{V}_\infty$ (m/s)	P_∞ (Torr)	T_∞ (K)	ρ_∞ (kg/m^3)	σ_{RMS} (deg)
2650	2.67	0.458	919	163.0	293.8	0.258	14.2

Station	time, s	x, m	y, m	z, m	V, m/s	M	Re_d (x 10^{-6})	ψ, deg	θ, deg
1	0.00000000	0.048	0.057	0.067	958.10	2.79	0.477	-0.3	-9.4
2	0.00160340	1.580	0.057	0.071	952.69	2.77	0.475	0.1	6.5
3	0.00321079	3.106	0.055	0.073	947.33	2.76	0.472	-0.3	18.3
4	0.00480798	4.615	0.054	0.073	942.05	2.74	0.469	-0.8	18.4
5	0.00643780	6.147	0.053	0.070	936.72	2.73	0.467	-0.5	6.9
6	0.00807500	7.675	0.052	0.069	931.43	2.71	0.464	-0.2	-10.0
7	0.00970644	9.190	0.051	0.068	926.20	2.70	0.461	0.9	-18.9
8	0.01135773	10.717	0.049	0.069	920.97	2.68	0.459	1.2	-16.4
9	0.01302687	12.249	0.048	0.071	915.75	2.67	0.456	0.6	-2.3
10	0.01468584	13.763	0.047	0.074	910.61	2.65	0.454	-1.1	12.8
11	0.01637032	15.293	0.046	0.076	905.45	2.64	0.451	-2.2	20.4
12	0.01806370	16.822	0.045	0.076	900.32	2.62	0.448	-1.6	14.3
13	0.01975763	18.345	0.043	0.072	895.26	2.61	0.446	-0.2	-0.8
14	0.02146713	19.869	0.044	0.070	890.20	2.59	0.443	1.6	-15.4
15	0.02317537	21.385	0.043	0.070	885.22	2.58	0.441	2.6	-19.4
16	0.02490569	22.913	0.042	0.072	880.23	2.56	0.438	1.6	-10.9

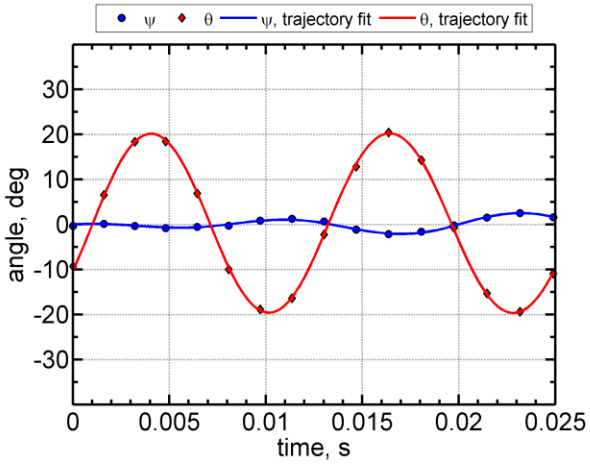

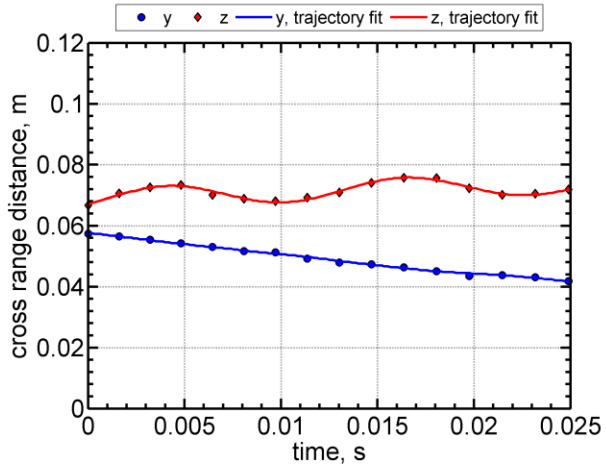

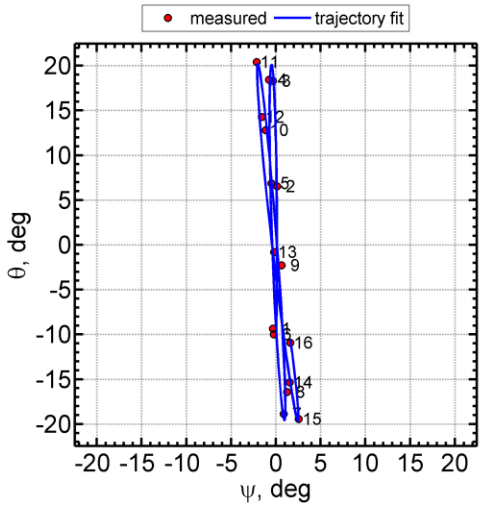

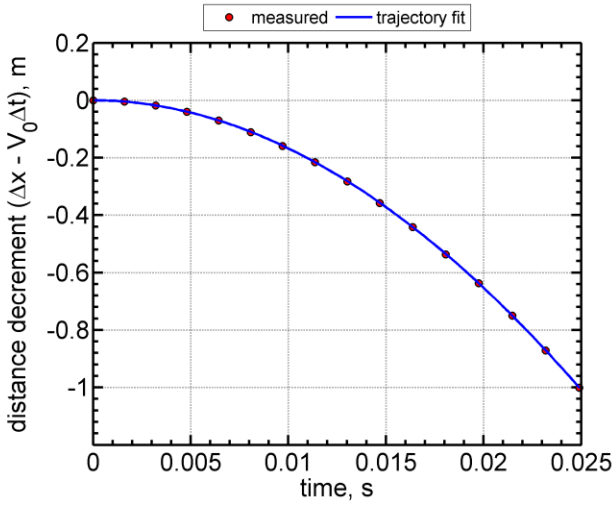

Shot	$\bar{M}_\infty$	$\overline{Re_d}$ (x 10^{-6})	$\bar{V}_\infty$ (m/s)	P_∞ (Torr)	T_∞ (K)	ρ_∞ (kg/m^3)	σ_{RMS} (deg)
2649	3.17	0.526	1088	158.0	293.6	0.250	15.7

Station	time, s	x, m	y, m	z, m	V, m/s	M	Re_d (x 10^{-6})	ψ, deg	θ, deg
1	0.00000000	0.049	0.055	0.068	1132.36	3.30	0.547	-0.5	-11.6
2	0.00135645	1.581	0.054	0.072	1126.31	3.28	0.544	-0.2	6.3
3	0.00271963	3.112	0.053	0.074	1120.29	3.26	0.541	-0.1	20.1
4	0.00406560	4.616	0.052	0.075	1114.39	3.24	0.538	0.1	21.1
5	0.00544285	6.146	0.050	0.072	1108.42	3.23	0.536	0.1	9.1
6	0.00682780	7.677	0.049	0.071	1102.48	3.21	0.533	-0.1	-8.9
7	0.00820481	9.191	0.048	0.070	1096.63	3.19	0.530	-0.5	-20.5
8	0.00959927	10.717		0.071	1090.76	3.18	0.527		-19.4
9	0.01100804	12.249	0.044	0.072	1084.89	3.16	0.524	-0.2	-5.7
10	0.01241307	13.769	0.044	0.076	1079.10	3.14	0.521	0.0	11.8
11	0.01383006	15.294	0.043	0.079	1073.32	3.12	0.519	0.3	21.7
12	0.01525713	16.821	0.041	0.079	1067.57	3.11	0.516	0.0	19.0
13	0.01668778	18.347	0.039	0.076	1061.86	3.09	0.513	0.2	3.4
14	0.01812863	19.871	0.038	0.074	1056.17	3.07	0.510	-0.2	-13.7
15	0.01956665	21.385	0.038	0.074	1050.56	3.06	0.508	-0.5	-21.6
16	0.02102686	22.916	0.036	0.075	1044.93	3.04	0.505	-0.7	-16.2

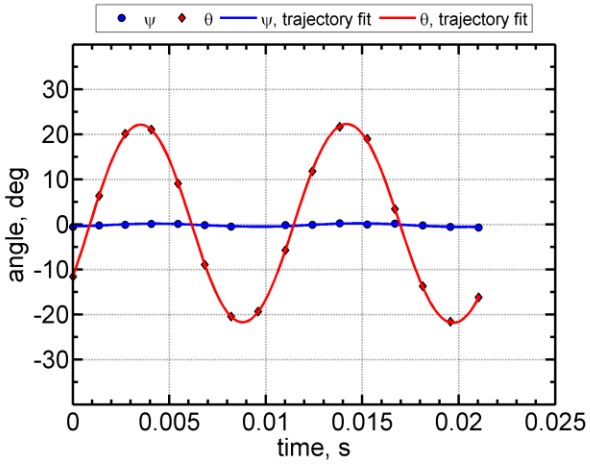

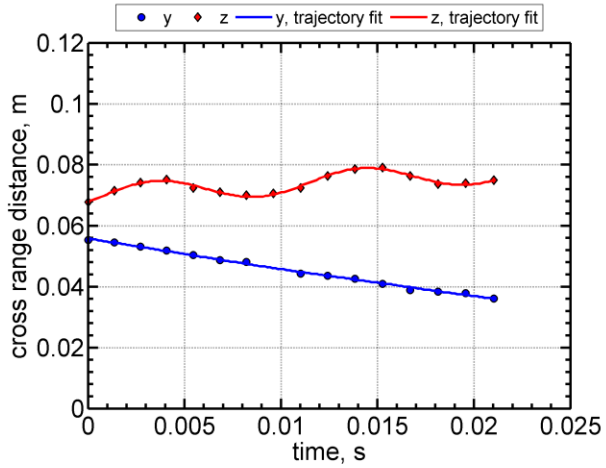

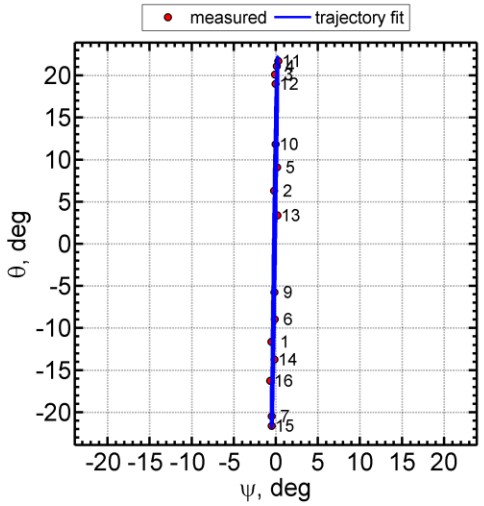

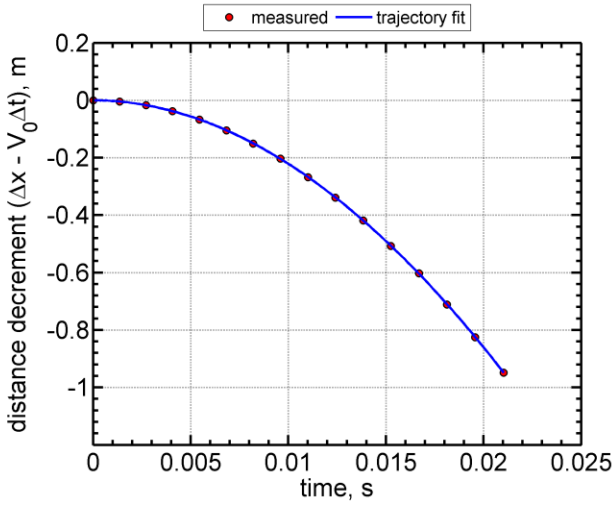

Shot	$\bar{M}_\infty$	$\overline{Re}_d$ (x 10^{-6})	$\bar{V}_\infty$ (m/s)	P_∞ (Torr)	T_∞ (K)	ρ_∞ (kg/m^3)	σ_{RMS} (deg)
2651	3.84	0.611	1323	152.0	294.5	0.240	16.0

Station	time, s	x, m	y, m	z, m	V, m/s	M	Re_d (x 10^{-6})	ψ, deg	θ, deg
1	0.00000000	0.052	0.057	0.066	1373.27	3.99	0.635	-1.6	-13.4
2	0.00111834	1.584	0.057	0.069	1366.40	3.97	0.632	-0.6	4.7
3	0.00224058	3.113	0.056	0.072	1359.56	3.95	0.629	0.5	18.7
4									
5	0.00448423	6.149	0.054	0.070	1346.07	3.91	0.622	1.0	12.0
6	0.00562493	7.680	0.053	0.069	1339.30	3.89	0.619	-0.3	-6.5
7	0.00675816	9.194	0.052	0.068	1332.64	3.87	0.616	-1.2	-20.3
8	0.00792147	10.719		0.068	1325.87	3.85	0.613		-21.7
9	0.00906494	12.253	0.049	0.069	1319.27	3.83	0.610	-1.0	-10.0
10	0.01021737	13.769		0.073	1312.69	3.82	0.607		7.4
11	0.01138344	15.296	0.048	0.076	1306.09	3.80	0.604	1.1	20.7
12	0.01255915	16.827	0.047	0.077	1299.50	3.78	0.601	1.5	21.4
13	0.01373202	18.350	0.045	0.074	1293.00	3.76	0.598	0.7	8.8
14	0.01491447	19.873	0.045	0.072	1286.50	3.74	0.595	-0.6	-9.4
15	0.01609447	21.387	0.044	0.071	1280.09	3.72	0.592	-1.9	-21.3
16	0.01729165	22.916	0.043	0.071	1273.65	3.70	0.589	-1.9	-20.3

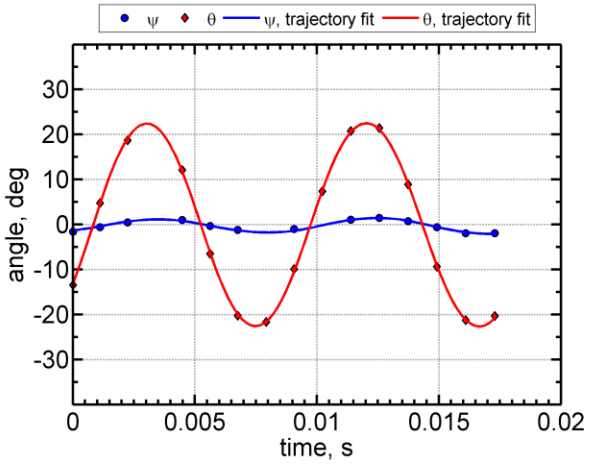

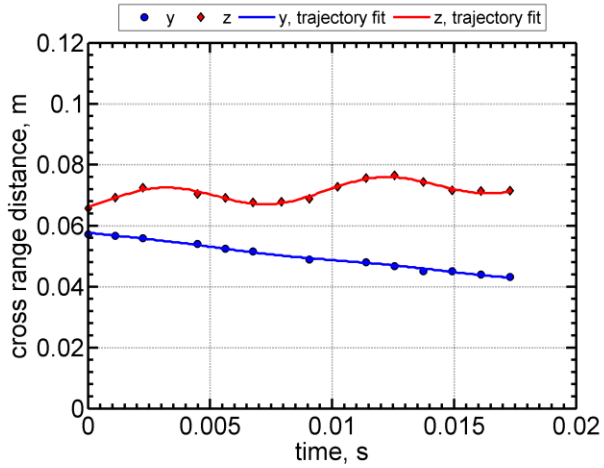

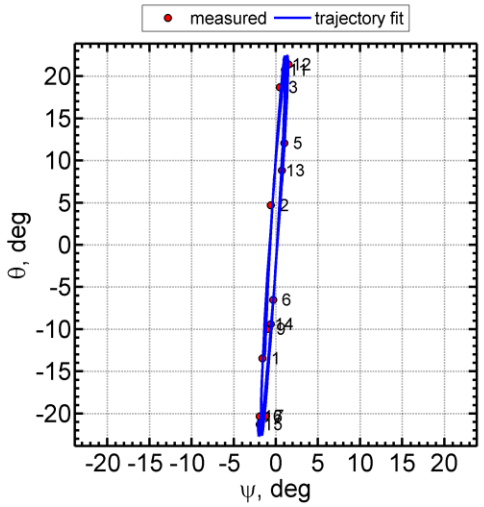

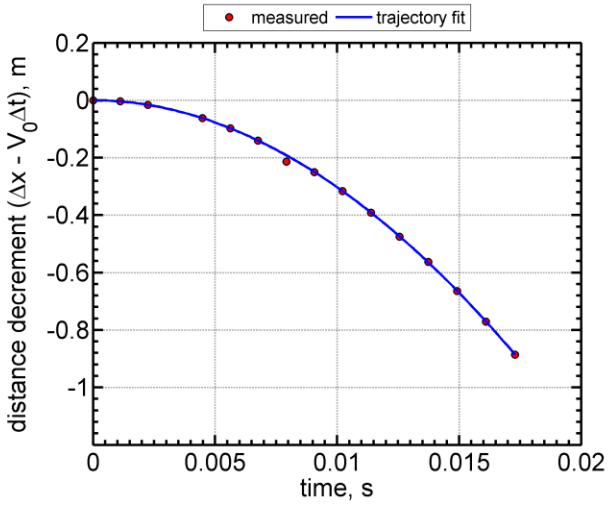

Shot	$\bar{M}_\infty$	$\overline{Re}_d$ (x 10^{-6})	$\bar{V}_\infty$ (m/s)	P_∞ (Torr)	T_∞ (K)	ρ_∞ (kg/m^3)	σ_{RMS} (deg)
2645	2.27	0.404	779	169.4	293.7	0.268	20.6

Station	time, s	x, m	y, m	z, m	V, m/s	M	Re_d (x 10^{-6})	ψ, deg	θ, deg
1	0.00000000	0.046	0.057	0.070	812.77	2.37	0.421	2.1	-15.7
2	0.00188971	1.578	0.057	0.076	808.20	2.35	0.418	1.5	6.7
3	0.00378523	3.105	0.055	0.082	803.67	2.34	0.416	-1.0	24.2
4	0.00566610	4.612	0.054	0.084	799.21	2.33	0.414	-3.1	27.8
5	0.00758682	6.144	0.053	0.082	794.70	2.31	0.411	-4.0	14.3
6	0.00951643	7.673	0.052	0.080	790.22	2.30	0.409	-1.1	-8.3
7	0.01143868	9.187	0.053	0.079	785.80	2.29	0.407	1.8	-25.1
8	0.01338694	10.714	0.051	0.080	781.37	2.27	0.405	5.0	-26.9
9	0.01535139	12.245	0.050	0.084	776.94	2.26	0.402	4.2	-12.5
10	0.01730717	13.760	0.048	0.090	772.59	2.25	0.400	-0.1	9.7
11	0.01929227	15.289	0.047	0.095	768.21	2.24	0.398	-4.8	26.3
12	0.02128536	16.815	0.045	0.097	763.87	2.22	0.396	-7.8	26.5
13	0.02328354	18.339	0.044	0.095	759.56	2.21	0.393	-5.2	11.4
14	0.02529525	19.862	0.045	0.092	755.27	2.20	0.391	1.2	-10.9
15	0.02731142	21.379	0.046	0.091	751.03	2.19	0.389	7.4	-25.8
16	0.02935203	22.908	0.044	0.093	746.78	2.17	0.387	8.9	-25.2

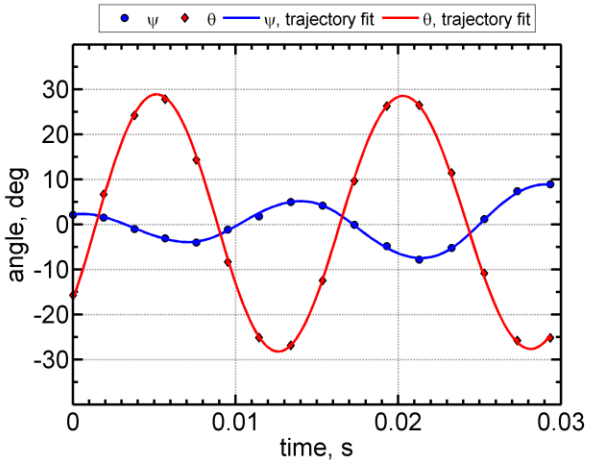

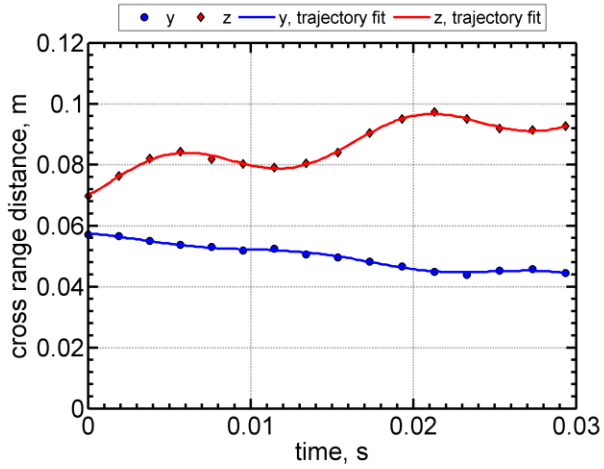

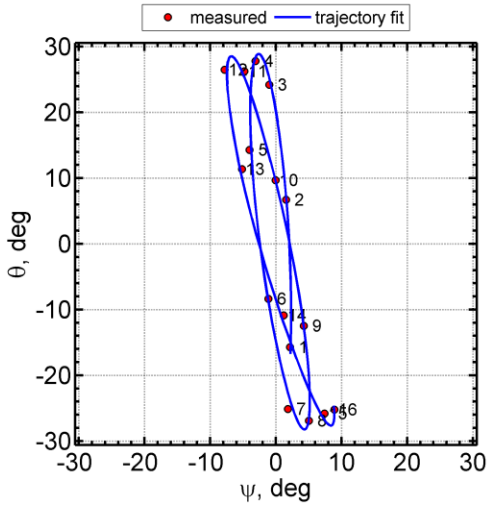

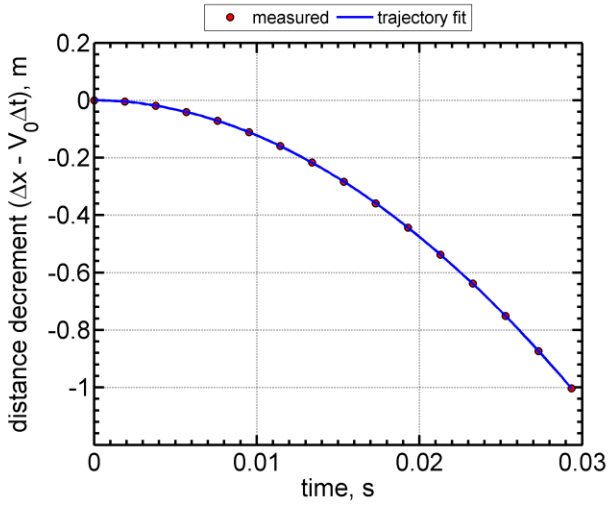

Shot	$\bar{M}_\infty$	$\overline{Re}_d$ (x 10^{-6})	$\bar{V}_\infty$ (m/s)	P_∞ (Torr)	T_∞ (K)	ρ_∞ (kg/m^3)	σ_{RMS} (deg)
2644	2.64	0.449	905	161.5	293.0	0.256	19.7

Station	time, s	x, m	y, m	z, m	V, m/s	M	Re_d (x 10^{-6})	ψ, deg	θ, deg
1	0.00000000	0.047	0.057	0.069	941.52	2.74	0.467	0.2	-16.0
2	0.00163177	1.579	0.057	0.076	936.50	2.73	0.464	-0.2	5.4
3	0.00326984	3.109	0.055	0.080	931.51	2.71	0.462	-1.8	23.6
4	0.00488924	4.613	0.054	0.083	926.63	2.70	0.460	-2.1	27.3
5	0.00654554	6.145	0.054	0.081	921.67	2.69	0.457	-1.6	15.6
6	0.00820928	7.674	0.053	0.080	916.74	2.67	0.455	0.8	-5.8
7	0.00986612	9.188	0.053	0.079	911.88	2.66	0.452	2.7	-23.2
8	0.01154414	10.715	0.051	0.080	907.00	2.64	0.450	3.3	-26.9
9	0.01323677	12.246	0.049	0.083	902.13	2.63	0.447	2.2	-14.7
10	0.01492080	13.761	0.049	0.089	897.33	2.62	0.445	-1.4	6.2
11	0.01662959	15.290	0.047	0.094	892.51	2.60	0.443	-3.4	24.1
12									
13	0.02006496	18.341	0.045	0.096	882.97	2.57	0.438	-2.7	14.3
14	0.02179636	19.865	0.046	0.093	878.24	2.56	0.436	1.6	-6.8
15	0.02352847	21.381	0.046	0.092	873.56	2.55	0.433	4.9	-23.5
16	0.02528118	22.908	0.045	0.093	868.87	2.53	0.431	6.2	-26.2

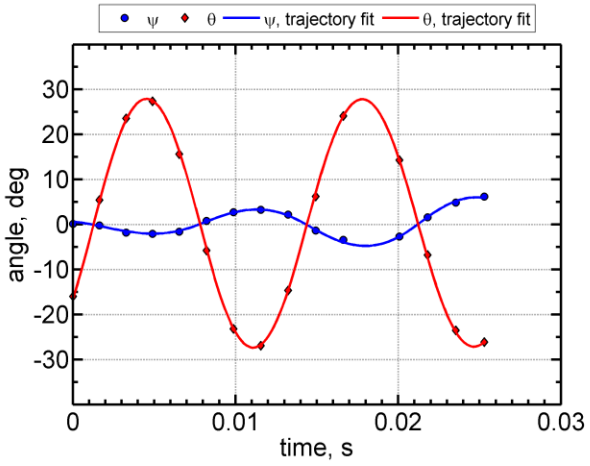

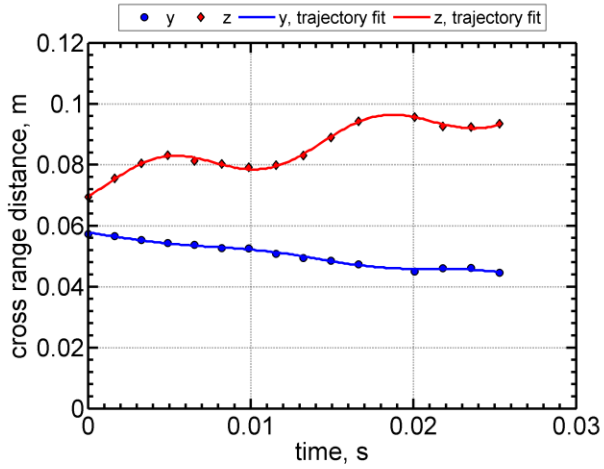

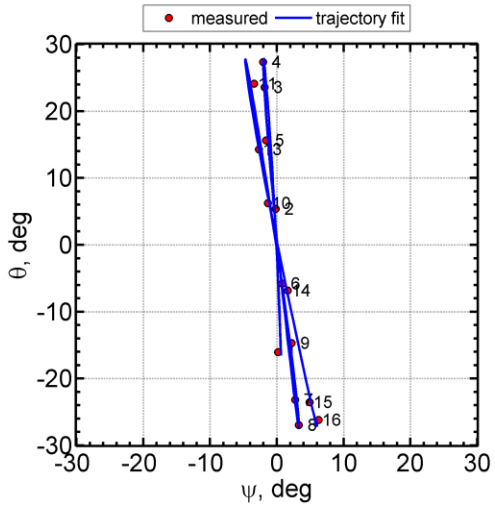

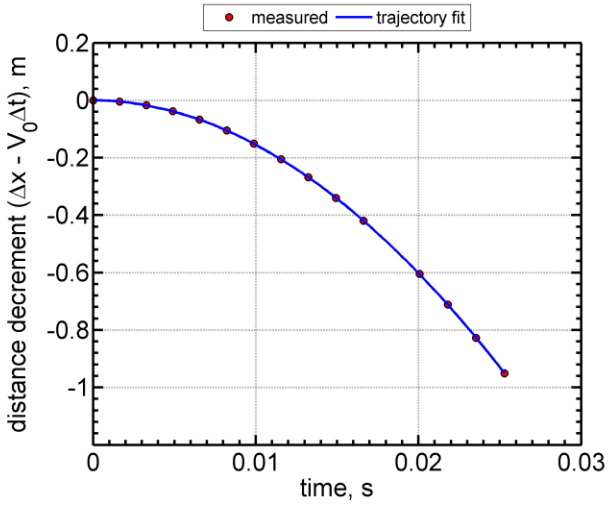

Shot	$\bar{M}_\infty$	$\overline{Re_d}$ (x 10^{-6})	$\bar{V}_\infty$ (m/s)	P_∞ (Torr)	T_∞ (K)	ρ_∞ (kg/m^3)	σ_{RMS} (deg)
2635	2.76	0.472	947	163.1	294.0	0.258	18.4

Station	time, s	x, m	y, m	z, m	V, m/s	M	Re_d (x 10^{-6})	ψ, deg	θ, deg
1	0.00000000	0.047	0.058	0.070	985.84	2.87	0.491	0.9	-11.5
2	0.00155709	1.578	0.058	0.076	980.49	2.85	0.488	-0.1	8.9
3	0.00311920	3.105	0.057	0.080	975.18	2.84	0.485	-2.0	24.1
4	0.00467075	4.614	0.056	0.082	969.95	2.82	0.483	-2.7	24.2
5	0.00625318	6.145	0.055	0.079	964.67	2.81	0.480	-1.4	9.1
6	0.00726083		0.055		961.33	2.80	0.478	0.6	
7	0.00942533	9.188	0.055	0.078	954.24	2.78	0.475	1.4	-24.5
8	0.01102937	10.715	0.053	0.080	949.04	2.76	0.472	2.1	-22.1
9	0.01264716	12.246	0.052	0.084	943.85	2.75	0.470	2.1	-7.0
10	0.01425748	13.761	0.051	0.089	938.75	2.73	0.467	-1.7	13.7
11	0.01589096	15.290	0.050	0.093	933.62	2.72	0.465	-4.0	25.3
12									
13	0.01917601	18.343	0.048	0.092	923.48	2.69	0.459	-1.5	4.8
14	0.02082927	19.864	0.049	0.091	918.46	2.67	0.457	2.8	-15.1
15	0.02248694	21.381	0.049	0.091	913.48	2.66	0.455	5.8	-24.7
16	0.02416247	22.909	0.048	0.093	908.51	2.64	0.452	4.7	-19.7

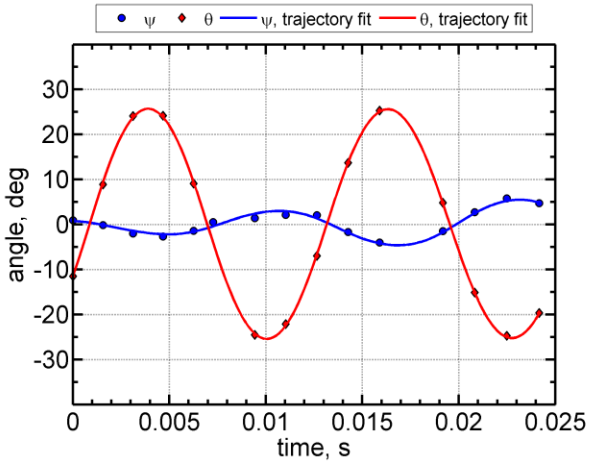

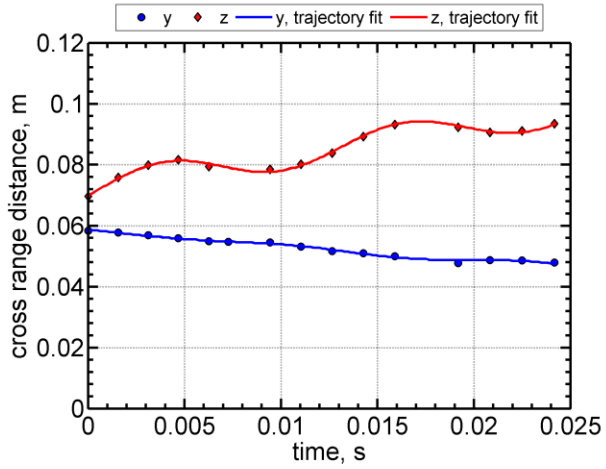

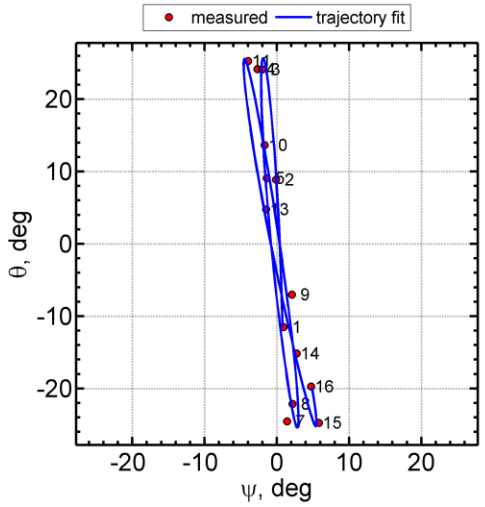

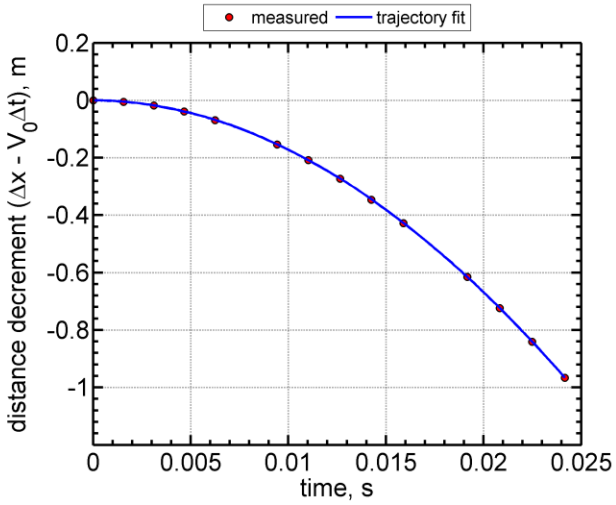

Shot	$\bar{M}_\infty$	$\overline{Re}_d$ (x 10^{-6})	$\bar{V}_\infty$ (m/s)	P_∞ (Torr)	T_∞ (K)	ρ_∞ (kg/m^3)	σ_{RMS} (deg)
2636	3.39	0.552	1165	155.0	293.7	0.245	20.5

Station	time, s	x, m	y, m	z, m	V, m/s	M	Re_d (x 10^{-6})	ψ, deg	θ, deg
1	0.00000000	0.049	0.055	0.067	1208.44	3.52	0.572	-1.6	-18.3
2	0.00127138	1.582	0.055	0.073	1202.50	3.50	0.570	-1.0	3.6
3	0.00254402	3.108	0.054	0.078	1196.59	3.48	0.567	0.6	23.0
4	0.00379756	4.615	0.052	0.080	1190.82	3.47	0.564	2.1	30.0
5	0.00509653	6.147	0.051	0.078	1184.90	3.45	0.561	2.1	19.8
6	0.00639222	7.679	0.049	0.076	1179.03	3.43	0.558	0.7	-1.0
7	0.00767707	9.190	0.048	0.074	1173.27	3.42	0.556	-1.4	-21.7
8	0.00898085	10.717	0.045	0.074	1167.48	3.40	0.553	-2.7	-29.0
9	0.01029507	12.246	0.044	0.076	1161.69	3.38	0.550	-2.2	-20.3
10	0.01160454	13.764	0.043	0.081	1155.97	3.36	0.548	-0.6	0.5
11	0.01293130	15.294	0.043	0.086	1150.23	3.35	0.545	1.8	21.9
12									
13	0.01559662	18.346	0.039	0.087	1138.87	3.31	0.539	2.6	22.3
14	0.01693890	19.870	0.038	0.084	1133.23	3.30	0.537	0.9	1.4
15	0.01827910	21.384	0.037	0.082	1127.65	3.28	0.534	-1.9	-19.6
16	0.01963686	22.912	0.035	0.081	1122.05	3.27	0.531	-3.0	-29.0

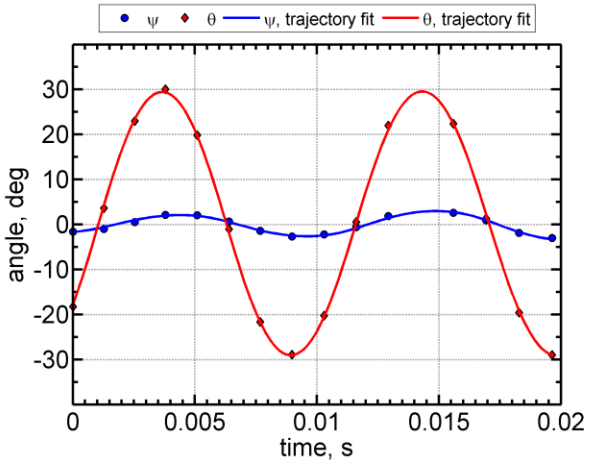

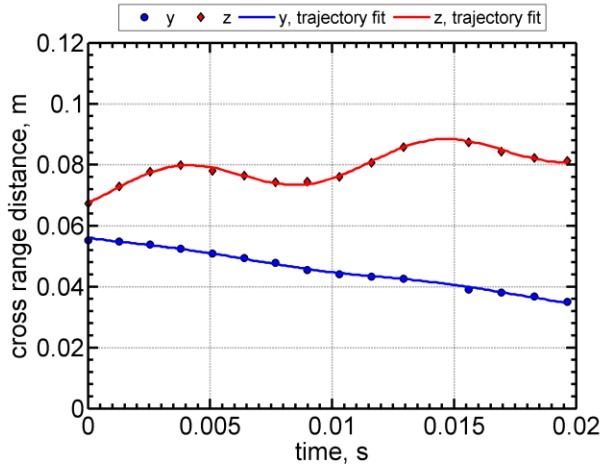

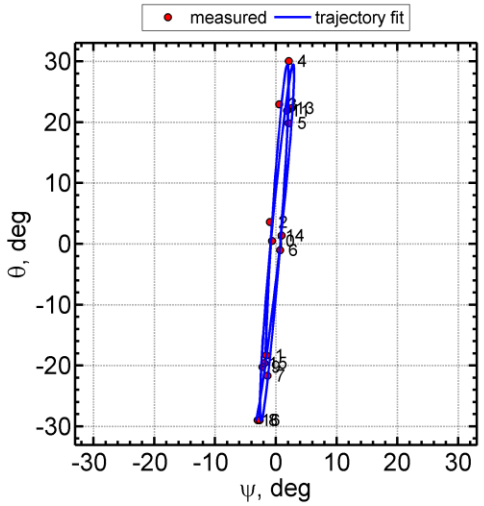

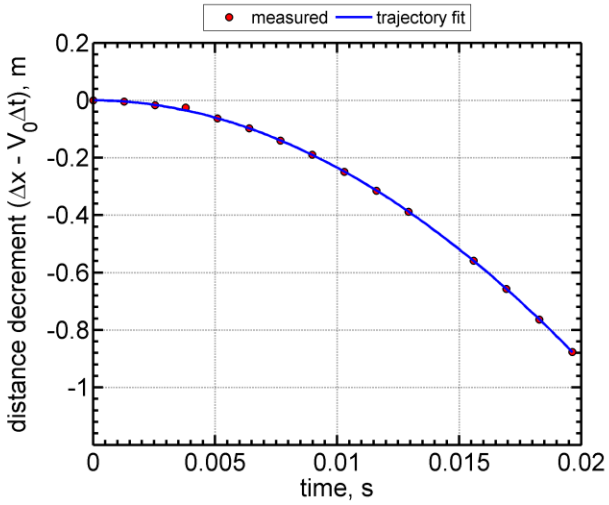

Appendix B: Measured Trajectory Values and Simulated Trajectories for the Stowed-SIAD Configuration

The data in this appendix are presented in order of shot number. The test conditions from Table 6 are repeated here, for convenience.

Test conditions for each shot of the stowed-SIAD configuration models.

Shot	$\bar{M}_\infty$	$\overline{Re}_d$ ($\times 10^{-6}$)	$\bar{V}_\infty$ (m/s)	P_∞ (Torr)	T_∞ (K)	ρ_∞ (kg/m^3)	σ_{RMS} (deg)
2659	3.46	0.341	1187	195.0	292.3	0.310	1.9
2660	3.44	0.338	1181	195.0	293.0	0.309	7.6
2661	3.46	0.339	1190	195.0	293.9	0.308	1.6
2662	3.51	0.344	1202	195.0	292.8	0.309	10.4
2663	3.45	0.338	1188	195.0	293.5	0.309	4.9
2664	3.48	0.343	1192	195.0	292.0	0.310	13.9
2665	3.20	0.312	1103	195.0	294.6	0.307	17.2
2666	3.17	0.308	1092	195.0	295.1	0.307	2.0
2667	3.18	0.310	1095	195.0	294.5	0.308	11.4
2668	3.18	0.310	1094	195.0	294.7	0.307	3.0
2669	3.18	0.310	1095	195.0	294.2	0.308	5.8
2670	3.67	0.357	1265	194.8	295.2	0.307	16.2

Shot	$\bar{M}_\infty$	$\overline{Re}_d$ (x 10^{-6})	$\bar{V}_\infty$ (m/s)	P_∞ (Torr)	T_∞ (K)	ρ_∞ (kg/m^3)	σ_{RMS} (deg)
2659	3.46	0.341	1187	195.0	292.3	0.310	1.9

Station	time, s	x, m	y, m	z, m	V, m/s	M	Re_d (x 10^{-6})	ψ, deg	θ, deg
1	0.00000000	0.054	0.072	0.071	1243.88	3.63	0.357	-0.1	0.7
2	0.00123726	1.588	0.074	0.072	1236.02	3.61	0.355	-0.1	-1.5
3	0.00247492	3.114	0.075	0.071	1228.25	3.58	0.353	0.4	-2.3
4	0.00370550		0.075		1220.61	3.56	0.350	-0.5	
5	0.00496299	6.151	0.076	0.071	1212.89	3.54	0.348	-0.5	0.9
6	0.00624035	7.695	0.077	0.072	1205.15	3.52	0.346	-0.3	2.8
7	0.00749225	9.199	0.079	0.073	1197.66	3.49	0.344	-0.4	2.5
8	0.00876983	10.724	0.079	0.072	1190.10	3.47	0.342	0.1	0.5
9	0.01006022	12.255	0.080	0.071	1182.56	3.45	0.340	0.9	-1.9
10	0.01134996	13.775	0.081	0.072	1175.13	3.43	0.337	0.4	-2.8
11	0.01265028	15.299	0.082	0.073	1167.73	3.41	0.335	-0.3	-1.7
12	0.01396820	16.833	0.082	0.073	1160.33	3.39	0.333	-0.7	1.0
13	0.01528305	18.354	0.082	0.073	1153.05	3.36	0.331	-0.8	2.5
14	0.01661801	19.887	0.085	0.073	1145.76	3.34	0.329	-0.6	2.0
15	0.01793633	21.393	0.086	0.074	1138.67	3.32	0.327	0.0	-0.1
16	0.01928174	22.921	0.087	0.073	1131.53	3.30	0.325	0.9	-1.9

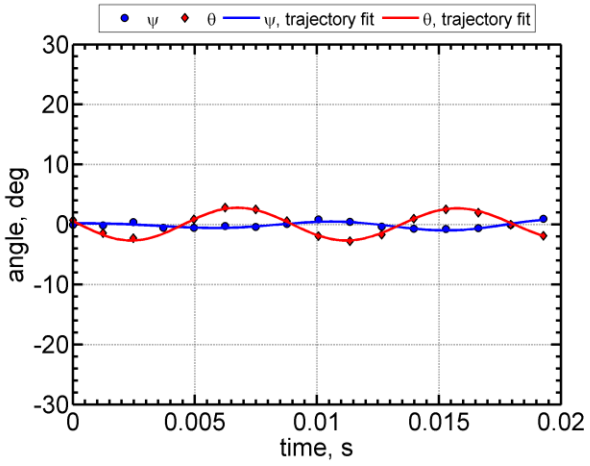

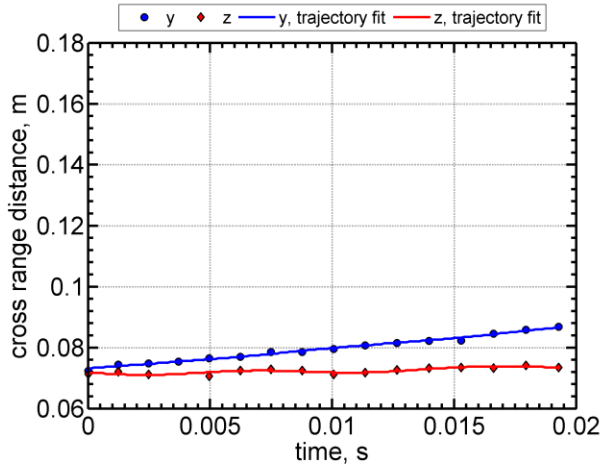

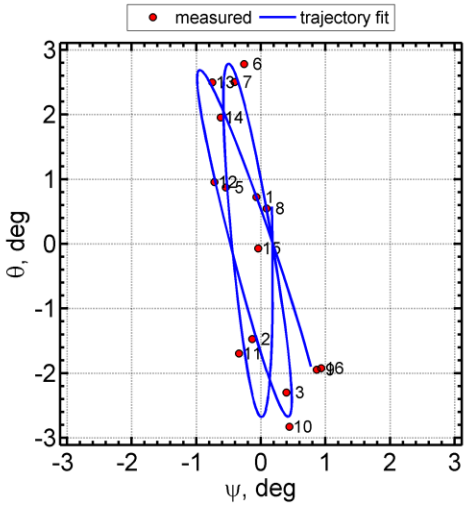

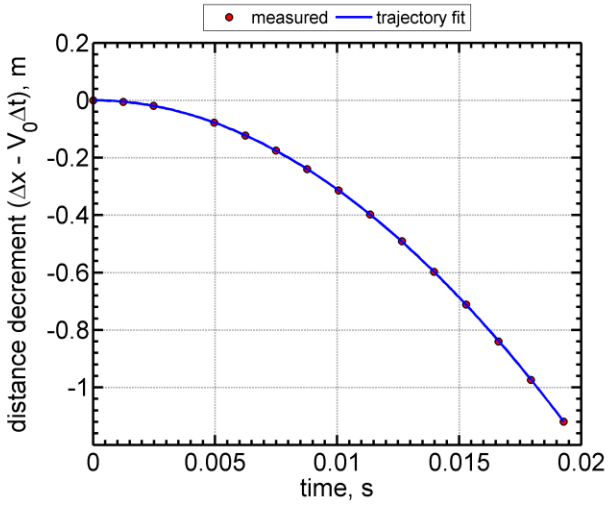

Shot	$\bar{M}_\infty$	$\overline{Re_d}$ (x 10^{-6})	$\bar{V}_\infty$ (m/s)	P_∞ (Torr)	T_∞ (K)	ρ_∞ (kg/m^3)	σ_{RMS} (deg)
2660	3.44	0.338	1181	195.0	293.0	0.309	7.6

Station	time, s	x, m	y, m	z, m	V, m/s	M	Re_d (x 10^{-6})	ψ, deg	θ, deg
1	0.00000000	0.053	0.076	0.075	1237.21	3.61	0.354	-0.2	-2.6
2	0.00124226	1.585	0.078	0.079	1229.50	3.58	0.352	-1.0	6.7
3	0.00248951	3.114	0.079	0.081	1221.85	3.56	0.350	-1.5	10.5
4	0.00372507	4.620	0.080	0.083	1214.35	3.54	0.347	-0.2	6.5
5	0.00498833	6.149	0.082	0.080	1206.77	3.52	0.345	0.3	-2.6
6	0.00627546	7.697	0.082	0.082	1199.14	3.49	0.343	1.1	-10.4
7	0.00753029	9.197	0.085	0.084	1191.79	3.47	0.341	-0.1	-9.1
8	0.00881372	10.722	0.085	0.087	1184.36	3.45	0.339	-1.1	-1.8
9	0.01011089	12.253	0.087	0.089	1176.94	3.43	0.337	-0.1	7.5
10	0.01140436	13.770	0.089	0.092	1169.64	3.41	0.335	0.5	11.4
11	0.01271152	15.295	0.090	0.093	1162.36	3.39	0.333	0.2	5.5
12	0.01403603	16.829	0.091	0.093	1155.08	3.37	0.330	-0.5	-3.6
13	0.01535682	18.351		0.093	1147.91	3.35	0.328		-10.4
14	0.01668857	19.875	0.095	0.095	1140.79	3.32	0.326	-1.9	-9.2
15	0.01801970	21.389	0.097	0.099	1133.76	3.30	0.324	-0.4	-0.7
16	0.01937207	22.917	0.099	0.102	1126.73	3.28	0.322	1.6	8.4

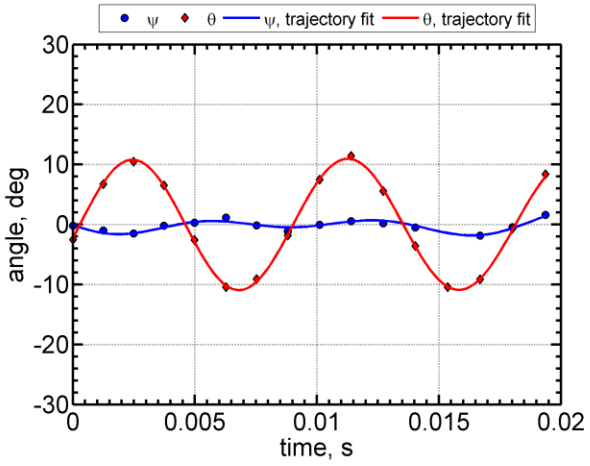

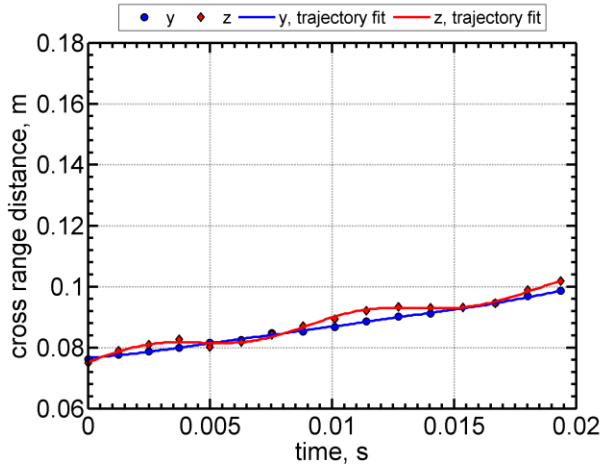

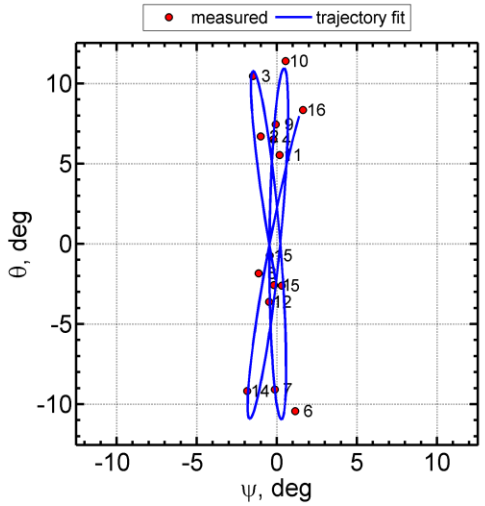

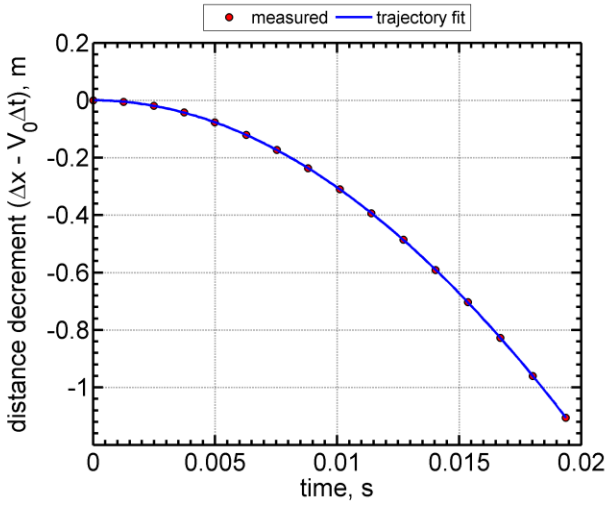

Shot	$\bar{M}_\infty$	$\overline{Re}_d$ (x 10^{-6})	$\bar{V}_\infty$ (m/s)	P_∞ (Torr)	T_∞ (K)	ρ_∞ (kg/m^3)	σ_{RMS} (deg)
2661	3.46	0.339	1190	195.0	293.9	0.308	1.6

Station	time, s	x, m	y, m	z, m	V, m/s	M	Re_d (x 10^{-6})	ψ, deg	θ, deg
1	0.00000000	0.054	0.076	0.070	1247.40	3.63	0.355	-0.8	0.0
2	0.00123322	1.587	0.078	0.071	1239.56	3.61	0.353	-0.6	1.3
3	0.00246976	3.114	0.080	0.070	1231.79	3.58	0.350	-0.4	2.2
4	0.00369689	4.622	0.081	0.071	1224.17	3.56	0.348	0.2	0.9
5	0.00495042	6.151	0.083	0.068	1216.47	3.54	0.346	0.5	-0.6
6	0.00621279	7.681	0.084	0.069	1208.81	3.52	0.344	0.4	-2.3
7	0.00747137	9.198	0.086	0.070	1201.27	3.50	0.342	-0.4	-1.9
8	0.00874744	10.726	0.087	0.070	1193.72	3.47	0.340	-1.3	-0.2
9	0.01003292	12.256	0.088	0.069	1186.20	3.45	0.337	-0.5	1.7
10	0.01131742	13.774	0.090	0.070	1178.79	3.43	0.335	-0.5	2.1
11	0.01261476	15.300	0.092	0.070	1171.40	3.41	0.333	0.3	0.7
12	0.01392596	16.830	0.094	0.070	1164.03	3.39	0.331	0.2	-0.9
13	0.01523896	18.355	0.095	0.069	1156.75	3.37	0.329	-0.3	-2.2
14	0.01656047	19.878	0.097	0.069	1149.52	3.35	0.327	-0.7	-1.7
15	0.01788368	21.393	0.099	0.071	1142.39	3.32	0.325	-1.1	-0.2
16	0.01922479	22.922	0.100	0.070	1135.26	3.30	0.323	-0.2	1.7

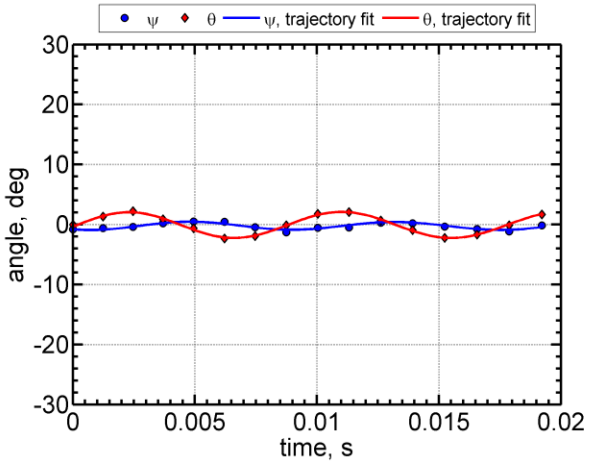

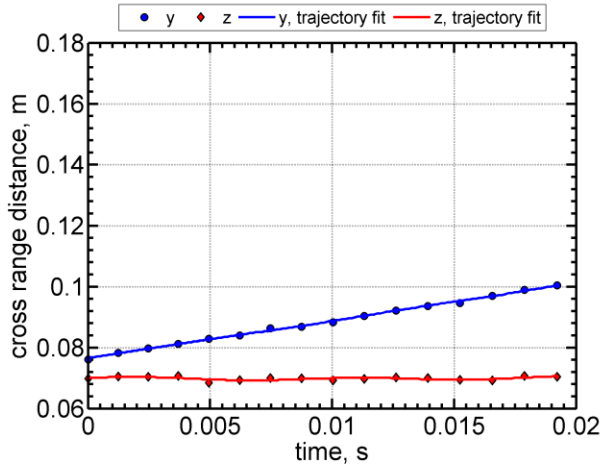

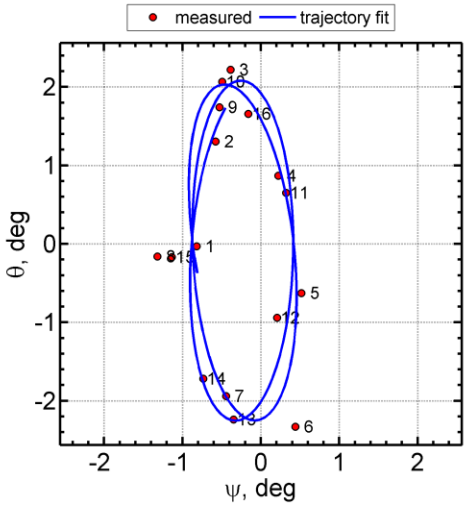

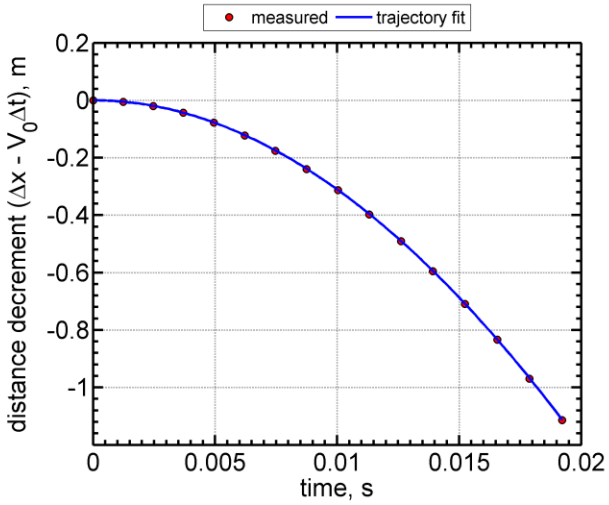

Shot	$\bar{M}_\infty$	$\overline{Re_d}$ (x 10^{-6})	$\bar{V}_\infty$ (m/s)	P_∞ (Torr)	T_∞ (K)	ρ_∞ (kg/m^3)	σ_{RMS} (deg)
2662	3.51	0.344	1202	195.0	292.8	0.309	10.4

Station	time, s	x, m	y, m	z, m	V, m/s	M	Re_d (x 10^{-6})	ψ, deg	θ, deg
1	0.00000000	0.052	0.074	0.081	1258.24	3.67	0.360	0.0	-4.0
2	0.00122199	1.584	0.077	0.088	1250.55	3.65	0.358	0.3	8.9
3	0.00244711	3.112	0.078	0.092	1242.94	3.62	0.356	1.0	15.0
4	0.00366198	4.618	0.079	0.096	1235.46	3.60	0.354	0.5	10.0
5	0.00490378	6.147	0.078	0.095	1227.91	3.58	0.352	-0.2	-2.3
6	0.00616101	7.685	0.080	0.098	1220.36	3.56	0.350	-1.7	-13.5
7	0.00740063	9.194	0.082	0.102	1212.99	3.54	0.347	-2.0	-13.7
8	0.00866209	10.719	0.082	0.107	1205.59	3.51	0.345	0.1	-4.3
9	0.00993526	12.250	0.084	0.112	1198.20	3.49	0.343	1.4	8.7
10	0.01120511	13.765	0.086	0.118	1190.93	3.47	0.341	2.7	14.7
11	0.01248803	15.290	0.087	0.121	1183.67	3.45	0.339	1.6	9.3
12	0.01378812	16.824	0.087	0.124	1176.41	3.43	0.337	-1.0	-2.9
13	0.01508416	18.344	0.087	0.125	1169.27	3.41	0.335	-3.5	-13.1
14	0.01639276	19.869	0.089	0.128	1162.15	3.39	0.333	-4.3	-13.9
15	0.01769943	21.381	0.092	0.135	1155.14	3.37	0.331	-1.8	-4.6
16	0.01902394	22.909	0.093	0.142	1148.13	3.35	0.329	2.6	8.0

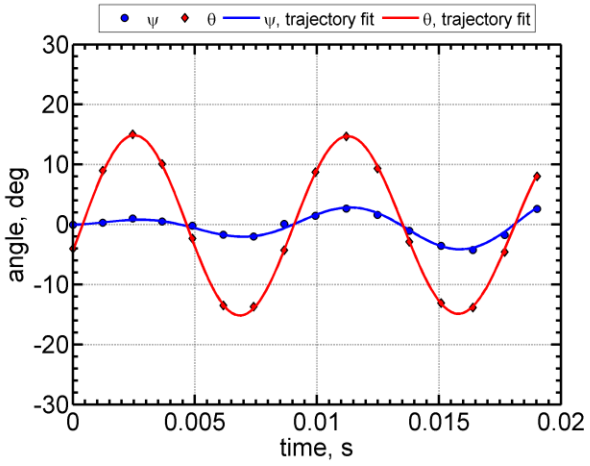

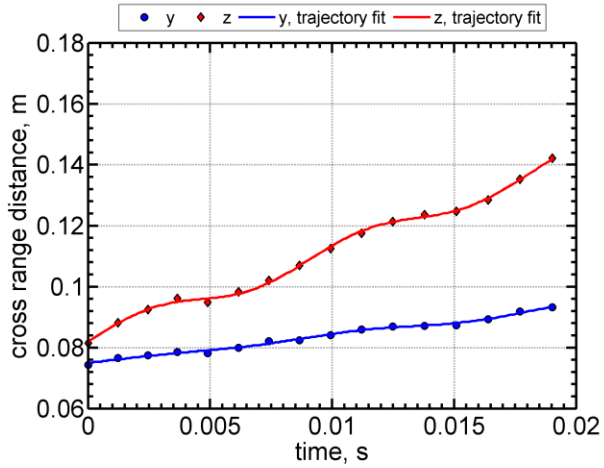

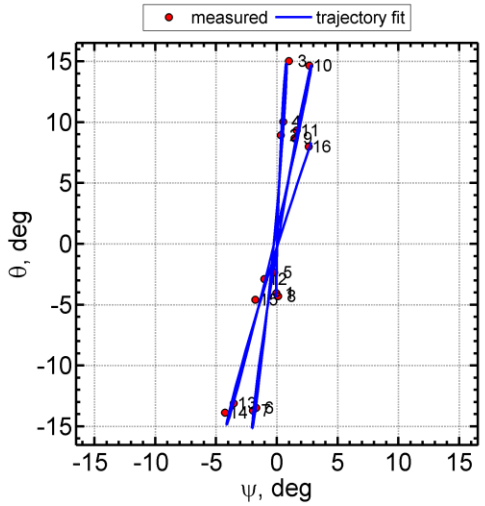

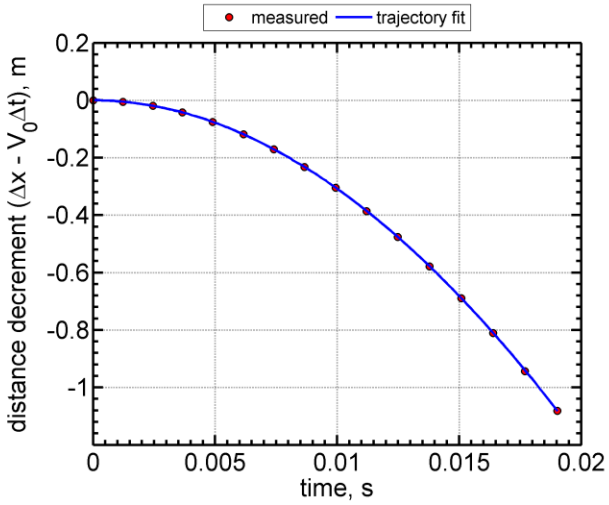

Shot	$\bar{M}_\infty$	$\overline{Re}_d$ (x 10^{-6})	$\bar{V}_\infty$ (m/s)	P_∞ (Torr)	T_∞ (K)	ρ_∞ (kg/m^3)	σ_{RMS} (deg)
2663	3.45	0.338	1188	195.0	293.5	0.309	4.9

Station	time, s	x, m	y, m	z, m	V, m/s	M	Re_d (x 10^{-6})	ψ, deg	θ, deg
1	0.00000000	0.054	0.075	0.072	1244.12	3.62	0.355	-0.9	-1.5
2	0.00123464	1.585	0.078	0.075	1236.35	3.60	0.353	0.6	4.2
3	0.00247379	3.113	0.079	0.076	1228.63	3.58	0.350	2.2	7.1
4	0.00370445	4.621	0.080	0.077	1221.06	3.56	0.348	1.5	4.3
5	0.00496132	6.150	0.081	0.075	1213.41	3.53	0.346	-0.1	-1.1
6									
7	0.00748912	9.198	0.084	0.077	1198.30	3.49	0.342	-2.3	-5.8
8	0.00876620	10.723	0.085	0.079	1190.81	3.47	0.340	-1.4	-1.5
9	0.01005614	12.255	0.086	0.080	1183.33	3.45	0.337	1.7	4.3
10	0.01134211	13.771	0.088	0.082	1175.98	3.42	0.335	2.4	5.5
11	0.01264297	15.297	0.089	0.082	1168.63	3.40	0.333	1.7	3.9
12	0.01395613	16.826	0.090	0.082	1161.31	3.38	0.331	-0.9	-1.6
13	0.01527325	18.351	0.090	0.082	1154.07	3.36	0.329	-2.9	-6.0
14	0.01660170	19.879	0.093	0.082	1146.87	3.34	0.327	-3.2	-6.0
15	0.01792410	21.391	0.095	0.085	1139.80	3.32	0.325	-1.1	-1.5
16	0.01926778	22.919	0.097	0.087	1132.72	3.30	0.323	2.2	4.2

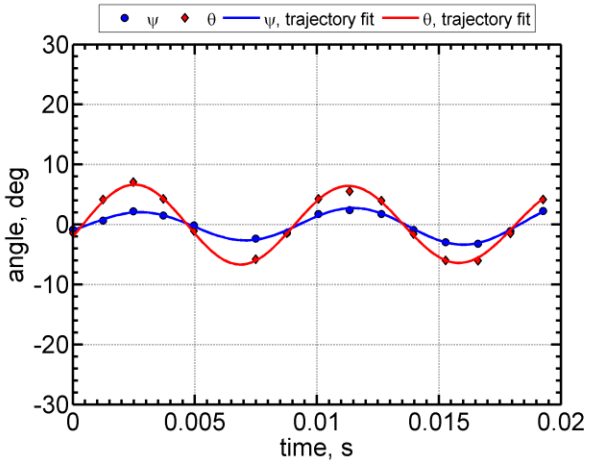

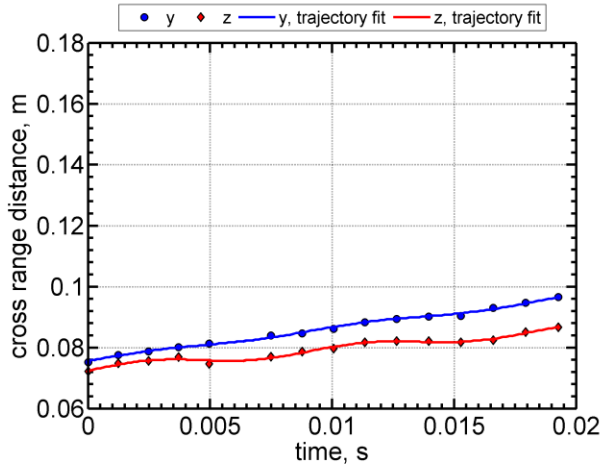

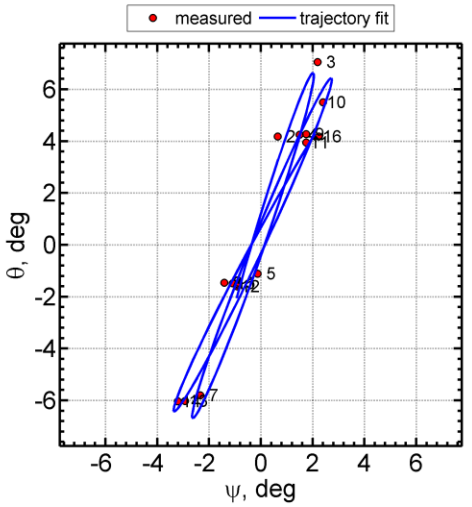

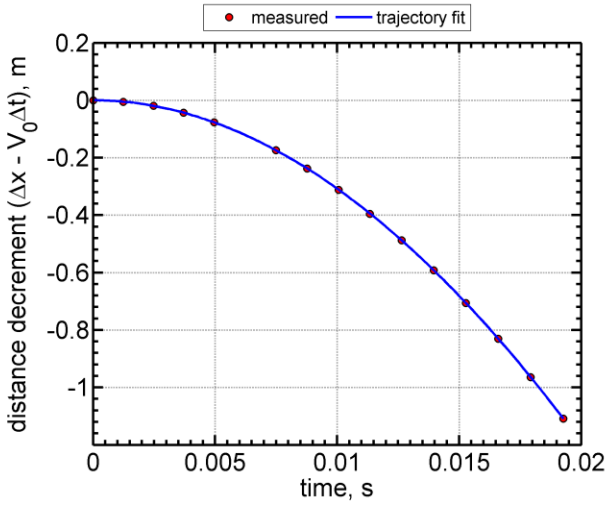

Shot	$\bar{M}_\infty$	$\overline{Re_d}$ (x 10^{-6})	$\bar{V}_\infty$ (m/s)	P_∞ (Torr)	T_∞ (K)	ρ_∞ (kg/m^3)	σ_{RMS} (deg)
2664	3.48	0.343	1192	195.0	292.0	0.310	13.9

Station	time, s	x, m	y, m	z, m	V, m/s	M	Re_d (x 10^{-6})	ψ, deg	θ, deg
1	0.00000000	0.050	0.073	0.088	1246.57	3.64	0.359	-1.6	-4.2
2	0.00123313	1.583	0.075	0.097	1239.06	3.62	0.356	1.8	12.8
3	0.00246942	3.110	0.076	0.103	1231.61	3.60	0.354	3.7	19.7
4	0.00369524	4.616	0.076	0.108	1224.29	3.57	0.352	2.6	11.9
5	0.00494854	6.146	0.077	0.107	1216.90	3.55	0.350	-0.3	-5.2
6	0.00621263	7.679	0.076	0.111	1209.52	3.53	0.348	-2.8	-18.1
7	0.00746739	9.192	0.078	0.117	1202.27	3.51	0.346	-3.7	-17.4
8	0.00873967	10.716	0.078	0.124	1195.01	3.49	0.344	-1.6	-2.7
9	0.01002393	12.247	0.079	0.131	1187.76	3.47	0.342	2.9	14.0
10	0.01130402	13.761	0.081	0.137	1180.63	3.45	0.340	5.0	19.4
11	0.01259825	15.287	0.081	0.141	1173.49	3.43	0.338	2.6	11.1
12	0.01390935	16.819	0.080	0.143	1166.36	3.40	0.336	-1.1	-7.0
13	0.01521691	18.340	0.080	0.145	1159.33	3.38	0.334	-4.5	-18.9
14	0.01653696	19.866	0.081	0.151	1152.32	3.36	0.331	-4.6	-16.7
15	0.01785313	21.376	0.083	0.159	1145.42	3.34	0.330	-1.1	-2.0
16	0.01918965	22.905	0.083	0.168	1138.51	3.32	0.328	3.8	14.5

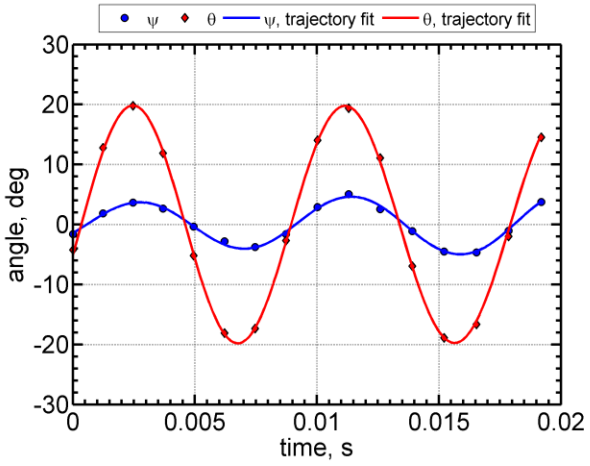

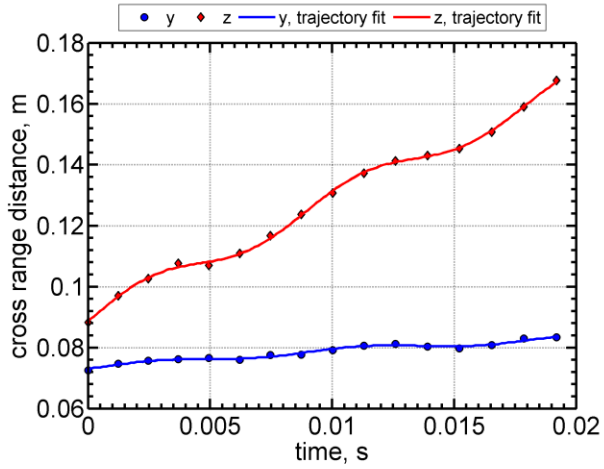

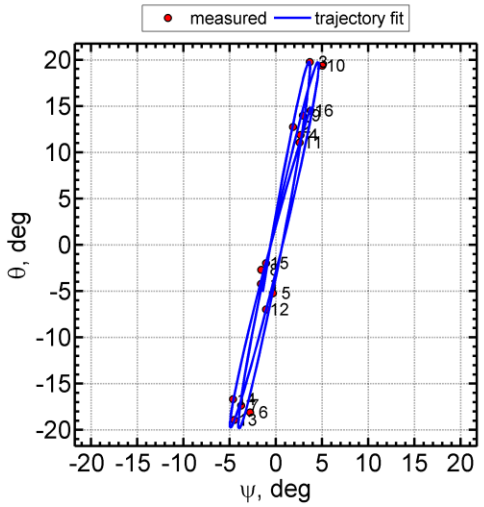

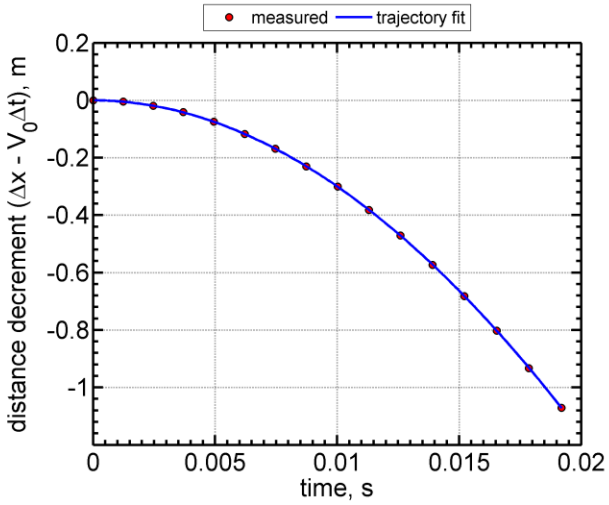

Shot	$\bar{M}_\infty$	$\overline{Re_d}$ ($\times 10^{-6}$)	$\bar{V}_\infty$ (m/s)	P_∞ (Torr)	T_∞ (K)	ρ_∞ (kg/m^3)	σ_{RMS} (deg)
2665	3.20	0.312	1103	195.0	294.6	0.307	17.2

Station	time, s	x, m	y, m	z, m	V, m/s	M	Re_d ($\times 10^{-6}$)	ψ, deg	θ, deg
1	0.00000000	0.052	0.074	0.083	1151.12	3.35	0.326	-0.9	-5.9
2	0.00133441	1.584	0.076	0.092	1144.49	3.33	0.324	1.4	15.0
3	0.00267244	3.111	0.077	0.097	1137.92	3.31	0.322	3.0	25.0
4	0.00399977	4.618	0.078	0.101	1131.46	3.29	0.320	2.4	17.2
5	0.00535466	6.146	0.079	0.098	1124.93	3.27	0.319	-0.8	-3.8
6	0.00671975	7.677	0.079	0.100	1118.41	3.25	0.317	-4.2	-21.1
7	0.00807887	9.193	0.080	0.105	1111.99	3.23	0.315	-5.0	-21.7
8	0.00945470		0.081		1105.56	3.21	0.313	-1.7	
9	0.01084337	12.249	0.083	0.117	1099.14	3.19	0.311	3.8	15.2
10	0.01222494	13.762	0.085	0.123	1092.82	3.18	0.309	6.8	23.7
11	0.01362591	15.290	0.086	0.125	1086.48	3.16	0.308	4.3	16.0
12	0.01504168	16.823	0.085	0.125	1080.15	3.14	0.306	-1.7	-4.3
13	0.01645333	18.344	0.085	0.126	1073.90	3.12	0.304	-7.5	-21.1
14	0.01787651	19.867	0.087	0.129	1067.68	3.10	0.302	-7.6	-22.4
15	0.01930039	21.381	0.089	0.135	1061.52	3.09	0.301	-2.6	-6.0
16	0.02074229	22.909	0.091	0.142	1055.37	3.07	0.299	5.6	13.5

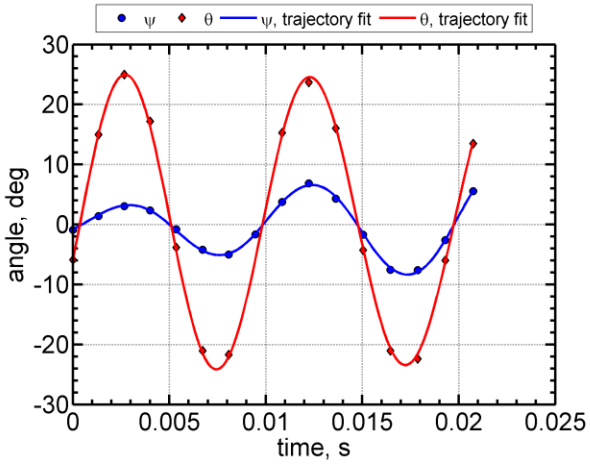

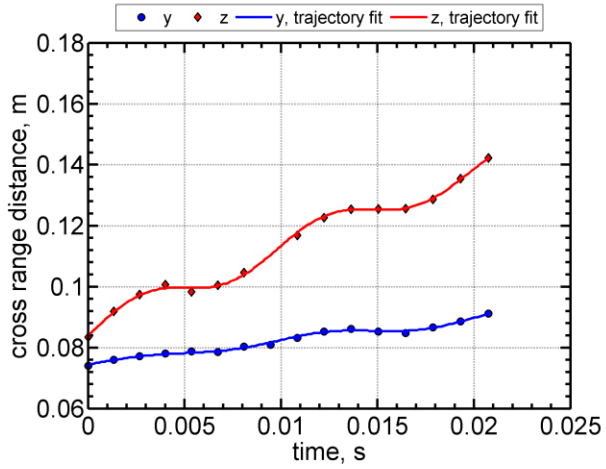

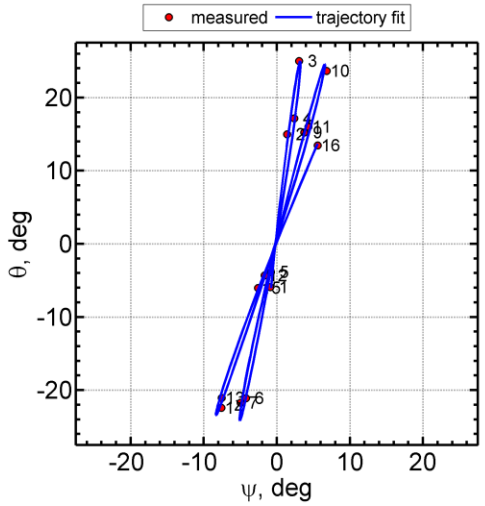

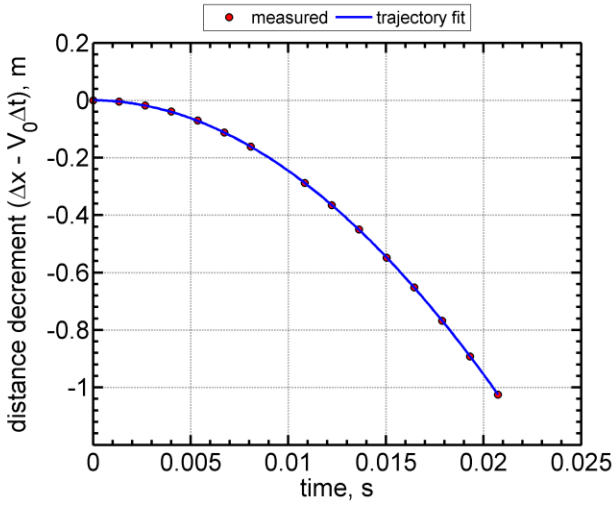

Shot	$\bar{M}_\infty$	$\overline{Re}_d$ (x 10^{-6})	$\bar{V}_\infty$ (m/s)	P_∞ (Torr)	T_∞ (K)	ρ_∞ (kg/m^3)	σ_{RMS} (deg)
2666	3.17	0.308	1092	195.0	295.1	0.307	2.0

Station	time, s	x, m	y, m	z, m	V, m/s	M	Re_d (x 10^{-6})	ψ, deg	θ, deg
1	0.00000000	0.052	0.073	0.075	1143.60	3.32	0.323	-0.8	1.1
2	0.00134437	1.584	0.074	0.076	1136.51	3.30	0.321	-0.7	-1.6
3	0.00269346	3.113	0.075	0.077	1129.48	3.28	0.319	0.0	-3.3
4	0.00403099	4.620	0.076	0.078	1122.59	3.26	0.317	0.5	-2.3
5	0.00539799	6.150	0.076	0.077	1115.63	3.24	0.315	0.2	0.0
6	0.00677410	7.680	0.078	0.080	1108.70	3.22	0.313	-0.3	1.7
7	0.00814644	9.196	0.079	0.081	1101.88	3.20	0.311	-0.7	2.7
8	0.00953617	10.723	0.079	0.082	1095.05	3.18	0.309	-0.8	0.8
9	0.01093776	12.253	0.080	0.082	1088.24	3.16	0.307	-0.2	-1.4
10	0.01234053	13.774	0.082	0.083	1081.52	3.14	0.305	-0.2	-3.3
11	0.01375144	15.296	0.084	0.085	1074.85	3.12	0.303	0.4	-2.4
12	0.01517985	16.826	0.084	0.087	1068.18	3.10	0.302	-0.1	-0.5
13	0.01661050	18.350	0.085	0.088	1061.59	3.08	0.300	-0.7	1.9
14	0.01805400	19.878	0.087	0.089	1055.03	3.06	0.298	-0.6	2.5
15	0.01949223	21.388	0.088	0.091	1048.58	3.05	0.296	-1.1	0.5
16	0.02095292	22.917	0.089	0.092	1042.13	3.03	0.294	-0.1	-1.5

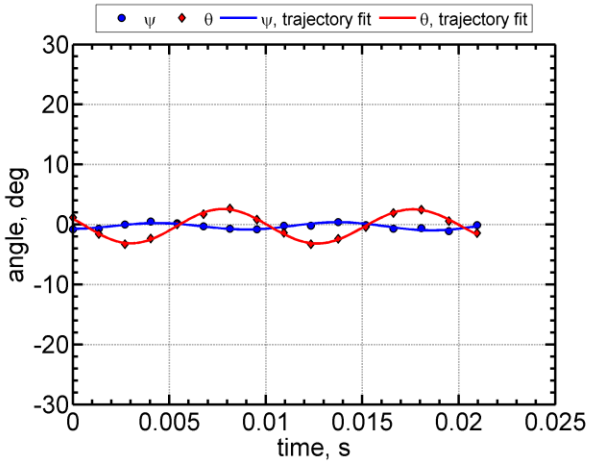

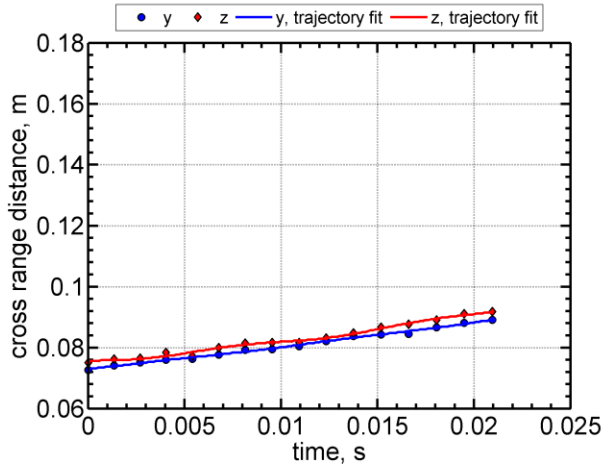

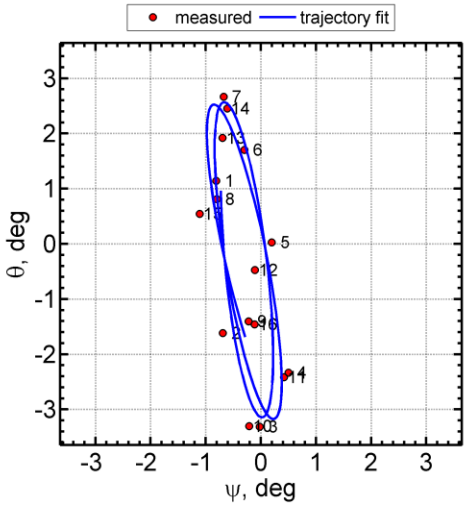

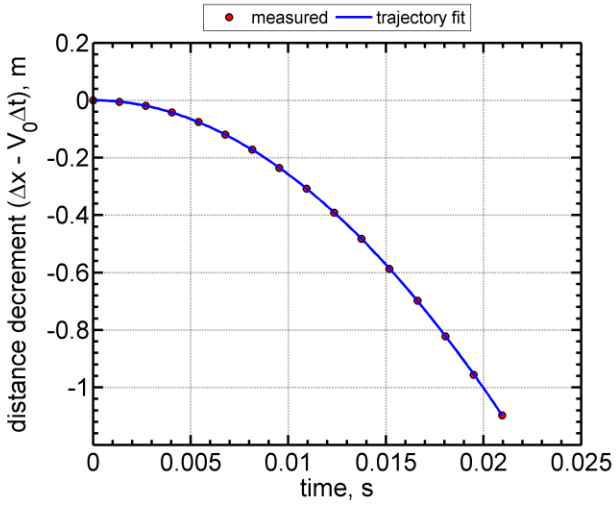

Shot	$\bar{M}_\infty$	$\overline{Re_d}$ (x 10^{-6})	$\bar{V}_\infty$ (m/s)	P_∞ (Torr)	T_∞ (K)	ρ_∞ (kg/m^3)	σ_{RMS} (deg)
2667	3.18	0.310	1095	195.0	294.5	0.308	11.4

Station	time, s	x, m	y, m	z, m	V, m/s	M	Re_d (x 10^{-6})	ψ, deg	θ, deg
1	0.00000000	0.051	0.076	0.083	1146.29	3.33	0.325	-0.4	-4.6
2	0.00134184	1.584	0.078	0.089	1139.31	3.31	0.323	-0.1	9.7
3	0.00268484	3.109	0.079	0.094	1132.39	3.29	0.321	0.8	17.1
4	0.00402028	4.618	0.080	0.098	1125.59	3.27	0.319	0.8	12.2
5	0.00538344	6.147	0.081	0.096	1118.73	3.25	0.317	-0.4	-2.0
6	0.00675571	7.676	0.082	0.099	1111.90	3.23	0.315	-2.1	-14.1
7	0.00812387	9.193	0.084	0.103	1105.17	3.21	0.313	-2.7	-14.9
8	0.00950949	10.719	0.085	0.107	1098.43	3.19	0.311	-1.3	-4.9
9	0.01090669	12.250	0.087	0.113	1091.71	3.17	0.309	1.9	8.9
10	0.01230134	13.767	0.089	0.118	1085.09	3.15	0.307	3.8	16.1
11	0.01370813	15.291	0.090	0.122	1078.50	3.13	0.305	3.2	11.4
12	0.01513743	16.826	0.090	0.122	1071.88	3.12	0.304	-0.9	-1.8
13	0.01655689	18.344	0.090	0.123	1065.39	3.10	0.302	-4.8	-12.5
14	0.01799182	19.868	0.092	0.126	1058.92	3.08	0.300	-6.5	-14.5
15	0.01942643	21.381	0.095	0.132	1052.54	3.06	0.298	-2.9	-5.5
16	0.02088065	22.909	0.096	0.138	1046.15	3.04	0.296	3.9	7.5

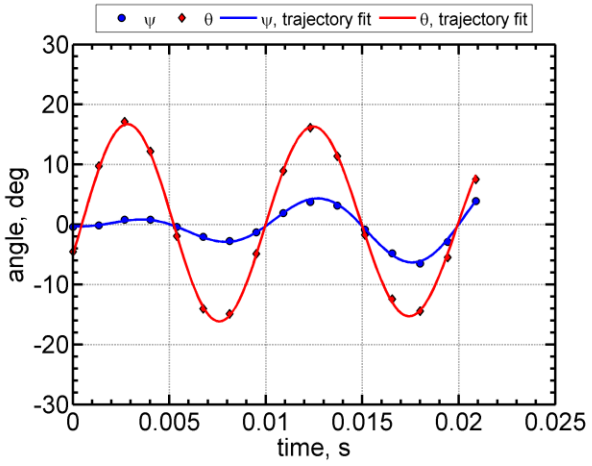

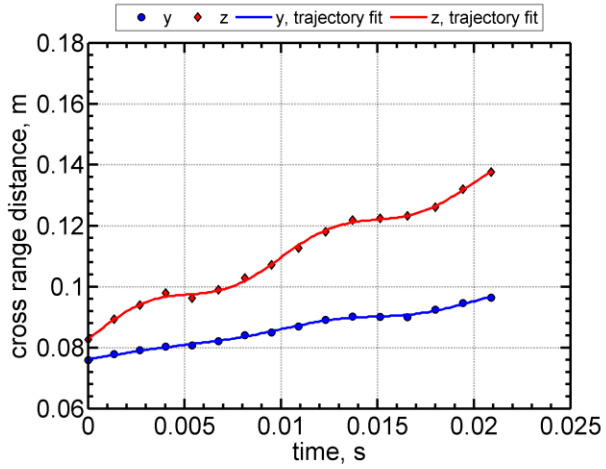

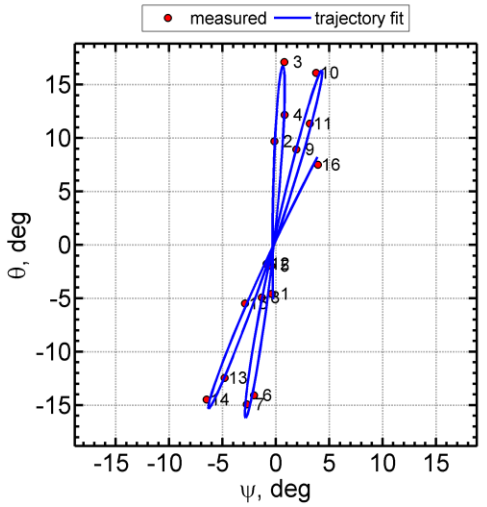

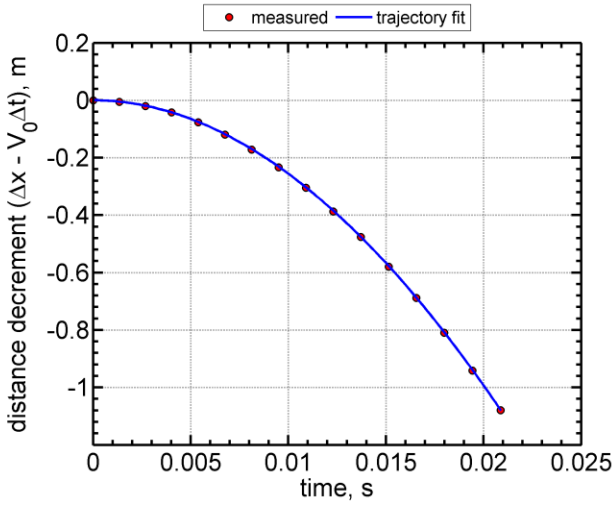

Shot	$\bar{M}_\infty$	$\overline{Re}_d$ (x 10^{-6})	$\bar{V}_\infty$ (m/s)	P_∞ (Torr)	T_∞ (K)	ρ_∞ (kg/m^3)	σ_{RMS} (deg)
2668	3.18	0.310	1094	195.0	294.7	0.307	3.0

Station	time, s	x, m	y, m	z, m	V, m/s	M	Re_d (x 10^{-6})	ψ, deg	θ, deg
1	0.00000000	0.053	0.076	0.077	1146.37	3.33	0.324	0.3	0.1
2	0.00133959	1.584	0.078	0.079	1139.22	3.31	0.322	-0.6	2.7
3	0.00268393	3.111	0.079	0.081	1132.12	3.29	0.320	-1.6	4.2
4	0.00402040	4.619	0.081	0.083	1125.14	3.27	0.318	-1.7	2.0
5	0.00538412	6.149	0.083	0.081	1118.10	3.25	0.316	-0.5	-1.6
6	0.00675900	7.681	0.085	0.084	1111.09	3.23	0.314	0.3	-4.4
7	0.00812679	9.196	0.087	0.086	1104.20	3.21	0.312	1.0	-3.1
8	0.00951237	10.720	0.088	0.087	1097.30	3.19	0.311	0.2	0.2
9	0.01091286	12.253	0.090	0.089	1090.42	3.17	0.309	-0.9	3.1
10	0.01230917	13.770	0.092	0.091	1083.64	3.15	0.307	-1.9	3.5
11	0.01371953	15.295	0.095	0.093	1076.89	3.13	0.305	-1.5	0.9
12	0.01514150	16.820	0.097	0.094	1070.16	3.11	0.303	-0.1	-2.5
13	0.01657326	18.349	0.099	0.095	1063.49	3.09	0.301	1.2	-4.3
14	0.01801356	19.875	0.102	0.097	1056.86	3.07	0.299	0.7	-3.1
15	0.01945055	21.388	0.104	0.100	1050.34	3.05	0.297	-0.3	0.3
16	0.02090863	22.916	0.107	0.102	1043.82	3.03	0.295	-1.9	2.9

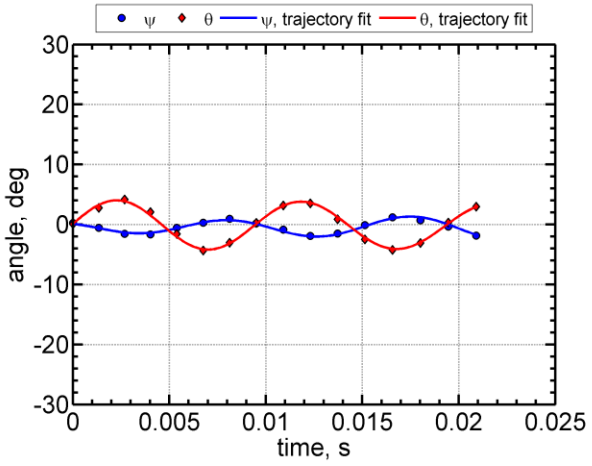

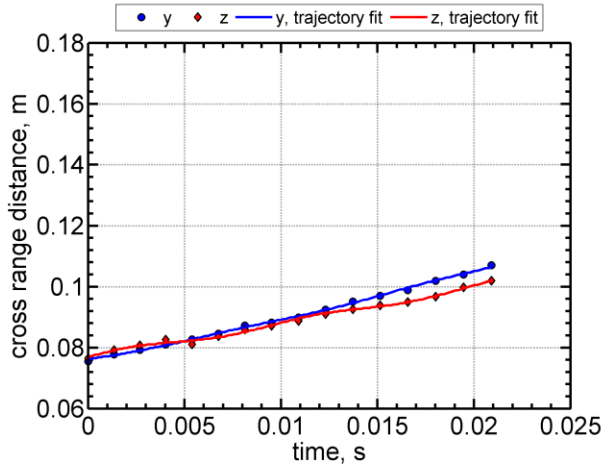

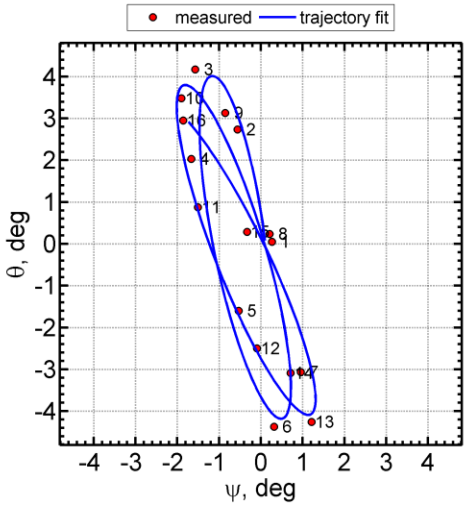

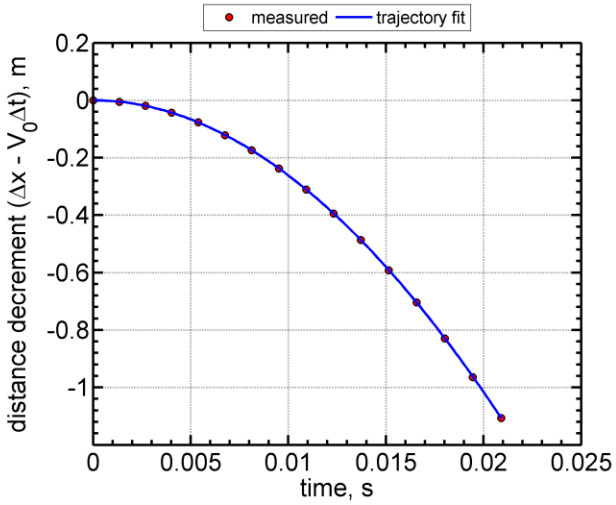

Shot	$\bar{M}_\infty$	$\overline{Re}_d$ (x 10^{-6})	$\bar{V}_\infty$ (m/s)	P_∞ (Torr)	T_∞ (K)	ρ_∞ (kg/m^3)	σ_{RMS} (deg)
2669	3.18	0.310	1095	195.0	294.2	0.308	5.8

Station	time, s	x, m	y, m	z, m	V, m/s	M	Re_d (x 10^{-6})	ψ, deg	θ, deg
1	0.00000000	0.052	0.074	0.080	1146.28	3.33	0.325	-0.9	-2.2
2	0.00134119	1.585	0.076	0.084	1139.17	3.31	0.323	0.6	4.4
3	0.00268604	3.112	0.077	0.087	1132.13	3.29	0.321	1.5	8.3
4	0.00401997	4.619	0.078	0.090	1125.21	3.27	0.319	1.3	5.3
5	0.00538358	6.148	0.079	0.089	1118.23	3.25	0.317	-0.7	-0.3
6	0.00675617	7.678	0.080	0.092	1111.28	3.23	0.315	-2.1	-6.5
7	0.00812559	9.195	0.082	0.094	1104.42	3.21	0.313	-2.8	-7.3
8	0.00951186	10.721		0.097	1097.57	3.19	0.311		-2.5
9	0.01091013	12.251	0.085	0.100	1090.75	3.17	0.309	1.1	4.6
10	0.01230554	13.768	0.087	0.104	1084.02	3.15	0.307	2.7	7.8
11	0.01371537	15.292	0.088	0.106	1077.31	3.13	0.306	1.9	5.4
12	0.01513962	16.821	0.089	0.108	1070.62	3.11	0.304	-0.8	-1.1
13	0.01656969	18.349	0.089	0.109	1064.00	3.09	0.302	-3.3	-7.3
14	0.01800814	19.873	0.092	0.111	1057.42	3.08	0.300	-3.7	-7.5
15	0.01944325	21.384	0.094	0.116	1050.95	3.06	0.298	-1.9	-3.1
16	0.02090148	22.914	0.096	0.119	1044.47	3.04	0.296	1.4	4.0

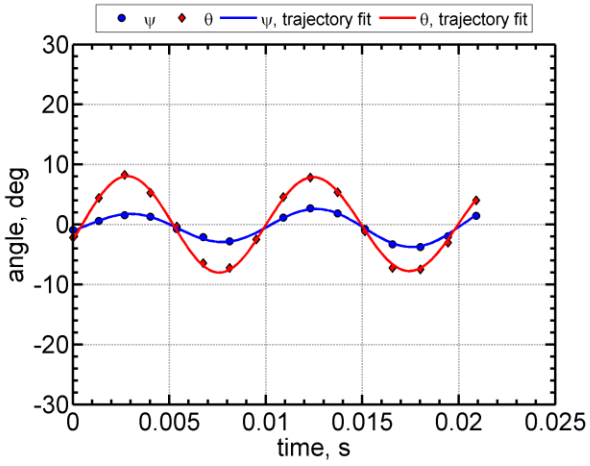

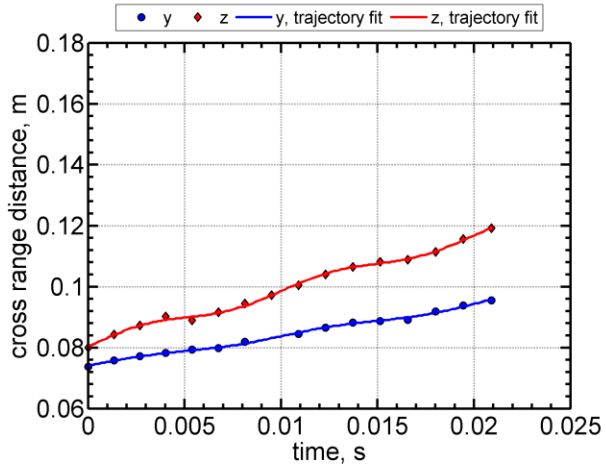

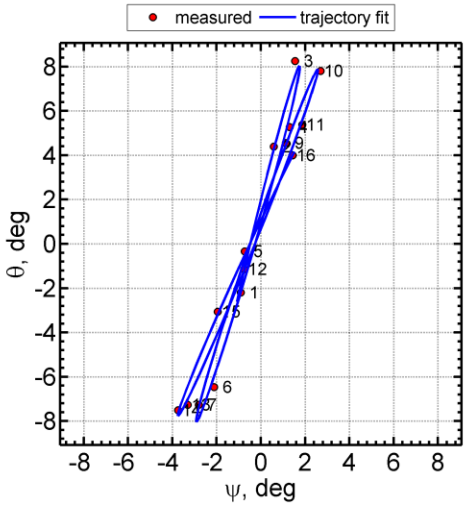

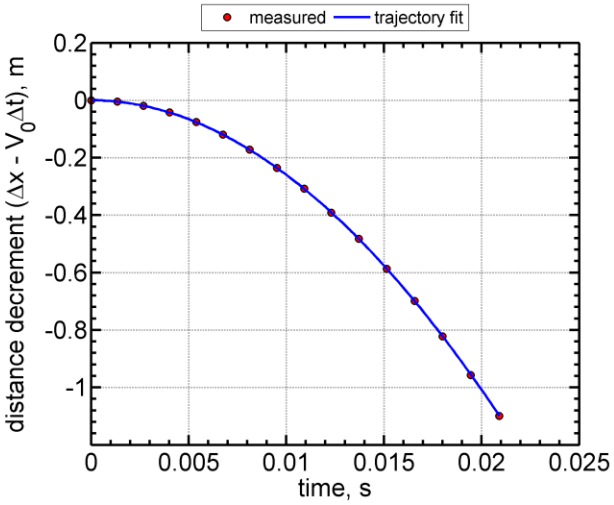

Shot	$\bar{M}_\infty$	$\overline{Re_d}$ (x 10^{-6})	$\bar{V}_\infty$ (m/s)	P_∞ (Torr)	T_∞ (K)	ρ_∞ (kg/m^3)	σ_{RMS} (deg)
2670	3.67	0.357	1265	194.8	295.2	0.307	16.2

Station	time, s	x, m	y, m	z, m	V, m/s	M	Re_d (x 10^{-6})	ψ, deg	θ, deg
1	0.00000000	0.053	0.073	0.084	1320.60	3.83	0.372	-0.5	-4.3
2	0.00116374	1.585	0.075	0.093	1313.00	3.81	0.370	2.1	15.4
3	0.00232947	3.111	0.076	0.098	1305.47	3.79	0.368	4.5	23.6
4	0.00348611	4.618	0.076	0.102	1298.07	3.77	0.366	2.5	13.5
5	0.00466805	6.147	0.075	0.101	1290.58	3.75	0.364	-2.0	-6.8
6	0.00586065	7.681	0.075	0.104	1283.10	3.73	0.362	-6.8	-21.1
7	0.00704256	9.194	0.077	0.109	1275.76	3.70	0.360	-7.6	-18.8
8	0.00824157	10.718	0.078	0.115	1268.39	3.68	0.358	-1.2	-2.5
9	0.00945259	12.250	0.080	0.122	1261.02	3.66	0.355	8.0	15.4
10	0.01065865	13.766	0.081	0.128	1253.77	3.64	0.353	10.2	20.4
11	0.01187620	15.290	0.081	0.132	1246.52	3.62	0.351	5.3	10.7
12	0.01311023	16.822	0.079	0.132	1239.25	3.60	0.349	-5.0	-7.1
13	0.01434131	18.344	0.078	0.134	1232.09	3.58	0.347	-13.1	-17.9
14	0.01558455	19.870	0.080	0.139	1224.93	3.56	0.345	-11.9	-14.9
15	0.01682130	21.379	0.084	0.146	1217.90	3.54	0.343	-0.3	-1.3
16	0.01807844	22.909	0.086	0.153	1210.83	3.52	0.341	12.2	12.7